Sediment Dynamics in a Transboundary Mangrove Habitat: A Perspective of Sediment Sources and Sedimentation in the Vanga Estuary, Kenya

Dissertation

for obtaining a Doctoral Degree in Science

(Dr. rer. nat)

at the Faculty of Geosciences (FB5),

the University of Bremen

Amon Kibiwot Kimeli

Bremen, May 2022

Printed and/or published with the support of the German Academic Exchange Service.

The work contained within this dissertation took place between October 2018 and March 2022 at the Leibniz Centre for Tropical Marine Research (ZMT) in Bremen, Germany.

Supported financially by the Deutscher Akademischer Austauschdienst (DAAD) Kenyan-German doctoral programme, the Flemish Interuniversity Council – University Development Cooperation (VLIR-UOS) research grant [ZEIN2016PR425], Western Indian Ocean Marine Science Association, Marine Research Grant [MARGI-2020-CO3] and the Leibniz Centre for Tropical Marine Research (ZMT), Bremen Germany through the ZMT Academy support.

First Reviewer:

Prof. Dr. Hildegard Westphal

University of Bremen, Germany

Leibniz Centre for Tropical Marine Research (ZMT), Bremen

Second Reviewer:

Prof. Dr. Matthias Hinderer

Technische Universität Darmstadt

Institute of Applied Geosciences

Colloquium: 12th May 2022

Table of Contents

Affirmation / Erklärung

Versicherung an Eides Statt / *Affirmation in lieu of an oath*

gem. § 5 Abs. 5 der Promotionsordnung vom 18.06.2018 /
according to § 5 (5) of the Doctoral Degree Rules and Regulations of 18 June, 2018

Ich / I, _____
(Vorname / First *Name*, Name / *Name*, Anschrift / *Address*, ggf. Matr.-Nr. / *student ID no., if applicable)*

versichere an Eides Statt durch meine Unterschrift, dass ich die vorliegende Dissertation selbständig und ohne fremde Hilfe angefertigt und alle Stellen, die ich wörtlich dem Sinne nach aus Veröffentlichungen entnommen habe, als solche kenntlich gemacht habe, mich auch keiner anderen als der angegebenen Literatur oder sonstiger Hilfsmittel bedient habe und die zu Prüfungszwecken beigelegte elektronische Version (PDF) der Dissertation mit der abgegebenen gedruckten Version identisch ist. / *With my signature I affirm in lieu of an oath that I prepared the submitted dissertation independently and without illicit assistance from third parties, that I appropriately referenced any text or content from other sources, that I used only literature and resources listed in the dissertation, and that the electronic (PDF) and printed versions of the dissertation are identical.*

Ich versichere an Eides Statt, dass ich die vorgenannten Angaben nach bestem Wissen und Gewissen gemacht habe und dass die Angaben der Wahrheit entsprechen und ich nichts verschwiegen habe*. / I affirm in lieu of an oath that the information provided herein to the best of my knowledge is true and complete.*

Die Strafbarkeit einer falschen eidesstattlichen Versicherung ist mir bekannt, namentlich die Strafandrohung gemäß § 156 StGB bis zu drei Jahren Freiheitsstrafe oder Geldstrafe bei vorsätzlicher Begehung der Tat bzw. gemäß § 161 Abs. 1 StGB bis zu einem Jahr Freiheitsstrafe oder Geldstrafe bei fahrlässiger Begehung. / *I am aware that a false affidavit is a criminal offence which is punishable by law in accordance with § 156 of the German Criminal Code (StGB) with up to three years imprisonment or a fine in case of intention, or in accordance with § 161 (1) of the German Criminal Code with up to one year imprisonment or a fine in case of negligence.*

_____ _____
Ort / *Place*, Datum / *Date* Unterschrift / *Signature*

Summary

Mangroves are essential providers of environmental, economic, and ecological ecosystem services. Mangroves of Vanga occur in the most southerly coastal area of Kenya. They transcend the Kenya-Tanzania border and receive fresh water and particulate materials from the transboundary Umba River. Consequently, they provide a unique opportunity to study system dynamics borne of both anthropogenic and natural disturbances. Cognizant of the universal threat that mangroves face with respect to sea-level rise (SLR), the need to understand sediments dynamics within the Vanga estuary is vital for their conservation and management. This is because sedimentation has been identified as one of the factors that will allow mangroves to mitigate and modulate the effects of SLR. However, our knowledge and understanding of the sediment dynamics in the Vanga Estuary are limited. Consequently, it jeopardizes plans on mitigation and adaptive measures to be undertaken in the face of SLR and other resource management issues. We hypothesized that most of the Vanga Estuary sediments are sourced from the Umba River catchment, with minimal contribution from tidal and *in-situ* production. Therefore, the overall aim of this doctoral study is to investigate the influence of the transboundary Umba River on the connectivity of downstream coastal habitats and the terrestrial catchment. To achieve the objectives of this study, we evaluated 1) the geochemical and mineralogical composition of the Umba River sediments 2) analyzed and modeled elemental carbon (C), nitrogen (N), and their stable isotopes to determine the possible sources of sediment organic matter delivered to the Vanga estuary and 3) measured current sedimentation rates in the Vanga estuary to evaluate the possible response of Vanga mangroves to current and future rates of SLR.

First, the Umba River sediments showed similar source geology along the river's course from the source to its mouth in the Vanga Estuary. This is reflected by the similarity in the mineralogy and the chemical composition of sediments evident by the dominant mafic to felsic minerals discernible in both upstream and downstream

sediments. The Umba River sediments also exhibit a moderate to high Chemical Index of Alteration (CIA) attributed to the variation from the dry to cold climate upstream (near the source) and humid climate further downstream. Secondly, based on the combined evaluation of elemental carbon (C) and nitrogen (N), C/N ratio, carbon ($\delta^{13}C$), and nitrogen ($\delta^{15}N$) isotopes, together with the results of the applied Stable Isotope Mixing Model, a mixed source of sediment organic matter in the Vanga Estuary was observed. The mixing is attributed to the daily hydrodynamic flushing and bioturbation under the mangrove canopy. The model results also indicated that riverine organic matter was the dominant source with ~60% contribution to the total sediment organic matter. It validated our hypothesis on the influence of the Umba River on the Vanga Estuary. With sediment organic matter as a proxy, we conclude that the terrestrial catchment and Vanga Estuary are connected, with Umba River supplying both freshwater and sediments. Finally, having determined the connectivity of the Umba River catchment, downstream mangrove habitat in Vanga, and the consequent sediment input, we further evaluated the fate of the sediments in terms of deposition and mangrove surface elevation. Our data indicate that mangrove surface elevation is experiencing shallow subsidence of up to -15 mm/yr. At the same time, sediments also accreted by a rate of up to 9 mm/yr on the mangrove surface. This accretion rate exceeds the current rates of local SLR (3.8 mm/yr) and global SLR (3.1 mm/yr). The mangroves of Vanga would therefore be able to keep pace and persist under the current rates of SLR. However, accelerated SLR would marginally outpace the net mangrove surface elevation in Vanga. Our study implies that adaptive measures on mangrove conservation and management in Vanga need to capture the complex intra- and interhabitat sediment dynamics and interactions. This would include policy interventions through comprehensive and integrated cross-border resource management and governance.

Zusammenfassung

Mangroven sind wichtige Lieferanten ökologische und wirtschaftlicher Ökosystemleistungen. Die Mangroven von Vanga kommen im südlichsten Küstengebiet Kenias vor. Sie überschreiten die Grenze zwischen Kenia und Tansania und erhalten Süßwasser und Schwebstoffe aus dem grenzüberschreitenden Umba-Fluss. Hier bietet sich eine einzigartige Gelegenheit zur Untersuchung der Systemdynamik, die sowohl von anthropogenen als auch von natürlichen Störungen abhängt. Angesichts der allgemeinen Bedrohung, der Mangroven durch den Anstieg des Meeresspiegels (SLR) ausgesetzt sind, ist das Verständnis der Sedimentdynamik im Vanga-Ästuar für ihre Erhaltung und Bewirtschaftung unerlässlich. Als einer der Faktoren, die es den Mangroven ermöglichen, die Auswirkungen des SLR abzumildern und zu modulieren, wurde die sedimentation identifiziert, die es den Mangroven ermöglichen, die Auswirkungen des SLR abzumildern und zu modulieren. Unser Wissen und Verständnis der Sedimentdynamik im Vanga-Ästuar ist jedoch begrenzt. Folglich gefährdet dies die Pläne für Abmilderungs- und Anpassungsmaßnahmen, die angesichts des SLR und anderer Fragen des Ressourcenmanagements ergriffen werden müssen. Wir gehen davon aus, dass der größte Teil der Sedimente im Vanga-Mündungsgebiet aus dem Einzugsgebiet des Umba-Flusses stammt und nur ein minimaler Anteil aus der Gezeiten- und In-situ-Produktion stammt. Das übergeordnete Ziel dieser Dissertation ist daher die Untersuchung des Einflusses des grenzüberschreitenden Umba-Flusses auf die Konnektivität der flussabwärts gelegenen Küstenlebensräume und des terrestrischen Einzugsgebiets. Um die Ziele dieser Studie zu erreichen, untersuchten wir 1) die geochemische und mineralogische Zusammensetzung der Sedimente des Umba-Flusses, 2) analysierten und modellierten elementaren Kohlenstoff (C), Stickstoff (N) und ihre stabilen Isotope, um die möglichen Quellen organischen Materials in den Sedimenten zu bestimmen, die in das Vanga-Ästuar gelangen, und 3) ermittelten die

aktuellen Sedimentationsraten im Vanga-Ästuar, um die mögliche Reaktion der Vanga-Mangroven auf die aktuellen und zukünftigen SLR-Raten zu bewerten.

Erstens wiesen die Sedimente des Umba-Flusses entlang des Flusslaufs von der Quelle bis zur Mündung in die Vanga-Mündung eine ähnliche Ausgangsgeologie auf. Dies spiegelt sich in der Ähnlichkeit der Mineralogie und der chemischen Zusammensetzung der Sedimente wider, die sich in den vorherrschenden mafischen bis felsischen Mineralien sowohl in den flussaufwärts als auch flussabwärts gelegenen Sedimenten zeigt. Die Sedimente des Umba-Flusses weisen außerdem einen mäßigen bis hohen chemischen Alterationsindex (CIA) auf, der auf den Wechsel zwischen dem trockenen bis kalten Klima flussaufwärts (in der Nähe der Quelle) und dem feuchten Klima weiter flussabwärts zurückzuführen ist. Zweitens wurde auf der Grundlage der kombinierten Auswertung von elementarem Kohlenstoff (C) und Stickstoff (N), des C/N-Verhältnisses sowie der Isotope von Kohlenstoff ($\delta^{13}C$) und Stickstoff ($\delta^{15}N$) zusammen mit den Ergebnissen des angewandten Mischungsmodells für stabile Isotopen eine gemischte Quelle von organischem Sedimentmaterial im Vanga-Ästuar festgestellt. Die Vermischung wird auf die tägliche hydrodynamische Spülung und die Bioturbation unter den Mangrovenbaumkronen zurückgeführt. Die Modellergebnisse zeigten auch, dass die organische Substanz aus dem Fluss mit einem Anteil von etwa 60 % an der gesamten Organik im Sediment die dominierende Quelle war. Dies bestätigte unsere Hypothese über den Einfluss des Umba-Flusses auf das Vanga-Ästuar. Mit der organischen Substanz im Sediment als Proxy kommen wir zu dem Schluss, dass das terrestrische Einzugsgebiet und das Vanga-Ästuar miteinander verbunden sind, wobei der Umba-Fluss sowohl Süßwasser als auch Sedimente liefert. Nachdem wir die Verbindung zwischen dem Einzugsgebiet des Umba-Flusses, dem flussabwärts gelegenen Mangrovenhabitat in Vanga und dem daraus resultierenden Sedimenteintrag ermittelt hatten, haben wir den Verbleib der Sedimente in Bezug auf die Ablagerung und die Höhe der Mangrovenoberfläche untersucht. Unsere

Daten deuten darauf hin, dass sich die Höhe der Mangrovenoberfläche mit bis zu -15 mm pro Jahr verringert. Gleichzeitig lagern sich die Sedimente mit einer Geschwindigkeit von bis zu 9 mm pro Jahr auf der Sedimentoberfläche der Mangroven ab. Diese Akkumulationsrate übersteigt die derzeitigen Raten des lokalen SLR (3,8 mm pro Jahr) und des globalen SLR (3,1 mm pro Jahr). Die Mangroven von Vanga wären daher in der Lage, mit den derzeitigen Raten des SLR Schritt zu halten und zu überleben. Allerdings würde ein beschleunigter SLR die Nettoerhebung der Mangrovenoberfläche in Vanga geringfügig übersteigen. Unsere Studie legt jedoch nahe, dass Anpassungsmaßnahmen zum Schutz und zur Bewirtschaftung der Mangroven in Vanga die komplexen Sedimentdynamiken und Interaktionen innerhalb und zwischen den Lebensräumen berücksichtigen müssen. Dies würde auch politische Interventionen durch umfassendes und integriertes grenzüberschreitendes Management und die Steuerung der Ressourcen beinhalten.

Conference and Workshop Contributions

During this doctoral study, part of the work has been presented in the conferences and workshop outlined below:

Kimeli A, Okello J, Koedam N**,** Westphal H, Kairo J – The 11th Western Indian Ocean Marine Science Association (WIOMSA) Scientific Symposium, July 2019, Réduit, Mauritius - Sediment dynamics in a transboundary mangrove habitat: a perspective of sediment sources, current and historical sedimentation in Vanga, Kenya.

Mangroves provide goods and services of ecological, economic and environmental values. The total coverage of mangroves along the Kenyan coast has declined due to both natural and anthropogenic impacts. Losses of mangroves due to sea-level rise (SLR) are least studied in the Western Indian Ocean region. Although mangroves can keep pace with SLR through several ways, their stability will partially depend on the balance between the rates of sediment accumulation SLR. However, it has been reported that the change in surface elevation could be slower compared to long-term and interannual rates of SLR. The project's main objective is to assist in collecting biophysical data towards establishing a transboundary conservation area (TBCA) between Kenya and Tanzania. This study investigates the source of sediments, amounts of sediments delivered by Umba River, sediment accumulation rates within mangroves and model historical sediment accumulation rates. We expect that the sediments deposited in the transboundary Vanga mangrove ecosystem are derived from the adjacent catchment and that the accumulation rates within the mangroves are still higher than reported rates of sea level rise. Sediment samples were collected longitudinally along the river channel and in the mangrove forest. Geochemical and mineralogical proxies were used to characterize the source of the sediments.

Kimeli A, Okello J, Westphal H, Kairo J – International Conference for Young Marine Researchers (ICYMARE), September, 2019, Bremen, Germany - Sediment dynamics

in a transboundary mangrove habitat: a perspective of sediment sources, current and historical sedimentation in Vanga, Kenya.

Mangrove coverage has been declining and it has been attributed to diverse factors, including sea-level rise (SLR). Although mangroves can keep pace with SLR, their stability will partially depend on the balance between sediment accumulation rates and SLR. Therefore, field studies to determine localized current and historical sediment accumulation rates remains vital. This study was premised on a collaborative project between Kenya-Tanzania seeking ecological and biophysical data that could help in understanding the hypothesized connectivity between the dynamic environment, ecological habitats and resource use. This study investigates the source of sediments, sediment accumulation rates within the mangroves and their implication in mitigation of SLR. Sediment samples were collected along the river channel from source to mouth. A combination of sediment-elevation tables and marker horizons are used to measure current sediment accumulation rates while a combination of $\delta^{15}N$ and $\delta^{13}C$, elemental C/N ratios were used to partition sources of sediments delivered to Vanga mangroves. Additionally, petrographic and geochemical analyses were used to determine the source geology of the sediments delivered to the Vanga transboundary mangroves. From the preliminary results, the sediments deposited in the mangroves of Vanga indicate a terrestrial origin. However, the marine origin of sediments is also evident.

Kimeli A, Cherono S, Mutisya B, Tamooh F, Okello, J, Westphal H, Koedam N, Kairo J. Estuaries and coastal seas in the Anthropocene (ECSA58 & EMECS 13) - September 2021, Hull, United Kingdom - Tracing the Sources of Organic Matter in Mangrove Sediments and Its Implication to Sediment Provenance in Vanga Estuary, Kenya.

Sediment accumulation in mangroves is vital in the growth of mangrove surface elevation against sea-level rise. Sedimentation within mangrove forests combines

autochthonous (in-situ) and allochthonous (terrigenous) material input and deposition. We utilized C/N, TOC, and $\delta^{13}C$ to disentangle sources of organic matter in sediments as a proxy for sediment provenance. We evaluated sediment samples collected along the entire gradient of the transboundary Umba River from mouth to source in seven stations during the dry (February - March 2019) and wet season (May - June 2019). According to the sampling locations, we broadly categorized the sediment samples as either riverine, estuarine, or marine. A Bayesian Stable Isotope Mixing Model in R-program (SIMMR) was used to estimate the proportional contribution of different potential sources of organic matter in surficial sediments to the mangroves of Vanga in Kenya. The C/N and $\delta^{13}C$ were significantly variable ($p<0.05$) between the stations and the broad categories. However, they did not vary significantly between the seasons. $\delta^{13}C$ was relatively depleted in estuarine and riverine samples compared to agricultural soil and oceanic samples. C/N ratios were >10 in all stations during the dry and wet season, reflecting a pronounced terrestrial origin of organic matter. The model results showed that the sediment OM delivered in the Vanga estuary had varied sources with discernible mixing. Additionally, riverine-derived OM was proportionately the dominant source of sediment OM compared to other sources during both the dry (60%) and wet season (70%). It indicated the significant influence of the Umba River on the downstream mangrove habitat and the sediment dynamics. This study forms part of the baseline information needed to set up and demarcate a proposed joint transboundary conservation area (TBCA) between Kenya and Tanzania, including the Vanga mangrove patch.

Kimeli A, Ocholla O, Okello J, Koedam N, Westphal H, Kairo J. The 3rd Leibniz Centre for Tropical Marine Research (ZMT) Annual Conference, Bremen, Germany, January 2022 - Geochemistry and mineralogy of sediments along the transboundary Umba River as indicators of provenance and weathering.

The transboundary Umba River traverses two countries, with its source in the Usambara Mountains in Tanzania and draining its water to the Indian Ocean in Vanga,

Kenya. Umba River delivers freshwater, nutrients and terrigenous sediments to the mangroves of Vanga and the Indian Ocean passing. Knowledge of the connectivity and influence of the larger Umba River catchment on the downstream coastal biotopes is therefore vital. From this basis, Kenya and Tanzania have jointly proposed to set up a transboundary conservation area (pTBCA) stretching ~120 km along the coastline from Diani, Kenya to Tanga, Tanzania. The pTBCA is based on rich contiguous biodiversity and the need for catchment-wide resource conservation and management. The source characteristics, degree of weathering, provenance and fate of the Umba River sediments were evaluated using geochemical and mineralogical proxies. Based on the chemical index of alteration, the Umba River sediments indicate moderate to high weathering. They are also rich in mafic and felsic minerals, characteristic of the source geology and the lithologies it drains. Additionally, the similarity of minerals in the Umba River sediments collected both in the upper catchment (close to the source) and downstream (in the estuary and coastal area) indicate a similar source. They also indicate the effects of transportation in their grain sizes, sorting and shapes.

List of Figures

List of Tables

Acknowledgements

This thesis is a culmination of support from various people and organizations providing financial, guidance, critical reviews, and moral support. First, many thanks to project partners Prof. Nico Koedam (Vrije Universiteit Brussels), Dr. James Kairo and Dr. Judith Okello (Kenya Marine and Fisheries Research Institute) for their support in field sampling, their contributions and critical reviews which significantly improved the manuscripts as well. Secondly, I want to thank Hildegard Westphal for accepting to supervise my study. Her comments, guidance and our constructive discussion on the manuscripts and the thesis are highly appreciated. She has been supportive, understanding, and accommodating as a supervisor and I will be forever indebted to her. I am equally and deeply indebted to the Leibniz Centre for Tropical Marine Research (ZMT), who hosted my doctoral study and provided the necessary infrastructure, support, and facilities to undertake the study. Specific mentions to the chemistry and geology laboratories personnel: Donata Monien, Dorothee Dasbach, Jule Mawick, and Sebastian Flotow for their eagerness to assist and guide. Many thanks to my fellow doctoral candidate Florian Hierl for being a friend and a brother away from home. The discussions of our projects, and the encouragement, especially at the height of COVID-19 pandemic, made the journey worthwhile. I also extend my regards to all of the Geoecology and Carbonate Sedimentology workgroup members for their encouragement, feedback, and wise counsel. I also owe a great deal of gratitude to my thesis committee members Martin Zimmer, Tim Jennerjahn, and Tim Rixen, for their valuable comments and guidance. Many thanks also to Matthias Hinderer for accepting to review this thesis albeit on a short notice. Last but not least, my deep and sincere gratitude to my family for their unparalleled and continued love, help, support and prayers. Many thanks to my wife Christine and my sons Jeremy and Joe, for the invaluable encouragement and I dedicate this milestone to you. To my parents, you are my sages, and it all started with and was nurtured by you. To my siblings, it has been a long way coming, but who would have thought!

Chapter 1 : General Introduction

1.1 Sediment elevation changes in estuarine mangrove ecosystems

Mangroves are halophytic coastal plants that occupy a dynamic region between the high and low watermarks in tropical and sub-tropical regions (Alongi, 2002; Donato et al., 2011). They occupy the interface between the terrestrial and the marine environments with freshwater inputs from rivers and saline water from tidal inputs (Yong et al., 2011; Sasmito et al., 2016). They are affected by short-term (sedimentation, decomposition, auto-compaction), long-term (sedimentation, compaction, eustatic sea-level changes, e.g., sea-level rise/drop), localized, regional, and more sudden changes (isostatic land level changes, e.g., subsidence) (Mcivor et al., 2013; Friess and McKee, 2021). All the above processes contribute and influence the net surface elevation of mangroves with respect to sea-level changes (McKee, 2011; Webb et al., 2013). Surface elevation changes in mangroves refer to the variations in the height of the sediment surface layer over a specific period (Cahoon and Lynch, 1997; Krauss et al., 2010; Day et al., 2011; Webb et al., 2013; Crosby et al., 2016; Schuerch et al., 2018). They result from both surface and sub-surface processes (McKee, 2011), acting on a local or regional scale (Nolte et al., 2013; Webb et al., 2013; Krauss et al., 2014; Ward et al., 2016). Therefore, the vertical elevation change of a mangrove surface is the total of surface, shallow and deep sub-surface processes (Webb et al., 2013) summarized by the equation below and Figure 1-1 below;

$$\mathbf{A = B\ (X_1, X_2, \ldots, X_n) + C\ (Y_1, Y_2, \ldots, Y_N) + D\ (Z_1, Z_2, \ldots, Z_n)}$$

where A is the total surface elevation change, B are the surface processes influenced by microprocesses (X_1, X_2, ..., X_n) including sedimentation (trapping, binding and retention, erosion and resuspension). C are the shallow subsurface processes

controlled by microprocesses (Y_1, Y_2, …, Y_n) including decomposition, compaction while D are the long-term processes controlled by microprocesses (Z_1, Z_2, …, Z_n) including deep subsidence due to regional geologic and seismic movements and long-term isostatic adjustments (McKee, 2011; Webb et al., 2013).

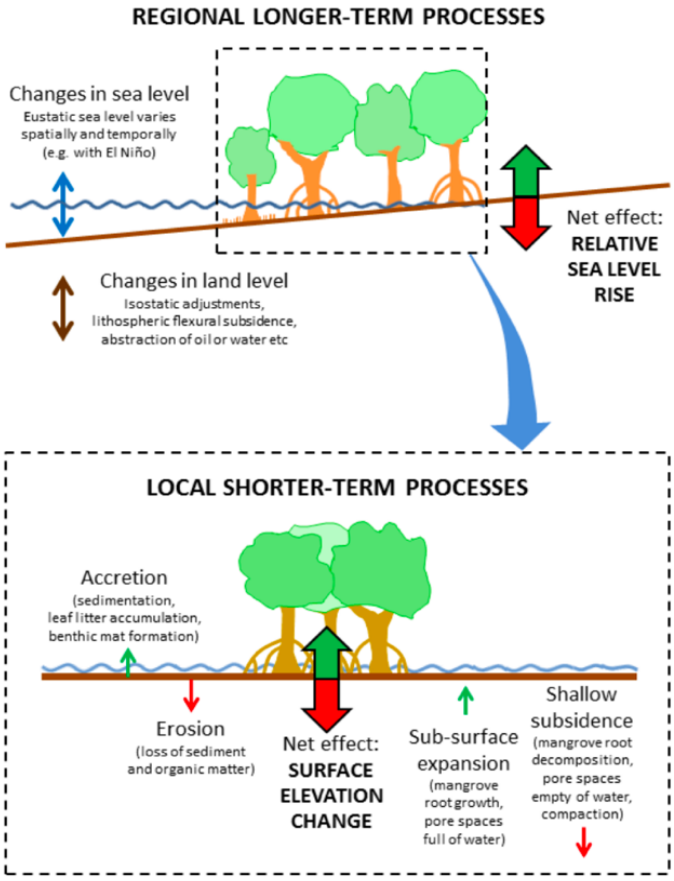

Figure 1-1: Regional and local macro- and microprocesses that control coastal wetland (marsh and mangroves) surface elevation changes relative to local datum of mean sea-level (MSL). Source: Mcivor et al., 2013.

Surface processes occur at or above the mangrove surface. They vary geographically and locally due to variations in availability and supply of sediments, hydrodynamic regimes, vegetation cover and density, exposure to strong waves, and anthropogenic impacts (McKee, 2011; Webb et al., 2013; Ward et al., 2016; Duvall et al., 2019). Shallow sub-surface processes occur below the mangrove surface but above the consolidated basement (Soares, 2009; McKee, 2011; Mcivor et al., 2013;

Ward et al., 2016). They include growth and decomposition of roots, shallow subsidence due to compaction, the weight of overlying material, loss of water and soil moisture content, and rebound due to weight changes (Cahoon and Turner, 1989; Cahoon and Lynch, 1997; Lang'at et al., 2014; Krauss et al., 2014).

Land subsidence is both a localized and a regional process that accounts for current sea-level fluctuations (Mimura and Horikawa, 2013; Brown and Nicholls, 2015). Land subsidence is the lowering or sinking of the land surface (Eggleston and Pope, 2013). It is caused by well-known and quantifiable processes, including groundwater abstraction, the weight of accumulated material, and rebound due to glacio-isostatic adjustments (Syvitski et al., 2009; Eggleston and Pope, 2013; Esteban et al., 2020). Therefore, large deltas trapping and storing huge amounts of sediments become susceptible to subsidence due to the weight of accumulated material (Meckel et al., 2007; Syvitski, 2008; Syvitski et al., 2009). Coupled with other human activities, including groundwater abstraction, rates of local subsidence are accelerated (Syvitski et al., 2009). However, some processes that can potentially cause land subsidence are not yet well studied and quantified, for example, bedrock dissolution and the effect of volcanic activities (Eggleston and Pope, 2013). Several deltas around the world have experienced or currently experience land subsidence. For example, the Ganges Delta in India has been reported to show local subsidence up to 20 mm/yr (Alam, 1996; Brown and Nicholls, 2015), the Nile delta up to 10 mm/yr (Saleh and Becker, 2018) and Mississippi delta up to 10 mm/yr (Törnqvist et al., 2008). In more extreme cases, up to 1 m of land subsidence can occur, as it was identified in New Orleans, the USA after Hurricane Katrina (Brown and Nicholls, 2015). Notably, these rates correspond to some of the largest deltas in the world, but subsidence information in smaller deltas/estuaries is currently limited. However, in areas experiencing both SLR and land subsidence, mangrove habitats face a double threat and would struggle to outpace, keep pace or even survive. Therefore, it is vital that

information on local subsidence is also considered in mitigating the effects of SLR on mangrove habitats.

1.2 Implications of elevation changes and mitigation of sea-level rise

The global mean sea level (MSL) is currently rising (Dangendorf et al., 2019), and it is predicted to accelerate in the coming decades as a result of global warming (Crosby et al., 2016; Saintilan et al., 2020). Historically, MSL has fluctuated over the geological timescale coinciding with glacial and interglacial periods (Cutler, 2003; Siddall et al., 2003; Alongi, 2008). The current rise in MSL has also been largely attributed to climate change effects (e.g., global warming) (Church and White, 2011). The effects of SLR on coastal wetlands and their futures have therefore generated immense concerns and interest (Alongi, 2015, 2008). The accelerated SLR can inundate and submerge low-lying coastal habitats and convert tidal marshes and mangroves habitats into open waters (Alongi, 2015; Lovelock et al., 2015; Temmerman and Kirwan, 2015; Darby et al., 2020). However, mangroves could survive the SLR by promoting sediment deposition and accretion (Krauss et al., 2014; Lovelock et al., 2015), thereby indirectly modulating and mitigating the effect of SLR (Crosby et al., 2016; Friess et al., 2019). The extensive and complex root structures of mangroves dampen the water flow velocities (Ellison and Stoddart, 1991; Furukawa and Wolanski, 1996; Soares, 2009; Sugden, 2020; Le Minor et al., 2021; Xia et al., 2021). This creates conducive environment that promotes the trapping of sediments, deposition, retention, and consequently accretion within the mangrove areas (Furukawa and Wolanski, 1996; Alongi, 2008). Their below-ground root growth also promotes the accumulation of peat, which accounts for surface elevation growth (Crosby et al., 2016). Adequate sediment accretion exceeding the rates of SLR would assist mangroves in maintaining their surface elevations within an appropriate tidal range (Webb et al., 2013; Krauss et al., 2014). Consequently, the sediment deposition on equilibrium with other inter- and intra-feedback mechanisms (erosion, subsidence, isostatic SL changes, decomposition, resuspension) would necessitate

accretion (Mcivor et al., 2013; Temmerman and Kirwan, 2015; Duvall et al., 2019; Howard et al., 2020). Accretion or accumulation of sediments substrate beneath mangrove enables mangrove surface elevation growth relative to mean sea-level (Webb et al., 2013). Mangroves and salt-marshes can also respond to SLR by retreating or regressing landward and replacing coastal terrestrial forests (Kirwan and Megonigal, 2013; Di Nitto et al., 2014; Temmerman and Kirwan, 2015; Schuerch et al., 2018; Woodroffe, 2018). They migrate towards higher grounds with ideal inundation regimes and salinity levels (Di Nitto et al., 2014). The migration is highly dependent on the availability of space that can accommodate the migration (Di Nitto et al., 2014; Fagherazzi et al., 2019; Rogers, 2021; Xia et al., 2021). These mechanisms would allow mangroves to colonize new and higher elevations and stay above rising sea levels (Di Nitto et al., 2014; Sasmito et al., 2016; Woodroffe, 2018). Additionally, mangroves have been shown to have historically persisted during periods of rapid post-glacial SLR (Crowley and Gagan, 1995; Hanebuth et al., 2000; Wooller et al., 2016; Saintilan et al., 2020). Mangroves first appeared in the fossil record during the late Cretaceous-Paleocene epoch (75 Mya) as descendants of the monotypic mangrove palm *Nypa* (Gee, 2001; Plaziat et al., 2001; Friess et al., 2019). The common mangrove genus *Rhizophora, Avicennia,* and *Lumnitzera* genetically diverged around 55, 42 and 23 Ma, respectively (Ricklefs et al., 2015) during the Paleocene-Eocene Thermal Maxima to late Oligocene (Xu et al., 2017; Zhang, 2017). After submergence during this warm period, mangroves became adapted to intertidal areas (Friess et al., 2019). Therefore, the mechanisms for mangroves to outpace, keep up or catch up with SLR (see Figure 1-2), as espoused by Woodroffe (2018), would support the historical and future response and persistence of mangroves to predicted and accelerated SLR. However, the responses would vary spatially from place to place depending on prevailing oceanographic conditions, geomorphology, hydrologic and ecologic settings (Webb et al., 2013; Fagherazzi et al., 2019; Friess and McKee, 2021). Therefore, this would require that local driving

factors be studied to evaluate the localized context of possible mangrove response and adaption to SLR.

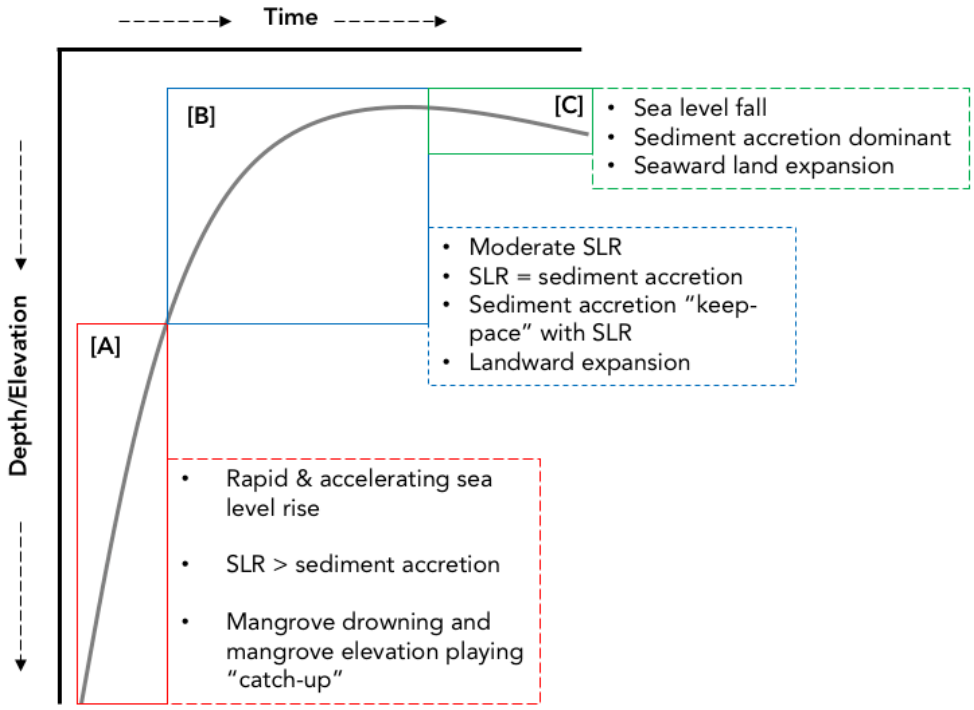

Figure 1-2: Showing the relationship between different rates of SLR and the expected response of mangrove surface elevation. A hypothetical sea-level curve (grey) is shown with the different responses with respect to elevation (inundation depths) and sediment accretion. [A] depict rapid and accelerating sea-level rise, [B] moderate to decelerating SLR and [C] gradual sea-level fall. Modified from Woodroffe (2018).

1.3 Geochemical and mineralogic characteristics of fluvial sediments

Both small and large rivers deliver large quantities of sediments to the global oceans. Close to a decade ago, the global fluvial sediment discharge stood at 19 billion metric tons annually (Milliman and Farnsworth, 2013; Milliman et al., 2016). These fluvial sediments provide an environmental archive of continental conditions. They provide avenues for reconstructing and identifying the weathering conditions, geographic, climatic and tectonic origin of fluvial sediments (McLennan et al., 1983; McLennan, 1993; Ali et al., 2014; Clift, 2016; Hu et al., 2016). From the context of understanding the dynamics and processes within the continuum of source to sink,

natural and human perturbation can be identified, quantified and predicted (Prizomwala et al., 2014). Consequently, the chemical and mineralogic composition of clastic and fluvial sediments has been investigated (McLennan et al., 1983; Singh et al., 2005). However, the interpretation of these archives and proxies to disentangle sediment provenance can be complicated. Mainly because of various factors, including catchment size, variability in sources and climate, sedimentary sorting, distance from source to mouth and anthropogenic impacts (Liu et al., 2008; Milliman and Farnsworth, 2013; Walling, 2013). For example, due to the steady population growth, anthropogenic impacts have consequently compounded the characterization of fluvial sediment provenance (Clift, 2016). The need for more land for settlement, expansion of agriculture and infrastructural development (e.g., dam construction along rivers) have impacted the composition of recent and modern fluvial sediments. Clift (2016) notes that there is currently more weathered material in fluvial sediments than historically, attributable to anthropogenic influences. Additionally, increased temperatures and precipitation due to climate change would hasten alteration processes like weathering. Consequently, this would alter the bulk chemistry and mineralogy of sediments making their use as proxies for sediment provenance more cumbersome (Clift, 2016; Hu et al., 2016).

1.3.1 Sediment provenance proxies

Several proxies and methods have been utilized to determine the post-weathering evolution and constrain fluvial sediments' provenance (McLennan et al., 1993; Nesbitt et al., 1996; McLennan, 2001). The different proxies are broadly categorized based on sediments' chemical, mineralogical and isotopic composition (Vermeesch, 2019). These broad categories define distinct data types; compositional data, point-counting data and distributional data (Vermeesch, 2019). Studies on the reconstruction and characterization of sediment sources have used the distribution of major and trace elements as a proxy (Hemming et al., 2015; Sajid et al., 2020). This is mainly due to the distinct behavior of these elements during weathering,

erosion, transport and post-deposition diagenesis (Dinis et al., 2020). These behaviors include mobility, dilution susceptibility, distribution in various grain sizes, and chemical alteration (McLennan, 1993). Major and trace element distribution and characteristics are preserved in transported sediment and therefore provide tracers for their origin and alteration processes (Sarkar et al., 2004; Sensarma et al., 2008). Various geological aspects have utilized different combinations of elements and elemental ratios as proxies. For example, studies on tracking of mantle evolution, ocean basalts, Neoproterozoic magmatism and age-dating terrestrial materials, have used the Strontium (Sr) and Neodymium (Nd) stable isotopes (White and Hofmann, 1982; Juteau et al., 1986; Maboko and Nakamura, 2002; Manya et al., 2007; Clift, 2016). Sr isotopes (Sr^{87}/Sr^{86}) have also been utilized to track the influence of anthropogenic Sr contamination (Zieliński et al., 2021). However, it is not a very reliable proxy because it is influenced by grain size and sedimentary sorting (Hu et al., 2016). Uranium-Lead (U-Pb) and Argon (Ar) ratio Ar/Ar ratio have been utilized in zircon and detrital muscovite geochronology, respectively (Bowring et al., 1998; Spencer et al., 2016) to constrain the provenance of Cenozoic sediments (Sun et al., 2018; Hollingworth et al., 2021). Potassium (K) to Aluminium (Al) (K/Al) ratios have been used to track precipitation variation. In contrast, K to Rubidium (Rb) (K/Rb) ratios have been used to evaluate weathering changes over a short time scale (Hu et al., 2016). Calcium (Ca) and Iron (Fe) to Ca (Fe/Ca) ratios, have also been used for provenance studies however, they are not ideal for terrestrial sediment reconstruction because they are too sensitive to dilution effects (Govin et al., 2012). Barium (Ba) and K concentrations have been associated with the weathering of K-feldspar ± biotite-rich minerals, while enrichment of ferromagnesian elements (e.g., Fe, Cr, Ni) or their ratios (e.g., Cr/Ni, Ni/Zr, Cr/Zr) have been utilized to constrain mafic to ultramafic igneous provenance and weathering intensities (Garver et al., 1996; Sarkar et al., 2004; Sensarma et al., 2008; Phillips et al., 2017). On the other hand, immobile major (e.g., Al_2O_3, Fe_2O_3, TiO_2), trace elements (e.g., Cr and Ni) and

rare earth elements (REEs) predominantly carried in the particulate load of rivers are useful indicators of the source of sediments/sedimentary rocks (Taylor and McLennan, 1985; Sarkar et al., 2004; Sensarma et al., 2008). Therefore, their relevance in studying the provenance of fluvial sediments is based on the hypothesis that they undergo less alteration during the sedimentary processes (Sensarma et al., 2008). Therefore, are ideal in revealing the nature and degree of weathering at the source region of sediments - controlled by climatic, geological factors and fluvial transport (McLennan, 1993). High concentrations of these elements coupled with a high chemical index of alteration (CIA) – a measure of degree of weathering in sediments, would suggest a high degree of alteration. But on the contrary, a high concentration of CaO, K_2O and Ba indicate supply of more quartzo-feldspathic material (Sensarma et al., 2008). Additionally, low K_2O contents are thought to result from diminished or lack of micas, which act as concentrators of K_2O (Silva et al., 2016). Another way of evaluating sediment provenance, is the use of element compositional proxies for example, the Al_2O_3 – (CaO + Na_2O) – K_2O (A-CN-K) and Al_2O_3 – (CaO + Na_2O +K_2O) – (Fe_2O_3 + MgO) (A-CNK-FM) ternary plots. They provide to evaluate the post-depositional clay components and weathering characteristics of sediments can be determined (Singh, 2009; Perri et al., 2011; Govin et al., 2012; Nyobe et al., 2018). Concentrations of major and trace elements can also be compared to known references, including the Upper Continental Crust (UCC) and Post Archean Australian Shale (PAAS) for a better understanding of their distribution and provenance (Sensarma et al., 2008; Ali et al., 2014; Baiyegunhi et al., 2017). The UCC is the top most part of the 35 km thick continental crust and, therefore, the most accessible. Its outcrops are widespread and provide continental crust's best constrained major and trace element composition (McLennan, 2001). From the above characteristics, decades-long measurements of the major and trace element composition of UCC have been taken and reliable estimates have been presented (Taylor and McLennan, 1985; Rudnick and Gao, 2003; Hacker et al., 2015; Hawkesworth et al., 2017).

Paleoclimate studies have used clay mineralogy as a proxies since the mid-20th century. Clay mineral assemblages reflect the climate of source areas and weathering of source rocks (Mackenzie and Mitchell, 1966; Power, 1969; Raigemborn et al., 2009; Dinis et al., 2020). Generally, high presence of clay minerals indicates intense weathering (Sensarma et al., 2008; Garzanti et al., 2014). For example, kaolinite reflects intense chemical weathering in wet and humid climates, while smectite reflects the sources area's warm and dry climate characterized by intense evaporation (Sarkar et al., 2004; Wu et al., 2011; Phillips et al., 2017). Additionally, climatically-driven weathering greatly influences clay composition, while source provenance, hydrodynamic and grain size sorting influence coarse mud sediments (Dinis et al., 2020). The correlation of K/Al and kaolinite and/or illite has shown that clay ratios can be used effectively in evaluating the intensity of weathering (Hu et al., 2016). Olivine, amphibole and pyroxene minerals preferentially host Fe and Mg (Dinis et al., 2020).

Evaluation of mineralogical and sediment maturity, chemical alteration and element mobility have used several chemical indices (Nesbitt and Young, 1982; McLennan et al., 1993; Gupta and Rao, 2001; Ceryan, 2018). The commonly used Chemical Index of Alteration (CIA) defined as $[Al_2O_3/(Al_2O_3 + CaO^* + K_2O + Na_2O)] \times 100$, where CaO* is CaO in silicate fraction only have been used to evaluate the degree of feldspar alteration (Mishra and Sen, 2012; Shao and Yang, 2012; Garzanti et al., 2014). The index of Compositional Variability (ICV) defined as $[CaO + K_2O + Na_2O + Fe_2O_3$ (t)+ MgO + MnO + $TiO_2/Al_2O_3]$, further incorporates Fe and Mg which caters for ultrabasic rocks, where Fe_2O_3 (*t*) represent the total Fe oxides while CaO includes all Ca sources (Cox et al., 1995; Hossain et al., 2017; Phillips et al., 2017). Several studies have utilized the ICV to indicate the sediment maturity and discrimination of parent rock types (Nesbitt and Young, 1984; Hu et al., 2016; Phillips et al., 2017). Provenance studies have used the plagioclase index of alteration (PIA) defined as

$[(Al_2O_3 – K_2O)/(Al_2O_3 + CaO^* + Na_2O – K_2O)] \times 100$ to identify plagioclase-rich silicate rocks (Phillips et al., 2017).

1.3.2 Influence of hydrodynamics and sedimentary sorting

In sediment provenance studies, chemical composition and mineralogy are evaluated by considering the transition from upstream/catchment sources to downstream depositional habitats (Kroonenberg, 1992; Vermeesch, 2019). From this continuum, weathering, transport, sediment sorting, deposition and post-depositional diagenesis come into play (Kroonenberg, 1992). For example, due to hydraulic sorting during fluvial transportation, the sediment grain size distribution can influence the geochemical and mineralogic properties of fluvial sediments (Wu et al., 2011; Govin et al., 2012; Ali et al., 2014; Hahn et al., 2018; Dinis et al., 2020). Consequently, varying the affinity of some elements to specific grain sizes, compositional variability is inevitable (Wu et al., 2011; Ali et al., 2014; Garzanti et al., 2018). For example, K and Al are enriched in clay fractions and in silicate minerals e.g., kaolinite, whereas silica (Si) is majorly associated with quartz and feldspars (Ali et al., 2014). Therefore, it is from the above that Al/Si and Fe/K ratios have been utilized as indicators of weathering and to track terrigenous input to continental margins (Govin et al., 2012). Additionally, the association of major and trace elements with clay and fine sediments, compared to the abundance of quartz and heavy minerals in sandy fractions, provides means to evaluate the effect of grain size sorting in fluvial sediments (Wu et al., 2011; Ali et al., 2014).

1.4 Estuarine sediment organic matter sources

Knowledge of the source of sediment organic matter (SOM) in estuaries and other marine depositional environments is vital. It allows for a better understanding of the biogeochemical cycles and sediment provenance (Gonneea et al., 2004; Krauss et al., 2014; Marwick et al., 2015; Blattmann et al., 2018; Friess et al., 2019). This understanding can inform better management practices as they provide indications

of key producers and sources of SOM in marine depositional environments (Geraldi et al., 2019). Sediment and OM source characterization is therefore imperative in transitional environments like in estuarine mangroves, characterized by a multiplicity of OM sources (Bouillon et al., 2000). Also, sources of OM provide information on the degree of inter- and intra-connectivity of marine and terrestrial ecosystems, subsequently supporting better habitat-specific, catchment-wide and eco-region management (Duarte and Cebrián, 1996; Dittmar et al., 2001; Bouillon et al., 2004; Tamooh et al., 2012; Canuel and Hardison, 2016). Understanding the sources of SOM, especially in mangrove ecosystems, allows for the determination of the fate of both autochthonous and allochthonous OM sources, detecting shift on ecosystem function and more, recently, the potential influence of Blue Carbon sequestration as a mitigating measure for CO_2 emission and global warming (Donato et al., 2011; Wylie et al., 2016). Additionally, investigations on carbon budgets and sequestration have and continue to underpin conservation and management interventions pertaining CO_2 levels and climate (Ouyang et al., 2017; Webb et al., 2018; Geraldi et al., 2019). Furthermore, knowledge of sources of SOM and by inference the sediment provenance, the fate of sediments assists in determining and monitoring mangrove surface elevation changes and the subsequent potential in modulating and mitigating the effects of SLR (Webb et al., 2013; Sasmito et al., 2016). OM delivered to estuaries originate from diverse sources, including from adjacent hinterlands/catchments (Jennerjahn et al., 2004; Marwick et al., 2014; Canuel and Hardison, 2016; Hapsari et al., 2019). They are delivered via river inputs, aeolian sources, from adjacent marine habitats (e.g., seagrass beds), point-discharge (e.g., sewage effluent) and *in-situ* sources through primary production (decomposition of mangroves leaves and litter) (Woodroffe, 1985; Neubauer, 2008; Prasad et al., 2017; Kusumaningtyas et al., 2019; Rahayu et al., 2019). The variation and distribution of bulk composition of sediments, including elemental carbon (C) and nitrogen (N) and their C/N ratios, coupled with C ($\delta^{13}C$) and N ($\delta^{15}N$) stable isotope, have been widely

used to disentangle and quantify sources of OM (Bouillon et al., 2003, 2008; Kennedy et al., 2004; Greiner et al., 2016; Nasir et al., 2016; Sasmito et al., 2020). They have been used as tracers/proxies in distinguishing between autochthonous (*in-situ* produced) and allochthonous OM (terrigenous, marine) sources of OM. They have also been utilized to differentiate within particular sources e.g., marine sources with distinct signatures such as seagrasses, macroalgae and epiphytes (Kennedy et al., 2010), as well as between C3 and C4 vegetation (Smith and Epstein, 1971). They have also been utilized in determining the influence of anthropogenic-driven changes in the coastal habitats (Dehairs et al., 2000; Pastene et al., 2019; Zhang et al., 2019). According to Bouillon et al. (2008), the utilization of OM concentrations and natural abundances of stable isotope ratios for source studies, especially in mangrove ecosystems, is based on the assumptions that:

i) different primary producers may have different stable isotope signatures; and

ii) the degradation process of the signatures in (i) above is maintained or altered predictably.

In this regard, therefore, source characterization of OM using C and N concentrations and their isotopic variations depends on accurate knowledge of potential sources/end-members, variation of concentration, and signature in both inter- and intra-source values (Andrews et al., 1998; Perdue and Koprivnjak, 2007; Bouillon et al., 2008; Xing et al., 2014; Sasmito et al., 2020). Due to sustained research and case studies now covering different regions and habitats, variation of concentration and signature of different material such as sediments types, plant tissue and water, average values for several potential end-members (see Figure 1-3) have been compiled (Lamb et al., 2006; Bouillon et al., 2008; Xiao and Liu, 2010).

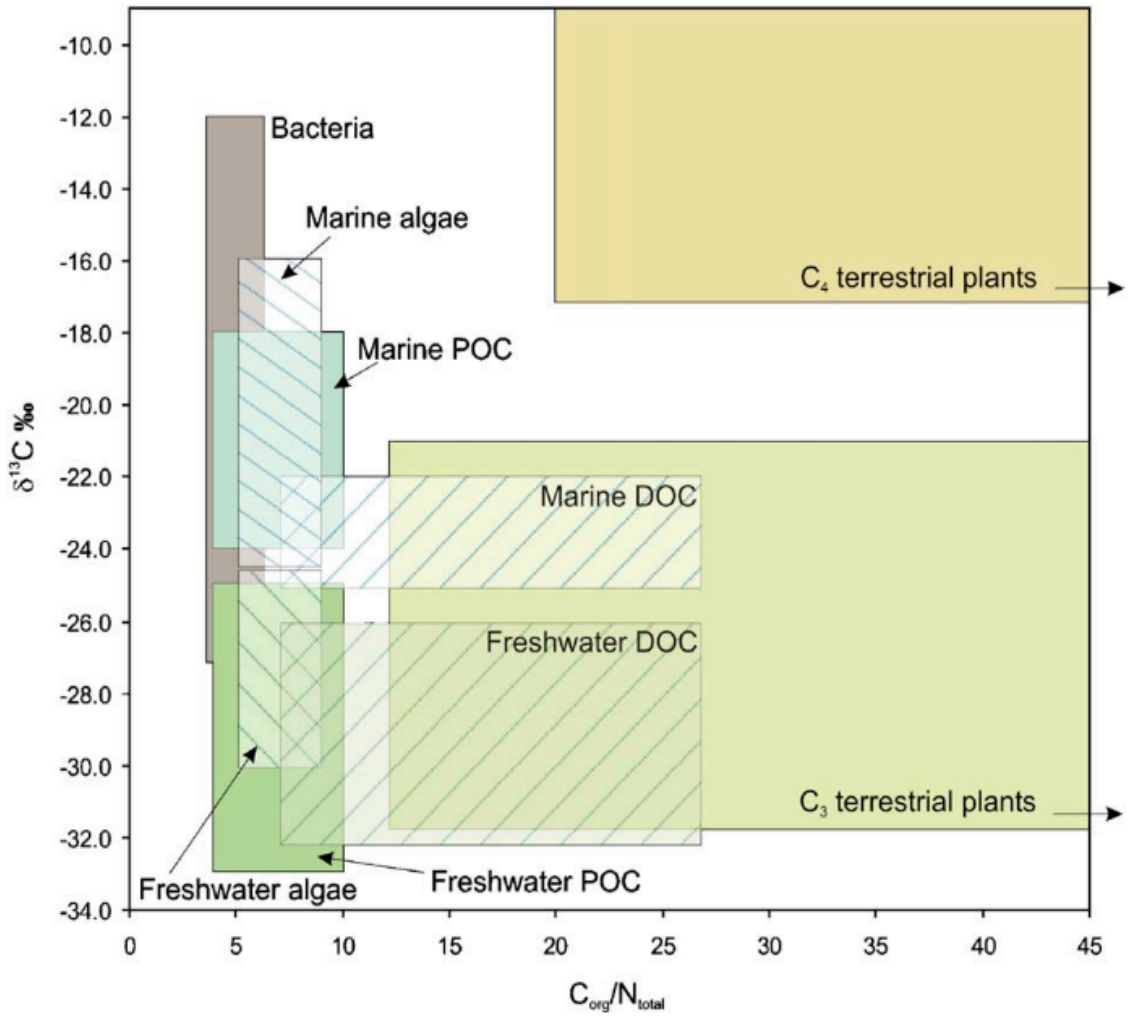

Figure 1-3: Typical $\delta^{13}C$ and C/N ranges for organic inputs to coastal environments from different sources (Source: Unmodified from Lamb et al., 2006).

1.5 Study area

The Umba River is a transboundary river transcending two East African countries (Kiteresi et al., 2012; Tesfamariam et al., 2018). The source of the Umba River is in the tectonically uplifted Usambara Mountains in Mkinga, Tanzania. It flows approximately 200 km southwards and transcends through the low-lying plains and drains its water to the Indian Ocean through its mouth in Vanga, Kenya (Figure 1-4). The Umba River drains a catchment area approximately 8000 km^2 (IUCN, 2003) with the majority (~5000 km^2) of it lying on the Tanzania side (Tesfamariam et al., 2021). The Umba River basin is composed of several ecosystems ranging from mountains

(the source), shrubland, riparian areas, wetlands, terrestrial forests, coastal forest, estuarine habitats, agricultural land, natural reserve and human developments including settlements (Figure 1-5).

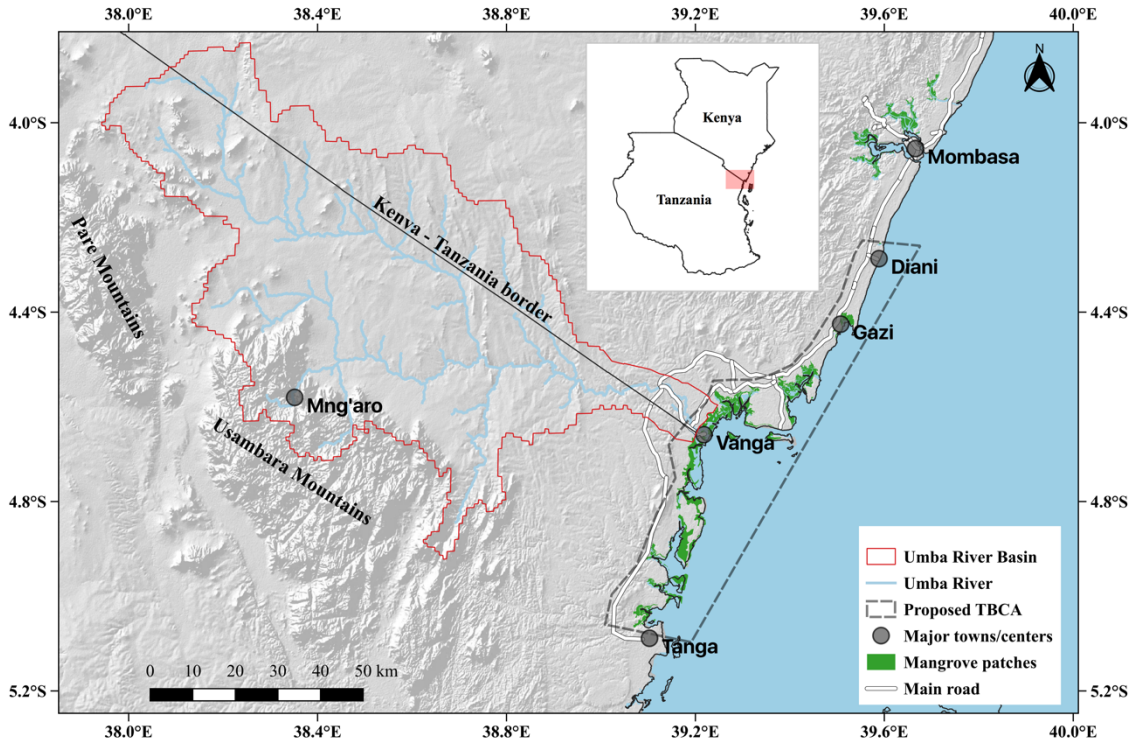

Figure 1-4: Study area showing the Umba River basin, the Umba River from source (Usambara mountains) to mouth, the proposed transboundary conservation area (pTBCA) and the coastal mangrove patches transcending the Kenya-Tanzania (Vanga) border.

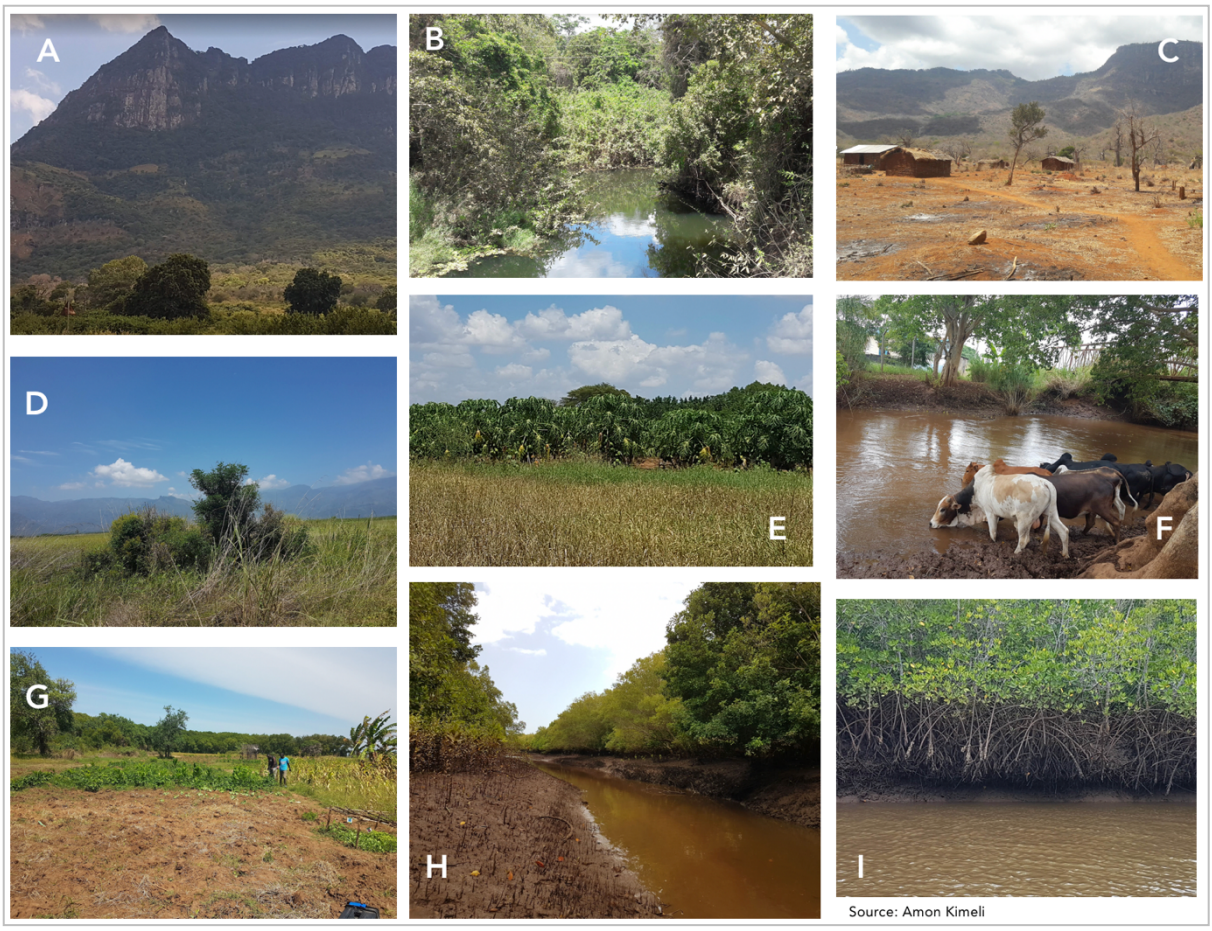

Figure 1-5: Photographs taken in different section of the Umba River indicating different ecosystems and land use within the Umba Basin with A) Usambara mountains (source of Umba River), B) forested initial stages of Umba River, C) settlement in the semi-arid middle section of the Umba River, D) grassland/wetland close to source of Umba River, E) Mango/Pawpaw farm on the banks of River Umba, F) animals watering on the Umba River further downstream, G) maize and banana farms adjacent to Umba River, H) Umba River mouth in Vanga and I) Estuarine mangroves of Vanga, Kenya.

1.5.1.1 Mangroves of Vanga

Most of the mangrove species occurring in the Western Indian Ocean (WIO) region are present in Vanga (Mungai et al., 2019). The common occurring species are *Rhizophora mucronata* (Rm), *Avicennia marina* (Am), *Ceriops tagal* (Ct) *Sonneratia alba* (Sa), *Xylocarpus granatum* (Xm), and *Bruguiera gymnorrhiza* (Bg). They occur mainly as mixed stands along and across the intertidal area. The mangroves of Vanga cover an area of ~3,000 ha, however, degradation and loss of up to 27 ha/yr due to

excessive human exploitation has been reported (Mungai et al., 2019). The over 6,000 inhabitants of Vanga (Fortnam et al., 2020), derive immense benefits from mangroves. They utilize them as energy sources (firewood) and source of building material for local use and as a revenue earner. Fishing, which is the village's main livelihood, depends on the mangroves as they act as fish nurseries which is important for local fish stocks (Igulu et al., 2014). These specific uses add to the other co-benefits of mangroves including acting as wave breakers (Dahdouh-Guebas et al., 2005), and important sediment, and carbon sinks in climate change mitigation (Lang'at et al., 2014; Rahayu et al., 2019; Rahman et al., 2021).

1.5.1.2 General geology of study area

The Usambara-Pare Mountains region in NE Tanzania is characterized by extensive and exposed amphibolite and granulite facies of the Upper Proterozoic Mozambique Belt (Shackleton, 1993; Maboko and Nakamura, 2002) (Figure 1-6). The geology of this area has also been demonstrated based on isotopic and geochemical data, showing that its is dominated ortho-gneisses of andesitic and dacitic origin (Maboko and Nakamura, 2002). They represent ~815 Ma old mantle-derived andesitic to dacitic magmatism of a Precambrian uplifted orogeny which was subsequently metamorphosed into the granulite facies at ~625–640 Ma (Fritz et al., 2013). Immediately eastwards of Usambara mountains and further downstream of the Umba River, Mozambiquian tilted Karoo Supergroup rocks are exposed (Figure 1-6). The Mozambique Belt is majorly characterized by distinct meta-sedimentary and meta-igneous geological formations (Akech et al., 2013). These formations varying between granitic-gneisses, meta-limestones, gneissic-schists, calc-silicates, sandstones and younger East African Rift basaltic extrusive igneous rocks (Schlüter, 1997; Maboko and Nakamura, 2002; Manya et al., 2007). The dominant rock formations include pyroxene-garnet-granulites interlaced with hornblende gneisses. The rocks are also highly weathered and degraded forming reddish-brown soils close to the source in Usambara (Schlüter, 1997). However, further downstream due to

extensive agriculture and transition to sedimentary rock lithologies the soils exhibit a dark-brown coloration.

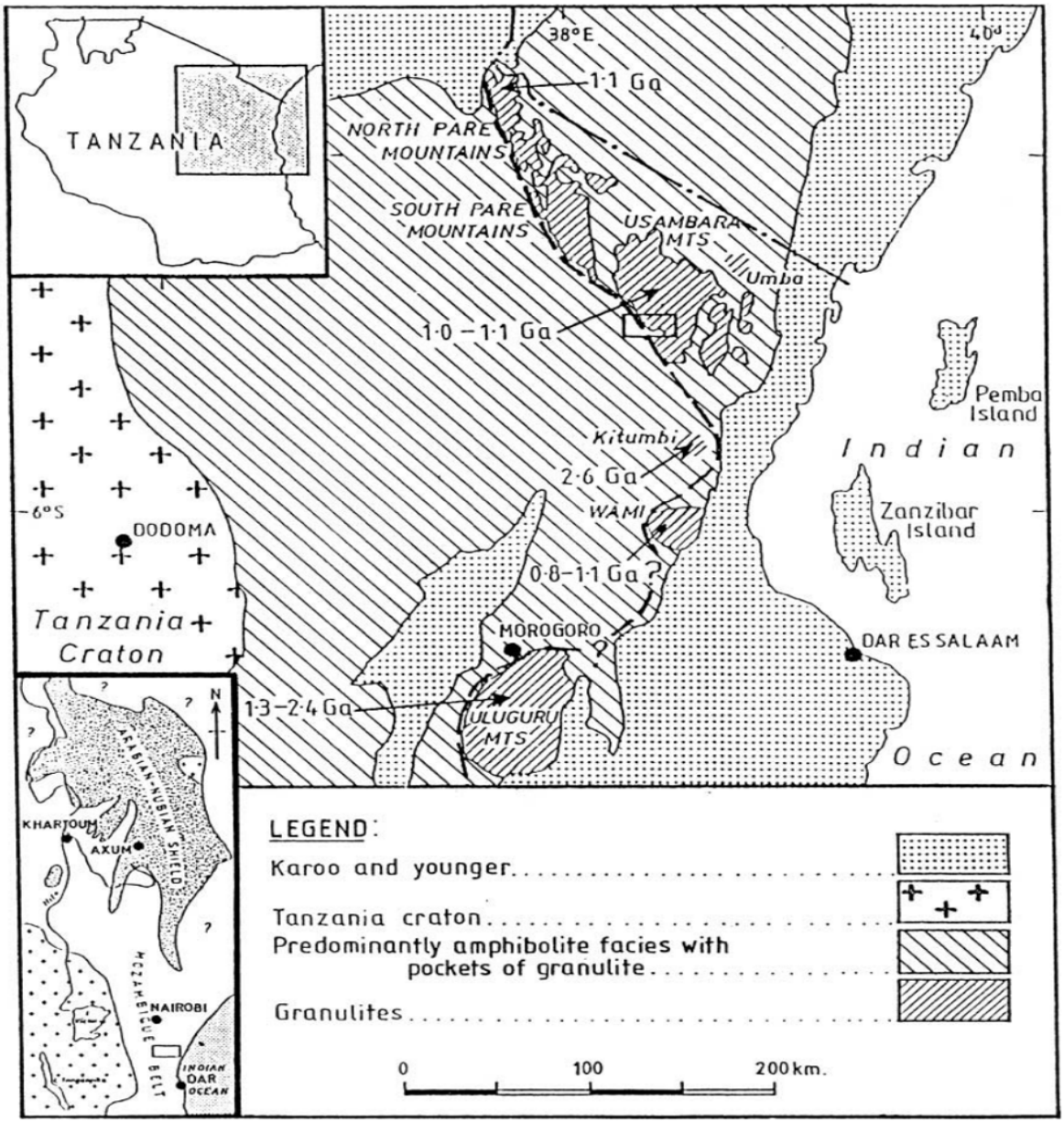

Figure 1-6: Geologic map of eastern Tanzania and southwestern Kenya showing the distribution of the main lithological units. Source: Unmodified from Maboko and Nakamura, (2002).

1.5.1.3 General climate of study area

The East African tropical climate is majorly influenced by changing monsoon winds (Ayugi et al., 2020). This is attributed to a combination of mesoscale convective

systems, globally propagating convection-triggering waves and the inertial instability in generating convection (Nicholson, 2018). The changing monsoon winds attributed to the annual and inter-annual migration of the Inter-tropical Convergence Zone (ITCZ), the large pressure systems of the Western Indian Ocean and orogenic effects of coastal hills, produces long and short wet seasons (Ayugi et al., 2020). The two rainy seasons occur between March and July and between October and November (Wang'ondu et al., 2009). Additionally, the Umba River catchment is comprised of a tropical monsoon (Am), a tropical savannah with dry summer (As) and a dry winter (Aw) according to Köppen-Geiger Climate classification (Kottek et al., 2006; Rubel et al., 2017). The average annual temperature in the Umba River catchment is ~25°C with a rainfall range between 500 mm and 1500 mm (Tesfamariam et al., 2021).

1.6 Project background

The mangroves of Vanga are within a proposed transboundary conservation area (pTBCA) (Figure 1-4) between Kenya and Tanzania (Tuda et al. 2019; UNEP, 2021). The pTBCA seeks to support conservation and management systems in adaptive transboundary governance (UNEP, 2021). The pTBCA stretches from Diani in Kenya to the north to Mkinga in Tanzania to the south. The pTBCA is sandwiched between the protected Diani-Chale Marine Reserve and the Tanga Coelacanth Marine Park (UNEP, 2021). Within it are other protected areas including the Kisite-Mpunguti Marine Park in Kenya and the Kirui Marine Park in Tanzania. The pTBCA has rich, contiguous and transboundary biodiversity and has been identified as a seascape of eco-regional importance (WWF-EAME, 2004). In order to effectively manage the resources within the pTBCA, the need to understand the intra- and interconnectivity between the coastal habitats and the extended terrestrial catchment arose. The mangroves of Vanga investigated in this thesis, occur at the mouth of Umba River at the Vanga Estuary (Figure1-4). Therefore, the influence of the Umba River catchment on sediment dynamics (sources, accretion) in the mangroves of Vanga and in particular the pTBCA were to be evaluated. This was done through a multi-

institutional collaboration project that sought to understand the "Transboundary coastal processes and human resource utilization patterns as a basis for a Kenya-Tanzania conservation area initiative". Through its different work packages, the project collected and collated biophysical, ecological and socio-economic data that could help understand the hypothesized connectivity between the dynamic environment, ecological habitats and resource use.

1.7 Motivation and objectives

The global mean sea-level (GMSL) has fluctuated over the geological timescale, rising and falling during interglacial and glacial periods, respectively (Cutler, 2003). Climate-driven GMSL rise has been reported since the 1960s (Mimura and Horikawa, 2013; Dangendorf et al., 2019; IPCC, 2019) and is currently rising at a rate of ~3 mm/yr (Santillan et al., 2020). Due to a 1.5°C increase in global warming, GMSL is projected to rise to between 0.26 and 0.77 m by 2100 (IPCC, 2019), at a rate of ≥3.4 mm/yr (Saintilan et al., 2020). SLR is currently one of the major threats to coastal communities and valuable ecosystems (Lovelock et al., 2015). With the ever-growing human population in the world's coastal areas (Zimmer, 2018), SLR poses a significant threat due to the potential conversion of human habitable spaces and coastal habitats to open water or tidal flats (Lovelock et al., 2015) and subsequent loss of ecosystems and the essential services (Alongi, 2008; Hamza et al., 2020; Rogers, 2021). Primary to this thesis is the potential loss of the Vanga Estuary mangroves and the associated ecosystem services due to current and projected SLR. As mentioned in Chapter 1.2, sediment availability can enable mangroves to adjust to SLR and maintain the mangrove surface elevation gain (Crosby et al., 2016). Sediment availability is a function of the supply and delivery of minerogenic and organogenic sediments (Nolte et al., 2013). Sediments delivered to an estuary are differently sourced, including terrigenous (from rivers), marine (from tides) and *in-situ* produced (roots and litter) sediments. Therefore, it is crucial to understand the sediment dynamics in a mangrove estuary entailing sediment sources, budgets, and their fate.

It allows the assessment of the possible responses of mangroves to SLR and their long-term sustainability (Lovelock et al., 2015; Woodroffe, 2018). The connectivity between the Vanga Estuary and the terrestrial catchment and its influence on the sediment supply is inadequate and lacks empirical evidence. This inadequacy jeopardizes the conservation, management and potential adaptive measures even within elaborate mechanisms like the integrated coastal zone management and the pTBCA. Therefore, the overarching aim, is the conservation of the mangroves of Vanga in the face of SLR underpinned by scientific data for the benefit of the current and future generations. Based on Chapter 1.1-1.6, the conservation of this critical transboundary habitat and indeed other coastal habitats is hinged on understanding the holistic sediment dynamics and interactions of the coastal habitat and the adjacent hinterland. Therefore, to effectively evaluate the possible response of the Vanga mangroves to SLR and their long-term sustainability, investigations and better understanding on both i) the source of Umba River sediments and ii) the assessment of the current mangrove surface elevation changes within the mangroves of Vanga is merited.

1.8 Research aims and approach

1.8.1 Research objectives

The overall goal of this doctoral study was to investigate the influence of the transboundary Umba River catchment, its geology, and the fluvial transport on the sediment provenance and dynamics in the mangrove sediments in the Vanga Estuary. To achieve the overall goal and identify the influence of the wider Umba River catchment, the following research questions were formulated:

i) What is the source geology and characteristics of the fluvial sediments transported by the transboundary Umba River and delivered to the Vanga Estuary?

ii) What are the contributing sources of sediment organic matter (as proxies for sediment province) delivered to the Vanga Estuary?

iii) Are the current rates of sediment accretion in the Vanga Estuary sufficient to sustain mangrove surface elevation relative to the current and predicted rates of sea-level rise?

In order to answer the research questions above, the following specific objectives were developed and pursued:

- Determine and interpret the geochemical and mineralogic composition and distribution Umba River sediments.
- Determine the source(s) of organic matter delivered and deposited in the Vanga Estuary.
- Measure the current sediment accumulation rates and surface elevation changes in the Vanga Estuary.

1.8.2 Materials and methods

To achieve the objectives outlined in chapter 1.8.1, surface sediments were collected along the Umba River from source in Mng'aro, Tanzania to its mouth in Vanga, Kenya (Figure 1-4). Additional sediment samples were collected under the mangrove canopy in Vanga and in the adjacent shallow coastal waters of the Indian Ocean. Field sampling campaigns were conducted during the dry season in February/March 2019 and the wet seasons in June/July 2019 and July 2020. Physico-chemical parameters, including temperature (°C), pH, dissolved oxygen (mg/L), salinity (psu) and total dissolved solids (g/L) were measured in-situ using a portable YSI™ multiparameter. Sediment-elevation tables-marker horizons (SET-MH) were set up within the mangroves of Vanga to measure and monitor the surface elevation changes during the study period. The detailed descriptions of the sampling, sample preparation, laboratory analyses, modeling and data analyses are contained in stand-alone sections within the individual manuscript chapters.

1.9 Thesis overview and declaration of author contributions

This doctoral thesis has a cumulative structure and consists of 6 chapters. It comprises an introductory chapter (Chapter 1), which highlights the general scientific context, the objectives and motivation of this thesis, as well as an introduction to the study area, geological setting and climate. Chapters 2, 3, and 4 have been developed into joint-authorship manuscripts and forms this doctoral thesis's body. They are succeeded by a general discussion (Chapter 5) and an outlook on future research (Chapter 6). The detailed author contributions to the manuscripts and their current status are provided below:

Chapter 2: Surface elevation changes in an estuarine mangrove forest in Vanga, Kenya: implications and mitigation of sea-level rise

Authors: Amon Kimeli, Shawlet Cherono, George Onduso, Margaret Mathinji, Judith Okello, Hildegard Westphal, Nico Koedam, and James Kairo

Status: To be submitted to Frontiers in Marine Science

This chapter focuses on the measurement of current sedimentation rates in the Vanga Estuary, Kenya, and compares them with the current and predicted local and global sea-level rise (SLR) rates, allowing for the evaluation and determination of the possible response of the mangroves to SLR.

Idea and concept: Personal contribution 85%

A. Kimeli proposed the combined sediment-elevation table-horizon marker (SET-MHs) methodology to measure sedimentation rates, with contributions from J. Okello, H. Westphal, N. Koedam, and J. Kairo. N. Koedam, J. Kairo, J. Okello, and A. Kimeli jointly obtained the funding.

Research and Analyses: Personal contribution 85%

A. Kimeli oversaw the setting up of the field plots and, together with S. Cherono, G. Onduso, M. Mathinji, J. Okello, monitored and collected periodic measurements during the study period. S. Cherono, G. Onduso and M. Mathinji assisted in data entry. G. Onduso, and A. Kimeli deployed and retrieved the hydrostatic pressure divers, downloaded and cleaned the data. A. Kimeli analysed all the datasets, generated all the figures and interpreted the data.

Manuscript writing: Personal contribution 85%

A. Kimeli wrote the whole initial sections of the manuscript, collated comments from co-authors, and incorporated suggested changes and textual improvements. H. Westphal and J. Okello made contributions to the introduction and methodology sections, respectively. All authors made significant intellectual contributions and critically reviewed the manuscript.

Chapter 3: Geochemical and petrographic characteristics of sediments along the transboundary (Kenya–Tanzania) Umba River as indicators of provenance and weathering

Authors: Amon Kimeli, Oliver Ocholla, Judith Okello, Nico Koedam, Hildegard Westphal, and James Kairo

Status: Published in Open Geosciences (De Gruyter) 13(1): 1064-1083. https://doi.org/10.1515/geo-2020-0275

This chapter seeks to determine the influence of the Umba River and its catchment on sedimentation and provenance in the Vanga Estuary. We utilize the geochemical and mineralogical characteristics of sediments to constrain the source geology and provenance of sediments delivered by the Umba River to the downstream mangrove of Vanga, Kenya.

Idea and concept: Personal contribution 85%

A. Kimeli conceived and pitched the idea to utilize the geochemical and mineralogical characteristics of Umba River sediments as proxies to constrain the source geology, weathering, and the possible influence of the Umba catchment on the sediment provenance. N. Koedam, J. Okello, and J. Kairo contributed to the concept as project partners and assisted in implementing the project, aligning it with the overall project objectives.

Research and Analyses: Personal contribution 85%

A. Kimeli, O. Ocholla, and J. Okello collected and prepared the samples for analysis. A Kimeli weighed, dried, and ground the sediments for geochemical analyses and conducted all the microscopic work on thin sections. A. Kimeli analyzed all the data, generated all the figures and tables, and interpreted the data.

Manuscript writing: Personal contribution 85%

A. Kimeli wrote the whole initial sections of the manuscript, aggregated the comments from co-authors as the corresponding author. H. Westphal contributed to the description of the study area's geological setting. Together with J. Okello, N. Koedam, and J. Kairo improved the manuscript through critical reviews and textual improvements.

Chapter 4: Tracing organic matter sources in the estuarine sediments of Vanga, Kenya, and provenance implications

Authors: Amon Kimeli, Shawlet Cherono, Bonface Mutisya, Fredrick Tamooh, Judith Okello, Nico Koedam, Hildegard Westphal, and James Kairo.

Status: Published in Estuarine, Coastal and Shelf Science, 263, p.107636. https://doi.org/10.1016/j.ecss.2021.107636

In order to further determine the sediment sources and contributing factors, this chapter focuses on disentangling sediment sources using stable isotope analysis of sediment organic matter and Bayesian modeling.

Idea and concept: Personal contribution 85%

A. Kimeli conceived the idea to utilize stable isotopes to determine the source of sediment organic matter in Vanga Estuary as a proxy for sediment provenance. A Kimeli also chose, studied, and applied the Bayesian model to partition sediment sources. N. Koedam, J. Kairo, H. Westphal, J. Okello, and F. Tamooh contributed to the project design.

Research and Analyses: Personal contribution 85%

A. Kimeli, J. Okello, S. Cherono, B. Mutisya collected and prepared the samples for laboratory analyses. At the laboratory, A. Kimeli further prepared the samples by drying, grinding, homogenizing and weighing. A. Kimeli generated all figures and tables, and interpreted the data.

Manuscript writing: Personal contribution 85%

A. Kimeli wrote the whole initial sections of the manuscript, collated comments from co-authors, and was the corresponding author. H. Westphal, J. Okello, and F. Tamooh proofread the reply letter to reviewers and, together with N. Koedam and J. Kairo, provided critical revision of the manuscript, subsequently improving it.

A. Kimeli has also co-authored articles/manuscripts related to this doctoral study but does not constitute chapters in this thesis:

1) **Effects of Umba River sedimentation on the distribution and morphology of mangroves of Vanga, Kenya (**Personal contribution: Idea and concept: 25%; Research: 25%; Writing: 25%)

   Authors: Shawlet Cherono, Judith Okello, Fredrick Tamooh, James Jumbe, Amon Kimeli, Nico Koedam

Status: Under review in Regional Studies in Marine Sciences Journal

Author contributions: The project and idea originated from N. Koedam and J. Kairo as principal investigators (PI) and A. Kimeli and J. Okello as co-PIs who obtained the funding. The project funded S. Cherono to carry out her MSc study. A. Kimeli jointly assisted in data collection, analysis, and manuscript submission and review.

2) **Mangroven als Sedimentfallen und Küstenschützer** (Personal contribution: Idea and concept: 10%; Research: 50% ; Writing: 50%)

   Authors: Martin Zimmer, Amon Kimeli

   Status: Published in the Journal Geographische Rundschau 7/8-2021.

   Author contribution: The concept originated from M. Zimmer. A. Kimeli did the research, literature review, developed the initial figures, and wrote the initial draft article. M. Zimmer improved the text, figures and corresponded with the publisher.

3) **Book Chapter on Mangrove Sedimentary Environment** (Personal contribution: Idea and concept: 10%; Research: 50%; Writing: 50%)

   Authors: Amon Kimeli, Martin Zimmer

   Status: In preparation to be submitted to and possibly published by Springer.

   Author Contribution: The concept originated from M. Zimmer. A. Kimeli does the literature review, and initial drafting of the book chapter.

Chapter 2 : Manuscript I

Surface elevation changes in an estuarine mangrove forest in Vanga, Kenya: implications and mitigation of sea-level rise

This work is under preparation for submission for peer review.

Kimeli A[a,b,c]*, Cherono S[c], Onduso G[c], Mathinji M[c], Okello J[c], Westphal H[a,b], Koedam N[d], and Kairo J[c].

[a] Faculty of Geoscience, University of Bremen, 28359 Bremen, Germany.

[b] Biogeochemistry and Geology Department, Leibniz Centre for Tropical Marine Research (ZMT), 28359 Bremen, Germany.

[c] Oceanography and Hydrography Department, Kenya Marine and Fisheries Research Institute, 81651 – 80100 Mombasa, Kenya.

[d] Laboratory of Plant Biology and Nature Management (APNA), Vrije Universiteit Brussels, 1050 Brussels, Belgium.

Highlights

- Sediment-elevation table -marker horizon (SET-MH) methodology is used to measure surface accretion and shallow subsidence
- Sediment accretion and shallow subsidence up to 9.9 mm/yr and -15 mm/yr, respectively is observed
- The mangrove surface accretion exceeds both local and global rates of sea level rise

Abstract

In order to assess and mitigate threats to mangroves caused by their vulnerability to sea-level rise, accurate location- and region-specific elevation information is required. The provision of land building services by mangroves is to a large extent sediment-dependent. It is therefore influenced by local factors including sediment availability and supply. In the present study from Kenya, we measured and examined the variations in surface elevation in mangroves at variable distance from the creek channel using a combination of surface elevation tables and horizon markers for a period of three years. Elevation changes varied with distance from the creek channel ($p < 0.05$), with both surface loss and gains being recorded. Elevation changes varied between -80 mm (greatest subsidence) and 42 mm (highest accretion) in stations closer to the creek, while farther from the creek (~200 m away), elevation changes ranged between -68 mm (greatest subsidence) and 29 mm (highest accretion). However, net surface elevation changes over the three years showed that shallow subsidence occurred in both stations closer to the creek (-45 ± 7.2 mm) and those farthest from the creek (-20 ± 7.1 mm). At the same time, an average of 18 mm of sediments were accreted above the horizon markers translating to ~9 mm yr^{-1} of accretion, a rate larger than both the current global rates of sea-level rise (~3.1 mm yr^{-1}) and local measured rates of sea-level rise (3.8 mm yr^{-1}) in Mombasa, a tide-gauge station nearest (~100 km) to the study site. Cumulatively, sediment elevation changes in Vanga indicate that they are outpacing the current rates of sea-level rise. However, they could be vulnerable to predicted and accelerated rates. It therefore calls for more holistic management and monitoring of the dynamics both within the mangrove forests and adjacent terrestrial hinterlands.

Keywords: Sediments, accretion, Mangrove, Vanga, Kenya, sea level changes, elevation, subsidence

2.1 Introduction

Mangroves are halophytic coastal plants that occupy the region between high and low water marks in tropical and sub-tropical regions. Mangroves provide numerous ecological and economic services including fish breeding habitats (Barbier et al., 2011; Igulu et al., 2014; Woodroffe et al., 2016; Saintilan et al., 2020), sediment traps and blue carbon sinks (Polidoro et al., 2010; Lang'at et al., 2014; Okello et al., 2013, 2020) and physical buffers against coastal erosion, wave action, flooding and Tsunamis (Dahdouh-Guebas et al., 2005; Mazda and Wolanski, 2009; Phan et al., 2015; Ellison, 2015). However, mangroves and other critical coastal habitats, including temperate marshes, coral reefs and seagrasses are confronted by challenges, both naturally and anthropogenically induced. One of the imminent threat to mangroves, is the rising and predicted acceleration of sea-level rise (SLR) owed to the consequential effects of climate change. This is inevitable as mangroves occupy a highly variable habitat that is sensitive to any sea-level change – be it upward or downward (Figure 2-1). For example, mangroves can be vulnerable due to low tidal range, e.g., the mangroves of Doula Cameroon, coastal subsidence for mangroves of Tikina Wai, Fiji (Ellison, 2015), and lack of space to migrate to, due to human settlement, e.g., in the mangroves of Gazi, Kenya (Di Nitto et al., 2014). However, mangroves are less vulnerable some regions due to favorable but localized dynamics, e.g., an uplifting coastline for the mangroves of Rufiji, Tanzania (Ellison, 2015). However, generally mangroves are able to indirectly moderate the effects of sea-level rise (SLR) and thus prevents possible loss of mangrove forests due to submergence (Krauss et al., 2014; Lovelock et al., 2015; Ward et al., 2016; Friess and McKee, 2021). Through their complex root structure, they attenuate wave velocities, enables sediment deposition, consolidation and accretion (Furukawa and Wolanski, 1996; Krauss et al. 2014). Mangroves are thus inherently adapted to relative sea-level changes. This is further evident from mangrove resilience observed with respect to paleo sea-level fluctuations, covering large time-scales dating back to the late

Oligocene (Soares, 2009; Collins et al., 2017; Woodroffe, 2018; Sugden, 2020). A combination of subsidence, sediment supply, enhanced tidal range and availability of space favors the mangroves of the South China Sea (Collins et al., 2017). Although SLR has been documented as the imminent threat to mangroves, sea-level drop (SLD), which has also been observed in the past could also be detrimental to mangroves. SLD could be occasioned by land subsidence which is both a localized and largely regional process (Figure 2-1).

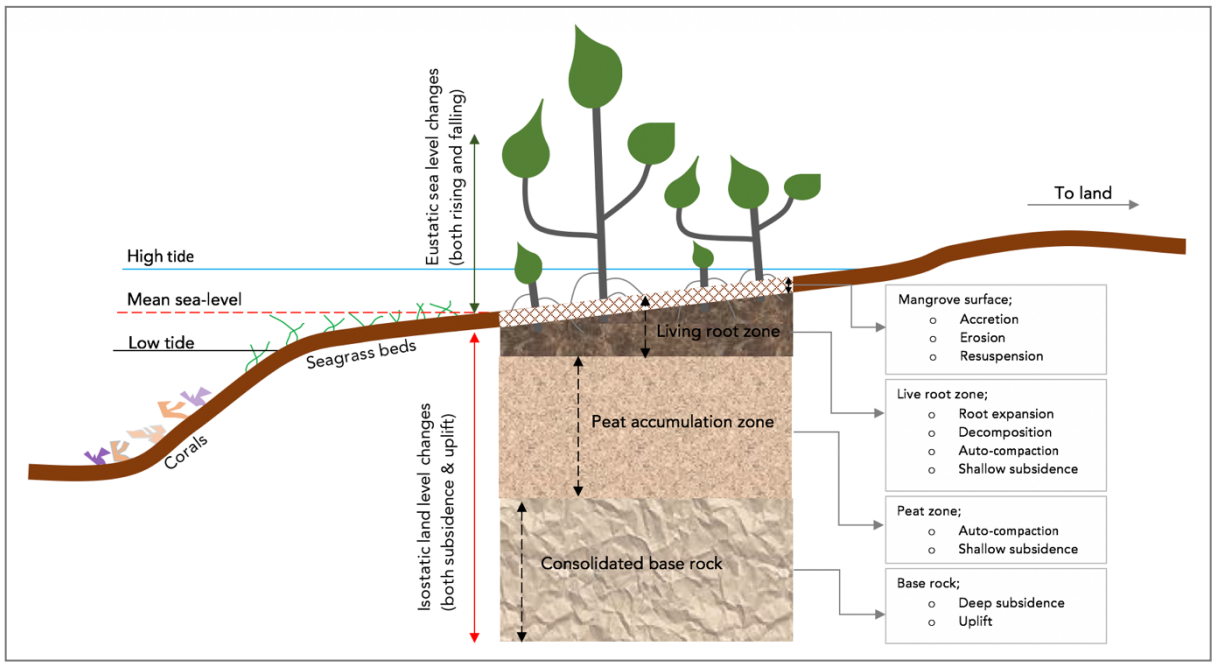

Figure 2-1: Diagram showing the regional and localized dynamic processes controlling both the short- and long-term mangrove surface elevation.

Mangrove habitats have developed strategies to cope with SLR and SLD (Woodroffe et al., 2016). However, SLR could be easier to mitigate than SLD mainly because SLR is gradual and would give time for a gradual response, adaptive measures, and other response/feedback mechanisms (Rogers, 2021). On the contrary, SLD due to tectonic subsidence would be sudden, and mangroves would have no time respond or adapt adequately. Research by Collins et al. (2017), has shown that that mangroves have been able to keep pace with localized tectonic subsidence of up-to 3 mm yr^{-1}. They attributed this to enhanced tidal range coupled with sediment supply, the reworking of sediments and the availability of accommodation space. SLR and SLD have varied

effects on mangrove habitats (Gilman et al., 2008; Neubauer, 2008; Polidoro et al., 2010; Ellison, 2015; Ward et al., 2016). High rates of SLR would lead to submergence of mangrove habitats and subsequent loss of entire ecosystems (Ellison, 2015). For example, with SLR rates of 20 mm yr^{-1}, the Indo-Pacific mangroves are predicted to be submerged by as early as 2070 and 2100 with less than 2 m and 4 m tidal ranges, respectively (Lovelock et al., 2015). SLD due to local subsidence, would enhance the tidal range, which would allow for more sediment supply, deposition, and increase tidal velocities that would assist in the reworking of sediments to suitable sizes (Collins et al., 2017).

Any loss of mangrove would result in a cascade of ecological, environmental and economic losses of local and global magnitudes (Barbier et al., 2011). Some of the losses would be loss of including loss of livelihoods (Hamza et al., 2020), wave and tsunami buffers (Dahdouh-Guebas et al., 2005) and ecological benefits (Barbier et al., 2011; Igulu et al., 2014). Loss of mangroves would also herald the loss of carbon sinks (Kusumaningtyas et al., 2019; Hamza et al., 2020) and ecosystem engineering services (Gutiérrez et al., 2012) that would be detrimental to other habitats.

Climate-change driven global mean sea-level (GMSL) as derived from satellite altimetry has been steadily rising since the 1960s and rose at an average rate of 3.2 ± 0.4 mm yr^{-1} between 1993 and 2009 (Nerem et al., 2018; Dangendorf et al., 2019). This was comparable to *in-situ* measured rates of 2.8 ± 0.8 mm yr^{-1} obtained for the same period in the tropical Pacific and the Indian Ocean Islands (Church and White, 2011). Mangrove habitat migration, adaptation and resilience towards current and projected SLR scenarios depend on the maintenance of elevation equilibrium between mangrove surface elevation and rates of SLR (McKee, 2011; Friess and McKee, 2021). One of the ways that mangroves would respond to sea-level rise, has been predicted to be a migration to higher grounds. (Di Nitto et al., 2014). This would largely depend on the availability of space to accommodate the migration (Rogers, 2021). Another is their indirect "engineering" through sediment trapping

and promotion of sediment accumulation. This would assist mangroves in elevating their surfaces with respect to SLR (Mcivor et al., 2013; Ellison, 2015). The equilibrium between mangrove surface elevation and rate of SLR is dependent on the net balance between material inputs (siliciclastic and organic material) and material removal via erosion and organic matter decomposition (Neubauer, 2008; Ward et al., 2016). Additionally, sediment compaction by sediment overload results in expulsion of water from the sediment column, which lead to compaction and elevation changes. Through constant supply of sediments and net accretion, it has been argued that mangroves are able to keep pace with sea-level rise and avoid submergence (Sanders et al., 2008; Ward et al., 2016; Woodroffe et al., 2016). Mangrove surface elevation is a direct function of several biophysical processes, including supply and deposition of both lithogenic and organogenic sediments. Sediments delivered by fluvial systems and flood tides all contribute to total sediment accumulation within the ecosystem. The cumulative effect of accretion, erosion, compaction, and subsidence (Figure 2-2) would lead to a net surface elevation. Localized and sudden or excessive input of sediments due to storm surges, floods or tsunamis to a mangrove habitat, would disrupt this net equilibrium. The disruption of would be detrimental to the survival of mangroves (Okello et al., 2013, 2020). For example, mangrove die-back and loss attributed to massive and sudden sedimentation after the 1997-1998 *El-Niño* event have been reported in Kenya (Kitheka et al., 2002; Bosire et al., 2014) and in Vietnam (Fagherazzi and Bryan, 2017; Nardin et al., 2021).

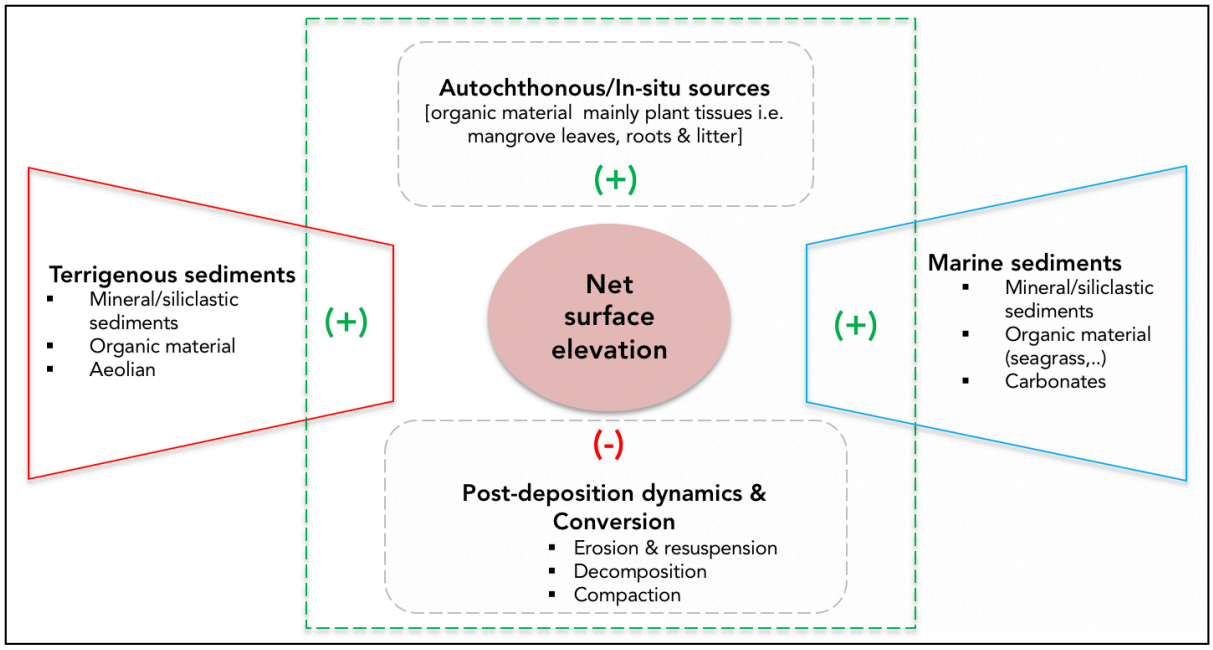

Figure 2-2: Conceptual model on the biophysical processes that control the localized net surface elevation in Mangrove. [+] indicating positive/incremental (accretion) influence while [-] indicate a negative (subsidence, loss of surface elevation) influence.

In general, sediment deposition has been described as episodes of emplacement of sediment particles to a surface. However, sediment accumulation is the net sum of deposition episodes which is a combination of deposition, resuspension and re-deposition (Cahoon and Lynch, 1997; Woodroffe et al., 2016). Net mangrove surface elevation is therefore the result of sediment accumulation, erosion, land uplift, subsidence, peat production and root zone expansion (Krauss et al., 2010; Friess et al., 2019). Direct shallow subsidence is caused by sub-surface processes including decomposition of organic matter, auto-compaction due to weight of subsequent deposition, and dissolution of minerals which tend to shrink the volume of sediments (Cahoon and Lynch, 1997; Krauss et al., 2010; Webb et al., 2013). Other studies have shown that biotic processes - peat accumulation controlled by belowground root growth, expansion and decomposition - can be the main driving factor of sediment accretion and surface elevation changes (Krauss et al., 2008; Kirwan et al., 2013; Crosby et al., 2016). Total sediment accumulation in mangrove ecosystems can also vary both in space and time mainly due to varying mangrove root density and/or type

(Cahoon and Lynch, 1997; Lovelock et al., 2015), lateral and longitudinal distances from the main river and creek channel (Neubauer, 2008). Mangrove habitats vulnerability to sea-level changes are extremely site-specific (Woodroffe, 2018), and the quantification of localized rates of sedimentation and monitoring of the same is required to assess the habitat stability of mangroves and their possible responses to sea-level changes (Neubauer, 2008; Adame et al., 2010; McKee, 2011).

To our knowledge there are no *in-situ* data or studies on vertical accretion or surface elevation changes done within the mangroves of Vanga (Kenya). Most studies in and around the mangroves of Vanga have focused more on fisheries, water quality, mangrove structure and socio-economics (Ochiewo et al., 2010; Kiteresi et al., 2012; Mungai et al., 2019; Fortnam et al., 2020; Kimani et al., 2020; Okuku et al., 2020). The mangroves of Vanga have suffered a great loss of cover than other adjacent mangrove areas both in Kenya and Tanzania (Mungai et al., 2019) and within the proposed transboundary conservation area (Figure 2-3). Due to observed losses, Vanga has been designated as a hotspot of mangrove loss, with an average annual loss of 25 ha (Mungai et al., 2019). This change has been attributed to anthropogenic activities, including harvesting, land use changes. However, natural factors such as sea-level change and subsequent influencing on the sediment dynamics have been assessed and considered. The objective of this study is therefore to investigate surface and subsurface elevation changes and to quantify current elevation change rates in the mangroves of Vanga.

2.2 Methodology

2.2.1 Study site

This study was conducted within the mangroves of Vanga Estuary (4° 39′ 18″ S and 39° 13′ 20″ E), ~100 km south of Mombasa, Kenya (Figure 2-3). Vanga Estuary is a river dominated system with a total mangrove cover area of 3,035 ha (Mungai et al., 2019). The dominant species of mangroves in the estuary are *Rhizophora mucronata,*

Ceriops tagal, *Sonneratia alba* and *Avicennia marina* species. This particular mangrove patch is part of the Vanga-Funzi mangrove block (Kiteresi et al., 2012; Mungai et al., 2019) within the proposed transboundary conservation area (TBCA) between Kenya and Tanzania (Figure 2-3). This region has a mean annual precipitation >1000 mm (IUCN, 2003) and the estuary experiences a semi-diurnal tidal influence. It also has a year-round discharge of allochthonous sediment and freshwater delivered by the transboundary Umba River (Tesfamariam et al., 2021). It also benefits from the deposition of autochthonous organic sediments derived from *in-situ* production and accumulation of biogenic material (leaves and roots).

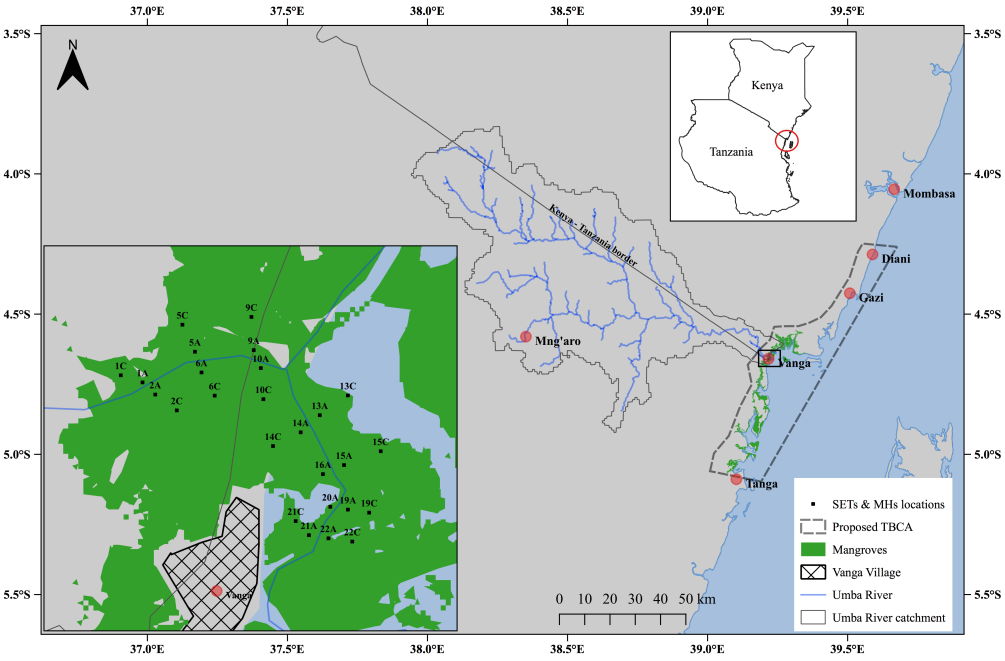

Figure 2-3: Location of study area in Vanga, Kenya with experimental plots perpendicular to the main creek channel.

2.2.2 Set up for measurement of surface elevation changes

Surface elevation changes were measured using a set of surfaceelevation tables (SET) and horizon markers (MH). SETs are mechanical, portable or fixed (or a combination of both) levelling set-up designed to assist in measuring vertical surface elevation changes (Cahoon and Lynch, 1997; Cahoon et al., 2002; Krauss et al., 2010; McKee,

2011; Webb et al., 2013; Callaway et al., 2015). Horizon markers (MH) are comprised of many different types of materials that are insoluble in water and easily distinguishable from sediments. They are used as references in sediments against which periodic measurement of accreted sediments can be made (Lang'at et al., 2014). In this study crystal violet (Ammonium oxalate) powder was used as our horizon marker mainly due to its local availability. In other studies, white feldspar (kaolin) markers have been utilized (Krauss et al., 2003; McKee, 2011; Lang'at et al., 2014). SETs are able to account for both positive (accretion) and negative (subsidence) elevation changes. On the contrary, MHs do not account for sub-surface processes but measures only positive elevation changes (accretion). A combination of both allows for the determination of both surface accretion and subsidence. Due to the dense mangrove, proximity to Vanga village and vulnerability to vandalism, sophisticated and relatively elaborate SET experimental set-up (Cahoon and Lynch, 1997; Krauss et al., 2010; Callaway et al., 2015) was not feasible in our study site. An improvised low-cost and low-maintenance experimental set-up (Figure 2-4) was therefore used in this study. The SET-MH were set up in 20 × 20 cm plots within the mangrove stands. In two opposite vertices (see Figure 2-4) of the plots, 3m-long stainless-steel rods (6 mm in diameter) were driven to refusal (e.g., bed rock). The rods were sunk below the ground and the length exposed above the surface set at 25. All the experimental SET-MH plots were set up perpendicular to the main channel. Some plots (A stations) were close (~10-20 m) to the main channel while others (C stations) were set up farther away (~150-200 m) from the main channel. The distance was to assess and apportion the influence that frequency and depth of tidal inundation had on sediment elevation changes. The assessment of the influence of mangrove species was not feasible because the Vanga-Funzi mangrove are characterized by mixed stands (Mungai et al., 2019).

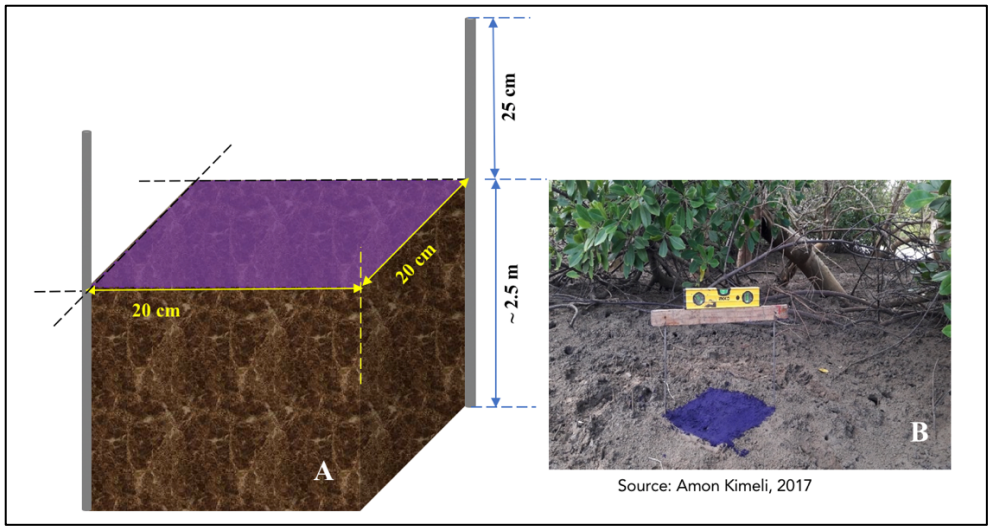

Figure 2-4. Conceptual illustration (not to scale) of the installation of surface-elevation table (left) within Vanga mangrove forest, Kenya. Measurements of elevation changes were done along the wooden board leveled using a spirit level (right).

Twelve (12) height measurements from the mangrove surface to the heights of the rods were made at twelve points along a spirit-leveled wooden board placed diagonally across each set of rods (Figure 2-4). The 12 measurements were averaged to obtained a single measurement per plot. Subsequent SET measurements over 3 years (between 2017 and 2021) were recorded. The elevation measurements were mostly taken every 3-4 months within the monitoring. However, there were long periods between i) April 208 and Feb 2019 and ii) July 2019 and August 2020 that elevation measurements were not taken owing to unavoidable project delays. Measurement of accretion above the MH was done by carefully obtaining 2 × 2 cm cores (blocks) on the edges of the plots using a sharp knife (Figure 2-4). The height (in cm) of sediment above the MH was recorded and the block returned to its position (Lang'at et al., 2014). Due to the perturbation of MH by sesarmid crabs, it was not possible to obtain MH cores and measurements beyond two years.

2.2.3 Sea-level and estimated mangrove surface elevation

Sea-level data was obtained from the Mombasa tide gauge – one of the only two tide gauges along the Kenyan coastline with data available for public use. The

Mombasa tide gauge (~100 km north of Vanga) was set-up and operationalized in 1986. The tide gauge is located at the mouth of Mwache Creek, Kilindini Harbor. The creek is geomorphologically different from Vanga estuary, however, sea-level variations along the entire Kenyan coastline are comparable (Kebede et al., 2010). It is currently part of the Global Ocean Observation System (GOOS) network in the context of the Tsunami early warning system. All the data from the GOOS network are stored in the centralized data repository of the GOOS network at the University of Hawaii Sea Level Centre (UHSLC, https://uhslc.soest.hawaii.edu/). Mean monthly and hourly sea-level data was obtained to assess the long-term sea-level and during-study variations, respectively.

The elevation of the study site with respect to sea-level, was estimated barometrically using *Van Essen*© hydrostatic divers. We obtained relative water levels by determining the hydrostatic pressure differences derived from barometric diver measurements and corrected for the atmospheric pressure. A diver (mini DI701 Cera diver) submerged during tidal flooding and measuring water pressure. The Cera diver was tied to mangrove roots close (approx. 3 cm) to the mangrove surface to minimize the error when the divers were not submerged. There is also a possibility to either underestimate or overestimate water levels above the mangrove surface in turbulent flood tides, however, waves are typically attenuated in dense mangrove vegetations (Furukawa and Wolanski, 1996; Ndirangu et al., 2017). This minimizes the variations due to the turbulence. The barometric diver (mini D1801 Baro diver) was placed high enough in mangrove branches, to avoid inundation including during spring tide. The D1801 Baro diver was used to measure only the atmospheric pressure. The readings from the Baro diver was considered as representative of the whole study area since atmospheric pressure does not vary over short distances. The two divers were both installed at station 14A (Figure 2-3).

By subtracting the measured atmospheric pressure (obtained using Baro diver) from the measured water pressure (obtained from the Cera diver), the hydrostatic

pressure is obtained. This can be transformed into a water column depth (in m) above the mangrove surface. The high-water levels (HWL, in m), measured by the tide gauge in Mombasa were correlated with the calculated water depths at the mangrove sites at high tides. The two daily high-water levels (HWL) referenced to the official chart datum, the lowest astronomical tide (LAT), recorded by the tide gauge were correlated with the corresponding high-water depths measured within the mangroves by the divers. Since the highest pressure is recorded during high water levels, the corresponding high diver pressure measurements represent the maximum water depth. The average of the difference between the corresponding tide gauge measurement (m LAT) and the water depth (m) measurement from the divers, gave an estimate of mangrove surface elevation (m LAT) in the study area.

2.3 Data Analysis

The average of elevation measurements from the 21 SETs (Figure 2-3), were obtained for between Dec 2017 and April 2021. Variation in elevation changes were examined between sites considering the distance from the creek and stations for normality and significance differences using Shapiro-Wilk test and Two-Way ANOVA respectively.

2.4 Results

2.4.1 Sea-level and mangrove surface elevation

At Mombasa (4° 4′ 12″ S and 39° 23′ 47.65″ E), ~100 km north of Vanga, the sea-level has been gradually rising. Based on the tide-gauge measurements, the MSL has been rising at a rate of 3.8 mm/year (Figure 2-5), represented by the slope of the linear trend. The sea-level has been referenced to the mean lowest astronomical tide (LAT).

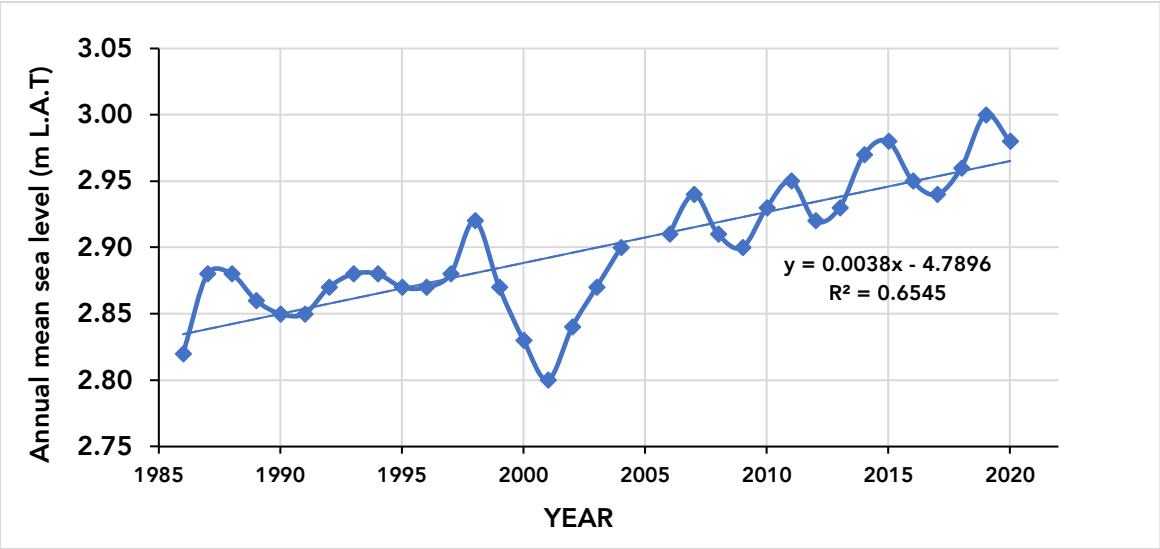

Figure 2-5: Plot showing a rising (increasing) trend of sea-level in Mombasa derived from tide gauge data between June 1986 and December 2020. From the linear trend, the sea-level in Mombasa has been rising at the rate of 3.8 mm/year.

The mean LAT derived from the tide gauge data is 0.81 m which is the average of all monthly mean low water (MLW). The comparison of water depths derived barometrically in the study (in Vanga), with water levels as recorded in Mombasa tide gauge, the estimated mangrove surface elevation in Vanga is 3.22 m above MSL.

2.4.2 Elevation changes of mangrove sediment surface

From the periodic measurement from the installed SET, we observed both accretion and elevation loss within the mangroves of Vanga. In stations near the creek channel (A stations), elevation changes over the 3 years varied between -80 and 20 mm (Figure 2-6), while those farther away from the creek channel (C stations) showed variation ranging between -68.5 and 29.3 mm (Figure 2-7). However, cumulatively over the monitoring period, A stations exhibited mean loss of elevation ranging between -77.7 and -16.4 mm with an average mangrove elevation loss of -45.2 ± 7.2 mm. C stations on the other hand experienced average loss of mangrove elevation between -76 and -2.2 mm with an average of -20 ± 7.1 mm.

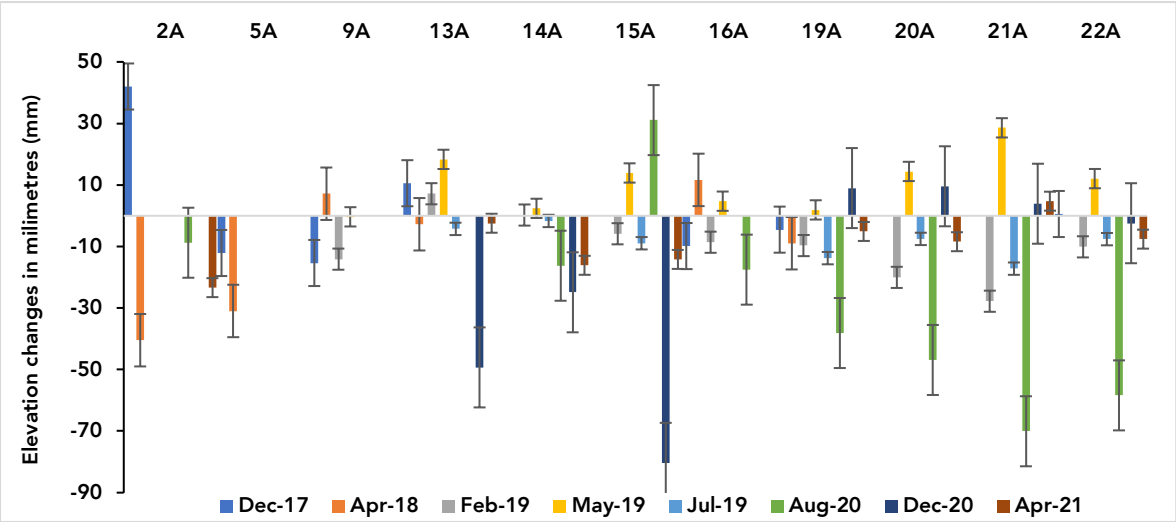

Figure 2-6. Mangrove surface elevation changes rates between Dec 2017 and April 2021 at stations close to main creek channel within the mangroves of Vanga. Top x-axis are the stations while the bottom x-axis are the monitoring time stamps. Error bars represent the standard deviation.

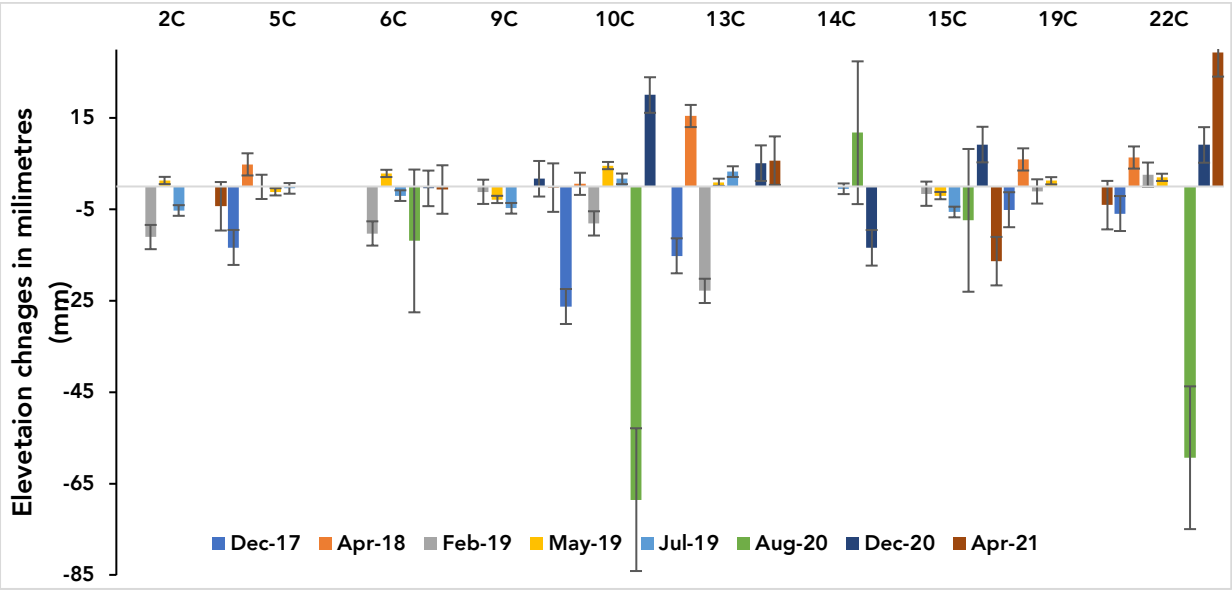

Figure 2-7. Mangrove surface elevation changes rates between Dec 2017 and April 2021 at stations farther away from the main creek channel within the mangroves of Vanga. Top x-axis are the stations while the bottom x-axis are the monitoring time stamps. Error bars represent the standard deviation.

It was evident that mangrove elevation loss was pronounced in stations closest to the main channel relative to stations farther away. The elevation changes also

showed significant variation between sites i.e. A stations and C stations (F-value = 7.87, p = 0.03), however, the variation between the individual stations although discernible in relative terms, was not significant (F-value = 1.43, p = 0.33). Two years (in 2019) after the placement of horizon markers, the cored subsamples in selected un-perturbed MH plots showed average positive sediment accretion above the MH ranging between 12.3 and 26.0 mm. For example, in station 13A, up to 1.5 cm equivalent to 15 mm of accretion was recorded (see Figure 2-8).

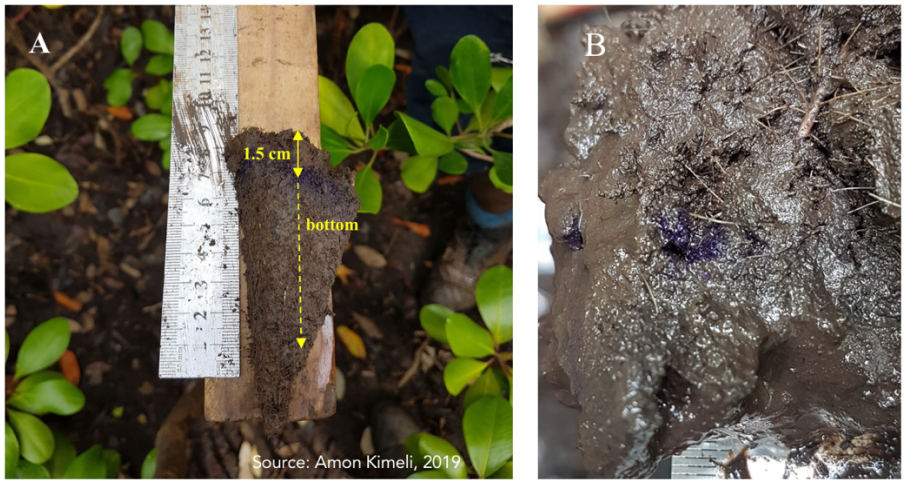

Figure 2-8. Showing the cored sediments with discernible sediment accretion (A) in station 13A and effects of crab mud overturning and mixing (B) in one of the plots set up (e.g., in stations 22A, 15A, 19C).

It represented a cumulative accretion of 7.5 mm yr^{-1}, a value higher than the rate of SLR (3.8 mm yr^{-1}), recorded at the Mombasa tide gauge (Figure 2-5). The average accretion of 18.0 mm equivalent to 9 mm yr^{-1} in all the stations was measured. On average, A stations showed lesser accretion (7.8 mm yr^{-1}) than the C stations (9.6 mm yr^{-1}). The cumulative elevation loss in A stations (-45.2 mm) and C stations (-20 mm) for 3 years, translates to a mangrove surface elevation loss of -15.1 mm yr^{-1} and -6.6 mm yr^{-1}, respectively. Comparing these elevation changes with the recorded accretion rates of 7.8 and 9.6 mm yr^{-1}, we can deduce a net mangrove surface loss of 7.3 mm yr^{-1} in the A stations and a net elevation gain of 3.0 mm yr^{-1} in the C stations.

2.5 Discussion

Mangroves promote sediment trapping, accumulation and consolidation through their dense and complex root structures. It is also from this functionality that mangroves are considered ecosystem engineers (Gutiérrez et al., 2012), where through sediment and organic matter retention, mangroves modify the physical environment and colonize new habitats and platforms. This is vital for mangroves themselves in the face of SLR and as they migrate to higher grounds, but this is also important for other flora and fauna. The mangroves of Vanga has exhibited sediment retention evident by the positive (up to 9.0 mm yr^{-1}, see Figure 2-8) accretion above the MH. However, there is also a marked shallow subsidence attributable to subsurface compaction, decomposition of buried OM (Gutiérrez et al., 2012; Lang'at et al., 2014) and possible collapse of fiddler sesarmid burrows. This leads to loss of surface elevation (Kristensen, 2007) and poses a huge challenge for the mangroves of Vanga, especially with the current and predicted rates of SLR. The surface elevation loss within the mangroves of Vanga of up-to -45 mm is relatively high but is comparable to those of Gazi Bay (~50 km north of Vanga) that reported up to -51 mm elevation loss (Lang'at et al., 2014). Such losses in elevation have been associated to mangrove die back and cover loss due to anthropogenic impacts (Krauss et al., 2014; Lang'at et al., 2014). Indeed, anthropogenic-driven loss of mangroves in Vanga has been reported (Mungai et al., 2019). We could therefore, partly attribute the localized subsidence to the loss. Additionally, during this study, upstream disruption of Umba River flow and discharge, occasioned by a road construction could have a had a negative impact on the sediment supply and mangrove surface elevation growth. It has been reported that the sediments deposited in most mangroves in Africa are mainly minerogenic (Balke and Friess, 2016), however, other studies have reported the dominance of organic sediments (roots, leaves) contribution in other tropical regions (Neubauer, 2008; Krauss et al., 2014). If indeed, the mangroves of Vanga receive more terrigenous sediments, we

can speculate that the disruption reduced the supply of minerogenic sediments. Consequently, the disruption could have further led to an increased dominance of the autochthonous organic sedimentation, predominantly root matter and aboveground biomass including leaf litter (Rogers et al., 2014; Woodroffe et al., 2016). The dominance of organogenic sediment accumulation and their subsequent decomposition would have led to the pronounced loss of elevation. Accretion has also been shown to be relatively lower in brackish/saline than in freshwater (Neubauer, 2008). This broad generalization has been attributed to acceleration of OM decomposition by saline water. But on the contrary, freshwater promotes the accumulation and preservation of OM, which would consequently translate to increased mangrove surface elevation. Therefore, applying this generalized conclusion, the mangrove surface elevation loss in Vanga could be qualified. However, this would require further assessment and evaluation. The relative high elevation loss in A stations compared to C stations, could be as a result of saline waters brought by flood tides reaching these stations both during spring and neap tides accelerating the decomposition unlike the C stations being inundated only during spring tides. The experimental plots both A stations and C stations, were set up in mixed mangrove stands (mostly a mixture of two or more). Therefore, the non-significance in elevation changes between stations would support the findings of Krauss et al. (2014), that different functional root types have no significant influence in elevation changes.

The loss of elevation recorded in this study is also within the ranges of -11.2 to 2.5 mm yr^{1}, documented for similar ecosystems of fringe and riverine mangroves (Krauss et al., 2014). It is projected that GMSL will rise between 4.3 mm (2.9 – 5.9 mm) and 8.4 mm (6.1 – 11 mm) by the end of this century (2100) under the low (RCP 2.6) and high (RCP 8.5) confidence scenarios, respectively (IPCC, 2019). Comparing the projected GMSL with elevation changes within the mangroves Vanga, it paints a picture of imminent threat but with informed interventions and adaptations, the

threats can be mitigated. This threat is also reported for similar habitats including the projected loss of ~50% of Mngazana, South Africa estuary mangroves with a 3.7 mm yr^{-1} SLR rate (Yang et al., 2014; Adams and Rajkaran, 2021), reported loss of >15,000 ha of mangroves due to SLR in Sundarbans (Rahman et al., 2011; Bomer et al., 2020). A regional assessment in Australia, Singapore, Indonesia, Philippines, Malaysia and Vietnam using a network of comparable SET elevation measurements, indicated a ~6 mm yr^{-1} elevation deficit with respect to current and predicted SLR rates (Alongi, 2008; Woodroffe et al., 2016). However, the key strength for the mangroves in Asia has been reported to be the presence of multiple species of mangroves (Ward et al., 2016; Woodroffe et al., 2016) that increases resilience due to interspecific interactions and organic matter input (Huxham et al., 2010).

In the context of long time-scales, mangroves have exhibited resilience and have hitherto adapted to various elevation changes due to paleo sea-level fluctuations (Krauss et al., 2008; Mcivor et al., 2013; Collins et al., 2017; Saintilan et al., 2020) and land elevation changes occasioned by both shallow and tectonically-driven deep subsidence (Collins et al., 2017). This is evident by the observed mangrove colonization and contribution to the net organic carbon budgets that have been identified for as far back as the Oligocene (Collins et al., 2017) and more pronounced in the Holocene (McKee, 2011; Mcivor et al., 2013). The inherent resilience of mangroves to sea-level changes, even in open fringe coasts, is borne from the indirect feedback mechanisms derived from the increased tidal ranges, tidal currents, sediment supply and accommodation space (Rogers, 2021). For example, enhanced tidal range and currents increases the reworking of sediments to sizes suitable for mangroves, and creation of numerous tidal channels that increases rugosity suitable for sediment trapping (Collins et al., 2017).

Information derived from this study, forms part of the site-specific empirical data that would inform management towards mitigation of the effects of the rising SLR. It adds to the growing but still minimal evidences and information of sediment dynamics,

elevation changes within the mangroves of the Western Indian ocean region (Okello et al., 2013; Lang'at et al., 2014; Stringer et al., 2015). The Information derived from this study, will also form part of a suite of baseline data that would inform the setting up and demarcation of a transboundary conservation area (TBCA) between Kenya and Tanzania (Figure 2-3). Most management and conservation strategies including restoration especially for mangroves, has hitherto focused on the ecological aspects but minimally on sediments which is one of the key pillars for their success. To mitigate the effects the of SLR, the use of artificial embankments and interventions to complement the nature-based adaptation and resilience have been suggested (Takagi, 2018; Dasgupta et al., 2019). These artificial embankments are intended to increase the efficiency of tidal damping, velocity attenuation and optimize the mangroves functionality of sediment trapping and consolidation. However, some studies have also cautioned on the long-term efficacies of the artificial embankments and dykes and other human-induced interventions (Romañach et al., 2018; Zimmer, 2018).

2.6 Conclusions

Vanga has been identified as a hotspot for mangrove degradation and loss (Mungai et al., 2019). It has been mainly attributed to anthropogenic factors. However, the effects of other biophysical factors, including sediment accretion, shallow and deep subsidence and expected sea-level rise have been minimally assessed. The current study provides data and information on the elevation changes within the mangroves of Vanga. It reveals the vulnerability to submergence and threat of the projected sea-level rise. It also gives impetus to the need for a more holistic look at the management and conservation of mangroves with incorporation of biophysical drivers likes sedimentation, within the context of land-use changes, sources and sinks. We also recommend for a more multi- and inter-disciplinary research on the Vanga ecosystem not only considering the sediment sources, but also freshwaters

and sediment discharge as well as sediment budgets in order to build a complete picture.

2.7 Acknowledgment

We acknowledge the Belgium Flemish VLIR-UOS for field funding through TEAM and Southern Initiatives (VLIR-UOS Project Code: ZEIN2016PR425) and the Deutscher Akademischer Austauschdienst (DAAD) doctoral programme scholarship awarded to AK and the Leibniz Centre for Tropical Marine Research (ZMT), Bremen Germany through the ZMT Academy support.

Chapter 3 : Manuscript II

Geochemical and petrographic characteristics of sediments along the transboundary (Kenya – Tanzania) Umba River as indicators of provenance and weathering

This work has been published in Open Geosciences (De Gruyter), September 2021 https://doi.org/10.1515/geo-2020-0275

Kimeli A[1,2,3]*, Ocholla O[3], Okello J[3], Koedam N[4], Westphal H[1,2], and Kairo J[3].

[1] Faculty of Geoscience, University of Bremen, 28359 Bremen, Germany.

[2] Biogeochemistry and Geology Department, Leibniz Centre for Tropical Marine Research (ZMT), 28359 Bremen, Germany.

[3] Oceanography and Hydrography Department, Kenya Marine and Fisheries Research Institute, 81651 – 80100 Mombasa, Kenya.

[4] Laboratory of Plant Biology and Nature Management (APNA), Vrije Universiteit Brussels, 1050 Brussels, Belgium.

Highlights

- Geochemical and mineralogical composition of Umba River sediments are evaluated
- The upstream and downstream Umba River sediments have a similar source geology
- The source characteristics match the geology of the Umba River catchment
- Grainsize has minimal influence on the distribution and composition of the Umba River sediments

Abstract

The Umba River basin is one of the smaller-scale hydrological basins in the East African region. It traverses two countries with its catchment in the Usambara mountains in Tanzania, while it drains its waters to the Indian Ocean in Vanga, Kenya. The chemical and mineralogical composition of riverbank and bottom sediments of the Umba River was analysed and evaluated to describe their source characteristics and provenance. The dominant minerals include quartz, K-feldspars, plagioclase, hornblende, pyroxenes, muscovite, biotite and likely presence of clays such as kaolinite. The chemical index of alteration (CIA) of the sediments indicate a moderate to high degree of alteration. They reflect a dominant mafic to intermediate igneous provenance consistent with the geology of the Umba River catchment that is characterized by the outcrops of the granitic Precambrian basement and the quartz-dominated Paleozoic Karoo Supergroup, overlain by Mesozoic and Cenozoic sediments dominated by both, mafic and felsic minerals. The similarity of the chemical and mineralogical composition of the Umba River sediments from source to mouth further indicates a uniform source in the upper course of the river and only subordinate contributions from the lower course where it passes the Karoo and younger sediments.

Keywords: Geochemistry, provenance, weathering, Umba River, petrography, mineralogy, Kenya, Tanzania, geology

3.1 Introduction

Rivers deliver large amounts of terrigenous sediments into the global oceans (Milliman et al., 2016). These sediments play a vital role in both, earth surface processes and the biogeochemical cycle. Fluvial sediments are typically heterogeneous being composed of weathered and eroded rocks along the river's course and are subsequently altered during downstream transportation. These alteration processes are generally characterized as either physical (e.g.,

fragmentation, abrasion, attrition) or chemical (e.g., dissolution, decay, and adsorption) (Lim et al., 2014; Wang and Liu, 2008). The final chemical sediment composition can be different from the source material because of secondary processes during fluvial transport, deposition and post-depositional early diagenesis (Cox et al., 1995; Taylor and McLennan, 1985). The rate of alteration of fluvial sediments is influenced by several factors including the primary composition determined by source geology, climatic conditions, topography and thus water energy, vegetation, transported distance, and human activities (e.g., land use, construction) (Sensarma et al., 2008). The mineralogical and chemical resemblance to the source rock is higher in sediments transported by relatively short rivers. This is because they are derived from a relatively smaller catchment, and therefore might drain fewer geological lithologies. Short rivers also transport sediments from source to mouth in shorter periods of time, allowing for less alteration (Sarkar et al., 2004; Sensarma et al., 2008). Additionally, the composition of sediments is altered by *in-situ* production of bio-clasts, mostly calcareous shells, and the formation of authigenic minerals (Taylor and McLennan, 1985). During transportation, fluvial sediments provide efficient sinks for major and trace elements to accumulate (Sarkar et al., 2004). Major and trace elements are introduced into aquatic environments (rivers, oceans, lakes) through both natural and anthropogenic ways. These ways include atmospheric deposition, weathering of source geology, erosion and surface runoffs and through anthropogenic activities like mining and discharge of sewage effluents (Amorosi, 2012). In the lowermost course of rivers such as in dynamic systems like estuaries, deltas, bays or creeks, the mixing of sediments from multiple sources alters the compositional characteristics. It therefore adds to the complexity when untangling sediment provenance using bulk mineralogical or chemical compositions in such systems. A combination of mineralogical and chemical composition of sediments and rocks has been utilized in numerous studies to constrain source characteristics and to evaluate the degree of weathering and

alteration during transportation (Ali et al., 2014; Sarkar et al., 2004; Sensarma et al., 2008). Source characteristics include the geological and tectonic setting of the source catchments as well as paleoclimate conditions (Ali et al., 2014; Dickinson et al., 1983). To evaluate these characteristics and improve the disentangling of sediment provenance, sediments can be chemically divided into the residual initial sediment composition and the labile fractions. The residual initial composition represents the close to source characteristics, while the labile fractions represent the altered composition as a function of fluvial transportation distance and time (Leleyter et al., 1999). Less mobile elements tend to be less susceptible to alteration thus are suitable proxies for evaluating the source area composition (Wang and Liu, 2008), and are thus used as tracers for sediment provenance. These elements include iron (Fe), vanadium (V), magnesium (Mg), thorium (Th), rare earth elements (REE) and their ratios to aluminum (Al), respectively (Cox et al., 1995; Jung et al., 2012). These elements are considered immobile due to their low solubility and relative retention of their characteristics during transport, reworking, deposition and diagenesis (Cox et al., 1995). However, it has also been shown that dominant minerals and some large labile fractions (mostly clays, carbonates and organic matter) can influence the chemical and mineralogical composition of sediments. Therefore, grain size can influence the chemical and mineralogical composition of fluvial sediments mainly because some grain sizes, especially highly cohesive and consolidated clays (< 125μm), provide better element sinks than relatively unconsolidated medium-grain sand (0.25 – 0.5 mm) to very fine sand or silt (62.5 – 125 μm) (Mil-Homens et al., 2014). Sediments with elevated sand content (up to > 80%) have been reported to act generally as inert dilutors of trace elements and conducive for enhanced accumulation of some including Cr, Ni and Co (Mil-Homens et al., 2014). The provenance of coastal sediments in our study area so far has received little attention. Our main hypothesis is that the sediments deposited along the Umba River including those that are deposited in the downstream estuary, reflect faithfully the geology of

the catchment that extends upstream to the Usambara mountains in southeast Tanzania. The primary purpose of our study is to characterize the geochemistry and mineralogy of the sediments along the Umba river and in the coastal area of Vanga, in order to provide information on the source characteristics, weathering, and their provenance. This study provides knowledge on this transboundary setting and thus contributes towards integrated cross-border management of common resources. Sedimentation is a vital component in this management endeavor not only because of the connectivity of the wider catchment land use but also their effects in downstream biotopes. For example, intensification of land use may increase the soil erosion and delivery of sediments to the downstream habitats, resulting in both negative and positive impacts. The positive effects would include delivery of particulate and dissolved nutrients – vital in the biogeochemical cycles, and sediments – with the accretion of sediments indirectly benefiting mangroves in response to the rising sea-level. Conversely, too high input of nutrients and sediments, as well as delivery of contaminants from the hinterland, is detrimental to downstream biotopes. For example, excessive sedimentation can lead to mangrove burial and die-back, and increasing turbidity can cause damage to coral reefs and seagrass beds in the adjacent coastal areas.

3.1.1 Climate

The tropical climate of this region is influenced by the monsoon winds attributed to the proximity of the warm Indian Ocean and the north-south inter-annual migration of the Inter-Tropical Convergence Zone (ITCZ) (Fortnam et al., 2020; Funk et al., 2016). This ITCZ migration and the resulting changes in wind directions coin two major seasons, namely the southeast monsoon (SEM) and the northeast monsoon (NEM). The NEM brings with it two rainy seasons, the "long rains" between March and June and the "short rains" between October and mid-December. Conversely, the SEM causes two dry seasons sandwiched between the two rainy (wet) seasons (Daron et al., 2015; Funk et al., 2016). The mean annual precipitation in this region

reaches 4000 mm, and the average annual temperature is at 25 °C. The "long rains" accounts for the majority of the annual rainfall, and consequently water discharge and annual sediment transport of the Umba River (IUCN, 2003).

3.1.2 Geological setting

The geology of the catchment area is dominated by the Precambrian basement, successively covered by younger lithologies towards the East (Figure 3-1a and 3-1b). A zone composed of Paleozoic to Jurassic rocks of the Karoo Supergroup (540 – 145 million years) stretches north-south (Figure 3-1a) along the East of the Tanzanian craton (Maboko and Nakamura, 2002), followed by a cover of inter-layered and inter-banded Mesozoic and Cenozoic lithostratigraphic deposits (Figure 3-1b). The Karoo Supergroup stretching from the Tanga basin in Tanzania to the southwest of Kenya comprises generally of sandstones, arkoses, arkosic sandstones, conglomerates and siltstones (Schlüter, 1997). The Precambrian (Neoproterozoic) basement is characterized by high-grade metamorphic gneisses, marbles, gneissic-schists and quartzites. These were intruded by younger East African Rift basaltic extrusive igneous rocks (Maboko and Nakamura, 2002; Schlüter, 1997) dominated by pyroxene-garnet-granulites interlaced with hornblende-gneiss lithologies. The upper reaches of the Umba River in the Usambara mountains consists of thick sequences of granulite facies ortho-gneisses (625 Ma) derived from andesitic to dacitic magmatism in a convergent margin (Maboko and Nakamura, 2002; Mutakyahwa et al., 2003). This formation is intercalated with pelitic, calc-argillaceous and calcareous meta-sediments (Maboko and Nakamura, 2002; Schlünz B., 2000; Shackleton, 1993). The meta-igneous rocks are also intruded by mafic and felsic bands of gabbro, anorthosite and hornblende/pyroxenite facies.

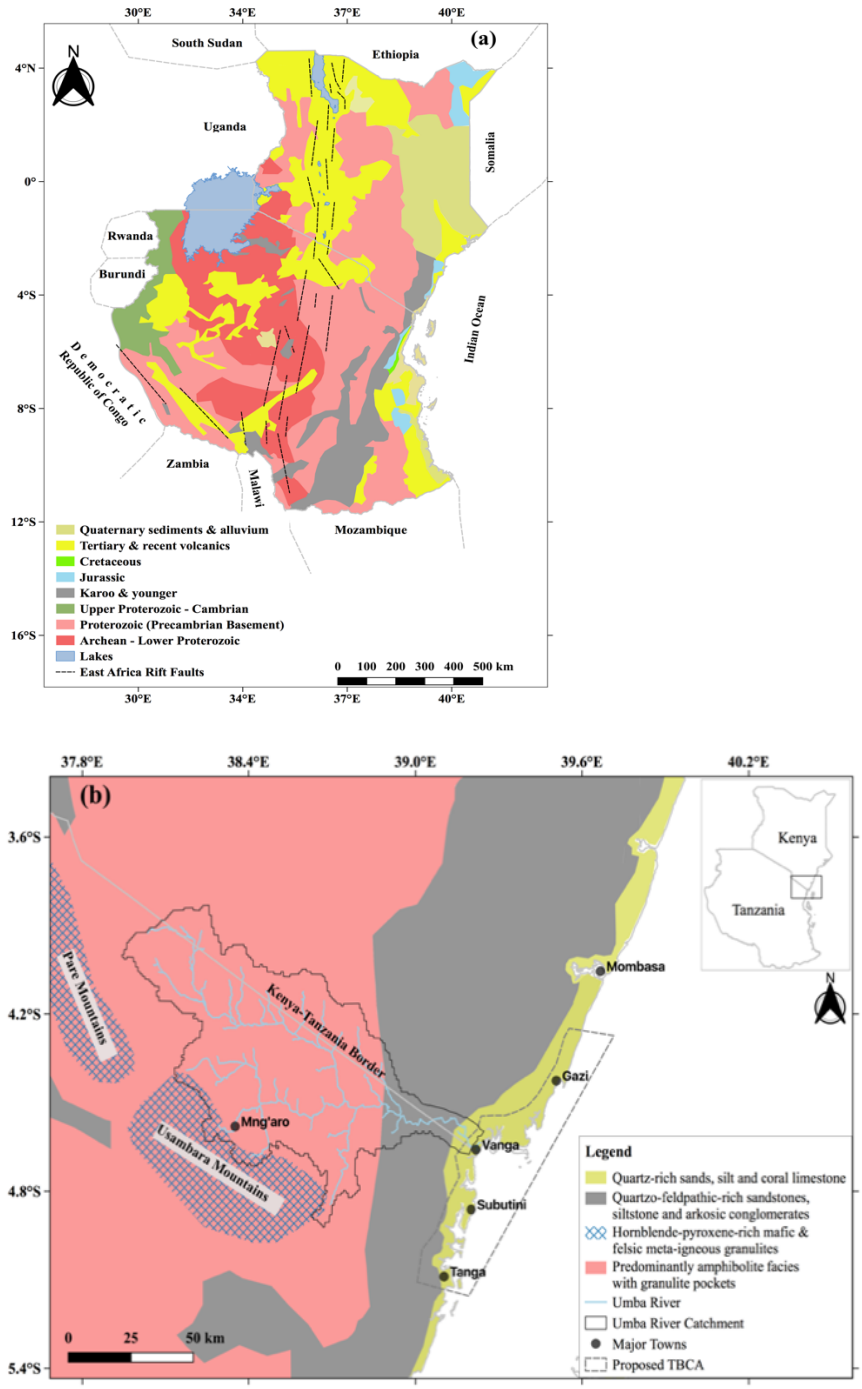

Figure 3-1: Map showing the regional geology and the key stratigraphic units (a) and the general geology and the dominant lithologies of the Umba River catchment from its upper reaches in Mng'aro, Tanzania to the river mouth in Vanga, Kenya in the lower reaches (b). Inset is a map of Kenya and Tanzania (b). Maps are modified from Akech et al., 2013; Maboko and Nakamura, 2002; Schlüter, 1997.

The quartzo-feldspathic and hornblende-pyroxene granulites area characterized by varying portions of quartz, K-feldspars, plagioclase, hornblende, pyroxenes, biotite, magnetite and accessorized by apatite, ilmenite and zircon (Maboko and Nakamura, 2002; Manya et al., 2007; Shackleton, 1993). Close to the source of the Umba River in Usambara mountains, the Precambrian basement and the associated lithologies are highly weathered and degraded at the surface, forming reddish-brown soils. Further downstream, warping along the eastern border of the Precambrian, towards our study site in both, Kenya and Tanzania towards our study site, Paleozoic rocks crop out, mainly belonging to the Karoo Supergroup. Here, due to extensive agriculture and transition to sedimentary and meta-sedimentary rock lithologies, the soils exhibit a dark-brown coloration (Akech et al., 2013; Maboko and Nakamura, 2002; Mutakyahwa et al., 2003). Close to the coast, the Umba River crosses Quaternary sediments (Figure 3-1b) composed mainly of quartz and calc-silicate minerals (Cairncross, 2019; Schlüter, 1997).

3.1.3 Study Site

The Umba River originates in the tectonically uplifted Usambara Mountains in Mkinga, Tanzania, with an elevation of *ca*. 2000 m above mean sea-level, and drains to the Indian Ocean in Vanga, Kenya (Figure 3-2). The mangroves of Vanga at the south coast of Kenya (Figure 3-2) receive terrigenous sediments from the relatively short, *ca*. 200 km long Umba River. It drains a catchment of *ca*. 8000 km^2 (IUCN, 2003). Part of the study area lies within a proposed Transboundary Conservation Area (TBCA) between Kenya and Tanzania (Figure 3-2), which extends south from Diani within the Kwale County in Kenya (39° 00′ E, 4° 25′ S) to Tanga within the Mkinga District in Tanzania (39° 40′ E, 5° 10′ S) covering a north-south distance of *ca.* 120 km and a narrow strip along the coastline in Kenya and Tanzania, with an estimated total area of *ca*. 2500 km^2. The TBCA intends to integrate and align coastal conservation and management in an ecologically connected region transcending the Kenya-Tanzania border. The proposed TBCA will have significant ecological

significance mainly because it is characterized by contiguous and connected marine and terrestrial habitats as well as similar and shared socio-economic status (Fortnam et al., 2020). Sampling for the present study was done at seven stations along the Umba River from source to mouth. Stations S1, S2, and S4 are located on the Tanzanian side while Stations S5, S6, S7, and S8 are on the Kenyan side (Figure 3-2).

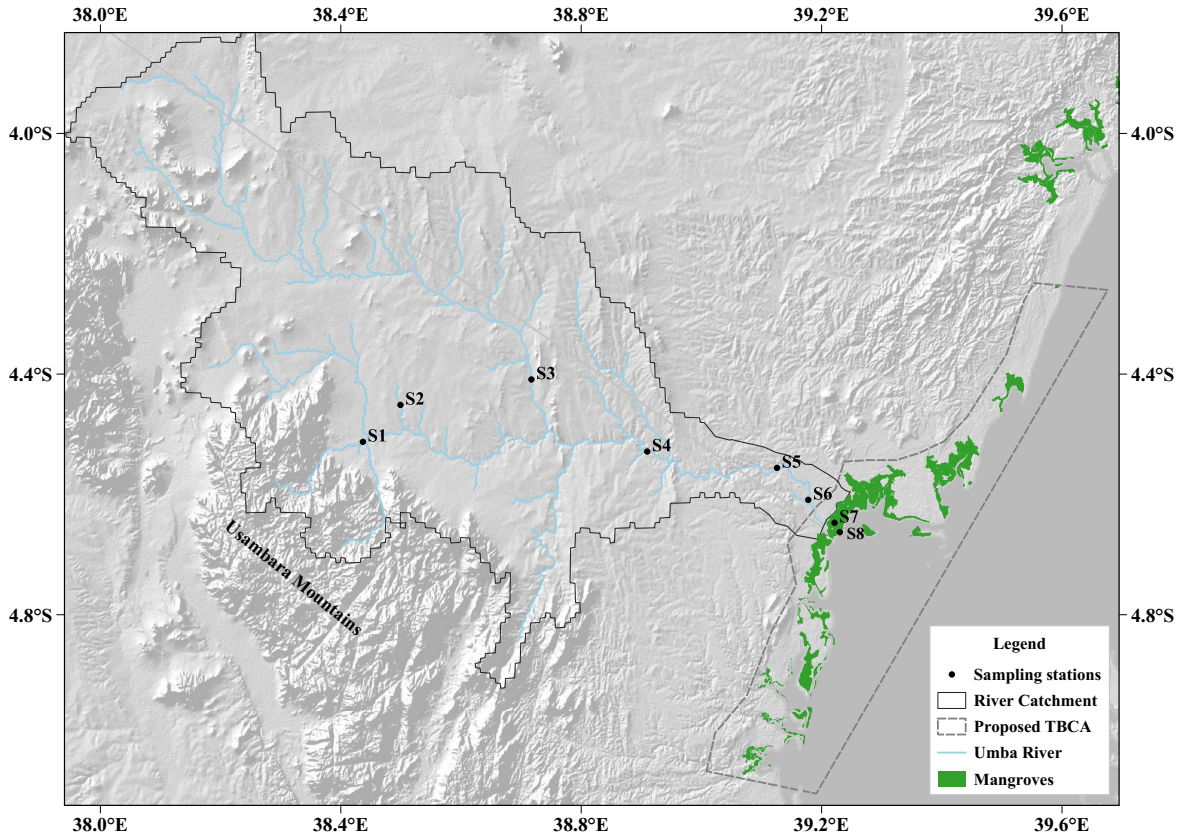

Figure 3-2: The study site within the Umba River catchment and sampling locations along the Umba River. Station S1, S2, S3 and S4 in Tanzania and S5, S6, S7 and S8 in Kenya.

3.2 Materials and samples

Riverbank (*n=32*) and bottom (*n=26*) sediment samples were collected from the Umba River in Tanzania and Kenya during the transition period between the dry season and the rainy seasons (June - July 2019). The sediment samples were collected along the course of the river at five upstream riverine stations (S1, S2, S4, S5 and S6), one downstream estuarine station (S7), and one marine station in the river mouth (S8). Riverbank samples were collected on either side of the river above

the waterline, while the bottom samples were taken - where accessible - in the middle of the river channel. All samples collected at station S7 and S8, were considered as bottom sediments due to the daily inundation by flood tides. Riverbank sediments were collected using a pre-cleaned hand-held shovel, while the estuarine and marine sediments were sampled using a hand-held Van Veen grab sampler at water depths between 5 and 10 m. The sediment samples were assumed to have been recently deposited, without significant post-depositional reworking. Three replicates of sediment samples in each station were collected and placed in sealed plastic bags for transport to the lab. Aliquots of the sampled sediments were obtained for petrographic, grain size and geochemical analyses

3.2.1 Grain size analysis

Grain size analysis of the bulk river sediment samples was conducted at the Kenya Marine and Fisheries Research Institute, Kenya, laboratory using a Malvern© Mastersizer 2000 laser diffraction particle size analyzer. Sediment pre-analysis treatment including removal of organic matter using 30% hydrogen peroxide and clastic grains >2 mm (Hossain et al., 2017) was undertaken before measurement of grain sizes. Mean grain size (μm) was estimated according to Folk and Ward (1957).

3.2.2 Petrographic analysis

Thin sections were prepared at the Leibniz Centre for Tropical Marine Research (ZMT), Germany, geology laboratory according to protocols in (Camuti and McGuire, 1999; Murphy, 1986). Small blocks (4 cm × 4 cm) of dried sediment samples were bound together with Araldite 20/20 resin. The blocks were hardened and after 24 hrs, one side of the block was ground to obtain a plain surface without scratches. The plain surface was cleaned in an ultrasonic-bath and dried. The dried block was fixed with resin on a glass-slide and bound together using a press-system. Once it was bound together and hard-dried again for another 24 hrs, the block was cut into 1 mm slices and polished parallel to the glass slide to obtain one single thin section.

The 1 mm sample was then ground on the slide down to 100 µm and further ground to 28 µm suitable for mineralogical analyses. The thin sections were examined under an optical polarized light in LEICA DM500-EP microscope.

3.2.3 Major and trace elements

In the laboratory, wet sediment samples were dried at 60 °C for 48-72 hrs, pulverized and homogenized using a Fritsch© Planetary Micro ball-mill Pulverisette 7. 700 mg of each sample was mixed with 4200 mg di-lithium tetraborate (Spectro-melt A10, $B_4Li_2O_7$) and pre-oxidized with 1000 mg ammonium nitrate at 500 °C. The sample mixtures were then digested (melted) at 1340 – 1350 ˚C in a CIMREX™ 10 microwave accelerated reaction system, using a combination of HF + HNO_3 + H_3BO_3 for major and trace element analyses (Gupta and Bertrand, 1995; Pruseth et al., 2005; Zhuchenko et al., 2008) and then fused to homogeneous glass pellets (beads). The pellets were then analysed in PANalytical© AXIO Max (3 kW) by wavelength-dispersive X-ray fluorescence (XRF). Major elements (as oxides) were reported in wt. % while the trace elements are given in ppm (Zindorf et al., 2020). The accuracy of the analytical procedures was verified by analyzing three certified standard reference materials (SRMs) namely PACS, MESS and PS-S. The major elements measured included Si, Ti, Al, Fe, Mn, Mg, Ca, K, Na and P. The oxides of major elements were also used to constrain and assign the sediment provenance using first and second discriminant functions (DF1 and DF2) analysis (Ali et al., 2014; Baiyegunhi et al., 2017; Bhat et al., 2019). Large-ion lithophile elements (LILE) including Rb, Ba, Sr, Th, U and Ce were measured. The high field strength elements (HFSE) including Zr, Y and Nb were also measured, as were the transition trace elements (TTE), i.e., Cr, Co, Cu, Ni, Zn, Ga, Mo and Pb.

3.2.4 Degree of weathering and chemical alteration

Several weathering indices are available to evaluate mineralogical maturity, chemical alteration and element mobility (Baiyegunhi et al., 2017; Depetris et al., 2014; Shao

et al., 2012; Shao and Yang, 2012). The underlying principle of weathering indices is the comparison of mobile elements with immobile elements such as Al as the reference (Campodonico et al., 2016). Such immobile elements are less susceptible to alteration and weathering. They therefore retain their chemical characteristics over longer periods and longer distances of transportation by rivers. In this study, the chemical index of alteration (CIA) was used to evaluate the degree of feldspar alteration, calculated using the equation of (Nesbitt and Young, 1984):

$$CIA = [Al_2O_3 / (Al_2O_3 + CaO^* + Na_2O + K_2O) \times 100]$$

The CIA is represented in molecular proportions, where CaO* represents the Ca in silicate fraction only, adjusted for other Ca-bearing minerals such as carbonates (Nesbitt and Young, 1982). The abundances of the major elements were used to evaluate the chemical composition and provenance of Umba River sediments following the rationale described in (Baiyegunhi et al., 2017; Campodonico et al., 2016; Sensarma et al., 2008). To further evaluate the effect of transport and weathering, ternary plots were generated from the major elements' composition of Umba River sediments (Nesbitt and Young, 1984). Specifically, ternary plots were created showing the concentration on Al_2O_3 - ($CaO + Na_2O$) - K_2O, hereafter referred to as A-CN-K, and Al_2O_3 - ($CaO + Na_2O + K_2O$) - ($Fe_2O_3 + MgO$), hereafter referred to as A-CNK-FM, ternary plots were used. The position of sediments within the ternary diagrams indicates the dominant minerals, degree of weathering, mineral sorting and therefore the source geology. Specifically, A-CN-K and A-CNK-FM plots assists in the understanding of feldspar weathering and the effects of sorting on weathering of Fe-Mg bearing minerals respectively (Baiyegunhi et al., 2017; Sensarma et al., 2008).

3.2.5 Provenance

The compositional data of the Umba River sediments was also used to constrain their sedimentary provenance. Discriminant function (DF) plots expresses oxides various

elements as ratios with the immobile Al_2O_3 (Baiyegunhi et al., 2017). DF analysis based on oxide ratios distinguishes the provenance of sediments between four fields, namely mafic igneous, felsic igneous, intermediate igneous, and quartzose (recycled) sedimentary provenance (Baiyegunhi et al., 2017; Hossain et al., 2017). DF analyses based on raw oxides are represented by the following equations;

Discriminant Function (DF1) = (30.638 TiO_2 / Al_2O_3) – (12.541 Fe_2O_3 / Al_2O_3) + (7.329 MgO / Al_2O_3) + (12.031 Na_2O / Al_2O_3) + (35.402 K_2O / Al_2O_3) – 6.382

Discriminant Function (DF2) = (56.500 TiO_2 / Al_2O_3) – (10.879 Fe_2O_3 / Al_2O_3) + (30.875 MgO / Al_2O_3) – (5.404 Na_2O / Al_2O_3) + (11.112 K_2O / Al_2O_3) – 3.89

3.3 Statistical analyses

Statistical analyses were performed using inbuilt R-program (v. 1.1.463) libraries and packages (R Core Team, 2020). Significant difference tests of major and trace elements concentrations, between sediment type (riverbank or bottom sediments) and environment (riverine, estuarine and marine) were assessed by performing an analysis of variance (ANOVA). Data conformity to normal distribution were examined using the Shapiro-Wilk test of normality.

3.4 Results

Mean concentrations of major and trace elements of the Umba River sediments are presented in Table 1 and the primary dataset in the Supplementary Information 3-1. Detailed results of the statistical analyses are summarized in Supplementary Information 3-2. From the performed statistical analysis, some oxides and trace elements showed significant variability ($p < 0.05$) between the sediment types (riverbank and bottom sediment), and some among environments (riverine, estuarine and marine). Despite the significance difference, both riverbank and bottom sediments showed similar distribution trends from source to mouth.

3.4.1 Grain size distribution

The Umba River sediments are composed of sand, silt and clay in different proportions (Table 3-1; Figure 3-3). The mean grain size (μm) of riverbank and bottom sediments is at 172 μm and 266 μm, respectively (see Table 1). The mean dominant fractions are sand and silt, ranging between 34% and 78%, and silt, ranging between 0.72 and 62% of total volume percentages. Clay constitutes less than 3% in both, riverbank and bottom sediments with an overall range between 0.07 and 2.90%. The grains size gradient is typical for rivers and transitions from predominantly coarse sandy sediments in the upper catchment (S1, S2, S4, S5 and S6), to sandy-silt-sized with clay in the estuary (S7) and silty-sand-sized sediment at the marine site (S8) (Figure 3-3 and Table 3-1). Clay-sized particles were most abundant in the estuarine stations (S7) compared to all the other stations.

Table 3-1: Grain size distribution (in μm), major element (in wt. %) and trace elements (in ppm) contents in riverbank and bottom sediments of Umba River.

Sample Station	Riverbank sediments					Bottom sediments				
	S1	S2	S4	S5	S6	S1	S2	S4	S7	S8
Grainsize distribution										
Mean grain size (μm)	160.36	90.44	394.14	109.88	106.37	90.41	141.41	861.41	72.49	166.32
Sorting (σ_g)	3.87	3.32	3.04	3.58	4.92	3.58	3.56	1.75	4.03	2.57
Skewness (Sk_g)	-0.23	-0.27	-0.25	-0.25	-0.28	-0.14	-0.18	-0.13	0.08	0.01
Kurtosis (K_g)	0.80	1.06	1.28	1.06	0.92	0.95	1.05	0.93	0.98	0.89
Sand (%)	60.78	63.75	67.04	58.51	57.79	59.12	70.94	65.69	34.23	78.83
Silt (%)	33.43	34.84	16.98	39.04	37.06	39.21	25.86	0.72	62.08	20.14
Clay (%)	0.22	1.41	0.07	1.75	2.06	0.72	0.81	0.07	2.90	1.03
Major elements (wt.%)										
SiO_2	57.05	56.26	70.43	62.39	53.30	61.70	63.75	76.22	55.67	71.47
TiO_2	1.12	0.82	1.76	1.45	0.90	0.97	1.04	0.73	0.80	0.70
Al_2O_3	16.50	18.50	10.45	15.33	19.06	15.43	14.60	9.90	17.12	11.18
Fe_2O_3	8.50	7.27	7.48	7.25	8.36	8.17	7.72	4.30	7.61	3.95
MnO	0.23	0.12	0.12	0.13	0.15	0.18	0.15	0.07	0.12	0.09
MgO	1.84	1.71	1.72	1.71	1.40	1.81	1.81	1.42	1.52	1.50
CaO	4.04	3.61	2.65	2.90	1.88	3.25	3.47	2.44	1.52	4.45
Na_2O	1.92	2.26	1.59	2.14	1.21	2.12	2.21	1.75	1.88	2.75

K_2O	1.23	1.50	1.40	1.66	1.48	1.12	1.34	1.58	1.39	1.53
P_2O_5	0.11	0.18	0.09	0.14	0.24	0.17	0.13	0.08	0.21	0.10
SO_3	0.01	0.02	0.02	0.03	0.02	0.00	0.01	0.01	0.13	0.04
LOI	7.01	7.56	2.04	4.60	11.79	4.91	3.60	1.26	11.86	2.04
Total	99.56	99.79	99.74	99.72	99.78	99.82	99.81	99.76	99.83	99.80
CIA	58.43	60.83	53.98	58.91	73.13	59.16	56.20	52.04	68.01	44.50
ICV	1.18	0.95	1.63	1.17	0.81	1.15	1.22	1.25	0.91	1.35
K_2O+Na_2O	3.15	3.76	2.99	3.81	2.68	3.24	3.54	3.33	3.27	4.28
K_2O/Na_2O	0.73	0.69	0.92	0.81	1.37	0.53	0.61	0.93	0.77	0.56
Al_2O_3/SiO_2	0.30	0.34	0.15	0.25	0.37	0.25	0.23	0.13	0.34	0.16
Fe_2O_3/SiO_2	0.15	0.13	0.11	0.12	0.16	0.13	0.12	0.06	0.15	0.06
Trace elements (ppm)										
Ce	51.33	46.00	86.17	76.50	70.60	47.00	47.67	32.33	55.53	34.00
Co	20.22	16.67	13.17	16.17	23.20	16.50	14.67	10.00	16.47	8.67
Cr	70.67	45.83	236.67	92.83	92.00	61.50	45.67	133.33	80.87	51.33
Cu	53.44	51.50	13.33	28.33	69.00	36.00	29.00	8.00	51.07	5.00
Ga	16.33	17.33	9.00	14.50	19.60	15.50	13.00	8.67	17.13	8.67
Mo	2.00	1.17	2.00	1.67	1.60	1.50	1.67	2.33	3.07	1.67
Nb	12.67	9.83	17.67	18.00	14.20	10.00	12.00	8.67	12.07	9.00
Ni	28.89	22.00	43.67	30.00	48.40	24.50	17.00	34.33	38.47	10.00
Pb	7.78	6.33	5.83	10.50	11.40	6.50	4.33	6.00	9.53	6.67
Ba	1004.6	1034.2	842.33	1065.33	898.40	803.50	895.67	959.33	635.33	974.00
Rb	34.44	35.67	29.50	45.00	60.00	28.50	27.67	31.67	55.00	28.67
Sr	350.00	438.17	300.17	382.83	263.20	333.50	387.33	329.67	232.80	472.67
Th	4.56	4.00	11.17	6.83	6.00	4.50	3.67	4.00	6.13	3.67
U	-0.67	-1.00	-0.33	-0.33	-0.60	-0.50	-1.33	-0.33	0.80	0.33
V	168.67	147.67	183.83	166.17	161.00	153.00	167.33	98.00	141.20	81.67
Y	19.44	17.00	20.33	21.67	23.80	17.00	20.67	11.67	19.33	13.00
Zn	105.22	74.83	53.67	70.33	89.20	87.50	64.33	34.00	74.60	39.67
Zr	258.78	184.83	541.00	417.50	169.80	238.00	266.33	349.33	255.27	291.33
Cr/Ni	2.63	2.15	3.54	3.71	1.96	2.55	2.77	3.99	2.51	5.11
Rb/Sr	0.10	0.08	0.10	0.12	0.26	0.09	0.07	0.10	0.24	0.06

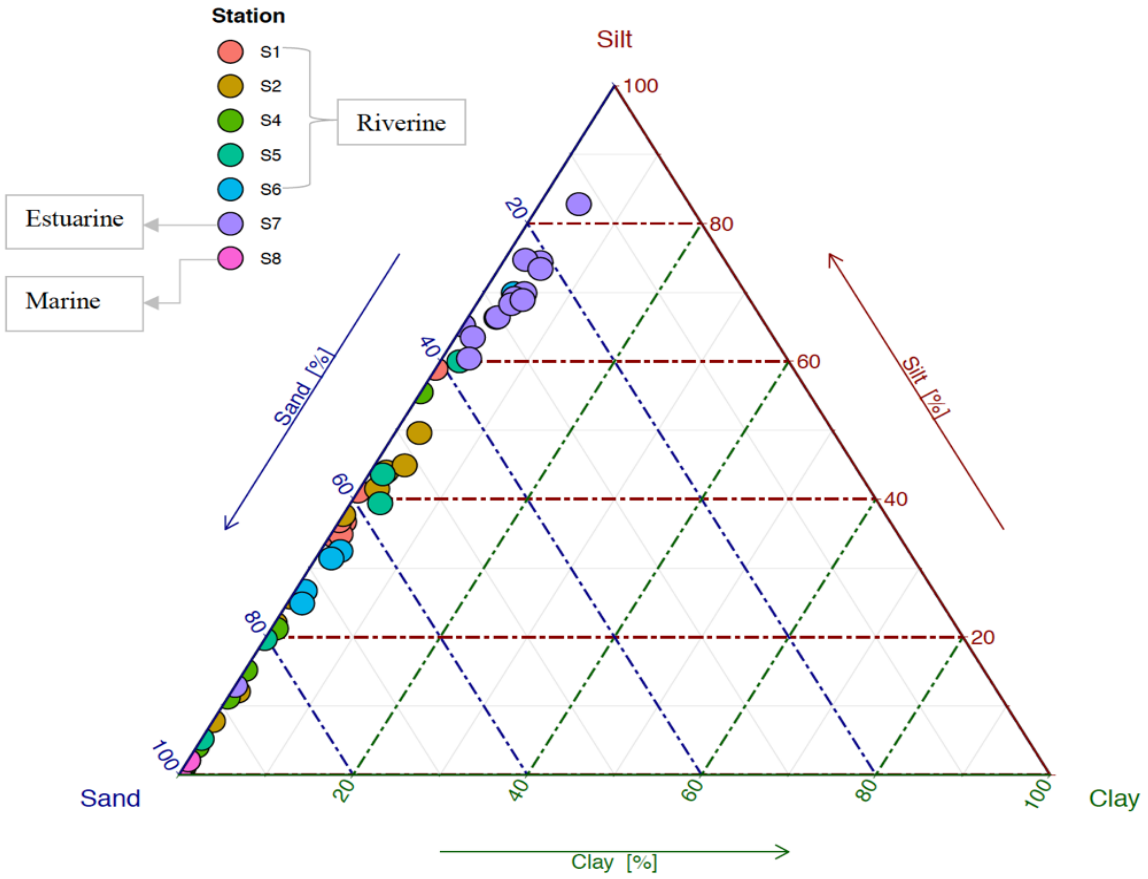

Figure 3-3: Ternary diagram showing textural distribution of sediments during the transition period (July 2019). With S1 -S6 being upstream riverine stations and S7 and S8 being downstream estuarine and marine stations respectively.

3.4.2 Mineralogy of Umba River sediments

The mineralogical composition identified by petrographic analyses is similar for the upstream riverine sediments and the downstream estuarine and marine sediments (Figure 3-4 and Figure 3-5). All sediments along the entire course of the Umba River (Figure 3-2) contain mainly K-feldspar, lamellar and striated plagioclase, quartz, muscovite, biotite and hornblende. Accessory minerals include opaque and clay minerals that were not further identified here. However, from comparison of site-relevant literature (Maboko and Nakamura, 2002; Mutakyahwa et al., 2003) we infer that the opaque minerals include magnetite, ilmenite and maghemite. Additionally, clay minerals such as kaolinite and illite are also reported for the Umba River catchment .

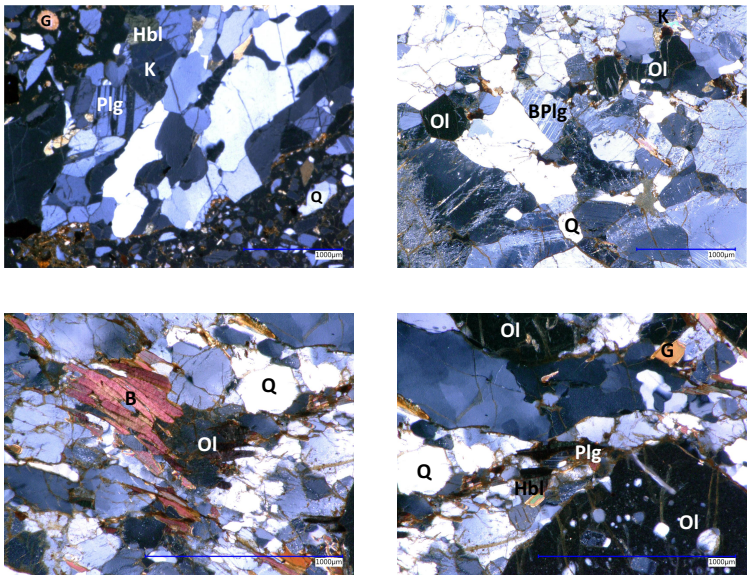

Figure 3-4: Photomicrographs of individual lithoclasts in upstream sediments (left to right: stations S1 and S4 (top row) and station S5 and S6 (bottom row). K = K-feldspar, BPlg = Banded plagioclase, G = Garnet, Q = Quartz, Hbl = Hornblende, B = Biotite, Ol = Olivine.

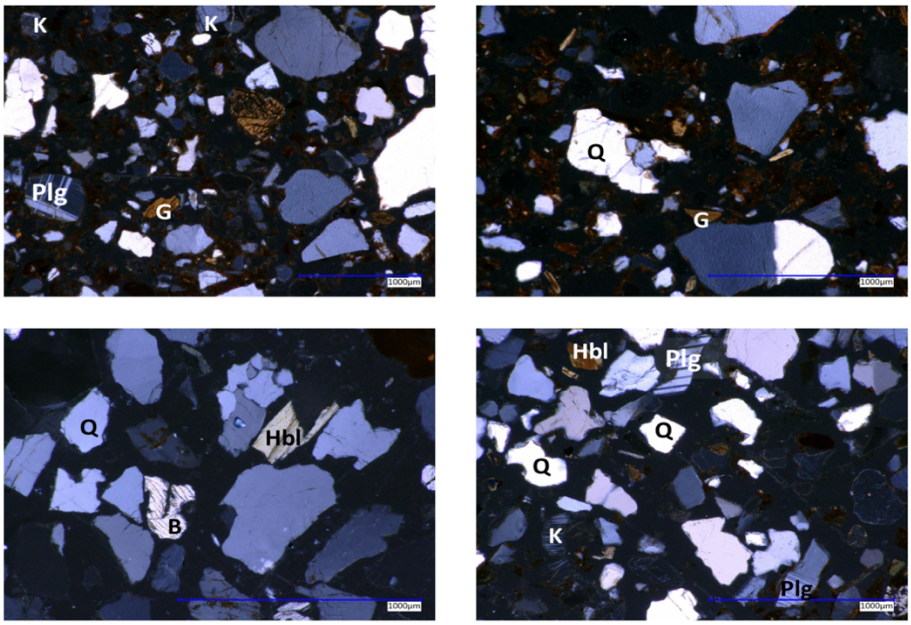

Figure 3-5: Photomicrographs of individual mineral lithoclasts in downstream sediments embedded in epoxy resin. Top row S7 (estuary), bottom row S8 (marine setting). K = K-Feldspar, Plg = Banded plagioclase, G = Garnet, Q = Quartz, Hbl = Hornblende, B = Biotite.

The quartz crystals occur as elongated and deformed lenticular grains. They are also present in lithoclasts, where they exhibit anhedral shapes adjacent and surrounding feldspar, biotite and other minerals. In the lithoclasts, the feldspars (K-feldspars and plagioclase) exhibit tabular and irregular crystals (Goswami and Bhattacharyya, 2014). The sediments collected in the downstream stations (S7 and S8) show evidence of river transportation or high energy environments characteristic of intertidal areas due to their relatively rounded shapes (Figure 3-5). From source to mouth, a decrease in lithoclasts sizes is observed that goes along with an increase of monocrystalline grains (as opposed to lithoclasts made up of multiple crystals) (Figure 3-4 and Figure 3-5). Downstream sediments (Figure 3-5) exhibit poor grain sorting and varying degrees of roundness of the individual clasts.

3.4.3 Major elements

The sediments exhibit a relatively narrow SiO_2 range in both, riverbank sediments (53.30 – 70.43 wt. %, with an average of 59.89 wt.%) and bottom sediments (55.57 – 76.22 wt.%, with an average of 65.76 wt. %) (see Table 1). Highest SiO_2 contents coincide with coarse-grained sediments, for example, in station S4 for riverbank, and S8 for bottom sediments. Low SiO_2 content (55.67 wt.%) is observed in the estuarine silty sands collected in station S7 (see Table 1). The Al_2O_3 content varies between 10.45 and 19.06 wt.% (average of 15.97 wt.%) in riverbank sediments, and between 9.90 and 17.12 wt.% (average of 13.64 wt.%) for bottom sediments (see Table 1 and Supplementary Information 3-1). Fe_2O_3 and TiO_2 contents were > 5 wt.% and < 2 wt.%, respectively, in both riverbank and bottom sediments. The immobile Al_2O_3 shows a clear negative relation with SiO_2 in both riverbank and bottom sediments (Figure 3-6a). There is no particular trend on Al_2O_3 versus TiO_2 in riverbank sediments but a positive relation in the bottom sediments (Figure 3-6b). Al_2O_3 also shows a positive relation with Fe_2O_3 and P_2O_5 in both, riverbank and bottom sediments (Figure 3-6c and 3-6d).

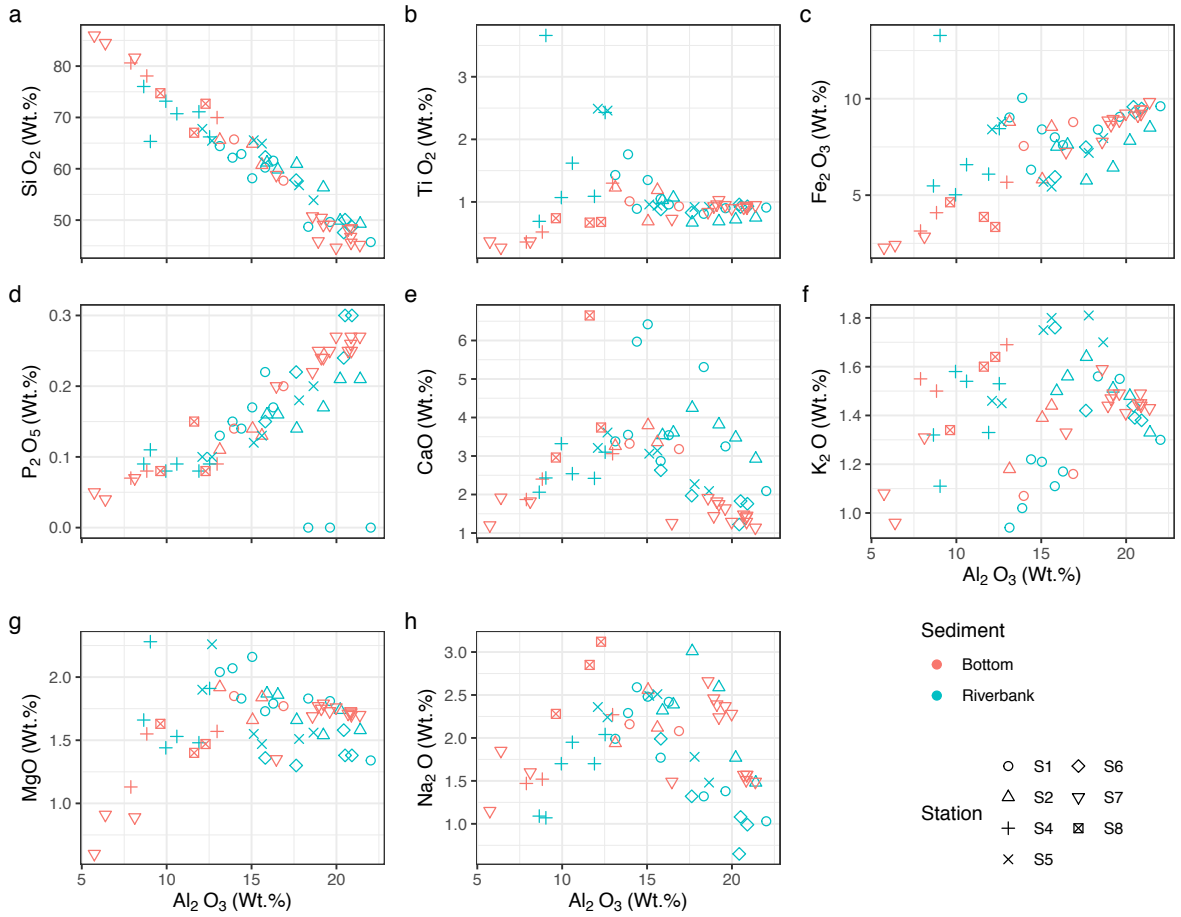

Figure 3-6: Major oxides (wt.%) plots for the Umba River riverbank and bottom sediments referenced to the immobile Al_2O_3. Strong relations are observed between the abundances of SiO_2 (negative), Fe_2O_3 (positive) and P_2O_5 (positive) with Al_2O_3 (Figure 3-6a, 3-6c and 3-6d respectively).

The alkaline oxides, i.e., K_2O, Na_2O and MgO, are relatively high (> 1 wt.%) in all stations and in both, riverbank and bottom sediments (see Table 1; Supplementary Information 3-1). However, on average K_2O and MgO are slightly higher in riverbank sediments compared to bottom sediments (1.46 and 1.68 wt.% respectively). Na_2O content is highest (2.14 wt.%) in bottom sediments (see Table 1). Additionally, the total alkali content (K_2O + Na_2O) and the alkali ratios (K_2O/Na_2O) in all stations is >2.5% and >0.5, respectively, in both riverbank and bottom sediments (see Table 1). The sediments exhibit a wide range of CaO values in riverbank (1.88 - 4.04 wt.%, average of 3.01 wt.%) and in bottom sediments (1.52 – 4.45 wt. %, average of 3.03

wt.%) (see Table 1). A negative relation between Al_2O_3 and CaO (Figure 3-6e) and K_2O (Figure 3-6f) is observed in riverbank as well as in bottom sediments. Additionally, CaO is relatively depleted in estuarine sediments (S7) compared to riverine and marine sediments. MgO and N_2O both show a positive but scattered relation with the immobile Al_2O_3 (Figure 3-6g and 3-6h respectively). Major element ratio Al_2O_3/SiO_2 vs. Fe_2O_3/SiO_2 exhibit a wide variation of all the grain size fractions and covering the entire quartz–clay spectrum (Figure 3-7). The larger grain size fractions (e.g., S4, S6, S8) show similar enrichment of Fe and Al, as exhibited by the fine fraction and relatively clay-rich estuarine sediments (S7).

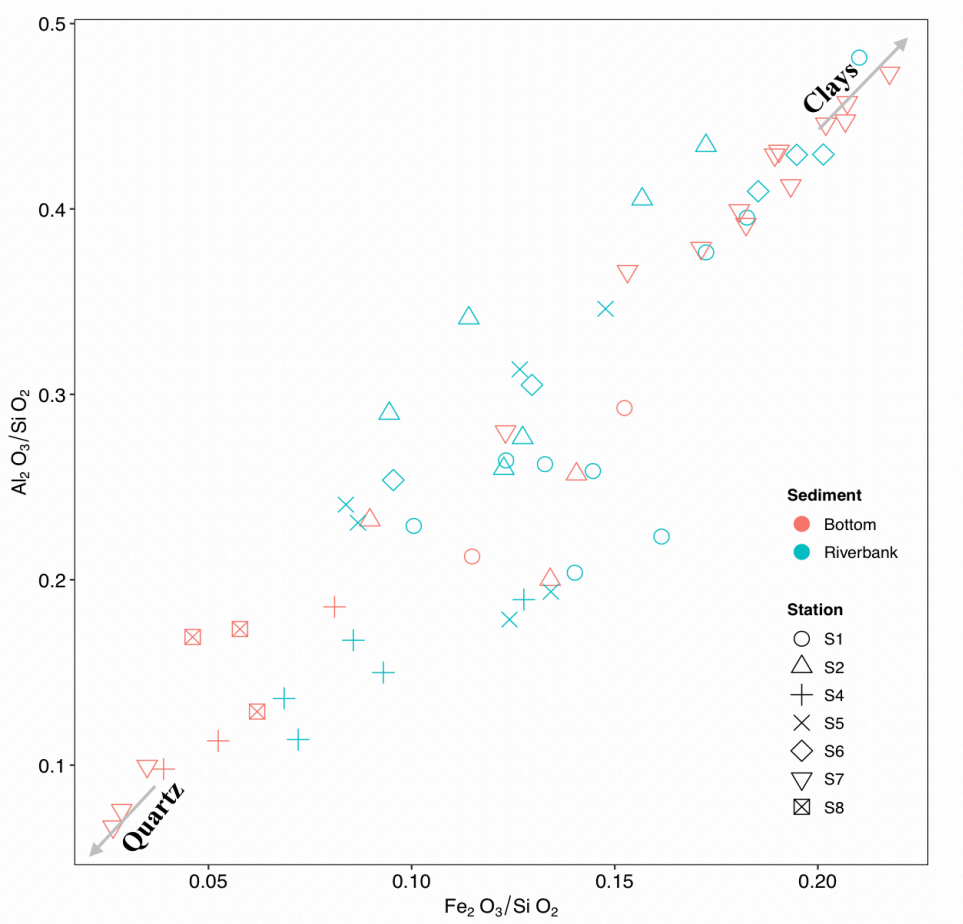

Figure 3-7: Variation of Al_2O_3/SiO_2 vs Fe_2O_3/SiO_2 ratios in Umba River sediments showing the distribution of Fe and Al elements in estuarine mud/silt sediment collected in station S7across the entire quartz-clay spectrum.

3.4.4 Trace elements

Average concentrations of the trace elements Cr, Ni and Zn are all enriched in riverbank sediments compared to bottom sediments (see Table 1, Supplementary Information 3-1). Cr concentration ranges between 25 and 346 ppm with an average of 107.60 and 34.59 ppm in riverbank and bottom sediments, respectively. Ni concentration ranges between 5 and 73, again showing a higher average of 34.59 ppm in riverbank sediments compared to bottom sediments (24.86 ppm) (see Table 3-1; Supplementary Information 3-1). Cr and Ni concentrations are depleted in marine bottom sediments collected in station S8 (see Table 3-1). Zr concentration shows values ranging between 169 and 541 ppm (average value of 314 ppm) for river bank sediments compared to bottom sediments that show slightly lower values ranging between 238 and 349 ppm (average of 280 ppm) (see Table 3-1). On the contrary, Sr concentration is enriched in marine (472 ppm) and riverine sediments (majority >300 ppm) (see Table 3-1) while they are depleted in bottom estuarine sediments (232.80 ppm). The Ba content is slightly enriched in both riverbank and bottom sediments (majority >800 ppm) while the lowest Ba content of 635.33 ppm is recorded in estuarine bottom sediments (see Table 3-1). The Rb/Sr ratios are similarly low (< 0.5) in all the stations and in both, riverbank and bottom sediments, ranging between 0.06 and 0.26 with average values of 0.13 and 0.11 in riverbank and bottom sediments, respectively (see Table 3-1). Such low Rb/Sr ratios indicates low to moderate chemical weathering. A less distinct and scattered relation is observed between Al_2O_3 and Sr (Figure 3-8a) while Al_2O_3 vs. Zr show a distinct negative relation (Figure 3-8b) in both riverbank and bottom sediments. On the contrary, strong positive relations are observed between Al_2O_3 and the immobile elements Ni, Zn, Cr and Rb (Fig 3-8c, 3-8d, 3-8e and 3-8f respectively). Relatively high positive relations are also observed between Sr and CaO as well as between the immobile Ba and K_2O (Figure 3-8g and 3-8h respectively) in both, riverbank and bottom sediments.

Generally, a low concentration of Sr and Ba in the bottom sediments collected in the estuarine station S7 is evident (see Figure 3-8a, 3-8g and 3-8h).

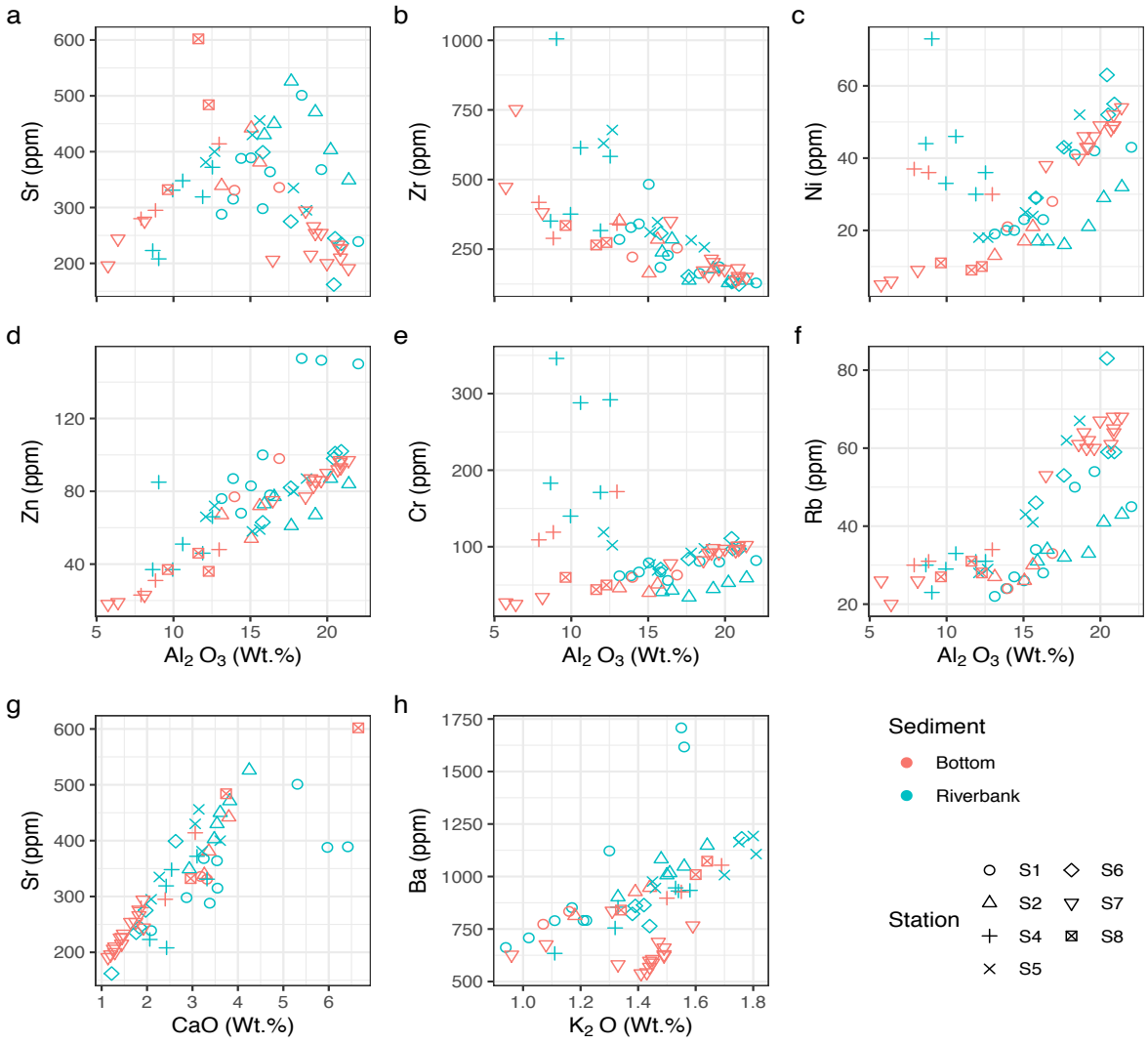

Figure 3-8: Showing selected trace element variations with respect to the immobile Al_2O_3 wt. % in Umba River sediments. Sr show positive but scattered (Figure 3-8a) relation compared with Zr (Figure 3-8b) which shows negative relation with Al_2O_3 (Figure 3-8b). Ni, Zn, Rb, Cr and Rb (in ppm) show good positive relation with Al_2O_3 in both riverbank and bottom sediments (Figure 3-8c, 3-8d, 3-8e and 3-8f respectively). Sr (Figure 3-8g) and Ba (Figure 3-8h) maintain a positive relation with alkali CaO and MgO respectively, with relatively low Sr and Ba (in ppm) in bottom estuarine sediments.

3.4.5 Elemental ratios and weathering indices

The major and trace elements were normalized to the upper continental crust (UCC) using values from Rudnick and Gao (2003). The relative averages of the major elements show similarity with UCC values, however, the relative Na_2O, K_2O and MgO (< 0.70) concentrations are generally low compared to UCC and relative to the immobile Al_2O_3 (Figure 3-9a). Additionally, SiO_2 show a marked similarity with UCC with no discernible enrichment. The average trace element compositions of the sediments show a variability that is quite comparable to other documented values from the same region (Maboko and Nakamura, 2002; Mutakyahwa et al., 2003). The general pattern shows a strong depletion in Rb relative to Ba, and depletion of Th and U relative to Sr (see Figure 3-9b).

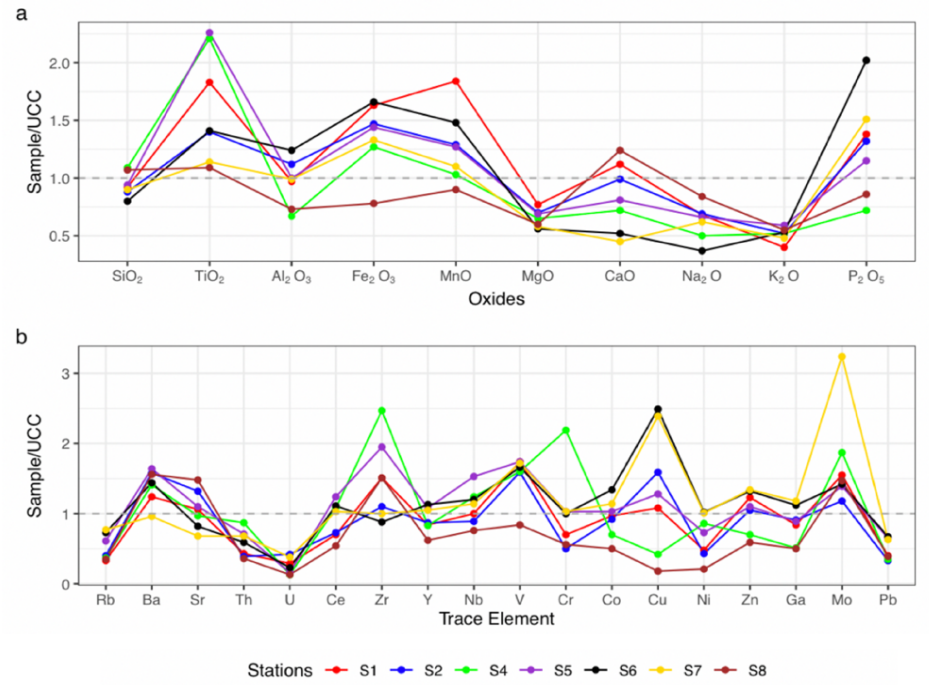

Figure 3-9: Major element oxides (a) and trace element (b) spider plot of Umba sediments normalized against the upper continental crust (UCC) values from Rudnick and Gao (2003). Major elements are normalized as oxides and trace elements as ppm. Mobile major elements (MgO, CaO, Na_2O and K_2O) and trace elements (Rb, Th and U) are relatively depleted relative to UCC.

The average upper continental crust (UCC) has a CIA value of 50, and weathered residual clay has a CIA value close to 100 (McLennan, 1993; Rudnick and Gao, 2003). The CIA of the Umba River sediments show a wide range, with CIA values ranging between 39 and 81 (Figure 3-10 and Supplementary Information 3-1).

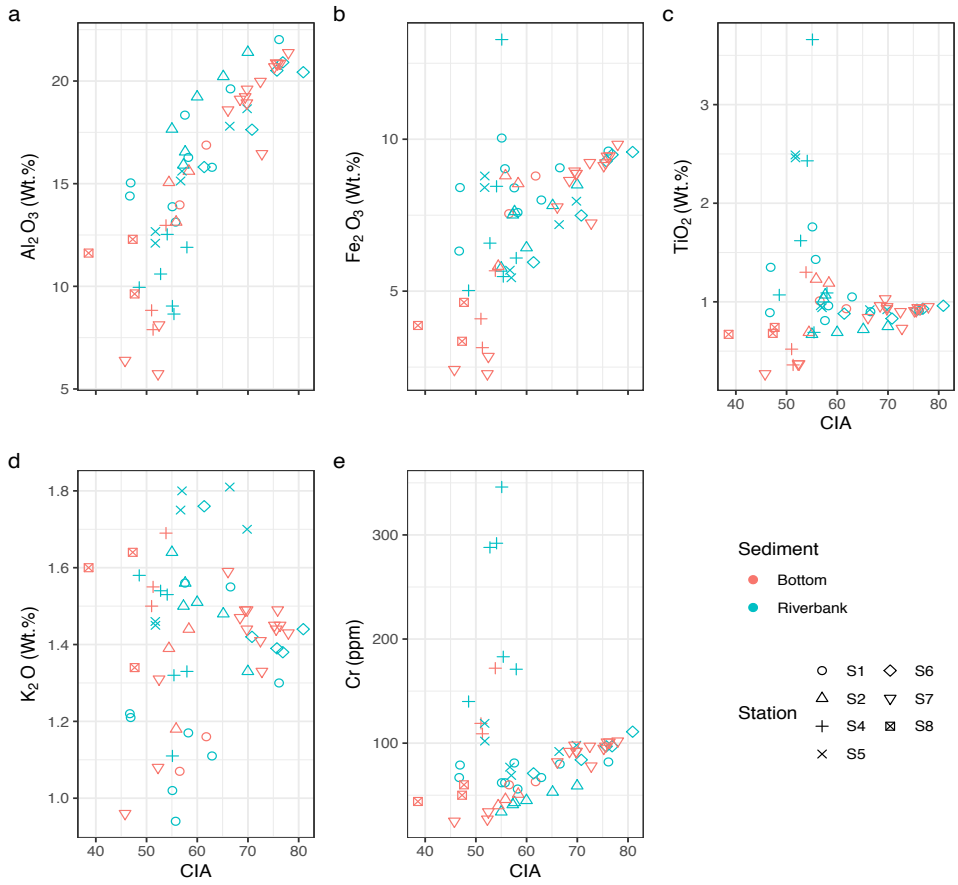

Figure 3-10: Plots of selected major and trace elements vs. the chemical weathering index (CIA) of Umba River sediments. CIA are defined as [Al_2O_3 / (Al_2O_3 + CaO + Na_2O + K_2O)] × 100 in molecular proportions [41,45]. Bottom estuarine samples (S7) show high major oxides variation at different contents CIA. Immobile and less soluble elements (Al_2O_3, TiO_2 and Cr) show increases with increasing CIA (Figure 3-10a, 3-10c and 3-10e respectively).

Within this range, the mean CIA values are higher in riverbank sediments ranging between 53.98 and 73.13 compared to the bottom sediments with values ranging between 52.04 and 68.01 (Table 3-1). The marine bottom sediments (collected in station S8) have the lowest CIA (Figure 3-10 and Table 3-1). The riverbank as well as

the bottom river sediments show a positive relation between CIA and Al_2O_3 and $Fe_2O_3 \geq 50$ (Figure 3-10a, 3-10b). They also show elevated Al_2O_3, Fe_2O_3 and TiO_2 at higher CIA values of > 70, while in contrast the bottom marine sediments have lower Al_2O_3, Fe_2O_3 and TiO_2 at CIA values of < 50 (Figure 3-10a, 3-10b, 3-10c). The bottom marine sediments are K_2O-enriched compared to the bottom estuarine sediments, however, the riverine riverbank sediments exhibited a scattered non-distinct variation at varying CIA (Figure 3-10d). There is also a strong relation between Cr concentration and CIA values in the Umba River sediments especially for downstream (estuarine and marine) bottom sediments (Figure 3-10e). On the A-CN-K plot, the sediments plot across the plagioclase – K-feldspar field (Figure 3-11a), while also maintaining a linear trend parallel to the A-CN edge towards the smectite field.

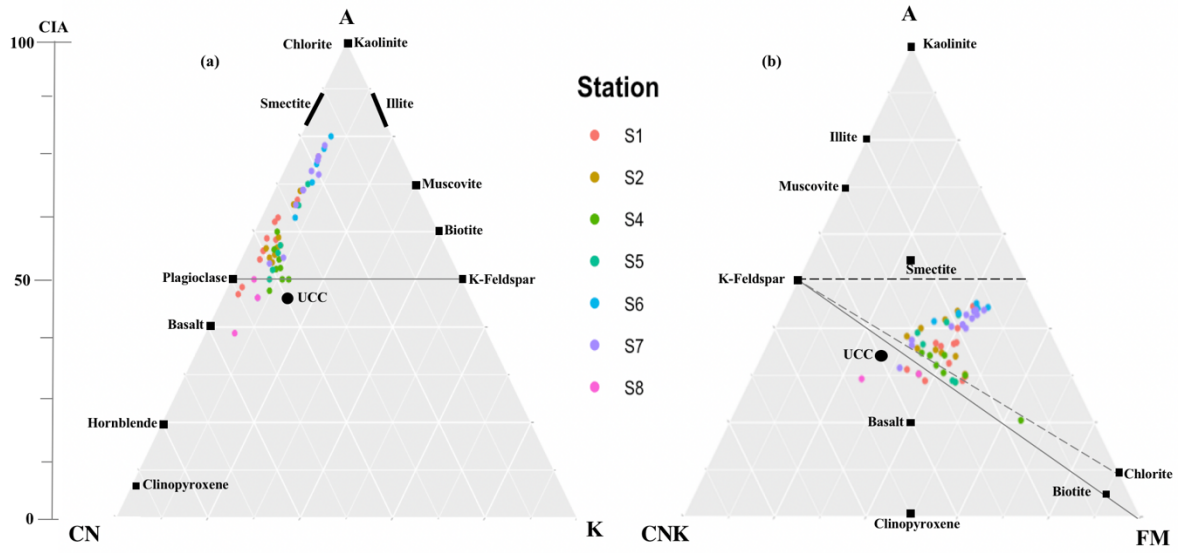

Figure 3-11: Ternary diagrams showing the common primary and secondary minerals and weathering trends of Umba River sediments. The CIA of Umba River sediments range from 39 - 81 with majority >50. On A-CN-K (a), Umba River sediments plot along a linear trend on the A-CN edge. On A-CNK-FM (b), the sediments plot below the smectite field. $A=Al_2O_3$, $CN= CaO^*+Na_2O$, $K=K_2O$, $CNK= CaO^* + Na_2O + K_2O$ and $FM = Fe_2O_3 + MgO$. Average values of basalt, UCC, and clinopyroxene taken from Wang and Liu (2008).

The trendline also starts at the pristine CIA value of ~40 to a highly weathered value of ~80. The sediments plot below the smectite and K-feldspar field and around the K-feldspar – chlorite and K-feldspar – biotite boundaries in the A-CNK-FM (Figure 3-11b) with a discernible trend away from the CNK-FM boundary.

Based on the calculated first and second discriminant functions (DF1 and DF2, respectively), the Umba River sediments plotted across three provenance fields, i.e., mafic igneous, intermediate igneous and quartzose sedimentary provenance fields (Figure 3-12). The majority of the sediments plot within the mafic igneous provenance field, which is consistent with the geology of the catchment and the associated dominant minerals.

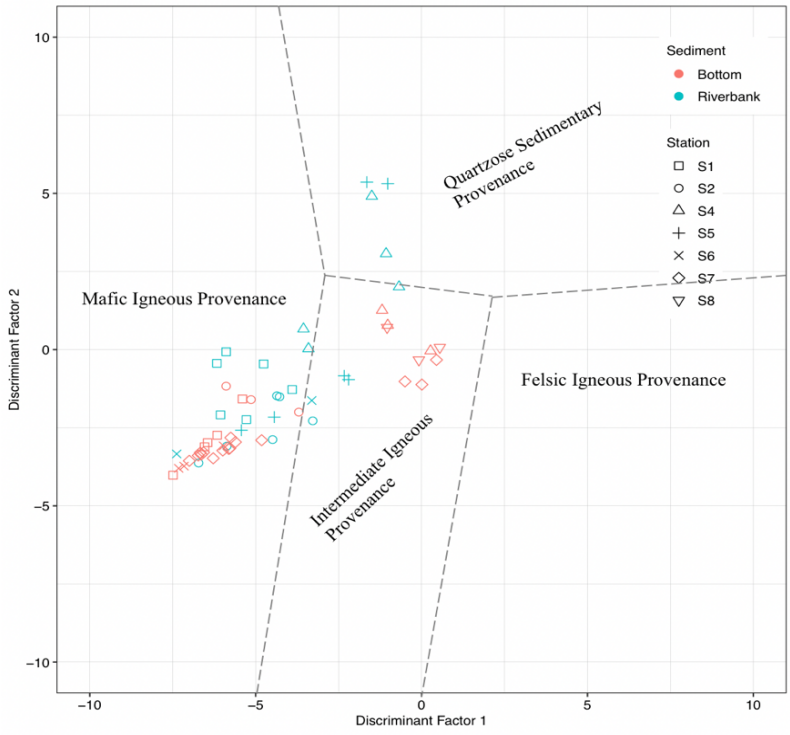

Figure 3-12: Major element provenance discriminant function (DF) plot. Major elements-based oxide ratios for the provenance signatures of Umba River sediments (Baiyegunhi et al., 2017; Bhat et al., 2019) plot across three provenance fields with majority in the mafic and intermediate igneous provenance.

3.5 Discussion

3.5.1 Influence of hydrodynamic and sedimentary sorting

Sediment sorting during fluvial transport, settling and deposition, can influence the mineral and chemical composition of sediments. Therefore, the influence of grain size sorting on sedimentary chemical composition has to be evaluated prior to any provenance determination (He et al., 2015; Hossain et al., 2017; McLennan, 1993; Sensarma et al., 2008). For example, major and trace elements, including Al, Fe, Mg, Ni and Cr, are known to be abundant in fine fractions of sediment rich in silt and clays while Si is abundant in sand fractions (He et al., 2013; Wu et al., 2011). In the Umba River sediments, grain sizes are distributed within a relatively narrow range between coarse sand (riverine), silty sand (marine) and sandy silt (estuarine) (Table 3-1; Figure 3-3). With minimal clay content of <3% in both riverbank and bottom sediments, these sediments fall within the broad class of sandy sediments (Table 3-1). The index of compositional variability (ICV) – which is used to indicate maturity of sediments - is >1 in all riverbank and bottom sediments (Table 3-1). Clay minerals have been shown to exhibit an ICV <0.8 (Hossain et al., 2017). Therefore, the ICV values derived here for Umba River sediments are consistent with the observation of a very low clay fraction (Table 3-1). Therefore, the effects of granulometric fractions and hydrodynamic sorting on the chemical composition of the sediments would be minimal. This is also reflected by the distribution of Fe and Al to the mud/sandy-silt fraction of sediments collected in estuarine station (S7) across the entire quartz-clay spectrum in the Al_2O_3/SiO_2 vs Fe_2O_3/SiO_2 ratio plot (Figure 3-7), reflecting the minimal effect of sorting (Sensarma et al., 2008; Wu et al., 2011). This is because the relative enrichment of Fe and Al in coarse sand (e.g., S1, S4, S8) as well as the sandy silt (S7), means that there is no control of grain size on their enrichment. This implies that the enrichment of Fe and Al in Umba River sediments is dominantly attributable to weathering inputs from the catchment. The enrichment of Fe (> 0.20) and Al (> 0.40) in estuarine (S7) samples could be attributed to the increased input of these

elements from the weathering of quartzo-feldspathic and hornblende-pyroxene rich downstream Karoo Supergroup and younger lithologies (Figure 3-1b). These lithologies and their associated minerals are rich in the Fe and Al elements in their chemical structure (Maboko and Nakamura, 2002; Sensarma et al., 2008). Additionally, the contribution of Karoo Supergroup lithologies to the increased input of Fe and Al, would be further promoted by a hot and humid climate due to the proximity to the Indian Ocean relative to upper catchment stations (Sensarma et al., 2008). The similarity of SiO_2 - the lack of either enrichment or depletion - relative to UCC, further indicate the reduced influence of hydrodynamic sorting on mineralogical and chemical composition of Umba River sediments (Garzanti et al., 2010; Hossain et al., 2017; McLennan, 1993).

3.5.2 Weathering indices and source area characteristics

The strong but negative relation between SiO_2 and Al_2O_3 (Figure 3-6a), the positive relation between Fe_2O_3 and Al_2O_3 (Figure 3-6c), and the positive relation between both Al_2O_3 and Fe_2O_3 with CIA (Figure 3-10a and 3-10b), indicate a shift that is expected from the replacement of easily weathered minerals towards a dominance of less mobile minerals, e.g., kaolinite composed of mainly the immobile Al^{3+}. The positive relation between Al_2O_3 and high CIA (Figure 3-10a) values in both riverbank and bottom sediments could be attributed to the initial weathering of sediments before the grains enter the fluvial system. Generally, fluvial sediments exhibit CIA values ~50 at the onset of weathering of a predominantly metamorphic and igneous source geology similar to the Umba River catchment. This value increases with reworking processes during transportation (Nesbitt and Young, 1982, 1984). The UCC has a mean CIA of ~47 (McLennan, 1993), however CIA values > 70 have also been reported to characterize intense weathering of source rock (Mishra and Sen, 2012). According to Campodonico et al. (2016), reworked fluvial sediments - through weathering, transport, deposition and diagenesis - have average CIA values of ~80. Clay minerals, which are an indicator of extensive weathering and chemical

alteration, have CIA values close to 100 (Campodonico et al., 2016; Shao and Yang, 2012). The large variation in CIA of the Umba River sediments ranging between 39 and 81, with a majority > 50 (Figure 3-11), signifies a low to high degree of weathering. This can be attributed to varying physico-chemical parameters including temperature, salinity and pH that vary along the longitudinal cross-section of the Umba River (Greber and Dauphas, 2019; Sensarma et al., 2008). The large variation in CIA values can also be attributed to the supply of pristine material to the fluvial system, supported by the smaller catchment of the Umba River and the short transport from source to mouth. However, the few high alterations recorded can be attributed to the alteration and input of feldspathic and clay minerals dominant in the downstream geology comprised of the Karoo Supergroup. The varying climate from the cold mountainous upstream to the hot and semi-arid midstream, and the hot and humid near coastal downstream could explain the variation in CIA (Sensarma et al., 2008). Low CIA values have been reported to be related to low weathering at source due to cooler conditions (Baiyegunhi et al., 2017) characteristic of higher elevations, e.g., mountainous regions and semi-arid conditions (Sensarma et al., 2008). These conditions are similar to the Umba River catchment near the source of the river in the Usambara and Pare mountains (Figure 3-1b and Figure 3-2). The likely presence of clay minerals e.g., illite and kaolinite in the Umba River sediments as discussed in section 4.2, and as observed in the grain size distribution (Table 3-1), could further explain the CIA variation. Additionally, the observed decrease in lithoclasts and the increase from source to mouth in grains made up of individual mineral crystals (Figure 3-4 and Figure 3-5) can indicate the gradual weathering with time exacerbated by river transport. The different roundness of grains within the downstream sediments (Figure 3-5) indicates that some clasts are incorporated in the bulk sediment later than others during fluvial transport. Part of these sediments thus have been minimally influenced by river transport, however, in the marine river mouth, wave action is expected resulting in increasing roundness of the grains.

The relatively low weathering in the downstream sediments compared to the upstream sediments, could be attributed to *in-situ* and proximal deposition devoid of fluvial transportation. Additionally, the occurrence of poorly rounded quartz mineral grains, being physically and chemically resistant to weathering (Figure 3-4 and Figure 3-5), is consistent with moderate reworking by river transport (Table 3-1 and Figure 3-3). The persisting presence of detrital feldspars (plagioclase and K-feldspars), a precursor of clay minerals, is an indication of low weathering of the gneissic granite, igneous and meta-igneous rocks sourced from the catchment.

The Umba River sediments plot across the plagioclase- K-feldspar line and reveal a narrow near-linear trend along the A-CN edge (Figure 3-11a). This trend has been attributed to possible higher removal rates of Na^{+} and Ca^{2+} from plagioclase compared to K^{+} removal rates during weathering, transport and other diagenetic processes (Baiyegunhi et al., 2017; Mishra and Sen, 2012). However, the linear trend parallel to the A-CN axis could be attributed to the supply and input of relatively pristine sediments to the fluvial system (Borges et al., 2008). This is consistent with the relatively short course of the Umba River and the small catchment it drains, consequently allowing faster delivery of newly weathered and pristine material into fluvial sediments. On the A-CNK-FM the sediments plot below the smectite and K-feldspar field and away from the CNK-FM edge (Figure 3-11b) further indicating a strong variable degree of weathering of the Umba River sediments. This corroborates the other findings that indicate high variability in weathering and reworking, attributed to progressive sediment input into the river and to varying climatic conditions along its course.

3.5.3 Source characteristics from bulk geochemical composition

In order to make inter-oxide comparisons, the abundance of Al_2O_3 was used as a reference factor, mainly because it is immobile and less soluble (Baiyegunhi et al., 2017). High positive inter-oxide relations are observed in the element bivariate plots between the immobile oxide Al_2O_3 and SiO_2, Fe_2O_3 and P_2O_5 (Figure 3-6a, 3-6c and

3-6d) in both, riverbank and bottom sediments. This can be attributed to less preferential fractionation during various sedimentary processes including weathering, transportation and deposition (Fiantis et al., 2010; Sarkar et al., 2004; Silva et al., 2016). It can also be the result of a relatively uniform source geology (Hossain et al., 2017) that would have similar mineralogy as reflected by these elements and observed in the mineral distribution (Figure 3-4 and 3-5). This preposition is further supported by the aforementioned influence of the relatively short course of the Umba River that drains a small catchment, limiting the amount of rock lithologies it crosses and therefore providing a uniform mineralogical and elemental composition. Short rivers tend to transport fresh sediments from source to mouth in a relatively short time, consequently reducing the degree of alteration of the chemical composition. The positive relation between Al_2O_3 and Fe_2O_3, on one hand, and P_2O_5 on the other, can be further attributed to abundances of these elements in platy and sheet phyllosilicates. The observed presence of muscovite, biotite, apatite and clay minerals in the Umba River sediments (Figure 3-4 and Figure 3-5) supports this observed trends (Maboko and Nakamura, 2002; Wu et al., 2011).

The bulk chemical composition of the sediments shows a comparable trend with average upper continental crust (UCC) chemical compositions (Figure 3-8a) and is similar to earlier studies within the region (Maboko and Nakamura, 2002). The relative depletion of Na_2O and K_2O observed here (Figure 3-8a) can be attributed to the result of increased leaching of the highly mobile elements and enrichment of the immobile and less soluble elements. Additionally, alkali elements including Na, Mg, Ca and K are largely lost as clay minerals are formed during weathering (Wu et al., 2011). Alteration of Al- and Mg-bearing minerals including plagioclase and phyllosilicates due to water percolation into rock fractures and crevices could accelerate the removal of mobile elements including Ca, Na, K and Mg (Sensarma et al., 2008). This is also consistent with moderate to high CIA as proxy for chemical weathering, with higher elemental values of these elements. Additionally, the

elevated MgO and CaO contents (Figure 3-6e, 3-6g respectively), coupled with a scattered relation between K_2O and Al_2O_3 (Figure 3-6f), also reflect a mixed source composition and varying degrees of weathering (Hossain et al., 2017). However, the observed high K_2O + Na_2O (>2.5%) and the relatively low K_2O / Na_2O ratio (<1) in the Umba River sediments (see Table 1), indicate an almost equal contribution of K-rich feldspar and Na-rich plagioclase (Baiyegunhi et al., 2017; Bhat et al., 2019; Rudnick and Gao, 2003).

Trace element concentrations vary along the longitudinal course of the Umba River in both riverbank and bottom sediments (Table 3-1). The less distinct and negative relation of Sr and Zr with Al_2O_3 (Figure 3-8a and 3-8b) can be attributed to the mixed geology from source to mouth of the Umba River. The weathering of the crystalline rocks of downstream geology (Figure 3-1) – rich in quartzo-feldspathic rock composition - would introduce increased amounts of Sr-rich K-feldspars and/or biotite to the sediments (Garzanti et al., 2018). Positive covariation and enrichment of Ni, Zn and Cr with Al_2O_3 in Umba River sediments (Figure 3-8c, 3-8d and 3-8e), can be attributed to the dominance of ferromagnesian elements. These elements are rich in mafic minerals dominant in the mafic granulites (Maboko and Nakamura, 2002; Manya et al., 2007; Sensarma et al., 2008) observed in the upper reaches of the Umba River in the Usambara Mountains (Figure 3-1). Cr/Ni have been used to indicate the mafic and ultramafic provenance (Sensarma et al., 2008). Low Cr/Ni values between 1.3 and 1.5 represent an ultramafic provenance. Both riverbank and bottom Umba River sediments, exhibit Cr/Ni >2 indicating a dominantly mafic to felsic provenance. The moderate to high abundances of both Ni (Figure 3-8c) and Cr (Figure 3-8e) in both riverbank and bottom sediments, suggests a mixed source of Umba River sediments. This mixture is occasioned by the changing lithologies and the subsequent variation of mafic and felsic minerals from source to mouth. The relative depletion and significant variation of Sr (Figure 3-8g) at low CaO and the depletion of Ba (Figure 3-8h) at moderate CaO in the estuarine bottom sediments has been

attributed to the physicochemical variations (salinity, dissolved oxygen, temperature) and the grain size (He et al., 2015; He and Xu, 2016, 2015; Wang et al., 2021). This is also supported by the significant variation ($p < 0.05$) of the two elements with environmental setting (see Supplementary Information 3-1). However, the observed depletion of Rb, Th and U in the Umba River sediments (Figure 3-9b) signifies a magmatic source geology with geochemical affinities of a meta-igneous granulite (Akech et al., 2013; Maboko and Nakamura, 2002; Schlüter, 1997). The sandstone lithology dominant in the lower reaches of Umba River (Figure 3-1b) is known be low in Rb and Sr (Baiyegunhi et al., 2017), therefore explaining the depletion of Rb relative to UCC.

3.5.4 Provenance

The sediments plot across three provenance fields, i.e., mafic igneous, intermediate igneous and quartzose sedimentary provenance fields (Figure 3-12) with the majority located in the mafic to intermediate igneous field. This indicates a strong influence of the upper and middle catchment geology, and a subordinate contribution of the lower catchment geology that is primarily composed of quartz-rich lithologies (Figure 3-1b). The Umba River catchment has pockets of mafic to ultra-mafic granulites (in the mountainous Mng'aro region) and mafic hornblende-pyroxene facies within the Karoo (Akech et al., 2013; Maboko and Nakamura, 2002) further downstream (Figure 3-1b). On the contrary, the lower catchment is dominated by quartzo-feldspathic-rich sandstones and siltstones that would explain the placement of some Umba River sediments in the quartzose provenance field (Figure 3-12). Further, the plot in the quartzose sedimentary provenance quadrant suggests the derivation of the Umba River sediments from a recycled orogen (Baiyegunhi et al., 2017; Bhat et al., 2019) – presumably, because the upstream Umba River is characterized by the geologically uplifted Usambara mountains (Maboko and Nakamura, 2002; Mutakyahwa et al., 2003; Shackleton, 1993).

3.6 Conclusions

The provenance of the sediments deposited along the course of the Umba River from source to mouth have been characterized using a combination of geochemical proxies and petrography. The chemical composition and elemental abundance of riverbank versus bottom sediments of Umba River, are significantly different, however, they show similar abundance and distribution trends along the course. The effect of hydrodynamic sorting on chemical and mineralogical composition of Umba River sediments is minimal, with the distribution of elements majorly attributed to inputs from weathering. The source geology, relative length of the river and the small catchment have a dominant influence on the element and mineral composition and abundances. This assessment has revealed that the Umba River sediments have a predominantly gneissic granite petrology consistent with the underlying catchment geology, characterized by a Precambrian craton and the Karoo Supergroup in its upper reaches and much younger Cenozoic outcrops and Quaternary sediments further downstream towards the coast. The Umba River sediments also exhibit a UCC-like chemical composition and further geochemical preservation of source characteristics, reflected by the similarity of mineralogy of upstream riverine sediments (close to source) and downstream sediments (estuarine). This is further supported by the moderate to high alteration reflected by the CIA, evident by the marked depletion of mobile and labile elements like MgO, CaO, Na_2O, K_2O and Sr relative to UCC.

3.7 Acknowledgments

We thank Simon Langat, Shawlet Cherono and George Onduso of Kenya Marine and Fisheries Research Institute, Kenya for assistance during sample collection and preparation and Donata Monien and Jule Mawick of ZMT and Carola Lehners of the Institute for Chemistry and Biology of the Marine Environment (ICBM) at the

University of Oldenburg for technical laboratory assistance, sample preparation and analysis.

3.8 Supplementary Information

- Supplementary Information 3-1. Geochemical data (major, trace and some rare earth elements) of Umba River.

- Supplementary Information 3-2. One-Way ANOVA analysis of major and trace elements contents of Umba River.

Supplementary Information 3-1

Table S1a. Major elements composition (in wt. %) of Umba River sediments (both riverbank and bottom sediments). n.d - not detected.

Major elements (in wt. %)																					
Station_code	Sediment_type	SiO_2	TiO_2	Al_2O_3	Fe_2O_3	MnO	MgO	CaO	Na_2O	K_2O	P_2O_5	SO_3	LOI	Total	CIA	ICV	Na_2O+K_2O	K_2O/Na_2O	Fe_2O_3/SiO_2	Al_2O_3/SiO_2	CaO*
S1	Riverbank	64.42	1.43	13.13	9.03	0.21	2.04	3.38	1.99	0.94	0.13	0.03	3.11	99.83	55.74	1.45	2.93	0.47	0.14	0.2	0.06
S1	Riverbank	61.58	0.96	16.28	7.59	0.16	1.79	3.54	2.42	1.17	0.17	-0.01	4.15	99.8	58.24	1.08	3.59	0.48	0.12	0.26	0.07
S1	Riverbank	62.16	1.76	13.88	10.04	0.2	2.07	3.55	2.29	1.02	0.15	0.01	2.6	99.81	55.10	1.51	3.31	0.45	0.16	0.22	0.07
S1	Bottom	57.68	0.93	16.88	8.79	0.2	1.77	3.18	2.08	1.16	0.2	n.d	6.93	99.81	61.78	1.07	3.24	0.56	0.15	0.29	0.06
S1	Bottom	65.72	1.01	13.97	7.55	0.15	1.85	3.32	2.16	1.07	0.14	n.d	2.89	99.83	56.54	1.22	3.23	0.50	0.11	0.21	0.06
S1	Riverbank	60.23	1.05	15.8	8.00	0.18	1.73	2.87	1.77	1.11	0.22	n.d	6.85	99.82	62.91	1.06	2.88	0.63	0.13	0.26	0.05
S1	Riverbank	58.15	1.35	15.04	8.41	0.20	2.16	6.42	2.48	1.21	0.17	0.01	4.16	99.77	46.87	1.48	3.69	0.49	0.14	0.26	0.12
S1	Riverbank	62.87	0.89	14.4	6.32	0.17	1.83	5.97	2.59	1.22	0.14	n.d	3.39	99.81	46.71	1.32	3.81	0.47	0.1	0.23	0.11
S1	Riverbank	48.7	0.81	18.34	8.40	0.32	1.83	5.31	1.32	1.56	0	0.04	12.37	99.7	57.57	1.07	2.88	1.18	0.17	0.38	0.11
S1	Riverbank	49.63	0.90	19.62	9.06	0.34	1.81	3.25	1.38	1.55	0	0.01	11.51	99.69	66.56	0.93	2.93	1.12	0.18	0.4	0.07
S1	Riverbank	45.72	0.91	22.02	9.61	0.27	1.34	2.09	1.03	1.3	0	0.04	14.91	99.77	76.14	0.75	2.33	1.26	0.21	0.48	0.04
S2	Riverbank	60.96	0.67	17.66	5.76	0.1	1.66	4.25	3.01	1.64	0.14	n.d	3.93	99.79	55.00	0.97	4.65	0.54	0.09	0.29	0.08
S2	Riverbank	61.21	1.03	15.91	7.51	0.13	1.87	3.54	2.32	1.5	0.16	0.02	4.59	99.8	57.28	1.13	3.82	0.65	0.12	0.26	0.07
S2	Riverbank	59.85	1.07	16.55	7.62	0.13	1.86	3.61	2.39	1.56	0.16	n.d	4.99	99.78	57.62	1.10	3.95	0.65	0.13	0.28	0.07
S2	Bottom	64.87	0.69	15.06	5.82	0.12	1.66	3.8	2.56	1.39	0.14	0.01	3.71	99.81	54.41	1.07	3.95	0.54	0.09	0.23	0.07
S2	Bottom	65.62	1.23	13.13	8.8	0.17	1.92	3.26	1.94	1.18	0.11	n.d	2.45	99.8	55.83	1.41	3.12	0.61	0.13	0.2	0.06
S2	Bottom	60.75	1.19	15.61	8.54	0.15	1.84	3.36	2.12	1.44	0.13	0.02	4.64	99.79	58.35	1.19	3.56	0.68	0.14	0.26	0.06
S2	Riverbank	49.89	0.72	20.22	7.82	0.13	1.74	3.48	1.77	1.48	0.21	0.01	12.34	99.79	65.13	0.85	3.25	0.84	0.16	0.41	0.07
S2	Riverbank	56.37	0.69	19.23	6.43	0.1	1.54	3.82	2.59	1.51	0.17	0.03	7.3	99.79	59.98	0.87	4.10	0.58	0.11	0.34	0.07
S2	Riverbank	49.29	0.75	21.4	8.5	0.13	1.58	2.93	1.48	1.33	0.21	0.03	12.18	99.81	69.97	0.78	2.81	0.90	0.17	0.43	0.06
S4	Riverbank	76.03	0.69	8.65	5.48	0.09	1.66	2.06	1.09	1.32	0.09	0.02	2.63	99.82	55.40	1.43	2.41	1.21	0.07	0.11	0.04
S4	Riverbank	70.72	1.62	10.6	6.58	0.09	1.53	2.54	1.95	1.54	0.09	0.04	2.37	99.74	52.77	1.50	3.49	0.79	0.09	0.15	0.05
S4	Riverbank	73.17	1.07	9.95	5.02	0.09	1.44	3.32	1.7	1.58	0.08	0.02	2.35	99.79	48.56	1.43	3.28	0.93	0.07	0.14	0.06
S4	Bottom	78.08	0.52	8.83	4.09	0.07	1.55	2.4	1.52	1.5	0.08	n.d	1.17	99.81	51.00	1.32	3.02	0.99	0.05	0.11	0.04

S4	Bottom	80.62	0.36	7.89	3.14	0.05	1.13	1.87	1.47	1.55	0.07	0.02	1.54	99.8	51.29	1.21	3.02	1.05	0.04	0.1	0.03
S4	Bottom	69.97	1.3	12.97	5.67	0.1	1.57	3.06	2.27	1.69	0.09	n.d	1.07	99.76	53.83	1.21	3.96	0.74	0.08	0.19	0.06
S4	Riverbank	71.1	1.09	11.9	6.09	0.11	1.48	2.42	1.7	1.33	0.08	0.04	2.47	99.81	57.96	1.19	3.03	0.78	0.09	0.17	0.04
S4	Riverbank	66.21	2.43	12.53	8.45	0.13	1.91	3.1	2.04	1.53	0.09	n.d	1.29	99.72	54.08	1.56	3.57	0.75	0.13	0.19	0.06
S4	Riverbank	65.33	3.66	9.04	13.28	0.2	2.28	2.43	1.07	1.11	0.11	0.01	1.15	99.67	55.10	2.66	2.18	1.04	0.2	0.14	0.04
S5	Riverbank	65.46	2.46	12.67	8.79	0.17	2.26	3.61	2.24	1.45	0.1	n.d	0.53	99.73	51.76	1.66	3.69	0.65	0.13	0.19	0.06
S5	Riverbank	67.77	2.49	12.1	8.41	0.15	1.9	3.21	2.36	1.46	0.1	0.01	-0.37	99.73	51.73	1.65	3.82	0.62	0.12	0.18	0.06
S5	Riverbank	65.56	0.96	15.13	5.69	0.1	1.55	3.06	2.49	1.75	0.12	0.01	3.29	99.76	56.71	1.03	4.24	0.70	0.09	0.23	0.06
S5	Riverbank	56.78	0.92	17.8	7.19	0.11	1.51	2.27	1.78	1.81	0.18	0.08	9.31	99.76	66.41	0.88	3.59	1.02	0.13	0.31	0.04
S5	Riverbank	53.88	0.92	18.65	7.96	0.14	1.56	2.09	1.48	1.7	0.2	0.03	11.18	99.79	69.83	0.85	3.18	1.15	0.15	0.35	0.04
S5	Riverbank	64.9	0.94	15.61	5.44	0.09	1.47	3.14	2.51	1.8	0.13	0.03	3.68	99.74	56.99	0.99	4.31	0.72	0.08	0.24	0.06
S6	Riverbank	47.58	0.96	20.43	9.58	0.21	1.58	1.22	0.65	1.44	0.24	0.02	15.91	99.82	80.91	0.77	2.09	2.22	0.2	0.43	0.03
S6	Riverbank	62.31	0.88	15.81	5.95	0.11	1.36	2.63	1.99	1.76	0.15	0.03	6.79	99.77	61.37	0.93	3.75	0.88	0.1	0.25	0.05
S6	Riverbank	50.08	0.92	20.51	9.28	0.15	1.38	1.83	1.08	1.39	0.3	0.01	12.83	99.81	75.71	0.78	2.47	1.29	0.19	0.41	0.04
S6	Riverbank	48.72	0.93	20.91	9.49	0.15	1.38	1.76	0.99	1.38	0.3	0.04	13.72	99.81	76.87	0.77	2.37	1.39	0.19	0.43	0.04
S6	Riverbank	57.79	0.83	17.63	7.49	0.12	1.3	1.97	1.32	1.42	0.22	0.01	9.7	99.81	70.79	0.82	2.74	1.08	0.13	0.31	0.04
S7	Bottom	45.88	0.93	18.93	8.87	0.13	1.77	1.44	2.46	1.44	0.25	0.46	17.23	99.85	69.78	0.90	3.90	0.59	0.19	0.41	0.03
S7	Bottom	44.64	0.9	19.98	9.23	0.15	1.76	1.29	2.28	1.41	0.27	0.13	17.78	99.84	72.46	0.85	3.69	0.62	0.21	0.45	0.03
S7	Bottom	48.21	0.91	20.69	9.13	0.13	1.71	1.48	1.57	1.45	0.25	0.18	14.12	99.84	75.21	0.79	3.02	0.92	0.19	0.43	0.03
S7	Bottom	81.66	0.37	8.12	2.85	0.06	0.89	1.82	1.6	1.31	0.07	0.1	0.99	99.83	52.46	1.10	2.91	0.82	0.03	0.1	0.03
S7	Bottom	85.97	0.37	5.74	2.28	0.04	0.6	1.2	1.15	1.08	0.05	0.05	1.31	99.85	52.27	1.17	2.23	0.94	0.03	0.07	0.02
S7	Bottom	84.51	0.27	6.39	2.42	0.06	0.91	1.92	1.85	0.96	0.04	0.05	0.43	99.82	45.76	1.31	2.81	0.52	0.03	0.08	0.03
S7	Bottom	50.74	0.84	18.59	7.77	0.1	1.69	1.91	2.66	1.59	0.22	0.06	13.66	99.83	66.06	0.89	4.25	0.60	0.15	0.37	0.04
S7	Bottom	49.09	1.03	19.23	8.95	0.17	1.79	1.75	2.24	1.49	0.24	0.17	13.69	99.83	69.46	0.91	3.73	0.67	0.18	0.39	0.04
S7	Bottom	50.45	0.96	19.11	8.64	0.15	1.75	1.82	2.39	1.47	0.24	0.02	12.84	99.83	68.45	0.90	3.86	0.62	0.17	0.38	0.04
S7	Bottom	48.42	0.91	20.88	9.22	0.14	1.7	1.45	1.57	1.44	0.25	0.06	13.79	99.83	75.56	0.79	3.01	0.92	0.19	0.43	0.03
S7	Bottom	58.81	0.73	16.46	7.24	0.1	1.35	1.26	1.49	1.33	0.2	0.16	10.68	99.83	72.75	0.82	2.82	0.89	0.12	0.28	0.03
S7	Bottom	45.17	0.95	21.38	9.83	0.14	1.7	1.14	1.49	1.43	0.27	0.08	16.26	99.84	77.97	0.78	2.92	0.96	0.22	0.47	0.02
S7	Bottom	49.1	0.95	19.6	8.87	0.16	1.73	1.64	2.37	1.49	0.25	0.22	13.43	99.82	69.83	0.88	3.86	0.63	0.18	0.4	0.03
S7	Bottom	46.74	0.94	20.84	9.44	0.13	1.73	1.41	1.51	1.49	0.26	0.03	15.31	99.83	75.86	0.80	3.00	0.99	0.2	0.45	0.03
S7	Bottom	45.6	0.93	20.86	9.45	0.14	1.72	1.29	1.57	1.45	0.27	0.14	16.42	99.83	76.33	0.79	3.02	0.92	0.21	0.46	0.03
S8	Bottom	72.67	0.68	12.29	3.35	0.08	1.47	3.74	3.12	1.64	0.08	0.02	0.67	99.8	47.28	1.15	4.76	0.53	0.05	0.17	0.07

S8	Bottom	74.72	0.74	9.63	4.63	0.11	1.63	2.96	2.28	1.34	0.08	0.06	1.64	99.83	47.65	1.42	3.62	0.59	0.06	0.13	0.05
S8	Bottom	67.02	0.67	11.62	3.87	0.08	1.4	6.65	2.85	1.6	0.15	0.05	3.81	99.79	38.57	1.47	4.45	0.56	0.06	0.17	0.12

Table S1b. Trace elements composition (in wt. %) of Umba River sediments (both riverbank and bottom sediments). n.d - not detected

Trace elements (in ppm)																						
Station_code	**Sediment _type**	**As**	**Ba**	**Ce**	**Co**	**Cr**	**Cu**	**Ga**	**Mo**	**Nb**	**Ni**	**Pb**	**Rb**	**Sr**	**Th**	**U**	**V**	**Y**	**Zn**	**Zr**	**Rb/Sr**	**Cr/Ni**
S1	Riverbank	n.d	662	52	18	62	17	12	2	13	19	4	22	288	5	-2	191	20	76	285	0.08	3.26
S1	Riverbank	-1	852	29	17	56	30	15	2	10	23	7	28	364	2	-1	145	15	78	228	0.08	2.43
S1	Riverbank	-1	708	42	17	62	21	14	2	16	20	5	24	315	4	-1	221	18	87	328	0.08	3.10
S1	Bottom	-1	834	61	19	63	53	17	1	10	28	7	33	336	5	-1	157	18	98	254	0.10	2.25
S1	Bottom	n.d	773	33	14	60	19	14	2	10	21	6	24	331	4	n.d	149	16	77	222	0.07	2.86
S1	Riverbank	-1	790	37	17	67	52	16	2	12	29	10	34	298	6	n.d	161	18	100	185	0.11	2.31
S1	Riverbank	-1	791	63	18	79	27	15	2	14	23	8	26	389	5	-1	189	21	83	483	0.07	3.43
S1	Riverbank	n.d	791	38	14	67	21	14	1	9	20	8	27	388	4	n.d	135	15	68	341	0.07	3.35
S1	Riverbank	-2	1617	62	25	81	103	19	3	12	41	8	50	501	4	n.d	148	21	153	163	0.10	1.98
S1	Riverbank	-2	1708	58	26	80	104	20	2	13	42	10	54	368	6	-1	160	22	152	187	0.15	1.90
S1	Riverbank	-2	1122	81	30	82	106	22	2	15	43	10	45	239	5	n.d	168	25	150	129	0.19	1.91
S2	Riverbank	-1	1148	33	13	34	28	16	2	8	16	6	32	526	3	-1	125	15	61	138	0.06	2.13
S2	Riverbank	-1	1007	53	15	41	36	15	n.d	11	17	6	31	430	4	-1	169	19	73	239	0.07	2.41
S2	Riverbank	-1	1048	40	15	43	41	16	2	11	17	7	34	450	4	-2	173	18	77	286	0.08	2.53
S2	Bottom	n.d	927	25	13	40	23	12	2	9	17	4	26	442	1	-1	124	16	54	164	0.06	2.35
S2	Bottom	n.d	813	45	15	46	21	12	1	13	13	4	27	339	5	-1	190	22	67	350	0.08	3.54
S2	Bottom	-1	947	73	16	51	43	15	2	14	21	5	30	381	5	-2	188	24	72	285	0.08	2.43
S2	Riverbank	-1	1083	52	20	53	78	19	1	10	29	6	41	403	5	-1	143	18	87	129	0.10	1.83
S2	Riverbank	-1	1017	43	16	45	47	17	1	9	21	7	33	471	3	n.d	126	13	67	179	0.07	2.14
S2	Riverbank	-2	902	55	21	59	79	21	1	10	32	6	43	349	5	-1	150	19	84	138	0.12	1.84
S4	Riverbank	2	755	29	12	183	16	7	2	10	44	5	30	223	5	n.d	106	18	37	351	0.13	4.16
S4	Riverbank	1	931	105	14	288	14	9	2	15	46	6	33	348	14	-1	166	15	51	614	0.09	6.26
S4	Riverbank	1	934	43	10	140	9	9	1	12	33	9	29	331	5	n.d	124	13	37	376	0.09	4.24
S4	Bottom	2	897	23	11	119	8	7	2	6	36	5	31	295	4	-1	84	11	31	289	0.11	3.31
S4	Bottom	2	927	16	8	109	6	7	3	6	37	6	30	280	2	n.d	67	8	23	418	0.11	2.95

S4	Bottom	n.d	1054	58	11	172	10	12	2	14	30	7	34	414	6	n.d	143	16	48	341	0.08	5.73
S4	Riverbank	1	854	35	12	171	13	10	2	13	30	5	31	319	4	n.d	132	19	46	317	0.10	5.70
S4	Riverbank	1	946	82	12	292	14	11	2	24	36	6	31	372	9	n.d	232	24	66	583	0.08	8.11
S4	Riverbank	3	634	223	19	346	14	8	3	32	73	4	23	208	30	-1	343	33	85	1005	0.11	4.74
S5	Riverbank	1	976	73	15	102	8	12	1	25	18	10	29	400	8	n.d	227	25	72	678	0.07	5.67
S5	Riverbank	1	945	99	13	119	6	11	3	25	18	9	28	381	9	-1	220	25	66	630	0.07	6.61
S5	Riverbank	n.d	1164	52	13	77	22	13	1	13	25	10	43	430	5	n.d	128	17	58	311	0.10	3.08
S5	Riverbank	n.d	1107	85	20	92	50	18	1	16	43	12	62	335	6	-1	144	23	80	282	0.19	2.14
S5	Riverbank	n.d	1007	82	23	98	62	19	2	15	52	12	67	295	8	1	154	24	87	257	0.23	1.88
S5	Riverbank	n.d	1193	68	13	69	22	14	2	14	24	10	41	456	5	-1	124	16	59	347	0.09	2.88
S6	Riverbank	n.d	764	92	28	111	78	22	1	18	63	14	83	162	9	-1	182	29	98	132	0.51	1.76
S6	Riverbank	n.d	1182	52	16	71	35	15	2	11	29	10	46	399	4	-1	127	17	63	307	0.12	2.45
S6	Riverbank	-2	860	75	26	97	84	22	2	15	52	12	59	245	7	-1	176	25	101	134	0.24	1.87
S6	Riverbank	-2	822	73	26	97	84	22	1	15	55	11	59	235	4	1	174	26	102	123	0.25	1.76
S6	Riverbank	n.d	864	61	20	84	64	17	2	12	43	10	53	275	6	-1	146	22	82	153	0.19	1.95
S7	Bottom	6	569	68	19	92	64	19	2	14	46	11	64	215	8	n.d	161	22	87	156	0.30	2.00
S7	Bottom	6	538	73	20	97	68	21	3	13	49	12	67	200	9	3	170	23	90	177	0.34	1.98
S7	Bottom	7	606	69	20	95	67	21	4	15	48	11	61	233	6	1	169	23	92	137	0.26	1.98
S7	Bottom	3	836	14	6	34	3	6	1	5	9	5	26	276	1	n.d	57	9	23	382	0.09	3.78
S7	Bottom	4	676	9	4	27	1	4	3	4	5	7	26	196	3	1	48	7	18	473	0.13	5.40
S7	Bottom	4	627	1	6	25	-1	4	2	6	6	3	20	244	2	-1	41	10	19	752	0.08	4.17
S7	Bottom	4	766	65	16	82	52	19	3	13	40	10	61	294	6	1	144	19	77	173	0.21	2.05
S7	Bottom	5	629	76	20	98	57	20	3	15	43	10	62	254	8	1	166	23	86	203	0.24	2.28
S7	Bottom	5	688	67	18	92	57	19	3	15	43	10	60	266	8	n.d	159	22	83	215	0.23	2.14
S7	Bottom	6	598	65	20	97	68	22	3	13	49	11	64	227	8	1	171	21	93	146	0.28	1.98
S7	Bottom	6	581	53	15	78	52	17	4	11	38	8	53	206	5	1	135	18	75	351	0.26	2.05
S7	Bottom	7	543	77	21	102	75	23	4	14	54	12	68	191	7	2	180	24	97	150	0.36	1.89
S7	Bottom	5	661	65	19	92	60	19	3	14	46	10	60	254	6	n.d	166	22	86	180	0.24	2.00
S7	Bottom	7	623	70	22	101	72	21	5	15	49	12	68	226	8	2	175	23	96	181	0.30	2.06
S7	Bottom	7	589	61	21	101	71	22	3	14	52	11	65	210	7	n.d	176	24	97	153	0.31	1.94
S8	Bottom	2	1073	22	7	50	5	10	1	8	10	7	28	484	3	1	76	11	36	274	0.06	5.00
S8	Bottom	4	840	34	9	60	5	7	2	11	11	6	27	332	2	n.d	90	16	37	335	0.08	5.45

S8	Bottom	5	1009	46	10	44	5	9	2	8	9	7	31	602	6	n.d	79	12	46	265	0.05	4.89

Supplementary Information 3-2

Table S2a. Results of one-way ANOVA test indicating variation of major elements contents with sediment type and environment. *, ** and *** indicate significance value at $p < 0.05$, 0.01 and 0.001, respectively.

Major elements	Sediment type				Environment			
	DF	Residuals	F-value	p-value	DF	Residuals	F-value	p-value
SiO_2	1	56	6.155	0.016*	2	55	0.753	0.476
TiO_2	1	56	6.583	0.013*	2	55	2.923	0.062
Al_2O_3	1	56	4.84	0.032*	2	55	0.605	0.550
Fe_2O_3	1	56	8.543	0.005**	2	55	0.585	0.561
MnO	1	56	7.189	0.009**	2	55	2.462	0.095
MgO	1	56	6.259	0.015*	2	55	2.996	0.058
CaO	1	56	1.138	0.291	2	55	6.995	0.002**
Na_2O	1	56	0.04	0.843	2	55	0.386	0.682
K_2O	1	56	1.252	0.268	2	55	0.685	0.508
P_2O_5	1	56	3.455	0.068	2	55	0.065	0.938

Table S2b. Results of one-way ANOVA test indicating variation of trace elements contents with sediment type and environment. *, ** and *** indicate significance value at $p < 0.05$, 0.01 and 0.001, respectively.

Major elements	Sediment type				Environment			
	DF	Residuals	F-value	p-value	DF	Residuals	F-value	p-value
Sr	1	56	4.51	0.0382*	2	55	19.15	4.87e-07***
Cr	1	56	2.80	0.099	2	55	1.28	0.287
Ni	1	56	0.36	0.553	2	55	4.81	0.0119*
Zr	1	56	0.88	0.352	2	55	0.51	0.606
Zn	1	56	4.07	0.0484*	2	55	2.32	0.107
Rb	1	56	1.03	0.315	2	55	9.32	3.28e-03***
Ba	1	56	15.96	0.00191***	2	55	16.52	2.39e-06***

Chapter 4 : Manuscript III

Tracing organic matter sources in the estuarine sediments of Vanga, Kenya, and provenance implications

This work has been published in Estuarine, Coastal and Shelf Science Journal, December 2021 https://doi.org/10.1016/j.ecss.2021.107636

Kimeli A[a,b,c]*, Cherono S[c], Mutisya B[c], Tamooh F[d], Okello J[c], Koedam N[e], Westphal H[a,b], and Kairo J[c].

[a] Faculty of Geoscience, University of Bremen, 28359 Bremen, Germany.

[b] Biogeochemistry and Geology Department, Leibniz Centre for Tropical Marine Research (ZMT), 28359 Bremen, Germany.

[c] Oceanography and Hydrography Department, Kenya Marine and Fisheries Research Institute, 81651 – 80100 Mombasa, Kenya.

[d] Department of Zoological Sciences, Kenyatta University, P.O. Box 16778-80100, Mombasa, Kenya

[e] Laboratory of Plant Biology and Nature Management (APNA), Vrije Universiteit Brussels, 1050 Brussels, Belgium.

Highlights

- Distribution of sediments organic matter in Vanga Estuary is evaluated
- Sources of sediment of organic matter in Vanga Estuary is modeled
- Riverine organic matter is the dominant contributor to Vanga Estuary

Abstract

Mangrove ecosystems can potentially and indirectly modulate the effects of sea-level rise due to their ability to trap and retain sediments. In order to gain a better understanding of the potential sediment dynamics in the mangroves of Vanga, Kenya, inter-seasonal riverine, estuarine and coastal/marine sediments together with agricultural soil and mangrove tissues were studied. Elemental ratios (C/N) and carbon ($\delta^{13}C$) stable isotope composition, were analysed to disentangle sources of sediment organic matter (SOM) in the Vanga, Estuary. The organic carbon (C) content, C/N ratios and $\delta^{13}C$ values ranged between 0.1 to 2.4%, 9.9 to 35.5 and -24.8 to -19.9‰ respectively. These contents were also as expected relatively higher in mangrove tissues than in all the sediment samples. $\delta^{13}C$ values of mangrove sediments were higher than those of the mangrove tissues, which was attributed to rapid decomposition, dilution by freshwater and mineral organic matter (OM) discharged by the Umba River as well as outwashing by ebb tides. On average, C/N ratios were also observed to be greater than 10 in all samples collected during both the dry and wet season. This has been shown to reflect a pronounced contribution of allochthonous organic matter. Using a combination of $\delta^{13}C$ values and C/N ratio, the dominance of riverine POM was also evident from a Bayesian Stable Isotope Mixing Model in R-program (SIMMR) that indicated OM source mixing but with a dominant (~60%) contribution of riverine OM. The observed and modeled variability of SOM in the Vanga estuary points to the hypothesized influence of the Umba River on Vanga Estuary sediments but with evidence of potential material exchange and influence of tidal fluxes within the estuary.

Keywords: Sediments, mangroves, organic matter, stable isotopes, modeling, Umba River, Tanzania, Kenya

4.1 Introduction

Fluvial systems are the vital link between the terrestrial biosphere and the oceans, delivering freshwater, nutrients, and sediments to the marine realm (Milliman et al., 2016; Tamooh et al., 2014). Tropical rivers transport approximately 60% of total riverine carbon and 35% of the total sediment fluxes to the global oceans (Milliman et al., 2016; Schlünz, 2000). Organic matter (OM) pools in mangrove ecosystems comprise dissolved OM and particulates originating from fluvial inputs, combined with marine-derived local production, and lateral inputs (Rumolo et al., 2011; Bouillon et al., 2004). Source characterization is therefore crucial in understanding factors that affect rates of sediment transport, budgets and dynamics in the context of land use changes, geographic locations and climate variability, as well as biogeochemical cycles (Jennerjahn et al., 2009; Khan et al 2015; Kennedy et al., 2004). Some of the OM sources in sediments include decayed plant biomass, *in-situ* production by phytoplankton, mangroves and submerged aquatic vegetation, as well as material derived from weathered organic-rich lithologies in the catchment (Blattmann et al., 2018; Petsch, 2013). Inevitably, the admixing of OM from the various sources occurs in mangrove habitats due to hydrodynamic effects of tidal loading and flushing (Rumolo et al., 2011; Jennerjahn et al., 2009). For example, adjacent coastal and marine OM and tidal influence dominate the source of sediment OM sources in mangroves with low organic carbon, while mangrove plants dominate the source of OM in mangroves with high sediment OM (Bouillon et. al., 2008). Therefore, in a combined tidal-river dominated estuary, the influence of both river and tidal flush coupled with *in-situ* production complicates the elucidation of material exchange, sources and importance of OM (Kristensen et. al., 2011; Jennerjahn and Ittekkot, 2002). Benthic consumers in mangrove ecosystems also play key role in the material production, consumption, conversion and export/exchange between ecosystems (Bouillon et. al., 2008; Kristensen et. al., 2011). Others have also shown that OM in large rivers carrying large loads have progressively older POC and low

organic carbon (Marwick et. al., 2015; Tamooh et. al., 2014) compared to smaller rivers draining smaller catchments and carrying smaller loads and transporting sediments for short distances. Among other proxies, carbon ($\delta^{13}C$) and nitrogen ($\delta^{15}N$) stable isotopes signatures of estuarine OM reflect the signatures of the above-mentioned sources, the riverine $\delta^{13}C$ values being determined by the plant biomass and soil OM dominant within their catchment and source (Tamooh et la., 2014). Consequently, considerable research has utilized both carbon (C) and nitrogen (N) stable isotopes coupled with elemental carbon to nitrogen (C/N) ratios as tracers to identify and partition organic matter provenance in estuaries (Bouillon et al., 2008; Kusumaningtyas et al., 2019; Nasir et al., 2016; Tamooh et al., 2012; Thornton and McManus, 1994). This methodology makes use of the natural variation in OM derived from different sources reflecting the dominant primary producers in their locality of origin (Rumolo et al., 2011). The variation in the isotope composition of OM is a consequence of distinct photosynthetic pathways by different groups of plants; the C3, C4 and CAM plants (Fry, 2006; Rahayu et al., 2019) from where the OM is sourced. It is from these distinct pathways that the sediments/soils retain the isotopic signatures of the plant materials dominant in their source location. However, stable isotope signature overlap is inevitable in river-tide dominant estuary (Bouillon et al., 2008) and this overlap can confound the interpretation and source characterization of OM (Donato et al., 2011; Kennedy et al., 2004). The $\delta^{13}C$ vs. C/N values can be utilized to effectively distinguish between terrestrial and aquatic OM end-members (Rumolo et al., 2011; Kennedy et al., 2004), while $\delta^{13}C$ and $\delta^{15}N$ values can be effectively used to distinguish marine- and sewage-derived OM mainly because sewage effluent is characterized by low $\delta^{13}C$ and $\delta^{15}N$ values relative to marine-derived OM. $\delta^{13}C$ and $\delta^{15}N$ values of terrestrial-derived OM can overlap with sewage-derived signatures, making their use in highly polluted waters difficult (Nasir et al., 2016). Sediment organic matter with C/N ratios values greater than 10 are considered to indicate a terrestrial source because terrestrial OM is depleted in N

compared to aquatic environments (Kennedy et al., 2004; Kristensen et al., 2008; Nasir et al., 2016). Similarly, $\delta^{13}C$ values have been used to distinguish plant-derived OM in catchments (von Fischer and Tieszen, 1995), with varying dominant vegetation e.g., terrestrial C3 and C4 plants has an average $\delta^{13}C$ of -30‰, mangrove leaves with average $\delta^{13}C$ values of -25 to -31‰ while marine derived OC has a typical $\delta^{13}C$ value of -20‰ (Bouillon et al., 2008) and bulk soil (Marin-Spiotta et al., 2009) with reported average $\delta^{13}C$ value of -27‰. On the other hand, the large $\delta^{15}N$ variability in marine OM can be attributed to the nitrogen fixing cyanobacteria that has much lower $\delta^{15}N$ values compared to the non-nitrogen fixing organisms (McKee et al., 2002). Based on this variability in OM signatures from various sources, end-member mixing models can be used to determine the proportions of the various contributing sources of OM, e.g., the open-source Bayesian isotope modeling packages like the Stable Isotope Mixing Model in R (SIMMR) (Kusumaningtyas et al., 2019; Parnell et al., 2013; Rahayu et al., 2019; Sasmito et al., 2020) or two-end mixing models (Bouillon et al., 2003; Kennedy et al., 2004; Thornton and McManus, 1994; Xiao and Liu, 2010). The aim of this study was therefore to determine the variation of sediment organic matter along Umba river by utilizing already developed and tested methodology of elemental and stable isotopes of carbon and nitrogen as natural tracers (Kusumaningtyas et al, 2019; Khan et al., 2015; Sasmito et al, 2020; Bouillon et al., 2003). Additionally, Bayesian modeling was utilized to constrain and characterize various sources of sediment OM (SOM) (Rahayu et al., 2019; Sasmito et al, 2020; Kusumaningtyas et al., 2019) within the Vanga, Estuary. In this study, a combination of $\delta^{13}C$ values and C/N ratios has been used to disentangle the sources contribution of different end members. Organic matter in estuarine systems with both riverine and tidal influences, are either produced autochthonous produced *in-situ*, allochthonous transported by rivers and tides or anthropogenic (Khan et al., 2015; Gonneea et al., 2004; Bouillon et al., 2008). Autochthonous OM plays key role in coastal ecosystem dynamics while terrigenous sediments have been shown to largely influence aquatic productivity

with increased supply of terrigenous OM shifting systems from autotrophic to heterotrophic production (Deininger and Frigstad, 2019). Knowledge of sediment sources, consequently assist in understanding the sediment budgets and sedimentation within an ecosystem. This is crucial for mangrove ecosystems as sediments indirectly assist mangroves to build-up their elevations against local sea-level rise (Woodroffe et al., 2016). Therefore, it is vital to understand the localized sources of sediments in tropical estuaries and mangrove habitats. Source characterization also allows for planning and determination of site-specific sediment budgets and mangrove surface elevation changes vital in understanding the potential response of mangroves to the current and predicted sea-level rise (Woodroffe et al., 2016) and consequently better mitigation measures. The holistic studies of sediment dynamics present an avenue for better understanding of carbon sequestration and climate change mitigation (Alongi, 2014; Woodroffe et al., 2016). In this study we hypothesize that the riverine OM sources are the dominant contributors to the total SOM in Vanga, Estuary. To test our hypothesis, we investigated the distribution of SOM in different sediment types from source to mouth and within the estuary. Based on the OM distribution we modeled the percentage contribution of each sediment type as an end-member source to the overall SOM in Vanga Estuary.

4.2 Materials and methods

4.2.1 Study area

The Vanga estuary is located along the south coast of Kenya (4˚ 39′ S and 39˚ 13′ E). It receives freshwater and terrigenous sediments from the transboundary Umba River. The river is approximately 200 km long and drains its catchment from its source in the Usambara Mountains in northeast Tanzania, before crossing the Kenyan-Tanzanian border and flowing into the Indian Ocean through a ~3,000 ha (Mungai et al., 2019) patch of mangroves at Vanga (Figure 4-1). This site was chosen because

Vanga Estuary is within the proposed transboundary conservation area (TBCA) between Tanzania and Kenya (Tuda et al., 2019). The proposed TBCA extends from Diani, Kenya in the north to Tanga, Tanzania in the south. (Figure 4-1). This stretch of the coastal strip harbors rich, contiguous and connected marine and coastal biodiversity transcending the Kenya-Tanzania border. Due to the rich biodiversity and associated contribution to the socio-economics of the area, the TBCA has been recognized by international agencies including the World Wildlife Fund (WWF) and Convention for Biological Diversity (CBD) as a biodiversity hotspot that needs conservation attention. Fishing, smallholder crop and animal farming on the riverbanks of the Umba River are the main activities of inhabitants of Vanga (Fortnam et al., 2020).

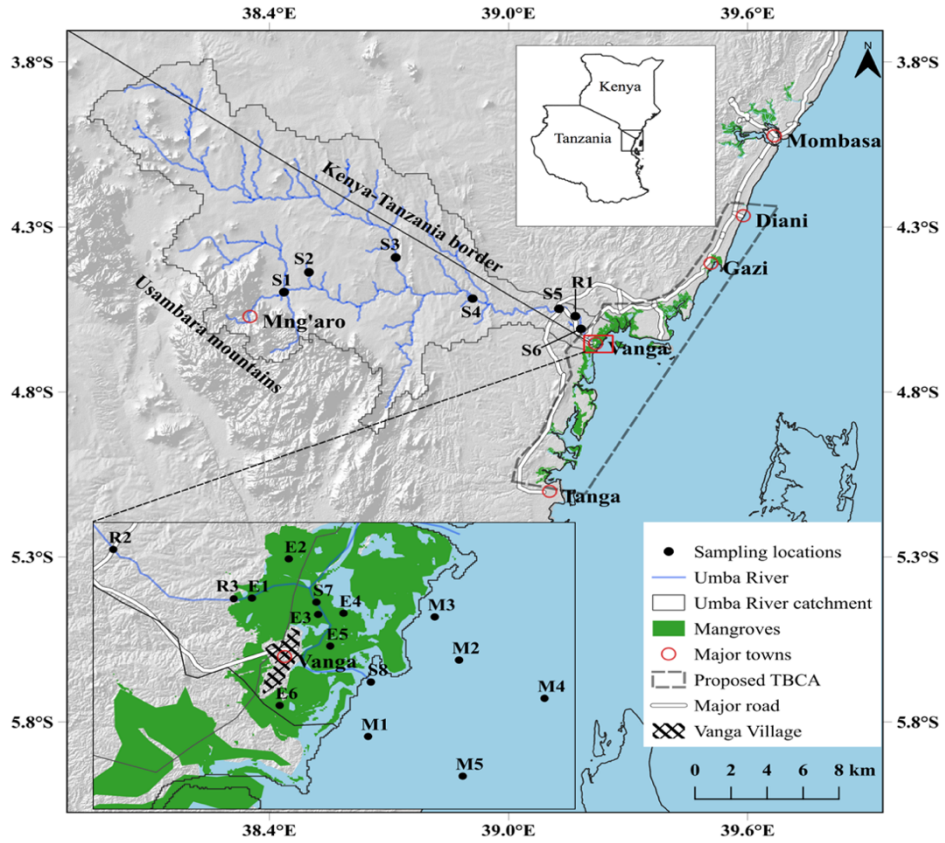

Figure 4-1. Map of study area showing the course of the Umba River and sampling stations, from its source in the Usambara mountains in Tanzania to its mouth in Vanga Estuary, Kenya.

4.2.2 Climate

East African tropical climate is controlled majorly by the large-scale pressure systems of the Western Indian Ocean and the two distinct monsoon periods (Ayugi et al., 2020). The pressure systems are attributed to a combination of mesoscale convective systems, globally propagating convection-triggering waves and the inertial instability in generating convection (Ayugi et al., 2020; Nicholson, 2018; Verschuren et al., 2009) with the effect of producing two rainy seasons between March and July and between October and November (Figure 4-2). Long-term historical precipitation data from three stations (Vanga, Lungalunga, and Mwena) in south coast Kenya manifests two rainy seasons (Figure 4-2). This pattern complements historical data from the Global Precipitation Climatology Centre (GPCC) online repository and shows a similar precipitation pattern (Fortnam et al., 2020).

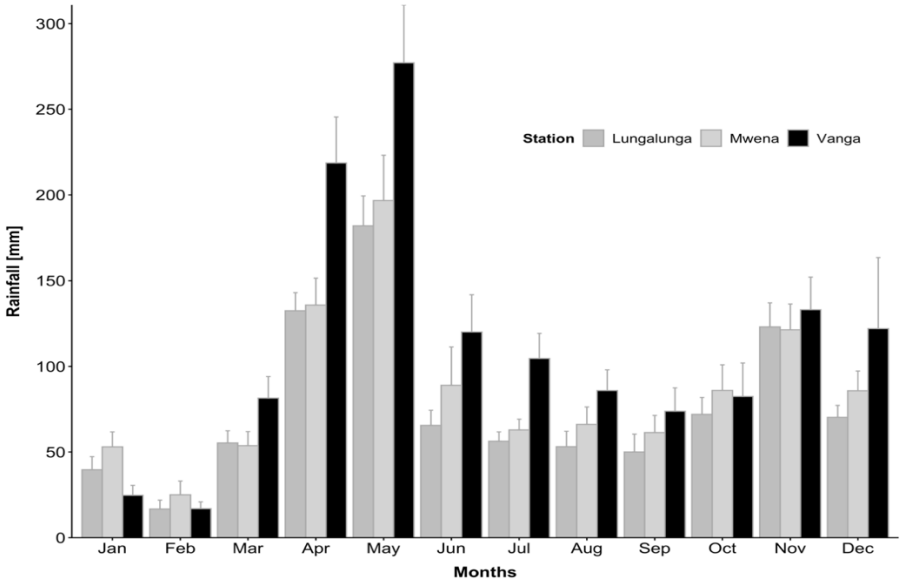

Figure 4-2. 35-year (1960-1995) average precipitation in Mwena, 42-year average (1960-2002) precipitation in Lungalunga and 31-year (1960-1991) average precipitation in Vanga. All the stations are located in south coast of Kenya at a distance of 20 km and 10 km between Vanga-Lungalunga and Vanga-Mwena respectively. The error bars represent the standard errors of the historical mean monthly precipitation. Source: Kenya Meteorology Department (https://www.meteo.go.ke/).

4.3 Field sampling and pretreatment

Field sampling campaigns were conducted during i) the dry season in February - March 2019, ii) the wet season in June - July 2019, and iii) at the end of the wet season in July 2020 (Table 4-2). Surface sediment samples were collected in ten riverine stations along the Umba River (Figure 4-1). Three of the sampling sites (S1, S2, S4) were on the Tanzanian side, while seven of the sampling sites (S5, S6, S7, S8, R1, R2, R3) were located on the Kenyan side. Estuarine intertidal surface sediments were collected in six stations close (10m) to the main channel (E1, E3, E5) and farther (50 m) away from the main channel (E2, E4 and E6). Coastal/marine subtidal (<20 m depth) sediment samples were collected stations M1, M2, M3, M4 and M5 (Figure 4-1). Surface (0-5 cm depth) sediment samples were collected using a hand-held corer and a mini Van Veen grab (Tamooh et al., 2012). Three replicate sediment samples were collected and placed in tight zip-lock plastic sample bags and placed in cooler boxes for further analysis in the laboratory. Sediment cores were taken in stations E1 to E5 using a 60 cm long *Hydrobios* sediment sampler. The extracted cores were subsampled every 5 cm in the top 20 cm and every 10 cm for the remainder of the core (Kusumaningtyas et al., 2019; Rahayu et al., 2019). Water sampling for suspended particulate organic matter (SPOM) was done using vacuum pump and Niskin bottle at depth 1-2 m below the river surface and 5 m below the sea surface. Subsequent extraction of SPOM from the water samples were done using the gravimetric method (Nasir et al., 2016). Environmental parameters were measured *in-situ* using Palin test and YSI multiparameter. Plant tissue samples comprising mature and freshly fallen yellow mangrove leaf samples and twig litter from *A. marina*, *R. mucronata*, *X. granatum*, *C. tagal* and *B. Gymnorrhiza* were collected by hand comprising of 2 leaves/sample. The leaves were washed and dried at 60°C for 72 h (Bouillon et al., 2003).

4.4 Analytical methods

4.4.1 Laboratory analysis

Grain size analyses were made using the principle of diffraction and diffusion of monochromatic laser beam on suspended particles suing a Malvern© 2000 Mastersizer particle analyzer. Mean grain size (μm) was estimated according to Folk and Ward (1957). The principle is based on forward scattering of laser beam by suspended sediment particles. A range of 0.02 and 2,000 μm can be measured. Sediment samples for OM analyses were dried at 60°C for 48 h, grinded and homogenized using a Fritsch© Pulverisette 7 ball mill (Khan et al., 2015; Kusumaningtyas et al., 2019). Subsamples for organic carbon (C) and carbon stable isotope ($\delta^{13}C$) analyses were washed with diluted 1N hydrochloric acid (HCl) first to remove potential carbonates and re-dried for 24 hrs at 40°C. The sediment samples were then flash-combusted in a CN elemental analyzer (Eurovector EA3000 Elemental Analyzer) to obtain total carbon content (TC), total nitrogen (N) and organic carbon (C) content in . The samples were then measured for C and N stable isotope composition using a Thermo Finnigan Deltaplus Mass Spectrometer coupled to a Flash EA1112 Elemental Analyzer. Measured $\delta^{13}C$ and $\delta^{15}N$ values are denoted by the conventional delta (δ) notation and expressed in parts per million (‰) deviations from a VPDB and atmospheric nitrogen standards for $\delta^{13}C$ and $\delta^{15}N$ respectively. The isotopic ratios of $^{13}C/^{12}C$ and $^{15}N/^{14}N$ were defined by the equation below:

$$\delta^{13}C\ (‰) \text{ or } \delta^{15}N\ (‰) = [(R_{sample} - R_{standard}) / R_{standard}] \times 1000$$

where $R = {}^{15}N/{}^{14}N$ or $^{13}C/^{12}C$. Data quality control throughout the analysis was ensured by running a reference standard (acetanilide) after every five runs. This was done mainly to permit corrections for machine drift and deviations to be incorporated prior to calculation of isotope abundances. The analytical precision of

instruments was determined by replicate analysis of the standards which resulted in standard deviations of C = ± 0.09%, N = ± 0.02% and $\delta^{13}C_{org}$ = ± 0.07‰.

4.4.2 Stable Isotope Mixing Model in R-program (SIMMR)

The Bayesian isotopic modeling package SIMMR was used to estimate the proportional contribution of potential sources to sedimentary OM in the mangroves of Vanga (Parnell et al., 2013; Sasmito et al., 2020; Kusumaningtyas et al., 2019; Rahayu et al., 2019). Various OM have distinct isotopic compositions borne of the different ways how different plants (the C3, C4 and CAM) fix carbon during photosynthesis (Rahayu et al., 2019, Kusumaningtyas et al., 2019). A combination of $\delta^{13}C$ and C/N was used as the input parameters in the model, because it solves the inherent challenge posed by the overlap of $\delta^{13}C$ values between C4 vegetation and marine-derived OM (Hemminga et al., 1994; Khan et al., 2015). Carbon to nitrogen (C/N) ratio can further distinguish aquatic and terrestrial OM due to relative high N content in marine-derived OM. SIMMR uses the Markov Chain Monte Carlo (MCMC) algorithm to disentangle the source and proportion of the contributing sources in an admixed sediment while incorporating uncertainties due to isotopic fractionation, concentration-dependencies and residual errors (Kusumaningtyas et al., 2019; Rahayu et al., 2019). The SIMMR model assumes that early degradation of organic matter in mangrove sediment does not significantly alter the stable isotope composition (Khan et al., 2015; Kusumaningtyas et al., 2019; Sasmito et al., 2020) and therefore the isotopic fractionation and concentration-dependencies are negligible. However, C/N ratios would expectedly vary with time as OM are degraded (Herbon and Nordhaus, 2013; Bouillon et al., 2003) and therefore, C/N ratios would potentially be underestimated in the model. To mitigate this, average of output proportions from a combination of different OM signatures has been utilized (Sasmito et al., 2020). In this study we have utilized a combination of i) $\delta^{13}C$ and C/N and ii) $\delta^{13}C$ and N/C which is a linear tracer for comparisons. Only the wet season was modeled because i) maximum riverine discharge and input (Tesfamariam

et al., 2018) and ii) riverine and marine POM were collected only during the 2020 wet season and therefore provided a complete dataset (Table 4-2). Having defined *a priori* the model inputs, four major end-members (marine POM, riverine POM, mangrove leaf and litter and terrestrial C3 plants) that are incorporated in sediments were modeled. Mangrove leaf and litter were not separated because the OM variation between them has been shown to be either overlapping (Kusumaningtyas et al., 2019) or minimal (Bouillon et al., 2003). The mean and standard deviation of each end-member was calculated and input into the model. Then the dataset containing the values of mangrove sediments were also loaded into the model in order to resolve their source and proportions through several model iterations up-to 1000 times. The results were presented using a boxplot which depicts the 50% credibility interval (Rahayu et al., 2019).

4.4.3 Statistical Analysis

Statistical analyses were performed using inbuilt packages in R-program (v. 1.1.463) (R Core Team, 2020). Differences of organic matter variables in sediments and plant tissues by stations, environment, species and sediment depths were analyzed using analysis of variance (ANOVA). Data conformity to normal distribution was examined using the Shapiro-Wilk test of normality. The data that did not pass the normality test were transformed prior to ANOVA analysis (for detailed results see Supplementary Information 4-4).

4.5 Results

4.5.1 Grain size distribution

Grain size distribution of Umba River sediments fall within a narrow range between sand and silty sand and the estuarine sediments were classified as sandy silt grain size due to the elevated silt content with minimal clay proportion compared to the riverine and marine sediments (Table 4-1).

Table 4-1: Showing grain size distributions of sediments along the Umba River

			Dry season grain size				Wet season grain size			
Station	Environment	Sample size (n)	%Sand	%Silt	%Clay	Sediment classification after Folk and Ward (1957)	%Sand	%Silt	%Clay	Sediment classification after Folk and Ward (1957)
S1	Riverine	3	61.5	38.4	0.1	Silty sand	65.1	34.7	0.2	Silty sand
S2	Riverine	3	87.6	12.4	0.0	Silty sand	66.9	31.8	1.2	Silty sand
S4	Riverine	3	76.1	23.6	0.3	Silty sand	85.1	11.5	0.1	Silty sand
S5	Riverine	3	70.6	27.9	1.4	Silty sand	59.2	39.0	1.8	Silty sand
S6	Riverine	2	41.8	55.4	3.1	Sandy silt	46.7	50.7	2.7	Sandy silt
S7	Estuarine	11	43.4	54.1	2.4	Sandy silt	36.0	61.1	2.8	Sandy silt
S8	Marine	4	99.4	0.6	0.0	Sand	99.3	0.70	0.0	Sand

4.5.2 Elemental and isotopic composition of sediment organic matter

The mean elemental and stable isotope data are presented in Table 4-2 and in Figure 4-3. Significant inter-station variation ($p < 0.05$) was observed for OM properties during both seasons as well as by sediment type except ($p > 0.05$) for TC, C and C/N ratio during the dry season and only C/N ratio during the wet season. There was no significant ($p > 0.05$) variation in the sediment OM content between the two seasons except for C/N ratios and $\delta^{13}C$ values (Supplementary Information 4-4). $\delta^{13}C$ values were higher ($p < 0.05$) in marine sediments (-20‰) compared to both agricultural soil, riverine and estuarine sediments (-23‰) during both seasons (Table 4-2, Figure 4-3a, 4-3b, 4-3d, 4-3e). A post hoc Tukey test further showed that the $\delta^{13}C$ values differed significantly ($p < 0.05$) between marine and estuarine sediment. Mean values of C/N, N/C, $\delta^{13}C$ and $\delta^{15}N$ intertidal and subtidal sediments differed significantly ($p < 0.05$) during both seasons except for $\delta^{13}C$ during the dry season (Supplementary Information 4-4) with further confirmation by a post hoc Tukey ($p = 0.033$, $\alpha = 0.05$). $\delta^{13}C$ values of intertidal sediments were lower than those of subtidal sediments

during both seasons (See Supplementary information 4-3). Overall, majority of the estuarine sediments showed C/N ratios >10 during both seasons and by both intertidal and subtidal sediments (Table 4-2 and Supplementary information 4-3).

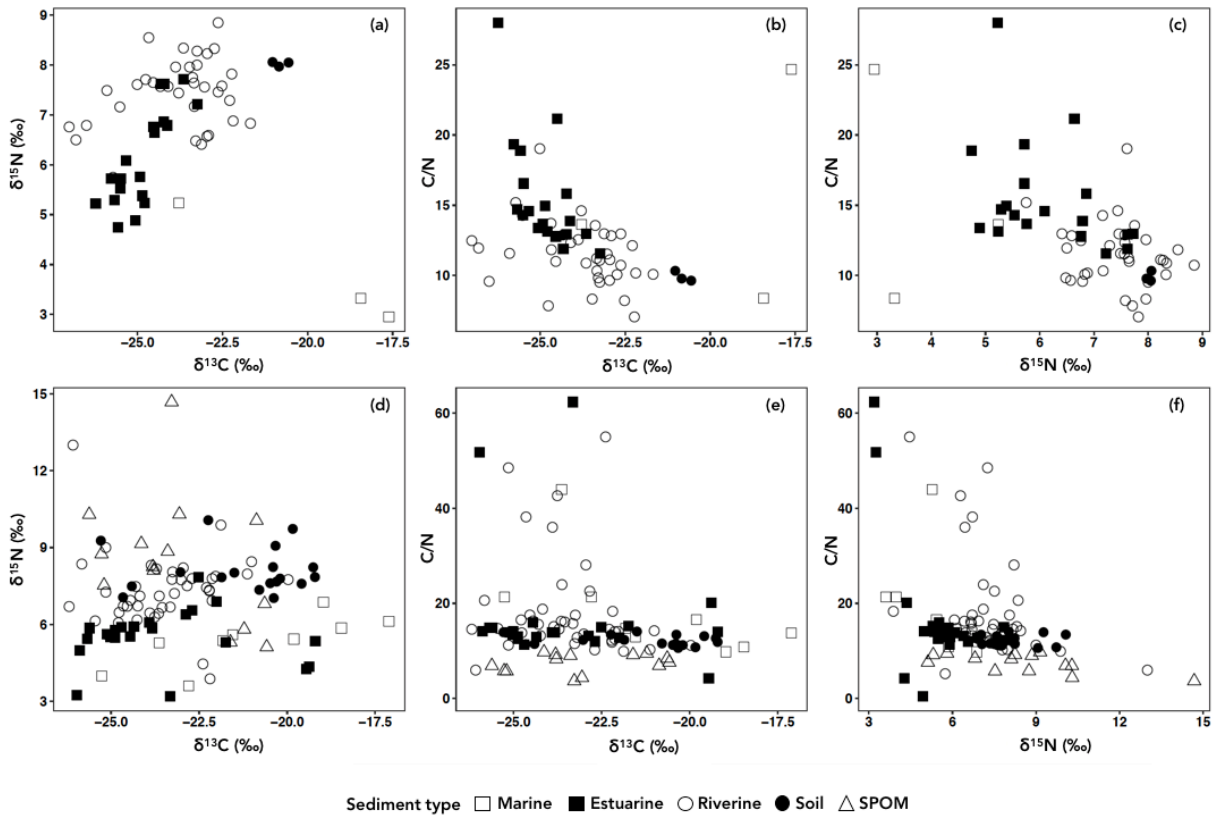

Figure 4-3. Relationships between $\delta^{13}C$, $\delta^{15}N$ and C/N in different sediment samples , environments and during different seasons (top row (a to c) represent the dry season and bottom row (d to f) represent the wet season).

Table 4-2: Mean values (± SD) of sediment elemental total carbon (TC), organic carbon (C) and total nitrogen (TN), C/N ratio (µg/ µg dry weight), $\delta^{15}N$ and $\delta^{13}C$ stable isotopes from all sampled stations along the transboundary Umba River during both the dry and wet season.

	TN (%)	**TC (%)**	**C (%)**	**C/N**	**$\delta^{15}N$ (‰)**	**$\delta^{13}C$ (‰)**
Dry Season 2019						
Riverine (n=36)	0.1 ± 0.1	1.3 ± 1.2	1.1 ± 1.2	11.5 ± 2.3	7.4 ± 0.7	-23.8 ± 1.4
Estuarine (n=19)	0.2 ± 0.1	2.1 ± 1.4	2.1 ± 1.3	15.5 ± 3.9	6.2 ± 0.9	-24.8 ± 0.8
Marine (n=3)	0.01 ± 0.004	0.2 ± 0.1	0.1 ± 0.03	15.6 ± 8.3	3.8 ± 1.2	-19.9 ± 3.4
Soil (n=3)	0.2 ± 0.01	2.7 ± 0.1	2.3 ± 0.1	9.9 ± 0.4	8.0 ± 0.1	-20.8 ± 0.2
Wet season (Jun - Jul 2019)						
Riverine (n=34)	0.1 ± 0.1	0.8 ± 0.7	0.7 ± 0.7	22.3 ± 20.7	7.1 ± 1.5	-23.9 ± 1.1
Estuarine (n=9)	0.2 ± 0.1	2.6 ± 1.4	2.6 ± 1.3	18.9 ± 16.7	5.1 ± 1.0	-24.9 ± 0.7
Marine (n=3)	0.1 ± 0.1	1.9 ± 1.6	1.7 ± 1.6	21.0 ± 11.9	5.0 ± 0.9	-24.5 ± 1.1
Soil n=6)	0.2 ± 0.1	2.4 ± 0.5	2.3 ± 0.5	11.2 ± 0.4	8.3 ± 0.9	-20.1 ± 0.5
Wet season (Jun - Jul 2020)						
Riverine (n=10)	0.03 ± 0.03	0.4 ± 0.4	0.4 ± 0.4	12.7 ± 1.8	8.0 ± 0.8	-21.9 ± 1.1
Estuarine (n=16)	0.1 ± 0.1	1.0 ± 1.2	0.9 ± 1.2	13.5 ± 3.9	5.9 ± 1.1	-23.8 ± 1.8
Marine (n=6)	0.01 ± 0.01	0.3 ± 0.2	0.1 ± 0.1	13.1 ± 2.5	5.9 ± 0.6	-19.6 ± 1.8
Soil (n=12)	0.2 ± 0.2	2.5 ± 1.9	2.5 ± 1.9	12.6 ± 0.9	8.0 ± 0.9	-21.9 ± 2.0
Riverine POM (n=5)	0.3 ± 0.1	2.4 ± 0.6	2.2 ± 0.6	7.7 ± 1.9	8.5 ± 0.7	-24.4 ± 0.8
Estuarine POM (n=4)	0.2 ± 0.1	1.2 ± 0.8	1.2 ± 0.8	6.0 ± 2.5	10.9 ± 2.7	-23.9 ± 1.2
Marine POM (n=5)	0.6 ± 0.4	7.3 ± 4.0	4.9 ± 2.2	8.3 ± 1.1	6.6 ± 2.0	-20.9 ± 0.4

Riverine sediments exhibited high $\delta^{15}N$ but relatively low $\delta^{13}C$ values (Figure 4-3a, 4-3d) coinciding with high C/N ratios (>10) (Figure 4-3b, 4-3c) during both seasons. On average, $\delta^{13}C$ values were highest (-19‰) in marine sediments during both the dry and wet season (Table 4-2). There was also a marked enrichment of ^{13}C in riverine (-21.9 ± 1.1‰) and agricultural soil (-21.9 ± 2.0‰) relative to estuarine sediments during the wet season (Table 4-2). High $\delta^{15}N$ values (>7‰) were observed in agricultural soils and riverine sediments (Table 4-2, Figure 4-3c, 4-3f) compared to marine and estuarine sediments values (<6‰) during both seasons. Mangrove leaves and litter showed significant variation ($p < 0.05$) in C, TN, C/N ratio and $\delta^{13}C$ contents between both the species and plant tissues (Figure 4-4 and Supplementary Information 4-4). On one hand, ^{13}C in *B. gymnorrhiza* leaves was relatively depleted (-30.4 ± 1.2‰) relative to *X. granatum* leaves (-27.9 ± 1.1‰) (Table 4-3). On the other hand, $\delta^{13}C$ values in mangrove litter was lowest in *A. marina* (-28.6 ± 1.3‰) compared to the marginally high values in *C. tagal* species (-27.9 ± 1.4‰). Generally, $\delta^{13}C$ values of leaves (-29.5 ± 0.4‰) and litter (-28.7 ± 1.0‰) in terrestrial C3 plants were lower compared to all the analysed mangrove species (Table 4-3, Figure 4-4). There was a general non-variation of OM content between the measured mangrove tissues material ($p > 0.05$, see Supplementary Information 4-4) but relatively high $\delta^{13}C$ values and C/N ratios in mangrove litter than in mangrove leaves in all species (Table 4-3, Figure 4-4). The C/N content in mangrove estuarine sediments showed high mean values (>13) during both seasons (Table 4-2, Figure 4-3b, 4-3c, 4-3e, 4-3f) and were considerably lower than in the mangrove leaf and litter the primary producers (Table 4-3, Figure 4-4). $\delta^{13}C$ values were higher in estuarine sediments including estuarine POM (-24‰) relative to mangrove leaves and litter (-28‰) (Table 4-2 and 4-3). C/N ratios and $\delta^{13}C$ values of SPOM were relatively lower than those of the other sediments (Figure 4-3e, 4-3f) but showed low and high $\delta^{15}N$ values in marine and estuarine POM respectively (Table 4-2).

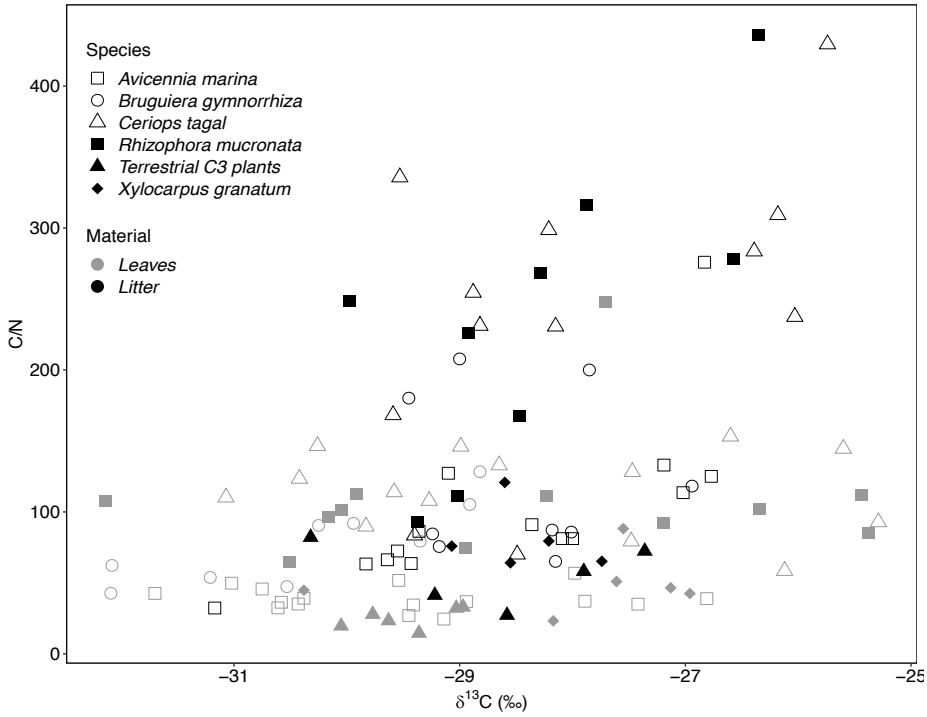

Figure 4-4: Bi-plot of stable carbon isotope and elemental C/N ratios of mangrove leaf and litter of different species found in Vanga, estuary. The grey colored represents the leaves while the dark colored represents the litter.

Table 4-3: Mean (± s.d.) elemental C/N ratios and carbon stable isotope ($\delta^{13}C$) of mangrove leaves and litter from the Vanga Estuary, Kenya. *n* = number of samples.

Species (no. of samples)	**Material**	**$\delta^{13}C$ (‰)**	**C/N**
C. tagal (n = 14)	Leaf	-28.3 ± 1.8	116.2 ± 27.4
C. tagal (n = 12)	Litter	-27.9 ± 1.4	244.4 ± 97.4
B. gymnorrhiza (n = 9)	Leaf	-30.4 ± 1.2	77.9 ± 27.2
B. gymnorrhiza (n = 9)	Litter	-28.5 ± 0.8	122.7 ± 53.9
R. mucronata (n = 12)	Leaf	-28.5 ± 2.1	109.0 ± 44.3
R. mucronata (n = 9)	Litter	-28.3 ± 1.2	238.3 ± 100.1
A. marina (n = 16)	Leaf	-29.5 ± 1.4	38.9 ± 8.36
A. marina (n = 14)	Litter	-28.6 ± 1.3	100.9 ± 55.9
X. granatum (n = 6)	Leaf	-27.9 ± 1.1	49.4 ± 19.5
X. granatum (n = 5)	Litter	-28.4 ± 0.4	81.1 ± 20.7
Terrestrial C3 plants (n = 6)	Leaf	-29.5 ± 0.4	25.1 ± 6.6
Terrestrial C3 plants (n = 5)	Litter	-28.7 ± 1.0	56.2 ± 20.0

4.5.3 Downcore profiles of organic matter composition

The bulk elemental and isotopic analyses of the estuarine sediments showed varied profiles, both, vertically within cores and spatially between different cores (Figure 4-5). There was a significant variation ($p < 0.05$, see Supplementary Information 4-4) of sediment OM properties in different stations except for C/N ($p > 0.05$). On the contrary variation of sediment OM properties with depth was not significant ($p > 0.05$) except for dry bulk density (gcm^{-3}) and C/N ratio ($p < 0.05$).

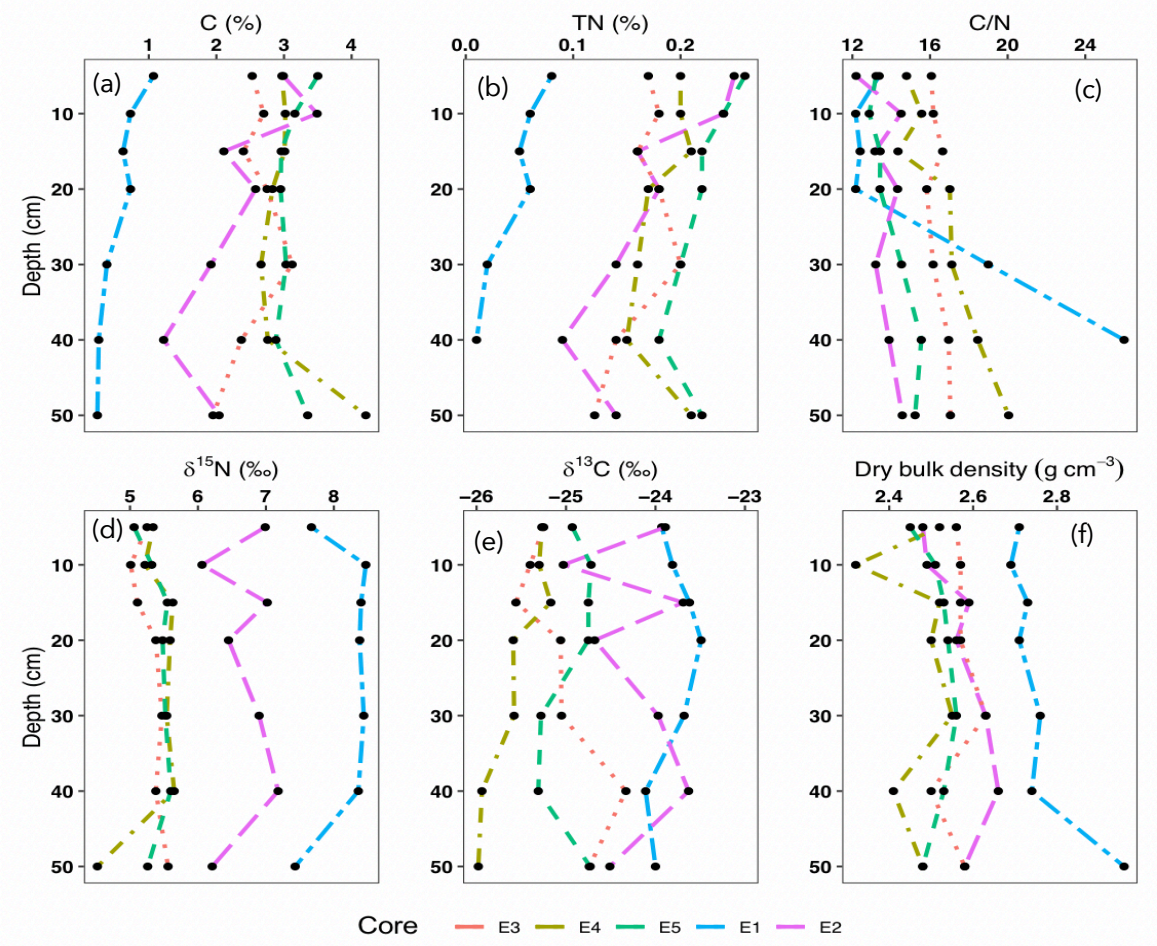

Figure 4-5: Downcore variation of (a) organic carbon, (b) total nitrogen, (c) C/N ratio, (d) $\delta^{13}C$ (e) $\delta^{15}N$ and (f) dry bulk density with soil depth of up to 50 cm in the Vanga Estuary.

Relative downcore decrease in C and TN was observed compared to an increase in C/N ratio and DBD (Figure 4-5). Particularly the core E1 taken at station E1 (Figure 4-1) showed a striking low C, TN, and relatively higher DBD values compared to the

other cores. There was also a subtle decreases in TN in all the cores in the top 40 cm (Figure 4-5b) and an increase at 50 cm.

4.5.4 Determination of proportional OM sources using SIMMR model

Model input parameters are presented in Supplementary Information 4-1. The model revealed that the sediment OM in the Vanga estuary, had varied sources with discernible mixing as seen in the bi-plots of $\delta^{13}C$ and C/N ratio (Figure 4-6, Supplementary Information 4-1). Riverine POM is the dominant OM source in the sediments that accumulated in the Vanga estuary (Figure 4-7). The riverine POM which would expectedly include both agricultural soil from surface runoff from the hinterland, contributed over 50% (median = 60%) of total sediment OM (Figure 4-7). Marine POM was the second largest contributor of OM to the estuarine sediments of Vanga with close to 20% (median = 18%). However, when N/C ratio was utilized (Supplementary Information 4-1), marine POM contributed slightly more up to 50% (median = ~40%) compared to riverine POM which contributed up to 40% (median = ~27%) (Figure 4-7, Supplementary Information 4-1). OM derived from mangroves and terrestrial C3 plants both contributed less than 20% to the overall sedimentary OM (Figure 4-7) but the contribution of terrestrial C3 plants was marginally high compared contribution of mangroves leaves and litter (Figure 7, Supplementary Information 4-1). Based on the average from the two combinations, $\delta^{13}C$ and C/N and $\delta^{13}C$ and N/C, the overall contribution from each end member was 45%, 32%, 13% and 8% for riverine POM, marine POM, terrestrial C3 plants and mangrove leaf and litter, respectively (Supplementary Information 4-1). There was a positive and relatively high correlation between marine POM and terrestrial C3 plants in both $\delta^{13}C$ and C/N (0.67) and $\delta^{13}C$ and N/C (0.55) combinations (Figure S1a in Supplementary Information 4-1). However, there was an observed low positive and high negative correlation between marine POM, riverine POM and mangroves leaf and litter.

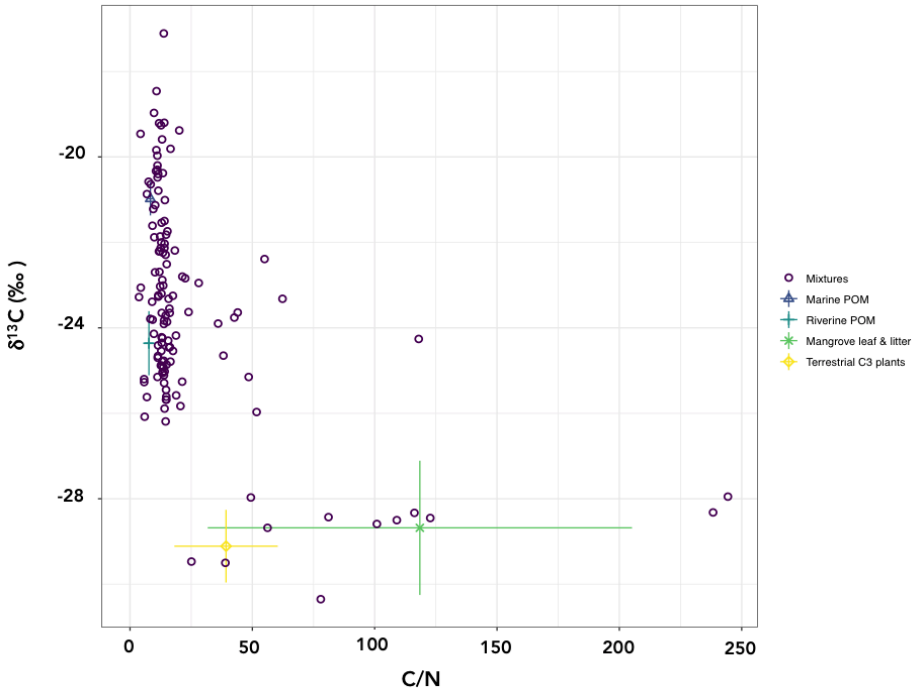

Figure 4-6. Bi-plot of $\delta^{13}C$ and C/N ratio of sediments from the study area along the Umba River and potential end-member mixing. The average values of the selected end members are shown.

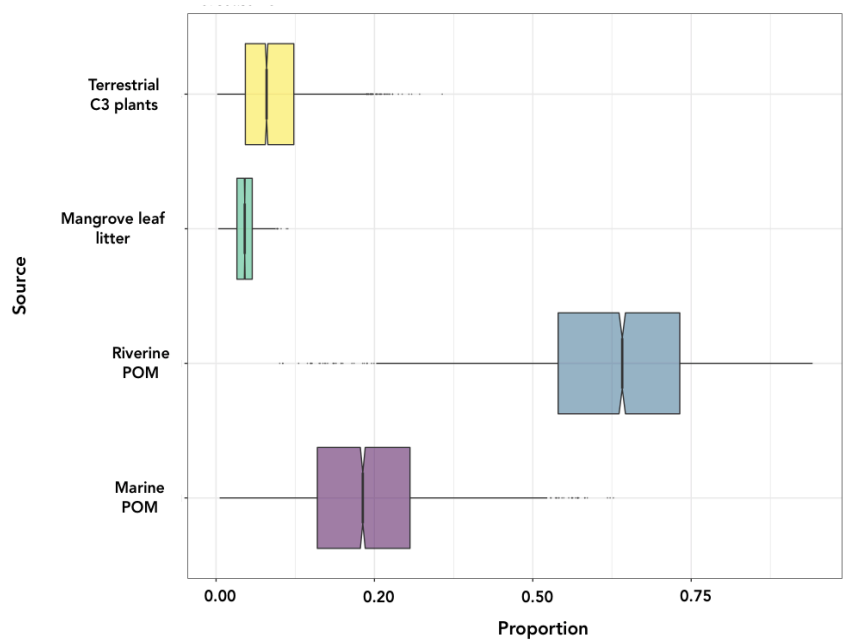

Figure 4-7. SIMMR model outputs of proportional contribution of end-members to total sediment organic matter during wet season (boxes represent the 50% credibility interval of individual end-member proportional contribution; lines within boxes represent median values).

4.6 Discussion

4.6.1 Spatio-temporal variability of sediment organic matter

Organic carbon (C) content in estuarine sediments were higher than marine sediments during both seasons (Table 2) attributable to proximity to mangroves the primary producer (Bouillon et al., 2003). Agricultural fertilizer input in the catchment farms could explain the high C values recorded in riverine sediments during the rainy seasons (Kiteresi et al., 2012; Ray et al., 2018). Further, the high C/N ratios between 13 and 19 during both seasons (Table 4-2) indicates the influence of the Umba River as it has been postulated that C/N ratios >10 are indicative of a terrestrial origin of detritus (Bouillon et al., 2003; Tamooh et al., 2012). Additionally, high C/N values in estuarine sediments (Figure 4-3b) during the dry season, reflect reduction in river discharge and dominance of tidal fluxes and the additional contribution of organic matter from the sea (Kusumaningtyas et al., 2019; Rahayu et al., 2019; Rumolo et al., 2011). The relatively high C/N ratios in estuarine sediments (Table 2) also suggests the variable contribution of both terrestrial (river-derived) and *in-situ* produced material (Bouillon et al., 2003) but the inverse proportionality of C and $\delta^{13}C$ values in estuarine sediments have been shown to reflect the contribution of terrestrial material (Middelburg et al., 1996). However, in this study there was no clear correlation between C and $\delta^{13}C$ values in estuarine sediments, which could mean multiplicity of sources of OM and mixing within the Vanga, Estuary. The grain size distribution of Umba River sediments is classified within a narrow range between sand, silty sand and sandy silt (Kimeli et al., 2021). The average sediment grain sizes in the Vanga Estuary (S7) classified under sandy silt (see Table 1), indicates that the influence of grain size on the OM distribution is minimal. We therefore conclude that the dynamics, variation and distribution of OM in the Vanga estuary is attributable to the different sources of OM and transportation, deposition and post-deposition processes. This processes include mixing, decomposition and dilution (Bouillon et al., 2003; Kristensen et al., 2008). The $\delta^{15}N$ and $\delta^{13}C$ signatures and the C and TN

values obtained in this study are comparable to those reported from other studies in similar settings (Hemminga et al., 1994; Jennerjahn and Ittekkot, 2002; Tamooh et al., 2014). Others have postulated that C/N ratio of SOM increases towards the range of proximal mangroves vegetation (Kennedy et al., 2004) but was not the case in this study. Estuarine sediments exhibited markedly low C/N (between 13 and 19 during both seasons) compared to the dominant primary producers, the mangroves with an average 118.7 (Table 2). $\delta^{13}C$ values were also higher in estuarine sediments (-24‰) relative to mangrove leaves and litter (-28‰) which we attributed to rapid decomposition and degradation of mangrove plant tissue as well as possibility of contribution by other low C/N primary producers (Kennedy et al., 2004). However, in river dominated estuaries, terrigenous OM is predominant due to freshwater runoff. This predominance of terrigenous OM diminishes seawards in sediment organic matter as it is replaced by POC as the freshwater flux is weakened by the increasing tidal push (Yu et al., 2010). $\delta^{13}C$ values were relatively higher (-21.9 ±1.1‰) in riverine sediments during the wet season. These values also match the $\delta^{13}C$ values of agricultural soil (-21.9 ± 2.0‰) during the same season. The increased contribution of highly enriched modern C4 plants could explain the high $\delta^{13}C$ values. Indeed, this is supported by field observation of small-scale maize cultivation along the Umba River especially in the middle section (Station S4) and most parts of the catchment on the Kenyan side. The $\delta^{15}N$ enrichment in agricultural soil and riverine sediments (Table 4-2, Figure 4-3a, 4-3c) can be attributed to possible input of organic fertilizer from animal waste (Garg and Bhatnagar, 1999) in the cultivated land in the upper catchment that end up in the river through erosion and surface runoff. The relatively low $\delta^{13}C$ values (~-24‰) in the estuarine samples can be attributed to the introduction of ^{13}C-depleted OM from proximal mangroves (Kristensen et al., 2008) however, dilution due to river inflow and the potential input of low $\delta^{13}C$ values from excessive mineralization within the water column or in the intertidal sediments could also explain the low $\delta^{13}C$ values (Bouillon et al., 2008; Kristensen et al., 2008). ^{13}C-

enrichment in marine POM relative estuarine POM sediments during both seasons (Table 4-2), agrees with the findings of others (Hemminga et al., 1994) in similar environments. They attributed this gradient and variation to inwelling of marine-derived OM including relatively ^{13}C-enriched seagrass materials. This could also explain the relatively high $\delta^{13}C$ values in subtidal sediments than in intertidal sediments (Supplementary Information 4-3) where the lighter ^{12}C have been preferentially utilized during decomposition by benthic organisms (Middelburg et al., 1996). SOM in intertidal and subtidal sediments represent different OM degradation states due to water depths variation, residence times and bed-load transportation (Dauwe et al., 2001; Dauwe and Middelburg, 1998). Therefore, fresh organic matter in mangrove-dominated intertidal areas are dominated by primary production from plant material mainly mangrove tissues (roots and leaves). Mixing, typical for a combined river-tide dominated systems, can cause a large range of values due to admixing of outwelled carbon with organic matter from other sources (Middelburg et al., 1996; Middelburg and Nieuwenhuize, 1998). Additionally, $\delta^{13}C$ values in suspension/settling particles and surficial sediments are identical in mangrove settings (Hemminga et al., 1994) and therefore, with no localized elevation in sediment C content e.g., close to point discharges, it is proposed that the dynamic processes in the mangroves of Vanga result in relatively efficient mixing and redistribution of sediment as postulated by Andreetta et al. (2014). The mixing and entangling of potential sources (Figure 4-6) could be attributed to bioturbation, burrowing and overturning the sediments. The overturning of sediments by the crabs could promote a reduction in C partly due to increased oxidation of organic matter due to increased gaseous exchange facilitated by sesarmid crab channels (Andreetta et al., 2014; Bouillon et al., 2008). Considering the inevitable mixing and reworking of sediments by microbial communities coupled with degradation of some tracers including C/N and $\delta^{15}N$, the main advantage of stable isotopes is the capability to

define "upper and lower limits" of proportional contributions to the sediment OM by different sources (Bouillon et al., 2008; Kristensen et al., 2008).

4.6.2 Downcore variation of sediment OM composition

Downcore variations of OM composition was observed in the different stations and were attributed to the varied sources of sedimentary OM in the estuarine sediments. However, the near-uniform profiles indicate the expected mixing typical for estuarine habitats like our study area. The non-varying content of $\delta^{13}C$ and $\delta^{15}N$ downcore ($p > 0.05$) has been attributed to reduced and limited microbial decomposition due to anoxia (Rumolo et al., 2011; Kusumaningtyas et al., 2019; Sasmito et al., 2020) and reduced microbial activity due to overturning of sediments. The striking variation of OM properties in core E1 (Figure 4-5) is probably attributed to its location within the study. This particular station is close to the river mouth (Figure 4-1) and relatively elevated and therefore only flooded during spring tide and extreme river discharge during peak wet season. Consequently, being starved of fresh OM, leading to the observed low C and TN and corresponding enrichment of the heavier $\delta^{13}C$ and $\delta^{15}N$ (Figure 4-5). Additionally, the increased dry bulk density (DBD) downcore is also associated with loss of moisture and dryness that causes more sediment sub-surface compaction. Downcore variations in the contents of TC content, C/N ratio and $\delta^{13}C$ values could also reflect temporal (tidal and seasonal) variability in the OM proportions from the different sources.

4.6.3 Modelled sources of sediment organic matter

The sediment OM that accumulates in the Vanga estuary showed a mixed source (Figure 4-6) with riverine POM contributing more 55 – 73 % (median= 60%) of total SOM (Figure 4-7). This can be attributed to the influence and Umba River terrigenous input and the increased discharge during the wet season (Tesfamariam et al., 2018). Marine POM was the second largest contributor of OM to the Vanga Estuary at 15 – 30% (median = 22%) (Figure 4-7, Supplementary Information 4-1). This confirms the

influence of the tidal fluxes and the material exchange within the estuary as espoused in Bouillon et al. (2003). Strikingly, the contribution of autochthonous sources of OM (<10%) predominantly mangrove tissue analysed in this study was the lowest (Figure 4-7). This is attributed to rapid degradation and possible dilution from the Umba River freshwater discharge and rapid outwashing by tidal ebbs (Kristensen et al., 2008; Sasmito et al., 2020) and further supported by the observed lower C content in estuarine sediments in Vanga during both the dry (2.1 ± 1.3 %) and the wet (1.9 ± 1.5%) seasons (Table 4-2). It could also be explained by the observed contribution of marine POM from adjacent habitats introduced ^{13}C-enriched seagrass OM (Rahayu et al., 2019). Dilution due to mineral OM derived from erosion in the wider Umba River catchment and delivered by the Umba River could have further reduced the influence of the mangrove tissue-derived OM to the overall sediment OM. Dittmar et al. (2001), also postulated that autochthonous aquatic primary production contribute subordinately to the total mangrove SOM. Evidently when N/C ratio was utilized in the model (Supplementary Information 4-1) with the dominance of marine POM to the total SOM marginally surpassed riverine POM. As mentioned earlier N/C is a linear tracer compared to C/N ratio which is bound to temporally and spatially vary markedly especially in plant tissues (Gonneea et al., 2004; Dittmar et al., 2001). Vanga has been identified as a mangrove loss hotspot (Mungai et al., 2019) mainly due to anthropogenic impacts and therefore this could exacerbate mangrove OM export to adjacent coastal habitats by tidal flush and reduces the retention of OM in the Vanga estuary sediments reducing their contribution to the overall SOM. However, this rather unusual minimal influence of mangrove-derived OM in the mangrove sediment in Vanga is not an isolated case as it has been shown that local plant production contribution to the overall sediment OM can be variable (Bouillon et al., 2003; Bosire et al., 2005; Middelburg and Niuwenheize, 1998). The low δ^{13}C values (more negative) exhibited in estuarine sediments during both during the dry (-24.9 ± 0.8‰) and the wet (-23.6 ± 2.1‰) seasons (Figure 4-3, Table 4-2) coupled

with low C content could be attributed to increased resuspension due to hydrodynamics (Jennerjahn et al., 2009; Kusumaningtyas et al., 2019) that subsequently promote enhanced decomposition. This relatively low $\delta^{13}C$ values are close to riverine $\delta^{13}C$ values support the observed pronounced contribution of riverine organic carbon sources to the cumulative sediment OM in the Vanga estuary. Large negative correlation between end-members (Supplementary Information 4-1) indicates the source contribution could not be resolved by the model. In this study, the high negative correlations between marine POM and river POM (-0.97) could further indicate the potential mixing of sediments and material exchange (Bouillon et al., 2003; Kristensen et al., 2011) within the Vanga Estuary. The non-distinction of marine POM from river POM could also indicate the influences of tidal fluxes and dilution by mineral OM delivered by Umba River. However, the positive but low correlation between marine POM and both terrestrial C3 plants (0.55) and mangrove tissues (0.37) indicate that these end-members are distinguishable however their contribution to the total SOM is not substantive (Sasmito et al., 2020). In this regard, more site-specific end-members, monthly and seasonal data need to be incorporated into the model for better source resolution and characterization.

4.6.4 Implications to sediment provenance

The comparison of $\delta^{13}C$ and C/N ratio values from different potential sources of OM to the mangrove estuary of Vanga coupled with analyses of bulk sediment samples allowed for the possible identification of dominant sources of OM to the estuary. In this study the C/N ratio recorded in estuarine sediments were >10 indicating a predominant terrestrial source of OM to the mangroves of Vanga, which confirms the hypothesized connectivity of Umba River catchment and the downstream sediment dynamics in the Vanga Estuary. The lack of damming along the Umba River means that sediment retention would occur mostly further downstream, especially in the mangrove forests where conditions for sediment deposition and retention are favorable. This study also showed that marine-derived OM contributes substantially

to the total sediment OM and brings to fore the material exchange between the estuary and adjacent coastal and marine habitats. With this realization, and coupled with the geochemical composition of Umba River bank and bottom sediments (Kimeli et al., 2021) which showed the influence of the geology of the Umba River catchment, further targeted research is merited. Umba River therefore would be a good case study for further long-term monitoring to further understand inter- and intra-seasonal quantitative sediment and OM fluxes and budgets. This further information would assist managers in having a holistic approach to a catchment-wide management, conservation and mitigation in regard to the response of the mangroves to sea-level rise.

4.7 Conclusions

This study gives insights into the contribution of different sources of OM deposited in the estuarine mangroves of Vanga. Seasonality influence is minimal in the OM distribution along the gradient of Umba River. Riverine OM has been shown to be the dominant contributor to the mangrove sediment OM and there is strong case for material exchange in the Vanga Estuary influenced mainly by physical mixing (hydrodynamics, freshwater input) both horizontally within the estuary and vertically in the sediments. This is supported mainly by the minimal contribution of from mangrove-derived OM to the sedimentary organic matter of Vanga. The relatively enhanced contribution of riverine POM compared to marine POM and *in-situ* production indicates the implications and concerns for better land use and catchment-wide management, especially, in the context of the proposed TBCA between Tanzania and Kenya. To further understand and resolve sources and the influences of the same, more site-specific and representative end-member samples and the hydrodynamic regime, river discharge and sediment budgets merit further in-depth study.

4.8 Acknowledgements

Thanks are due to the managing editor and the two reviewers for their helpful comments on a previous version of this manuscript. This study was supported by the Flemish Interuniversity Council – University Development Cooperation [VLIR-UOS] through "Transboundary coastal processes and human resource utilisation patterns as a basis for a Kenya-Tanzania conservation area initiative (Trans-Coast) Project" [grant number ZEIN2016PR425]. Further funding was obtained from the Western Indian Ocean Marine Science Association (WIOMSA) small grant [grant number MARGI_2020_CO3]. We would also like to thank George Onduso, Oliver Ocholla and Simon Langat of Kenya Marine and Fisheries Research Institute, Kenya, for the assistance during sample collection and preparation, and Donata Monien and Dorothee Dasbach of ZMT for technical laboratory assistance.

4.9 Supplementary Information

- Supplementary Information 4-1. SIMMR mixing model input values and results

- Supplementary Information 4-2. Physico-chemical parameters variation along the gradient of Umba River

- Supplementary Information 4-3: Variation of OM between estuarine intertidal and subtidal sediment samples

- Supplementary Information 4-4. *F*-values of one-way ANOVAs indicating variation of OM matter in bulk sediment and mangrove tissues with station, species, site and depth.

Supplementary Information 4-1

SIMMR Mixing model

Table 1Sa: Showing the average values of model input parameters that were used in the SIMMR simulation

	Means			**Standard deviation**		
End-Members	δ^{13}C (‰)	C/N	N/C	δ^{13}C (‰)	C/N	N/C
Marine POM	-20.98	8.33	0.12	0.39	0.96	0.01
River POM	-24.36	7.73	0.14	0.75	1.67	0.03
Mangrove detritus	-28.68	118.46	0.01	1.57	86.70	0.01
Terrestrial C3 plants	-29.11	39.25	0.03	0.85	21.11	0.02

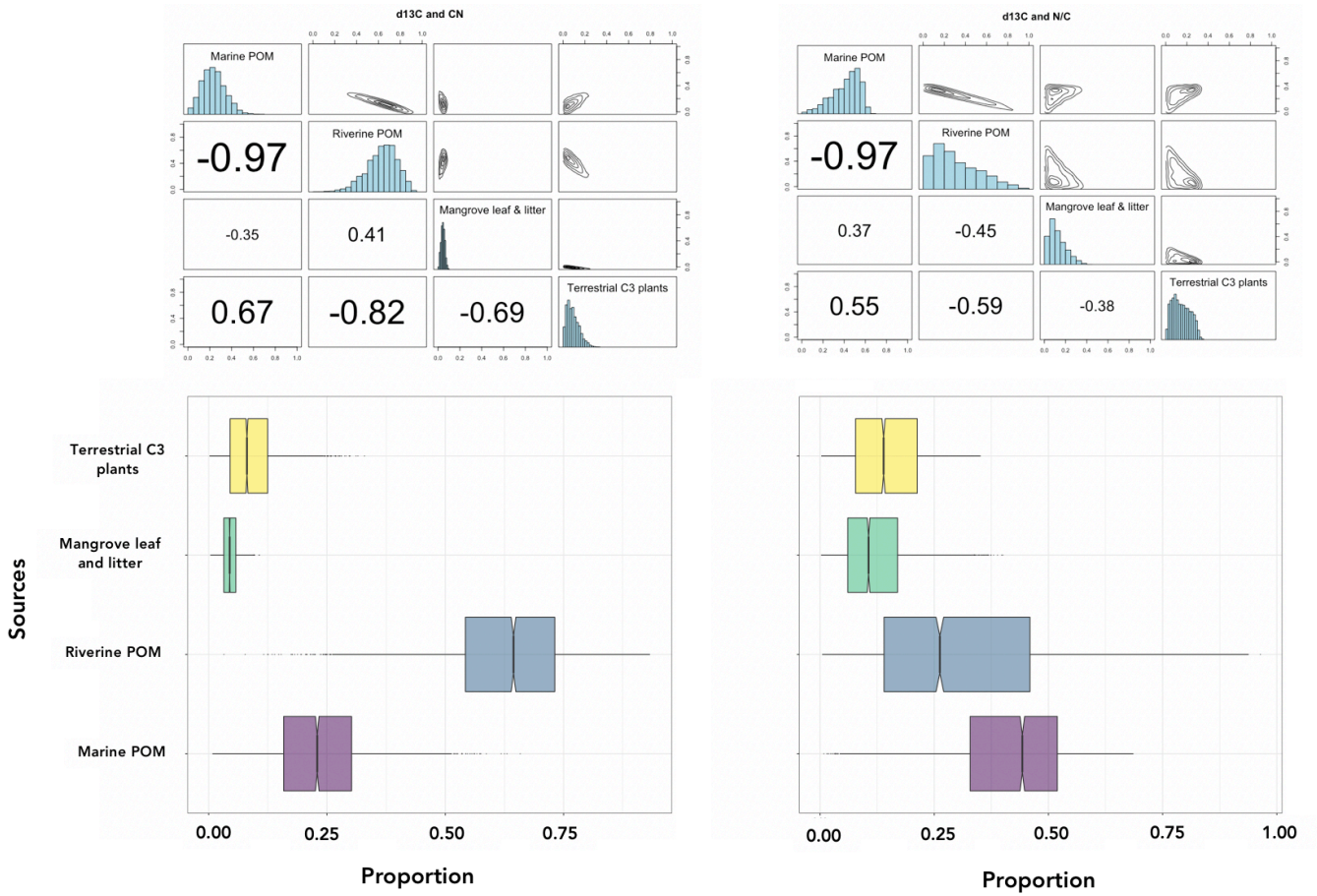

Figure S1a. Combined end-members mixing model results using a) $\delta^{13}C$ and C/N ratio (left column) and b) $\delta^{13}C$ and N/C ratio (right column) variables input.

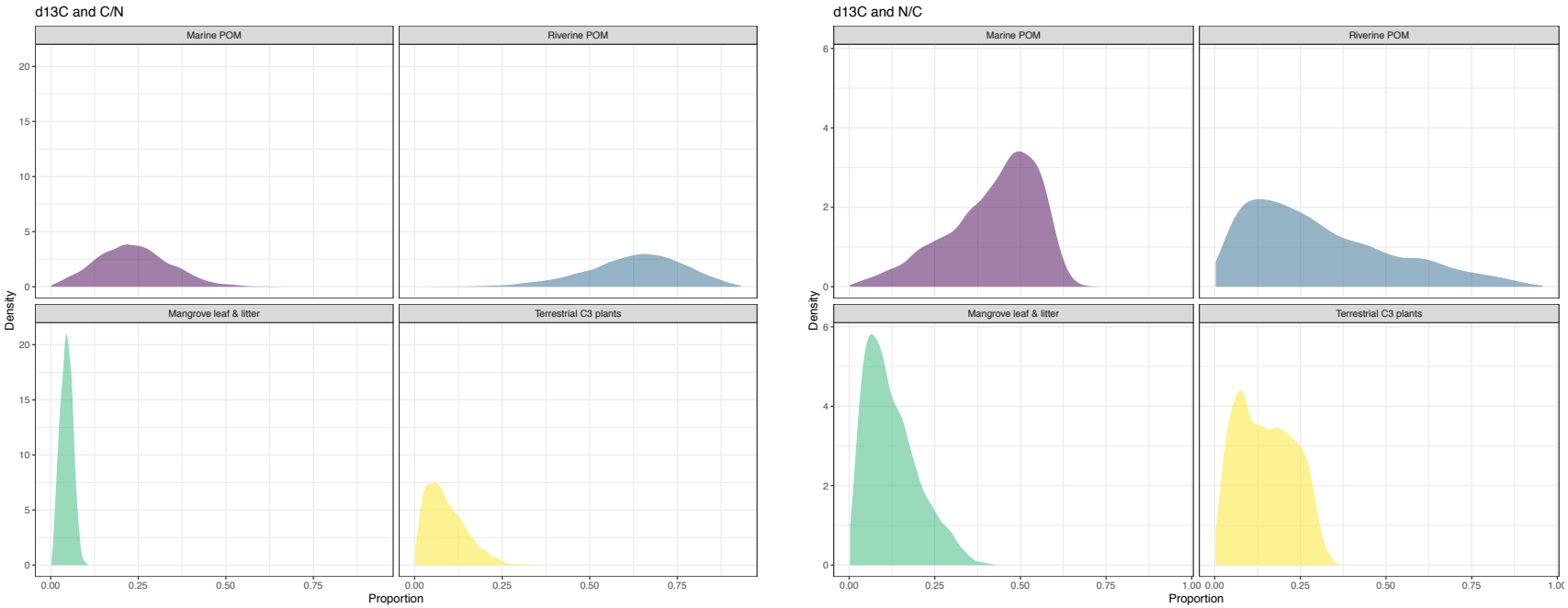

Figure S1b. Combined end-members mixing model results using a) $\delta^{13}C$ and C/N ratio, b) $\delta^{13}C$ and N/C variables/model input and their associated density distribution.

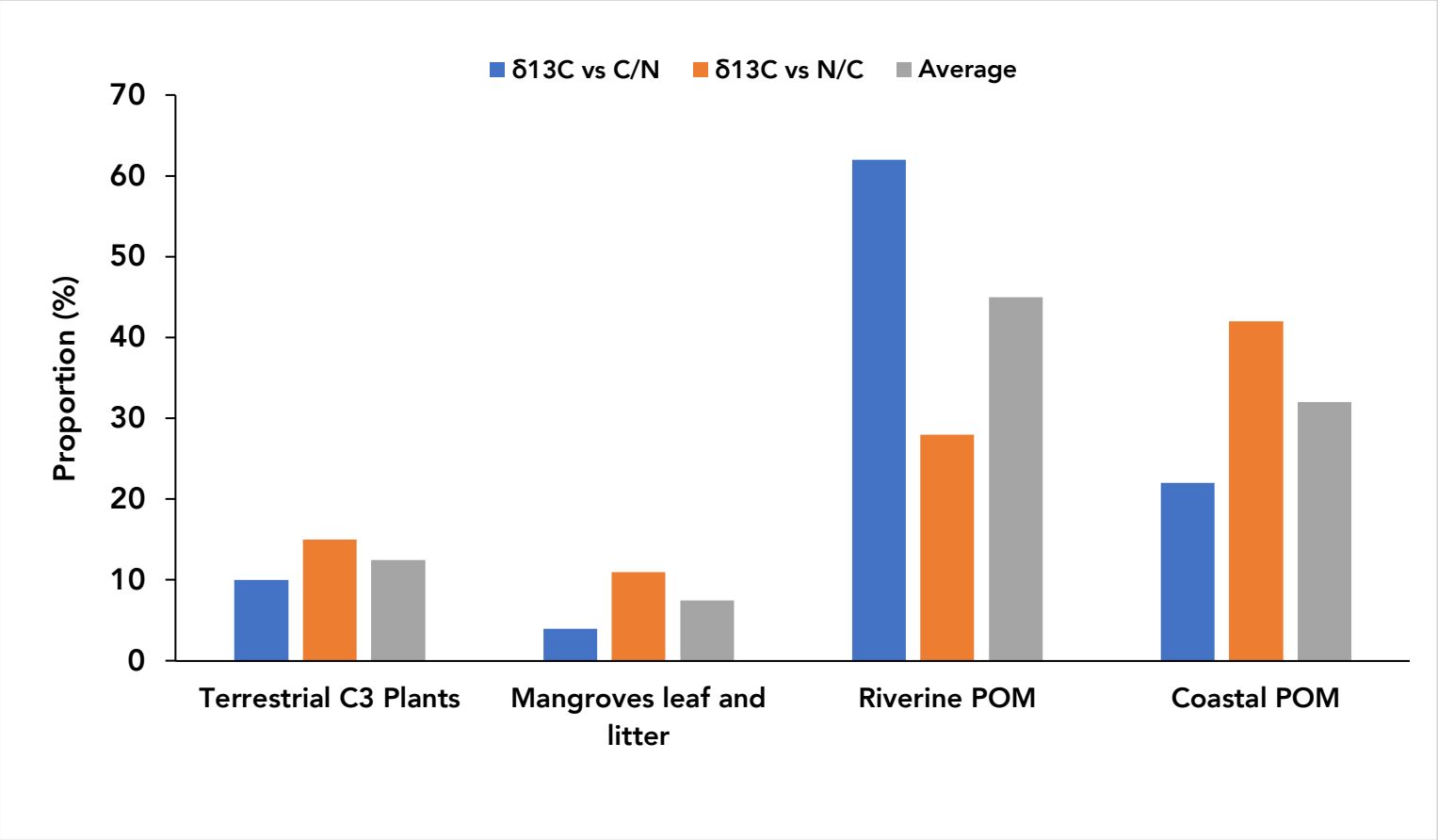

Figure S1c. Relative contribution of different source end-members to the total mangrove sediment organic matter in Vanga, Estuary.

Supplementary Information 4-2

Table S2a. Physicochemical parameters measured in-situ during both the dry (March) and wet (July) season

Station	Location	Temperature (°C)	pH	Salinity (psu)	DO (mg/L)	TDS (g/L)
		Dry season				
S1	Riverine	28.0	8.51	0.16	5.4	0.215
S4	Riverine	29.2	7.96	0.37	5.7	0.5
S5	Riverine	30.2	8.3	0.41	3.9	0.546
S6	Riverine	29.6	8.32	0.4	3.4	0.533
S7	Estuarine	30.3	7.87	34.31	5.3	33.995
S8	Marine	29.1	7.99	35.33	7.4	34.905
		Wet Season				
S1	Riverine	22.8	7.66	0.18	4.8	0.25
S2	Riverine	22.5	7.72	0.13	5.1	0.19
S4	Riverine	25.5	7.86	0.065	7.3	0.845
S5	Riverine	27.6	7.83	0.22	6.7	0.2977
S6	Riverine	26.6	7.91	0.22	6.5	0.299
S7	Estuarine	28.5	7.99	23.18	7.1	23.907
S8	Marine	27.5	8.14	33.25	6.3	32.045

Supplementary Information 4-3

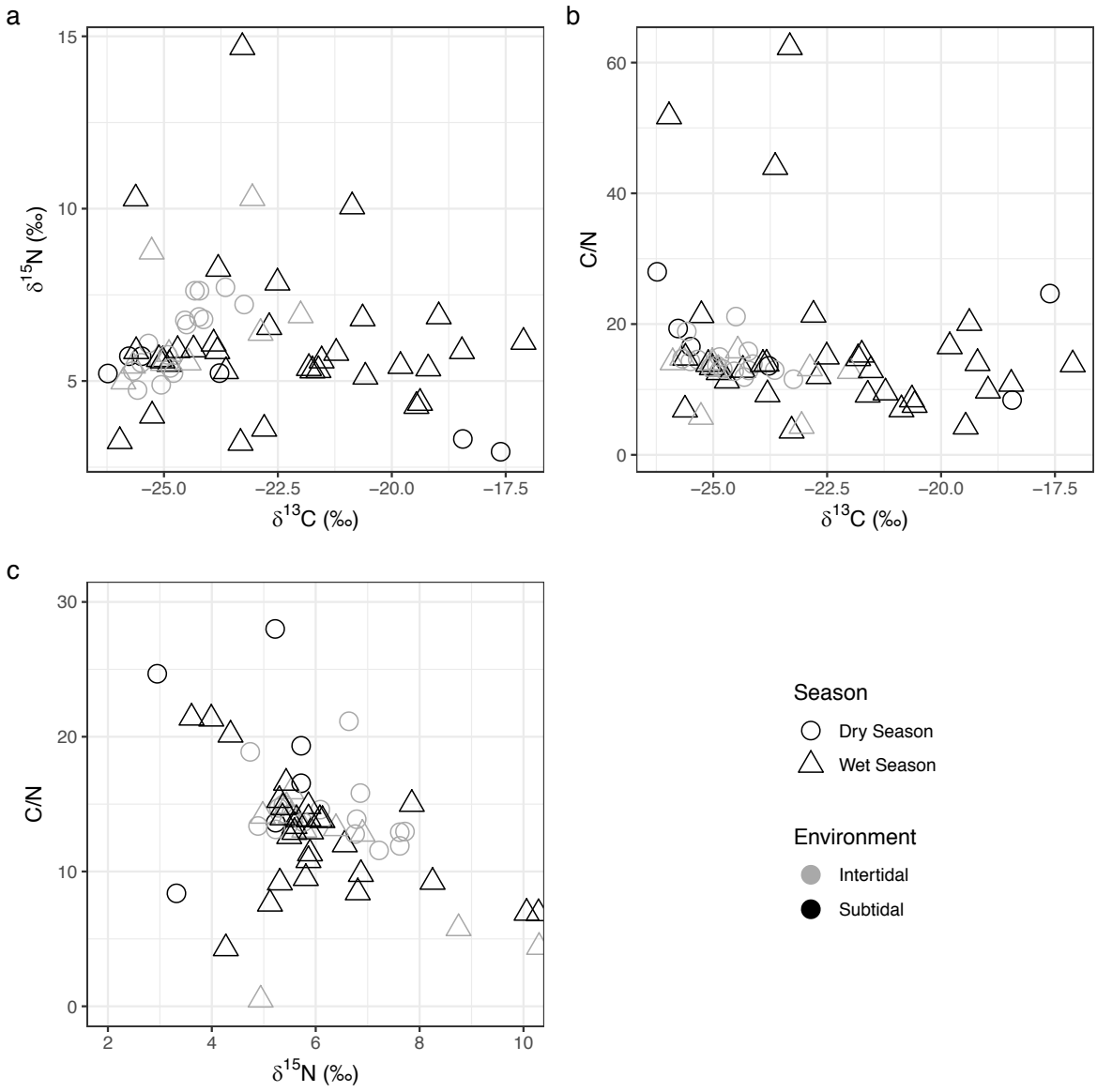

Figure 3Sa: Showing the variation in OM based on environmental setting (intertidal and subtidal).

Supplementary Information 4-4

Table S4a. F-values of one-way ANOVA test indicating variation of mangrove leaves, surface and core sediment OM properties species, station, environment, depth and season. *, ** and *** indicate significance value at $p < 0.05$, 0.01 and 0.001, respectively.

Sample type	SOM property	Station	Sediment type	Season	Environment	Depth	Species	Material
Surface sediments	**Dry season**							
	TC	F(6,44) = 0.002**	F(3,47) = 0.087	F(1,145) = 0.942	F(2,107) = ***			
	TOC	F(6,44) = 0.001**	F(3,47) = 0.126	F(1,145) = 0.773	F(2,107) = **			
	TN	F(6,44) = 0.002**	F(3,47) = 0.035*	F(1,145) = 0.969	F(2,107) = ***			
	C/N	F(6,44) = 0.01*	F(3,47) = 0.131	F(1,145) = 0.015*	F(2,107) = **			
	C_{org}/N	F(6,44) = 0.024**	F(3,47) = ***	F(1, 142) = 0.01*	F(2,57) = ***			
	$\delta^{15}N$	F(6,43) = ***	F(3,46) = ***	F(1,144) = 0.275	F(2,57) = ***			
	$\delta^{13}C$	F(6,43) = ***	F(3,47) = ***	F(1, 141) = 0.02*	F(2,57) = 0.052			
	Wet season							
	TC	F(18,77) = 0.0016**	F(3,92) = ***	F(1,145) = 0.942	F(2,107) = **			
	TOC	F(18,77) = ***	F(3,92) = ***	F(1,145) = 0.773	F(2,107) = **			
	TN	F(18,77) = 0.001**	F(3,92) = ***	F(1,145) = 0.969	F(2,107) = **			
	C/N	F(18,77) = 0.002**	F(3,92) = 0.0037**	F(1,145) = 0.015*	F(2,107) = ***			
	C_{org}/N	F(18,77) = 0.541	F(3,89) = 0.206	F(1, 142) = 0.01*	F(2,107) = 0.043*			
	$\delta^{15}N$	F(18,77) = ***	F(3,92) = ***	F(1,144) = 0.275	F(2,107) = ***			
	$\delta^{13}C$	F(18,77) = ***	F (3,88) = ***	F(1, 141) = 0.02*	F(2,107) = ***			
Core sediments	TC	F(4,29) = ***				F(6,28) = 0.92		
	TOC	F(4,30) = ***				F(6,28) = 0.95		
	TN	F(4, 29) = ***				F(6,27) = 0.61		
	C/N	F(4,29) = 0.1819				F(6, 27) = 0.05*		
	DBD	F (4,30) = ***				F(6,28) = 0.05*		
	$\delta^{15}N$	F(4,30) = ***				F(6,28) = 0.98		
	$\delta^{13}C$	F(4,30) = ***				F(6,28) = 0.99		
Mangroves leaf & litter	TC						F(5,111) = 0.0049**	F(1,111) = 0.02**
	TN						F(5,111) = ***	F(1,115) = ***
	C/N						F(5,111) = ***	F(1,115) = ***

	$\delta^{13}C$						F(5,111) = 0.036*	F(1,115) = 0.03*
A. marina	TC							F(1,28) = 0.06
	TN							F(1,28) = ***
	C/N							F(1,28) = ***
	$\delta^{13}C$							F(1,28) = 0.08
C. tagal	TC							F(1,24) = 0.77
	TN							F(1,24) = 0.0137*
	C/N							F(1,24) = ***
	$\delta^{13}C$							F(1,24) = 0.57
B. gymnorrhiza	TC							F(1,16) = 0.09
	TN							F(1,16) = 0.102
	C/N							F(1,16) = 0.052
	$\delta^{13}C$							F(1,16) = 0.01**
R. mucronata	TC							F(1,19) = 0.24
	TN							F(1,19) = ***
	C/N							F(1,19) = ***
	$\delta^{13}C$							F(1,19) = 0.82
X. granatum	TC							F(1,9) = 0.033*
	TN							F(1,9) = 0.086
	C/N							F(1,9) = 0.042**
	$\delta^{13}C$							F(1,9) = 0.457
Terrestrial C3 plants	TC							F(1,9) = 0.353
	TN							F(1,9) = 0.0102*
	C/N							F(1,9) = 0.0028**
	$\delta^{13}C$							F(1,9) = 0.151

Chapter 5 : Extended Discussion

5.1 Transboundary connectivity of the Vanga Estuary and the Umba River catchment

The key aim of this doctoral study was to identify whether the Vanga Estuary is connected with the larger Umba River catchment. This was mainly to evaluate the influence of the transboundary Umba River on the Vanga Estuary, specifically on sediment supply and deposition in the downstream mangrove forest. This was achieved by 1) identifying source characteristics and sediment provenance of the Umba River sediments using geochemical and mineralogical fingerprinting and 2) determining the contribution of different sources of sediment organic matter as proxies for sediment provenance. This was achieved by evaluating the distribution and the amounts of elemental carbon (C), nitrogen (N), C/N ratio and their stable isotopes in the Umba River sediments. We also estimated the contribution of each potential source using a Bayesian Stable Isotope Mixing Model implemented in R Program (Chapter 4).

This study shows that the estuarine sediments of Vanga are partially sourced from the larger Umba River catchment (Chapter 3 and 4) extending from the Usambara Mountains in Tanzania down to Kwale at the coastline in Kenya as shown by the similarity in the geochemical and mineralogical compositions of both upstream and downstream sediments. We attributed this similarity to uniform geology within the upstream and midstream sections of the Umba River catchment. This validated our hypothesis and indeed agreed with other studies with similar conclusions (Sensarma et al., 2008; Garzanti et al., 2011; He et al., 2015). Additionally, the geochemical composition of Umba River sediments, is predominantly controlled by weathering, climate, and rapid sediment replenishment with grain size distribution and sorting having minimal influence (Chapter 3). Conventionally, grain size distribution would

have a bearing on the geochemical composition of fluvial sediments (Garzanti et al., 2011; Greber and Dauphas, 2019; Álvarez-Vázquez et al., 2020). However, this was not the case for the sediments sampled from the Umba River. We attributed this to the narrow grain size distribution spectrum (Chapter 3), minimal clay content in the Umba River sediments, and the rapid supply of fresh sediments and the short distance of sediment transportation from source to sink. In addition, sediments delivered by the Umba River and deposited to the Vanga Estuary exhibited a mixed source as evidenced from the sediment organic matter (Chapter 4). The main contributions are from terrestrial inputs (brought by Umba River), marine-derived sediments (brought by the tides) and *in-situ* contributions from leaves and roots (Chapter 4). The degree of mixing was not quantified in this study, but the relative percentage contribution of the different end-members was low, signifying considerable mixing.

The results of this thesis, especially on the sediment provenance (Chapter 3 and 4), suggest that the geographic, hydrological, and environmental aspects play a major role in the connectivity of the Umba River catchment to the downstream habitats. It is from this conclusion that a holistic and catchment-wide management is merited. This is because any changes within the catchment will be felt in the downstream coastal habitat. For example, anthropogenic activities (e.g., agriculture, dam constructions) coupled with the effects of climate change (e.g., increased precipitation) would alter sediment supply, bulk geochemistry and mineralogy (Clift, 2016). The impact of these potential alterations would be felt further downstream and in the coastal habitats. In addition, the hydrodynamic influence and the mixing of sediment organic matter, further indicate the spatial connectivity of the Vanga Estuary with the adjacent coastal and marine environment. This is important for future research and considerations for monitoring of mechanisms that induce and control material exchange and dynamics (Bouillon et al., 2003; Yong et al., 2011; Tamooh et al., 2012).

5.2 Estuarine sediment dynamics and mitigation of sea-level rise (SLR)

The current rates of sea-level rise (SLR) are estimated at ~3 mm/yr globally (Dangendorf et al., 2019; Saintilan et al., 2020). The geographic variability in rates of sea-level change is due to variation in thermal expansion dependent on ocean depth and location, the influx of freshwater from continents through river inputs, melting land ice (glaciers and ice caps) and land subsidence (Cazenave et al., 2008; Church and White, 2011). Based on tide gauge data recorded in Mombasa, Kenya, the last three decades have seen a relative sea-level rise at a rate of 3.8 mm/yr (Figure 2-5, Chapter 4), which is comparable to the global rates (Church and White, 2006). The potential threat from this SLR and possible response for the Vanga Estuary mangroves remain unclear. However, others have shown that the equilibrium between relative SLR, sedimentation (both accretion and shallow subsidence) and eustatic sea-level changes would play a key role in the response, adaptation, and survival of mangroves (Gilman et al., 2008; Payo et al., 2016; Woodroffe, 2018). In this regard, sufficient elevation gains through deposition and accretion of sediments, with rates higher than SLR, would allow mangroves to keep pace with SLR (Lovelock et al., 2015; Crosby et al., 2016; Woodroffe, 2018).

Presently, anthropogenic stressors contribute primarily to the loss of mangroves (up to 2% per year), but it has been predicted that relative SLR would be the major cause of mangrove loss globally (up to 20% per year) by the year 2100 (Gilman et al., 2008). This holds for Vanga as it has been recently designated as a mangrove loss hotspot due to human factors (Mungai et al., 2019). This study (Chapter 2) has shown that sediment accretion still exceeds the rates of SLR. However, accelerated rates in the future would pose a threat. The envisaged equilibrium that would allow mangroves to respond adequately and adapt to SLR varies spatially both locally (within mangrove ecosystems), regionally, and globally. For example, the Sundarbans at 2 m above mean sea level and with high sediment supply will persist and survive even

at the highest SLR scenarios of up to 1.4 m by 2100 (Lovelock et al., 2015; Payo et al., 2016). Based on a synthesis of several publications on sediment accretion, Crosby et al. (2016) showed that the predicted rates of SLR could outpace up to 90% of salt marshes. However, increasing rates of SLR would also trigger positive ecogeomorphic feedback mechanisms that would facilitate sediment deposition and accretion. SLR would increase the inundation depths and the period (Crosby et al., 2016, Woodroffe, 2018). Prolonged inundation would allow for more sediment to settle out of suspension and lead to increased accretion. In this study, the accretion rates in the Vanga Estuary are still higher (9 mm/yr) compared to the current rates of sea-level rise (3.8 mm/yr, see Chapter 2). This is very promising for the survival of the mangroves of Vanga. Considering the current sediment accretion rates, it is even more promising that a 5mm/yr mean rate of SLR under low-emission scenarios in tropical and subtropical locations (Saintilan et al., 2020) would see the mangroves of Vanga persist. However, regional and localized factors play significant roles in the ultimate response and survival of mangroves facing the threat of SLR. For example, this study also showed localized variations of accretion and shallow subsidence rates within the same system with distance from the main creek channel. This has also been reported in other studies where the same sites can experience variable sedimentation rates spatially and temporally (Bricker-Urso et al., 1989; Neubauer et al., 2002). The variation mainly depends on the extended duration and increased inundation frequency in sites closer to the main creek channels. Therefore, they exhibit higher deposition rates. This study further showed that the sites closer to the creek channel exhibit higher subsidence rates as indicated by mangrove elevation loss (average of -45 mm, see Chapter 2). This is attributable to higher amounts of fresh organic matter resulting from frequent inundation that gradually decomposes, causing local subsidence (Neubauer et al., 2002; Day et al., 2011; Bomer et al., 2020). Estuaries are also affected by other drivers acting on local, regional and sub-global scales. These drivers include elevation loss through subsidence and local and

regional catchment land-use practices. In some areas, these drivers are interconnected, for example, land-use within a catchment, including dam construction and crop cultivation could alter sediment supply to an estuary (Syvitski, 2008; Geeraert et al., 2015; Okuku et al., 2018) and groundwater abstraction could cause land subsidence (Brown and Nicholls, 2015; Karegar et al., 2016). Low frequency but high impact weather events including flooding, *El Niño* Southern Oscillation, tsunamis, cyclones, and hurricanes, also greatly influence estuaries and deltas (Kitheka et al., 2002; Dahdouh-Guebas et al., 2005; Sippo et al., 2018). The effects of these events are mainly the disturbance of the equilibrium, especially sediment supply and the total destruction of habitats. Although these were not evaluated in this study, they merit further integrated analysis to enable the understanding of the drivers, their effects and implications, as well as the interactions of the transboundary Umba River, the catchment and downstream Vanga Estuary connectivity.

5.3 Conclusions

The need for conservation and management of transboundary resources is borne by human, habitat, resource and geographic connectedness. Specifically related to this doctoral study, the Vanga Estuary is part of a proposed transboundary conservation area (pTBCA) between Kenya and Tanzania. The pTBCA is habitat-connected along the coastline by the marine associated biotopes (mangroves, coral reefs, and seagrass). It is also connected geographically to the larger terrestrial catchment and functionally by the transboundary Umba River. Therefore, the downstream coastal habitats are influenced by intra- and inter-habitat material exchange and by materials from the hinterland delivered by the transboundary Umba River. This doctoral study contributes to the required body of biophysical data and information on the poorly studied Vanga Estuary. This information is vital in the demarcation of the pTBCA, and better resource management and conservation of the area. The results of this thesis have demonstrated the connectivity of the Vanga estuary to the terrestrial

catchment. Moreover, the demonstration of connectivity through geochemical, mineralogical and source provenance analyses gives further impetus to the need for integrative management and the consideration of a broader scope in the demarcation of the pTBCA. This study has also given an insight into the present equilibrium between SLR and mangrove surface elevation upon which possible response of Vanga mangroves to predicted SLR under the different scenarios will be evaluated. Subsequently, better mitigation and adaptive measures to sustain the transboundary resources will be drawn by policymakers, managers and resource users.

Chapter 6 : Outlook and Future Research

This chapter highlights and discusses the potential future research directions to fill some of the knowledge gaps identified by the present research. Some of the highlights would build on the current study and further assist in the holistic understanding of the Vanga Estuary with respect to the environmental and socio-economic dynamics. This is borne of the connectivity between coastal and marine biotopes with the extended upstream catchment. For example, the intertemporal, interspatial and intergenerational aspects of the biophysical environment and anthropogenic aspects merit further study. However, this would be further complicated and compounded concerning transboundary resources that would require bilateral or multilateral joint transboundary management (Turner, 2000; Tuda et al., 2019; Mason et al., 2020). Due to documented biodiversity loss and degradation, global, regional and national efforts have been prompted to curb the decline through coordinated transboundary conservation, land use management and joint research (Kark et al., 2015; Mason et al., 2020). It is in the backdrop of the above-mentioned that transboundary conservation is also taking root through joint information sharing and management. Indeed, part of the study in this thesis is within a proposed joint transboundary conservation area (between Kenya and Tanzania.

6.1 Historical sedimentation, habitat formation and response to historical sea-level changes

The availability and delivery of sediments in mangrove habitats allow for a sustainable equilibrium and conducive mangrove surface elevation maintenance, whereupon the mangrove 'land-building' and 'coastal protection' capabilities can be realized (McKee, 2011). It has been shown by other studies that successful mangrove conservation, rehabilitation and restoration is partially a function of sufficient sediment supply and deposition (Syvitski et al., 2009; López-Portillo et al., 2017;

Nicholls et al., 2020; Li et al., 2021). However, when this conditionality and pre-requisite is overlooked, mangrove rehabilitation and conservation projects are prone to fail (López-Portillo et al., 2017; Rivera-Monroy et al., 2017; Zimmer, 2018; Le Minor et al., 2021). This is connected to the merited need for a historical perspective to determine the persistence and the previous response of mangroves to historical sea-level changes or shifts in delta mouth position. For example, the Volta delta in Ghana and Nile Delta in Egypt have been shown to have oscillated and migrated partly due to natural and anthropogenically driven variations in sediment supply (Addo et al., 2018; Darby et al., 2020; Aagaard et al., 2021). Indeed, it is reported that historically, the Volta deltas' mouth was 20 km east of the current location (Addo et al., 2018). Due to dynamics inherent to deltas, and the variability in sediment supply this oscillation and migration produce geomorphologic shifts between protuberance and delta loss due to erosion. Delta loss and associated habitat re-engineering potentially leads to loss of mangrove ecosystems (Rahman et al., 2011). Site-specific delta and estuarine dynamics also alter the critical threshold of vertical sediment accretion in mangroves, while beyond this threshold, mangrove ecosystems fail (Ellison and Stoddart, 1991; Fujimoto et al., 1996). Through self-sustaining bio-morphodynamic feedbacks controlling surface-elevation (Swales et al., 2007; Fagherazzi et al., 2019; Xie et al., 2020), mangroves have persisted and survived various sea-level changes documented as far back as ~7000 cal yr BP in different geographic regions and habitats (Fujimoto et al., 1996; Alongi , 2008; Krauss et al., 2014; Sugden, 2020; Bozi et al., 2021). Therefore, it is vital to determine historical sea-level curves for a region or habitat considering local subsidence rates. Combined with sediment age dating, habitat changes and historical responses can be evaluated (Woodroffe, 1981; Lamb et al., 2006). On average, globally, 0.1 mm/yr delta subsidence based on weighted coastal length, has contributed to the relative sea-level changes (Nicholls et al., 2021). However, this varies from region to region. For example, based on radiocarbon dating, Holocene deposits of the Venice Lagoon in Italy showed average

subsidence rates of up to 1.3 mm/year estimated for corresponding periods of excess and low sediment supply (Zanchettin et al., 2021). The Nile delta in Egypt and the Ganges-Brahmaputra-Meghna in Asia have recorded subsidence rates of up to 12 mm/year (Saleh and Becker, 2018) and 41 mm/year (Brown and Nicholls, 2015), respectively. Based on GPS data analyses, The East Coast of North America experiences subsidence rates < 3 mm/yr (Karegar et al., 2016). Although other studies have shown that mangrove ecosystems in low-lying coastal wetlands could outpace SLR rates between 0.8 and 0.9 mm/yr, these ecosystems could be under stress or even collapse at higher rates (Ellison and Stoddart, 1991). This stress could be exacerbated and compounded by subsidence. This information is an outstanding gap in the East African coast and a possible area of research interest. A relative SLR would affect the existing mangrove environment. Mangroves would survive a transgressive phase depending on the equilibrium between the rate of relative SLR and the rate of mangrove surface growth through sediment accretion (Islam and Tooley, 1999). Therefore, the historical perspective of the Vanga Estuary would provide a viable focus for future research on estuary mouth dynamics, sea-level changes, mangrove edge oscillations and a basis for better mitigation and management strategies. Several methods have been developed and applied to dating mangrove sediments, including lead-210 (^{210}Pb) for younger (up to 100 yrs) sediments (Sanders et al., 2008; Ruiz-Fernández et al., 2018; Kusumaningtyas et al., 2021), Cesium-137 (^{137}Cs) (Baskaran et al., 2014) and radiocarbon dating for more extended periods (up to 50,000 yrs) (Törnqvist et al., 2008; Khan et al., 2019).

6.2 Sediment and nutrient budgets of the Vanga Estuary

Current and historical land-use dynamics, the Umba River discharge, sediment and nutrient budgets remain an outstanding gap in this study area. They would assist in further understanding the extensive Umba River catchment connectivity with the Vanga Estuary. For example, knowledge of sediment budgets combined with the estuarine sedimentation rates, would give robust information on the influence of

sediments on mitigation of SLR impacts. Additionally, as discussed in this thesis (Chapter 4), the Vanga estuary experiences material exchange and source mixing. Therefore, the determination of the sediment budgets would allow the estimation of the exact contribution of marine and terrestrial sources to the total estuarine organic matter and sedimentation. In addition, the comparison of land-use dynamics through analyses of historical images with historical sedimentation rates would assist in the evaluation and assessment of the influence of land use changes over time on fluvial sediments supply and subsequently in the downstream mangrove sediments. Other studies on sediment and nutrient budgets have integrated climate change and socio-economic development scenarios for better understanding of localized dynamics within catchment land use and potential influences in mangrove conservation (Turner, 2000; Holzkämper et al., 2012; Honti et al., 2017).

6.3 Incorporation of modeling for sound management

Modeling is a vital tool in combining and assessing the interactions between local and global changes within a coastal habitat. Integrated modeling considering environmental and anthropogenic processes also supports integrated management. Low-lying tropical and sub-tropical mangrove coastal wetlands face threats from combined natural and anthropogenic impacts (Crosby et al., 2016; Rogers, 2021). However, mangrove habitats have been shown historically and currently, to be able to respond adequately and rebound from the effects of such impacts including overexploitation and sea-level changes (Krauss et al., 2014; Woodroffe et al., 2016; Okello et al., 2020). In order to evaluate the potential response and adaptation to future impacts, mapping and modeling based on current and historical trends is vital (Temmerman and Kirwan, 2015; Schuerch et al., 2018). However, current modeling of mangrove sedimentation, especially in the Western Indian Ocean (WIO) region, remains insufficient and primarily do not account for the hydro-geomorphic connection between mangrove sediment accretion and upstream hydrology, geology, geography and even human activities compared to other regions (Syvitski

and Milliman, 2007; Pietrafesa et al., 2019; Paprotny et al., 2020; Xie et al., 2020). Although mapping techniques have continued to improve, partly through open access to remote sensing data, precision to track sediment accretion, subsurface processes or quantify coastal and riverine flooding is still limited. The complex interrelations between geographic influences (basin area, runoff and relief), climate (temperature, humidity, rainfall), geology (lithology, tectonics), and human activities (reservoir trapping, land use and soil erosion), compounds the current constraints to better modeling efforts (Inman and Jenkins, 1999; Syvitski and Milliman, 2007). Together with inadequate hydrometeorological monitoring network, paucity of historical data and limited data or single-point observations, the aforementioned challenges in developing tropical countries reveal inadequacies that need to be bridged for better mitigation, planning and management of natural resources. It would be worthwhile to evaluate the historical sedimentation rate in the Vanga Estuary and compare it with historical land use in the Umba River catchment. This would provide information on the level of influence of the catchment on the estuary and a basis of data-based mitigation and future management adaptations.

In conclusion, the literature and information from this study and future extension, of as espoused in this chapter would form the basis essential for setting and evaluating contemporary and future Vanga estuarine dynamics. It will also assist in streamlining mitigation targets, strategic adaptation needs and response to potential habitat and ecosystem services loss and damage. Specifically, the information from this study would be incorporated and considered in the demarcation and management of the proposed transboundary conservation area between Kenya and Tanzania. As this was part of the envisaged outcomes of this doctoral study, the direct transfer of knowledge to policy would be beneficial policymakers and resource users through better resource stewardship.

References

Aagaard, T., Anthony, E.J., Gillies, B., Laursen, S.N., Sukstorf, F.N., Breuning-Madsen, H., 2021. Holocene development and coastal dynamics at the Keta Sand Spit, Volta River delta, Ghana. Geomorphology. 387, 107766.

Adame, M.F., Neil, D., Wright, S.F., Lovelock, C.E., 2010. Sedimentation within and among mangrove forests along a gradient of geomorphological settings. Estuar. Coast. Shelf Sci. 86, 21–30.

Adams, J.B., Rajkaran, A., 2021. Changes in mangroves at their southernmost African distribution limit. Estuar. Coast. Shelf Sci. 248, 107158.

Addo, K.A., Nicholls, R.J., Codjoe, S.N.A., Abu, M., 2018. A Biophysical and Socioeconomic Review of the Volta Delta, Ghana. J. Coast. Res. 34(5), 1216–1226.

Akech, N.O., Omuombo, C.A., Masibo, M., 2013. General Geology of Kenya, in: Developments in Earth Surface Processes. Elsevier B.V., pp. 3–10.

Alam, M., 1996. Subsidence of the Ganges—Brahmaputra Delta of Bangladesh and Associated Drainage, Sedimentation and Salinity Problems. Springer Dordrecht. Pp. 169–192.

Ali, S., Stattegger, K., Garbe-Schönberg, D., Frank, M., Kraft, S., Kuhnt, W., 2014. The provenance of Cretaceous to Quaternary sediments in the Tarfaya basin, SW Morocco: Evidence from trace element geochemistry and radiogenic Nd-Sr isotopes. J. African Earth Sci. 90, 64–76.

Alongi, D. M., 2014. Carbon cycling and storage in mangrove forests. Annual review of marine science. 6, 195-219.

Alongi, D.M., 2002. Present state and future of the world's mangrove forests. Environ. Conserv. 29, 331–349.

Alongi, D.M., 2008. Mangrove forests: Resilience, protection from tsunamis, and

responses to global climate change. Estuar. Coast. Shelf Sci. 76(1), 1-13.

Alongi, D.M., 2015. The Impact of Climate Change on Mangrove Forests. Curr. Clim. Chang. Reports. 1(1), 30-39.

Álvarez-Vázquez, M.Á., Hošek, M., Elznicová, J., Pacina, J., Hron, K., Fačevicová, K., Talská, R., Bábek, O., Grygar, T.M., 2020. Separation of geochemical signals in fluvial sediments: New approaches to grain-size control and anthropogenic contamination. Appl. Geochemistry 123, 104791.

Hamza, A.J., Esteves, L.S., Cvitanovic, M. and Kairo, J., 2020. Past and present utilization of mangrove resources in Eastern Africa and drivers of change. Journal of Coastal Research. 95(SI), 39-44.

Amorosi, A., 2012. Chromium and nickel as indicators of source-to-sink sediment transfer in a Holocene alluvial and coastal system (Po Plain, Italy). Sediment. Geol. 280, 260–269.

Andreetta, A., Fusi, M., Cameldi, I., Cimò, F., Carnicelli, S., Cannicci, S., 2014. Mangrove carbon sink. Do burrowing crabs contribute to sediment carbon storage? Evidence from a Kenyan mangrove system. Journal of Sea Research. 85, 524–533.

Andrews, J.E., Greenaway, A.M., Dennis, P.F., 1998. Combined carbon isotope and C/N ratios as indicators of source and fate of organic matter in a poorly flushed, tropical estuary: Hunts Bay, Kingston Harbour, Jamaica. Estuar. Coast. Shelf Sci. 46, 743–756.

Ayugi, B., Tan, G., Gnitou, G.T., Ojara, M., Ongoma, V., 2020. Historical evaluations and simulations of precipitation over East Africa from Rossby centre regional climate model. Atmospheric Research. 232, 104705.

Baiyegunhi, C., Liu, K., Gwavava, O., 2017. Geochemistry of sandstones and shales from the Ecca Group, Karoo Supergroup, in the Eastern Cape Province of South Africa: Implications for provenance, weathering and tectonic setting. Open Geosci. 9, 340–360.

Balke, T., Friess, D.A., 2016. Geomorphic knowledge for mangrove restoration: a pan-tropical categorization. Earth Surf. Process. Landforms. 41, 231–239.

Barbier, E.B., Hacker, S.D., Kennedy, C., Koch, E.W., Stier, A.C. and Silliman, B.R., 2011. The value of estuarine and coastal ecosystem services. Ecological monographs. 81(2), 169-193.

Baskaran, M., Nix, J., Kuyper, C., Karunakara, N., 2014. Problems with the dating of sediment core using excess 210Pb in a freshwater system impacted by large scale watershed changes. J. Environ. Radioact. 138, 355–363.

Bhat, N.A., Singh, B.P., Bhat, A.A., Nath, S., Guha, D.B., 2019. Application of Geochemical Mapping in Unraveling Paleoweathering and Provenance of Karewa Deposits of South Kashmir, NW Himalaya, India. J. Geol. Soc. India 93, 68–74.

Blattmann, T.M., Letsch, D., Eglinton, T.I., 2018. On the geological and scientific legacy of petrogenic organic carbon. American Journal of Science. 318(8), 861–881.

Bomer, E.J., Wilson, C.A., Hale, R.P., Hossain, A.N.M., Rahman, F.M.A., 2020. Surface elevation and sedimentation dynamics in the Ganges-Brahmaputra tidal delta plain, Bangladesh: Evidence for mangrove adaptation to human-induced tidal amplification. Catena. 187, 104312.

Borges, J.B., Huh, Y., Moon, S., Noh, H., 2008. Provenance and weathering control on river bed sediments of the eastern Tibetan Plateau and the Russian Far East. Chem. Geol. 254, 52–72.

Bosire, J. O., Dahdouh-Guebas, F., Kairo, J. G., Kazungu, J., Dehairs, F., Koedam, N., 2005. Litter degradation and CN dynamics in reforested mangrove plantations at Gazi Bay, Kenya. Biological Conservation. 126(2), 287-295.

Bosire, J.O., Kaino, J.J., Olagoke, A.O., Mwihaki, L.M., Ogendi, G.M., Kairo, J.G., Berger, U., Macharia, D., 2014. Mangroves in peril: unprecedented degradation rates of peri-urban mangroves in Kenya. Biogeosciences. 11, 2623–2634.

Bouillon, S., Chandra Mohan, P., Sreenivas, N., Dehairs, F., 2000. Sources of suspended organic matter and selective feeding by zooplankton in an estuarine mangrove ecosystem as traced by stable isotopes. Mar. Ecol. Prog. Ser. 208, 79–92.

Bouillon, S., Connolly, R.M., Lee, S.Y., 2008. Organic matter exchange and cycling in mangrove ecosystems: Recent insights from stable isotope studies. Journal of Sea Research. 59(1-2), 44–58.

Bouillon, S., Dahdouh-Guebas, F., Rao, A., Koedam, N., Dehairs, F., 2003. Sources of organic carbon in mangrove sediments: variability and possible ecological implications. Hydrobiologia. 495(1), 33–39.

Bouillon, S., Moens, T., Dehairs, F., 2004. Carbon sources supporting benthic mineralization in mangrove and adjacent seagrass sediments (Gazi Bay, Kenya). Biogeosciences. 1(1), 71–78.

Bowring, S.A., Erwin, D.H., Jin, Y.G., Martin, M.W., Davidek, K., Wang, W., 1998. U/Pb Zircon Geochronology and Tempo of the End-Permian Mass Extinction. Science. 280(5366), 1039–1045.

Bozi, B.S., Figueiredo, B.L., Rodrigues, E., Cohen, M.C.L., Pessenda, L.C.R., Alves, E.E.N., de Souza, A. V., Bendassolli, J.A., Macario, K., Azevedo, P., Culligan, N., 2021. Impacts of sea-level changes on mangroves from southeastern Brazil during the Holocene and Anthropocene using a multi-proxy approach. Geomorphology. 390, 107860.

Bricker-Urso, S., Nixon, S.W., Cochran, J.K., Hirschberg, D.J., Hunt, C., 1989. Accretion rates and sediment accumulation in Rhode Island salt marshes. Estuaries. 12, 300–317.

Brown, S., Nicholls, R., 2015. Subsidence and human influences in mega deltas: the case of the ganges–brahmaputra–meghna. Sci Total Env. 527, 362–374.

Cahoon, D., Lynch, J., 1997. Vertical accretion and shallow subsidence in a mangrove forest of southwestern Florida, U.S.A. Mangroves Salt Marshes. 1, 173–186.

Cahoon, D.R., Lynch, J.C., Hensel, P., Boumans, R., Perez, B.C., Segura, B., Day, J.W., 2002. High-precision measurements of wetland sediment elevation: I. Recent improvements to the sedimentation-erosion table. J. Sediment. Res. 72, 730–733.

Cahoon, D.R., Turner, R.E., 1989. Accretion and canal impacts in a rapidly subsiding wetland II. Feldspar marker horizon technique. Estuaries. 12, 260–268.

Cairncross, B., 2019. Minerals & Gemstones of East Africa. Penguin Random House, Pippa Parker, Cape Town.

Callaway, J.C., Cahoon, D.R., Lynch, J.C., 2015. The Surface Elevation Table-Marker Horizon Method for Measuring Wetland Accretion and Elevation Dynamics.10, 901–917.

Campodonico, V.A., García, M.G., Pasquini, A.I., 2016. The geochemical signature of suspended sediments in the Parana River basin: Implications for provenance, weathering and sedimentary recycling. Catena. 143, 201–214.

Camuti, K.S., McGuire, P.T., 1999. Preparation of polished thin sections from poorly consolidated regolith and sediment materials. Sediment. Geol. 128, 171–178.

Canuel, E.A., Hardison, A.K., 2016. Sources, Ages, and Alteration of Organic Matter in Estuaries. Ann. Rev. Mar. Sci. 8, 409-434.

Cazenave, A., Lombard, A. and Llovel, W., 2008. Present-day sea level rise: A synthesis. Comptes Rendus Geoscience. 340(11), 761-770.

Ceryan, S., 2018. Weathering indices used in evaluation of the weathering state of rock material, in: Handbook of Research on Trends and Digital Advances in Engineering Geology. Igi Global, pp. 132–186.

Church, J.A., White, N.J., 2006. A 20th century acceleration in global sea level rise. Geophys. Res. Lett. 33, L10602.

Church, J.A., White, N.J., 2011. Sea level Rise from the Late 19th to the Early 21st Century. Surv. Geophys. 32, 585–602.

Clift, P.D., 2016. Assessing effective provenance methods for fluvial sediment in the

South China Sea. Geol. Soc. London, Spec. Publ. 429, 9–29.

Collins, D.S., Avdis, A., Allison, P.A., Johnson, H.D., Hill, J., Piggott, M.D., Hassan, M.H.A., Damit, A.R., 2017. Tidal dynamics and mangrove carbon sequestration during the Oligo-Miocene in the South China Sea. Nat. Commun. 8, 1–12.

Cox, R., Lowe, D.R., Cullers, R.L., 1995. The influence of sediment recycling and basement composition on evolution of mudrock chemistry in the southwestern United States. Geochim. Cosmochim. Acta 59, 2919–2940.

Crosby, S.C., Sax, D.F., Palmer, M.E., Booth, H.S., Deegan, L.A., Bertness, M.D., Leslie, H.M., 2016. Salt marsh persistence is threatened by predicted sea level rise. Estuar. Coast. Shelf Sci. 181, 93–99.

Crowley, G.M., Gagan, M.K., 1995. Holocene evolution of coastal wetlands in wet-tropical northeastern Australia. Holocene 5, 385–399.

Cutler, K., 2003. Rapid sea level fall and deep-ocean temperature change since the last interglacial period. Earth Planet. Sci. Lett. 206, 253–271.

Dahdouh-Guebas, F., Jayatissa, L.P., Di Nitto, D., Bosire, J.O., Seen, D. Lo, Koedam, N., 2005. How effective were mangroves as a defence against the recent tsunami?. Current Biology. 15(2), 443-447.

Dangendorf, S., Hay, C., Calafat, F.M., Marcos, M., Piecuch, C.G., Berk, K., Jensen, J., 2019. Persistent acceleration in global sea level rise since the 1960s. Nat. Clim. Chang. 9, 705–710.

Darby, S.E., Appeaning Addo, K., Hazra, S., Rahman, M.M., Nicholls, R.J., 2020. Fluvial Sediment Supply and Relative Sea level Rise, in: Nicholls, R.J., Adger, W.N., Hutton, C.W., Hanson, S.E. (Eds.), Deltas in the Anthropocene. Springer International Publishing, Cham, pp. 103–126.

Daron, J.D., Sutherland, K., Jack, C., Hewitson, B.C., 2015. The role of regional climate projections in managing complex socio-ecological systems. Reg. Environ. Chang. 15, 1–12.

Dasgupta, S., Islam, M.S., Huq, M., Huque Khan, Z., Hasib, M.R., 2019. Quantifying

the protective capacity of mangroves from storm surges in coastal Bangladesh. PLoS One 14, e0214079.

Dauwe, B., Middelburg, J. J., 1998. Amino acids and hexosamines as indicators of organic matter degradation state in North Sea sediments. Limnology and Oceanography. 43(5), 782-798.

Dauwe, B., Middelburg, J. J., Herman, P. M., 2001. Effect of oxygen on the degradability of organic matter in subtidal and intertidal sediments of the North Sea area. Marine Ecology Progress Series. 215, 13-22.

Day, J.W., Kemp, G.P., Reed, D.J., Cahoon, D.R., Boumans, R.M., Suhayda, J.M., Gambrell, R., 2011. Vegetation death and rapid loss of surface elevation in two contrasting Mississippi delta salt marshes: The role of sedimentation, autocompaction and sea level rise. Ecol. Eng. 37, 229–240.

Dehairs, F., Rao, R.G., Chandra Mohan, P., Raman, A.V., Marguillier, S., Hellings, L., 2000. Tracing mangrove carbon in suspended matter and aquatic fauna of the Gautami–Godavari Delta, Bay of Bengal (India). Hydrobiol. 431(2), 225–241.

Deininger, A., Frigstad, H., 2019. Reevaluating the Role of Organic Matter Sources for Coastal Eutrophication, Oligotrophication, and Ecosystem Health. Front. Mar. Sci. 0, 210.

Depetris, P.J., Pasquini, A.I., Lecomte, K.L., 2014. Weathering and the Riverine Denudation of Continents, SpringerBriefs in Earth System Sciences. Springer Netherlands, Dordrecht.

Dickinson, W.R., Beard, L.S., Brakenridge, G.R., Erjavec, J.L., Ferguson, R.C., Inman, K.F., Knepp, R.A., Lindberg, F.A., Ryberg, P.T., 1983. Provenance of North American Phanerozoic sandstones in relation to tectonic setting. GSA Bull. 94, 222–235.

Di Nitto, D. Di, Neukermans, G., Koedam, N., Defever, H., Pattyn, F., Kairo, J.G., Dahdouh-Guebas, F., 2014. Mangroves facing climate change: landward migration potential in response to projected scenarios of sea level rise.

Biogeosciences 11, 857–871.

Dinis, P.A., Garzanti, E., Hahn, A., Vermeesch, P., Cabral-Pinto, M., 2020. Weathering indices as climate proxies. A step forward based on Congo and SW African river muds. Earth-Science Rev. 201, 103039.

Dittmar, T., Lara, R.J., Kattner, G., 2001. River or mangrove? Tracing major organic matter sources in tropical Brazilian coastal waters. Mar. Chem. 73, 253–271.

Donato, D.C., Kauffman, J.B., Murdiyarso, D., Kurnianto, S., Stidham, M., Kanninen, M., 2011. Mangroves among the most carbon-rich forests in the tropics. Nature Geoscience. 4(5), 293–297.

Duarte, C.M., Cebrián, J., 1996. The fate of marine autotrophic production. Limnol. Oceanogr. 41, 1758–1766.

Duvall, M.S., Wiberg, P.L., Kirwan, M.L., 2019. Controls on Sediment Suspension, Flux, and Marsh Deposition near a Bay-Marsh Boundary. Estuaries and Coasts. 42, 403–424.

Eggleston, J., Pope, J., 2013. Land subsidence and relative sea level rise in the southern Chesapeake Bay region. US Geol. Surv. Circ. 1392, 30.

Ellison, J.C., 2015. Vulnerability assessment of mangroves to climate change and sea level rise impacts. Wetl. Ecol. Manag. 23, 115–137.

Ellison, J.C., Stoddart, D.R., 1991. Mangrove ecosystem collapse during predicted sea level rise: Holocene analogues and implications. J. Coast. Res. 7, 151–165.

Esteban, M., Takagi, H., Jamero, L., Chadwick, C., Avelino, J.E., Mikami, T., Fatma, D., Yamamoto, L., Thao, N.D., Onuki, M., Woodbury, J., Valenzuela, V.P.B., Crichton, R.N., 2020. Adaptation to sea level rise: Learning from present examples of land subsidence. Ocean Coast. Manag. 189, 104852.

Fagherazzi, S., Anisfeld, S.C., Blum, L.K., Long, E. V., Feagin, R.A., Fernandes, A., Kearney, W.S., Williams, K., 2019. Sea Level Rise and the Dynamics of the Marsh-Upland Boundary. Front. Environ. Sci. 7, 25.

Fagherazzi, S., Bryan, K.R., 2017. Buried Alive or Washed Away: The Challenging Life

of Mangroves in the Mekong Delta. Nardin Source Oceanogr. 30, 48–59.

Fiantis, D., Nelson, M., Shamshuddin, J., Goh, T.B., Van Ranst, E., 2010. Determination of the Geochemical Weathering Indices and Trace Elements Content of New Volcanic Ash Deposits from Mt. Talang (West Sumatra) Indonesia. Eurasian Soil Sci. 43, 1477–1485.

Folk, R.L. and Ward, W.C., 1957. Brazos River bar [Texas]; a study in the significance of grain size parameters. J. Sedimentary Res. 27(1), 3-26.

Fortnam, M., Atkins, M., Brown, K., Chaigneau, T., Frouws, A., Gwaro, K., Huxham, M., Kairo, J., Kimeli, A., Kirui, B., Sheen, K., 2020. Multiple impact pathways of the 2015–2016 El Niño in coastal Kenya. Ambio. 50(1), 1–16.

Friess, D.A., McKee, K.L., 2021. The history of surface-elevation paradigms in mangrove biogeomorphology, in: Dynamic Sedimentary Environments of Mangrove Coasts. Elsevier, pp. 179–198.

Friess, D.A., Rogers, K., Lovelock, C.E., Krauss, K.W., Hamilton, S.E., Lee, S.Y., Lucas, R., Primavera, J., Rajkaran, A., Shi, S., 2019. The state of the world's mangrove forests: past, present, and future. Annu. Rev. Environ. Resour. 44, 89–115.

Fritz, H., Abdelsalam, M., Ali, K.A., Bingen, B., Collins, A.S., Fowler, A.R., Ghebreab, W., Hauzenberger, C.A., Johnson, P.R., Kusky, T.M., Macey, P., Muhongo, S., Stern, R.J., Viola, G., 2013. Orogen styles in the East African Orogen: A review of the Neoproterozoic to Cambrian tectonic evolution. J. African Earth Sci. 86, 65-106.

Fry, B., 2006. Stable Isotope Ecology, Stable Isotope Ecology. Springer New York. Vol. 521.

Fujimoto, K., Miyagi, T., Kikuchi, T., Kawana, T., 1996. Mangrove Habitat Formation and Response to Holocene Sea level Changes on Kosrae Island, Micronesia. Mangroves Salt Marshes. 1(1), 47–57.

Funk, C., Hoell, A., Shukla, S., Husak, G., Michaelsen, J., 2016. The East African Monsoon System: Seasonal Climatologies and Recent Variations, in: Springer

Climate. Springer, pp. 163–185.

Furukawa, K., Wolanski, E., 1996. Sedimentation in mangrove forests. Mangroves Salt Marshes 1, 3–10.

Garg, S.K., Bhatnagar, A., 1999. Effect of different doses of organic fertilizer (cow dung) on pond productivity and fish biomass in stillwater ponds. Journal of Applied Ichthyology 15(1), 10–18.

Garver, J.I., Royce, P.R., Smick, T.A., 1996. Chromium and nickel in shale of the taconic foreland: A case study for the provenance of fine-grained sediments with an ultramafic source. J. Sediment. Res. 66, 100–106.

Garzanti, E., Andó, S., France-Lanord, C., Censi, P., Vignola, P., Galy, V., Lupker, M., 2011. Mineralogical and chemical variability of fluvial sediments 2. Suspended-load silt (Ganga-Brahmaputra, Bangladesh). Earth and Planetary Science Letters. 302(1-2), 107-120.

Garzanti, E., Andò, S., France-Lanord, C., Vezzoli, G., Censi, P., Galy, V., Najman, Y., 2010. Mineralogical and chemical variability of fluvial sediments. 1. Bedload sand (Ganga-Brahmaputra, Bangladesh). Earth Planet. Sci. Lett. 299, 368–381.

Garzanti, E., Andò, S., Limonta, M., Fielding, L., Najman, Y., 2018. Diagenetic control on mineralogical suites in sand, silt, and mud (Cenozoic Nile Delta): Implications for provenance reconstructions. Earth-Science Rev. 185, 122-139.

Garzanti, E., Padoan, M., Setti, M., López-Galindo, A., Villa, I.M., 2014. Provenance versus weathering control on the composition of tropical river mud (southern Africa). Chem. Geol. 366, 61–74.

Gee, C.T., 2001. The mangrove palm Nypa in the geologic past of the New World. Wetl. Ecol. Manag. 93, 181–203.

Geeraert, N., Omengo, F.O., Tamooh, F., Paron, P., Bouillon, S., Govers, G., 2015. Sediment yield of the lower Tana River, Kenya, is insensitive to dam construction: sediment mobilization processes in a semi-arid tropical river system. Earth Surf. Process. Landforms. 40, 1827–1838.

Geraldi, N.R., Ortega, A., Serrano, O., Macreadie, P.I., Lovelock, C.E., Krause-Jensen, D., Kennedy, H., Lavery, P.S., Pace, M.L., Kaal, J., Duarte, C.M., 2019. Fingerprinting Blue Carbon: Rationale and Tools to Determine the Source of Organic Carbon in Marine Depositional Environments. Front. Mar. Sci. 6, 263.

Gilman, E.L., Ellison, J., Duke, N.C., Field, C., 2008. Threats to mangroves from climate change and adaptation options: A review. Aquat. Bot. 89(2), 237-250.

Gonneea, M. E., Paytan, A., Herrera-Silveira, J. A., 2004. Tracing organic matter sources and carbon burial in mangrove sediments over the past 160 years. Estuarine, Coastal and Shelf Science. 61(2), 211-227.

Goswami, B., Bhattacharyya, C., 2014. Petrogenesis of shoshonitic granitoids, Eastern India: Implications for the late Grenvillian post-collisional magmatism. Geosci. Front. 5, 821–843.

Govin, Aline, Holzwarth, Ulrike, Heslop, David, Keeling, Lara Ford, Zabel, Matthias, Mulitza, Stefan, Collins, James A, Chiessi, Cristiano M, Govin, A, Holzwarth, U, Heslop, D, Keeling, L Ford, Zabel, M, Mulitza, S, Collins, J A, Chiessi, C M, 2012. Distribution of major elements in Atlantic surface sediments (36°N-49°S): Imprint of terrigenous input and continental weathering. Geochemistry, Geophysics, Geosystems. 13(1).

Greber, N.D., Dauphas, N., 2019. The chemistry of fine-grained terrigenous sediments reveals a chemically evolved Paleoarchean emerged crust. Geochemica Cosmochim. Acta. 255, 247–264.

Greiner, J.T., Wilkinson, G.M., McGlathery, K.J.J., Emery, K.A., 2016. Sources of sediment carbon sequestered inrestored seagrass meadows. Mar. Ecol. Prog. Ser. 551, 95–105.

Gupta, A.S., Rao, S.K., 2001. Weathering indices and their applicability for crystalline rocks. Bull. Eng. Geol. Environ. 60(3), 201–221.

Gupta, J.G.S., Bertrand, N.B., 1995. Direct ICP-MS determination of trace and ultratrace elements in geological materials after decomposition in a microwave

oven. Part II. Quantitation of Ba, Cs, Ga, Hf, In, Mo, Nb, Pb, Rb, Sn, Sr, Ta and Tl. Talanta. 42, 1947–1957.

Gutiérrez, J.L., Jones, C.G., Byers, J.E., Arkema, K.K., Berkenbusch, K., Commito, A., Duarte, C.M., Hacker, S.D., Lambrinos, J.G., Hendriks, I.E., Hogarth, P.J., Palomo, M.G., Wild, C., 2012. Physical Ecosystem Engineers and the Functioning of Estuaries and Coasts. Treatise on Estuarine and Coastal Science. Elsevier Inc. pp. 53-81.

Hacker, B.R., Kelemen, P.B., Behn, M.D., 2015. Continental Lower Crust. Annual Review of Earth and Planetary Sciences. 43, 167–205.

Hahn, A., Miller, C., Andó, S., Bouimetarhan, I., Cawthra, H.C., Garzanti, E., Green, A.N., Radeff, G., Schefuß, E., Zabel, M., 2018. The Provenance of Terrigenous Components in Marine Sediments Along the East Coast of Southern Africa. Geochemistry, Geophys. Geosystems 19, 1946–1962.

Hanebuth, T., Stattegger, K., Grootes, P.M., 2000. Rapid flooding of the Sunda Shelf: A late-glacial sea level record. Science. 288(5468), 1033–1035.

Hapsari, K.A., Jennerjahn, T.C., Lukas, M.C., Karius, V., Behling, H., 2019. Intertwined effects of climate and land use change on environmental dynamics and carbon accumulation in a mangrove-fringed coastal lagoon in Java, Indonesia. Glob. Chang. Biol. 26(39), 1414-1431.

Hawkesworth, C.J., Cawood, P.A., Dhuime, B., Kemp, T.I.S., 2017. Earth's continental lithosphere through time. Annu. Rev. Earth Planet. Sci. 45, 169–198.

He, M., Zheng, H., Clift, P.D., Tada, R., Wu, W., Luo, C., 2015. Geochemistry of fine-grained sediments in the Yangtze River and the implications for provenance and chemical weathering in East Asia. Prog. Earth Planet. Sci. 2, 1–20.

He, M., Zheng, H., Huang, X., Jia, J., Li, L., 2013. Yangtze River sediments from source to sink traced with clay mineralogy. J. Asian Earth Sci. 69, 60–69.

He, S., Xu, Y.J., 2015. Concentrations and ratios of dissolved Sr, Ba and Ca Concentrations and ratios of Sr, Ba and Ca along an estuarine river to the Gulf

of Mexico-implication for sea level rise effects on trace metal distribution Concentrations and ratios of dissolved Sr, Ba and Ca Concentrations and ratios of dissolved Sr, Ba and Ca. Biogeosciences Discuss. 12, 18425–18461.

He, S., Xu, Y.J., 2016. Spatiotemporal distributions of sr and ba along an estuarine river with a large salinity gradient to the Gulf of Mexico. Water. 8(8), 323.

Hemming, S.R., McLennan, S.M., Hanson, G.N., 2015. Geochemical and Nd/Pb Isotopic Evidence for the Provenance of the Early Proterozoic Virginia Formation, Minnesota. Implications for the Tectonic Setting of the Animikie Basin. J. Geol. 103, 147–168.

Hemminga, M.A., Slim, F.J., Kazungu, J., Ganssen, G.M., Nieuwenhuize, J., Kruyt, N.M., 1994. Carbon outwelling from a mangrove forest with adjacent seagrass beds and coral reefs (Gazi Bay, Kenya). Marine Ecology Progress Series. 106, 291–302.

Herbon, C. M., & Nordhaus, I., 2013. Experimental determination of stable carbon and nitrogen isotope fractionation between mangrove leaves and crabs. Marine Ecology Progress Series. 490, 91-105.

Hollingworth, R.S., Leary, R.J., Heizler, M.T., 2021. Detrital U-Pb zircon and 40Ar/39Ar muscovite geochronology from Middle Pennsylvanian strata in the Anadarko Basin, Texas Panhandle, USA. Palaeogeogr. Palaeoclimatol. Palaeoecol. 579, 110573.

Holzkämper, A., Kumar, V., Surridge, B.W.J., Paetzold, A., Lerner, D.N., 2012. Bringing diverse knowledge sources together - A meta-model for supporting integrated catchment management. J. Environ. Manage. 96, 116–127.

Honti, M., Schuwirth, N., Rieckermann, J., Stamm, C., 2017. Can integrative catchment management mitigate future water quality issues caused by climate change and socio-economic development? Hydrol. Earth Syst. Sci. 21, 1593–1609.

Hossain, H.M.Z., Kawahata, H., Roser, B.P., Sampei, Y., Manaka, T., Otani, S., 2017.

Chemie der Erde Geochemical characteristics of modern river sediments in Myanmar and Thailand: Implications for provenance and weathering. Chemie der Erde 77, 443–458.

Howard, R.J., From, A.S., Krauss, K.W., Andres, K.D., Cormier, N., Allain, L., Savarese, M., 2020. Soil surface elevation dynamics in a mangrove-to-marsh ecotone characterized by vegetation shifts. Hydrobiologia. 847, 1087–1106.

Hu, D., Clift, P.D., Wan, S., Böning, P., Hannigan, R., Hillier, S., Blusztajn, J., 2016. Testing chemical weathering proxies in Miocene–Recent fluvial-derived sediments in the South China Sea. Geol. Soc. London, Spec. Publ. 429, 45–72.

Huxham, M., Kumara, M.P., Jayatissa, L.P., Krauss, K.W., Kairo, J., Langat, J., Mencuccini, M., Skov, M.W., Kirui, B., 2010. Intra- and interspecific facilitation in mangroves may increase resilience to climate change threats. Philos. Trans. R. Soc. B Biol. Sci. 365, 2127–2135.

Igulu, M.M., Nagelkerken, I., Dorenbosch, M., Grol, M.G.G., Harborne, A.R., Kimirei, I.A., Mumby, P.J., Olds, A.D., Mgaya, Y.D., 2014. Mangrove Habitat Use by Juvenile Reef Fish: Meta-Analysis Reveals that Tidal Regime Matters More than Biogeographic Region. PloS one. 9(12), e114715.

Inman, D.L., Jenkins, S.A., 1999. Climate change and the episodicity of sediment flux of small California Rivers. J. Geol. 107, 251–270.

IPCC, 2019. Climate Change and Land: an IPCC special report on climate change, desertification, land degradation, sustainable land management, food security, and greenhouse gas fluxes in terrestrial ecosystems [P.R. Shukla, J. Skea, E. Calvo Buendia, V. Masson-Delmot Masson-Delmotte, V., Pörtner, H.O., Roberts, D.C., Zhai, P., Slade, R., Connors, S., van Diemen, S. and Ferrat, M.]

Islam, M.S., Tooley, M.J., 1999. Coastal and sea level changes during the Holocene in Bangladesh. Quat. Int. 55, 61–75.

IUCN, 2003. Eastern Africa Programme 2003: The Pangani Basin: A Situation Analysis; xvi + 104pp.

Jennerjahn, T.C., Ittekkot, V., 2002. Relevance of mangroves for the production and deposition of organic matter along tropical continental margins. Naturwissenschaften. 89(1), 23–30.

Jennerjahn, T.C., Ittekkot, V., Klöpper, S., Adi, S., Purwo Nugroho, S., Sudiana, N., Yusmal, A., Prihartanto, Gaye-Haake, B., 2004. Biogeochemistry of a tropical river affected by human activities in its catchment: Brantas River estuary and coastal waters of Madura Strait, Java, Indonesia. Estuar. Coast. Shelf Sci. 60, 503–514.

Jennerjahn, T.C., Nasir, B., Pohlenga, I., 2009. Spatio-temporal variation of dissolved inorganic nutrients related to hydrodynamics and land use in the mangrove-fringed Segara Anakan Lagoon, Java, Indonesia. Regional Environmental Change 9(4), 259–274.

Jung, H.-S., Lim, D., Choi, J.-Y., Yoo, H.-S., Rho, K.-C., Lee, H.-B., 2012. Rare earth element compositions of core sediments from the shelf of the South Sea, Korea: Their controls and origins. Cont. Shelf Res. 48, 75–86.

Juteau, M., Michard, A., Albarede, F., 1986. The Pb-Sr-Nd isotope geochemistry of some recent circum-Mediterranean granites. Contrib. to Mineral. Petrol. 1986 923 92, 331–340.

Karegar, M.A., Dixon, T.H., Engelhart, S.E., 2016. Subsidence along the Atlantic Coast of North America: Insights from GPS and late Holocene relative sea level data. Geophys. Res. Lett. 43, 3126–3133.

Kark, S., Tulloch, A., Gordon, A., Mazor, T., Bunnefeld, N., Levin, N., 2015. Cross-boundary collaboration: key to the conservation puzzle. Curr. Opin. Environ. Sustain. 12, 12–24.

Kebede, A.S., Nicholls, R.J., Hanson, S., Mokrech, M., 2010. Impacts of climate change and sea level rise: A preliminary case study of Mombasa, Kenya. J. Coast. Res. 28, 8–19.

Kennedy, H., Beggins, J., Duarte, C.M., Fourqurean, J.W., Holmer, M., Marbà, N.,

Middelburg, J.J., 2010. Seagrass sediments as a global carbon sink: Isotopic constraints. Global Biogeochem. Cycles. 24(4).

Kennedy, H., Gacia, E., Kennedy, D.P., Papadimitriou, S., Duarte, C.M., 2004. Organic carbon sources to SE Asian coastal sediments. Estuarine, Coastal and Shelf Science 60(1), 59–68.

Khan, N.S., Vane, C.H., Engelhart, S.E., Kendrick, C., Horton, B.P., 2019. The application of **δ**13C, TOC and C/N geochemistry of mangrove sediments to reconstruct Holocene paleoenvironments and relative sea levels, Puerto Rico. Mar. Geol. 415, 105963.

Khan, N.S., Vane, C.H., Horton, B.P., 2015. The application of stable carbon isotope and C/N geochemistry of coastal wetland sediments as a sea level indicator, in: Shennan, I., et al. (Eds.), Handbook of Sea Level Research: Wiley-Blackwell, Hoboken. pp. 295–311.

Kimani, P., Wamukota, A., Manyala, J.O., Mlewa, C.M., 2020. Actors' perceptions of government performance in support of value chain development in marine small-scale fisheries in Kenya. Mar. Policy. 122, 104221.

Kimeli, A., Ocholla, O., Okello, J., Koedam, N., Westphal, H., & Kairo, J. (2021). Geochemical and petrographic characteristics of sediments along the transboundary (Kenya–Tanzania) Umba River as indicators of provenance and weathering. Open Geosciences, 13(1), 1064-1083.

Kirwan, M.L., Langley, J.A., Guntenspergen, G.R., Megonigal, J.P., 2013. The impact of sea level rise on organic matter decay rates in Chesapeake Bay brackish tidal marshes. Biogeosciences 10, 1869–1876.

Kirwan, M.L., Megonigal, J.P., 2013. Tidal wetland stability in the face of human impacts and sea level rise. Nature 504, 53–60.

Kiteresi, L.I., Okuku, E.O., Mwangi, S.N., Ohowa, B., Wanjeri, V.O., Okumu, S., Mkono, M., 2012. The influence of land based activities on the phytoplankton communities of Shimoni-Vanga system, Kenya. International Journal of

Environmnetal Research. 6(1), 151–162.

Kitheka, J.U., Ongwenyi, G.S., Mavuti, K.M., 2002. Dynamics of suspended sediment exchange and transport in a degraded mangrove creek in Kenya. Ambio 31, 580–587.

Kottek, M., Grieser, J., Beck, C., Rudolf, B., Rubel, F., 2006. World Map of the Köppen-Geiger climate classification updated. Meteorol. Zeitschrift 259–263.

Krauss, K.W., Allen, J.A., Cahoon, D.R., 2003. Differential rates of vertical accretion and elevation change among aerial root types in Micronesian mangrove forests. Estuar. Coast. Shelf Sci. 56, 251–259.

Krauss, K.W., Cahoon, D.R., Allen, J.A., Ewel, K.C., Lynch, J.C., Cormier, N., 2010. Surface elevation change and susceptibility of different mangrove zones to sea level rise on Pacific high islands of Micronesia. Ecosystems.13, 129–143.

Krauss, K.W., Lovelock, C.E., McKee, K.L., López-Hoffman, L., Ewe, S.M.L., Sousa, W.P., 2008. Environmental drivers in mangrove establishment and early development: A review. Aquat. Bot. 89(2), 105-127.

Krauss, K.W., Mckee, K.L., Lovelock, C.E., Cahoon, D.R., Saintilan, N., Reef, R., Chen, L., 2014. How mangrove forests adjust to rising sea level. New Phytol. 202, 19–34.

Kristensen, E., 2007. Mangrove crabs as ecosystem engineers; with emphasis on sediment processes. Journal of sea Research. 59(1-2), 30-43.

Kristensen, E., Bouillon, S., Dittmar, T., Marchand, C., 2008. Organic carbon dynamics in mangrove ecosystems: A review. Aquatic Botany. 89(2), 201-219.

Kristensen, E., Mangion, P., Tang, M., Flindt, M. R., Holmer, M., Ulomi, S., 2011. Microbial carbon oxidation rates and pathways in sediments of two Tanzanian mangrove forests. Biogeochemistry. 103(1), 143-158.

Kroonenberg, S.B., 1992. Effect of provenance, sorting and weathering on the geochemistry of fluvial sands from different tectonic and climatic environments. In Proceedings of the 29th international geological congress, part A. 69, pp. 81.

Kusumaningtyas, M.A., Hutahaean, A.A., Fischer, H.W., Pérez-Mayo, M., Ransby, D., Jennerjahn, T.C., 2019. Variability in the organic carbon stocks, sources, and accumulation rates of Indonesian mangrove ecosystems. Estuarine, Coastal and Shelf Science. 218, 310–323.

Kusumaningtyas, M.A., Kepel, T.L., Solihuddin, T., Lubis, A.A., Putra, A.D.P., Sugiharto, U., Ati, R.N.A., Salim, H.L., Mustikasari, E., Heriati, A., Daulat, A., Sudirman, N., Suryono, D.D., Rustam, A., 2021. Carbon sequestration potential in the rehabilitated mangroves in Indonesia. Ecol. Res. 37(1), 87-91.

Lamb, A.L., Wilson, G.P., Leng, M.J., 2006. A review of coastal palaeoclimate and relative sea level reconstructions using **δ**13C and C/N ratios in organic material. Earth-Science Rev. 75, 29–57.

Lang'at, J.K.S., Kairo, J.G., Mencuccini, M., Bouillon, S., Skov, M.W., Waldron, S., Huxham, M., 2014. Rapid losses of surface elevation following tree girdling and cutting in tropical mangroves. PLoS One. 9, 1–8.

Le Minor, M., Zimmer, M., Helfer, V., Gillis, L.G., Huhn, K., 2021. Flow and sediment dynamics around structures in mangrove ecosystems—a modeling perspective. Dyn. Sediment. Environ. Mangrove Coasts. 83–120.

Leleyter, L., Probst, J.-L., Depetris, P., Haida, S., Mortatti, J., Rouault, R., Samuel, J., 1999. REE distribution pattern in river sediments: partitioning into residual and labile fractions. Comptes Rendus l'Académie des Sci. - Ser. IIA - Earth Planet. Sci. 329, 45–52.

Li, J., Knapp, D.E., Lyons, M., Roelfsema, C., Phinn, S., Schill, S.R., Asner, G.P., 2021. Automated Global Shallow Water Bathymetry Mapping Using Google Earth Engine. Remote Sens. 13(8), 1469.

Lim, D., Jung, H.S., Choi, J.Y., 2014. REE partitioning in riverine sediments around the Yellow Sea and its importance in shelf sediment provenance. Mar. Geol. 357, 12–24.

Liu, J.P., Liu, C.S., Xu, K.H., Milliman, J.D., Chiu, J.K., Kao, S.J., Lin, S.W., 2008. Flux

and fate of small mountainous rivers derived sediments into the Taiwan Strait. Mar. Geol. 256, 65–76.

López-Portillo, J., Lewis, R.R., Saenger, P., Rovai, A., Koedam, N., Dahdouh-Guebas, F., Agraz-Hernández, C., Rivera-Monroy, V.H., 2017. Mangrove Forest Restoration and Rehabilitation. Mangrove Ecosyst. A Glob. Biogeogr. Perspect. Springer, Cham. pp. 301–345.

Lovelock, C., Cahoon, D., Friess, D., Guntenspergen, G., Krauss, K., Ruth, R., Saunders, M., Sidik, F., Swales, A., Saintilan, N., Xuan, T., Triet, T., 2015. The vulnerability of Indo-Pacific mangrove forests to sea level rise. Nature. 426, 559–563.

Maboko, M.A.H., Nakamura, E., 2002. Isotopic dating of Neoproterozoic crustal growth in the Usambara Mountains of northeastern Tanzania: Evidence for coeval crust formation in the Mozambique Belt and the Arabian-Nubian Shield. Precambrian Res. 113, 227–242.

Mackenzie, R.C., Mitchell, B.D., 1966. Clay mineralogy. Earth-Science Rev. 2, 47–91.

Manya, S., Maboko, M.A.H., Nakamura, E., 2007. Geochemistry and Nd-isotopic composition of potassic magmatism in the Neoarchaean Musoma-Mara Greenstone Belt, northern Tanzania. Precambrian Res. 159, 231–240.

Marin-Spiotta, E., Silver, W.L., Swanston, C.W., Ostertag, R., 2009. Soil organic matter dynamics during 80 years of reforestation of tropical pastures. Global Change Biology. 15(6), 1584–1597.

Marwick, T.R., Tamooh, F., Ogwoka, B., Teodoru, C., Borges, A. V., Darchambeau, F., Bouillon, S., 2014. Dynamic seasonal nitrogen cycling in response to anthropogenic N loading in a tropical catchment, Athi-Galana-Sabaki River, Kenya. Biogeosciences.11, 443–460.

Marwick, T.R., Tamooh, F., Teodoru, C.R., Borges, A. V, Darchambeau, F., Bouillon, S., 2015. Global Biogeochemical Cycles A global perspective. Global Biogeochem. Cycles. 29, 122–137.

Mason, N., Ward, M., Watson, J.E.M., Venter, O., Runting, R.K., 2020. Global opportunities and challenges for transboundary conservation. Nat. Ecol. Evol. 4(5), 694–701.

Mazda, Y., Wolanski, E., 2009. Hydrodynamics and Modeling of Water Flow in Mangrove Areas, First edit. ed, Coastal Wetlands: An Integrated Ecosystem Approach. Elsevier. 8, 231-262.

Mcivor, A., Spencer, T., Möller, I., Spalding, M.D., 2013. The response of mangrove soil surface elevation to sea level rise Natural Coastal Protection Series: Report 3, Natural Coastal Protection Series ISSN.

McKee, K.L., 2011. Biophysical controls on accretion and elevation change in Caribbean mangrove ecosystems. Estuar. Coast. Shelf Sci. 91, 475–483.

McKee, K.L., Feller, I.C., Popp, M., Wanek, W., 2002. Mangrove isotopic (δ15N and δ^{13}C) fractionation across a nitrogen vs. phosphorus limitation gradient. Ecology. 83(4), 1065–1075.

McLennan, S.M., 1993. Weathering and global denudation. J. Geol. 101, 295–303.

McLennan, S.M., 2001. Relationships between the trace element composition of sedimentary rocks and upper continental crust. Geochemistry, Geophys. Geosystems. 2(4).

McLennan, S.M., Hemming, S., McDaniel, D.K., Hanson, G.N., 1993. Geochemical approaches to sedimentation, provenance, and tectonics. Spec. Pap. Soc. Am. pp. 21-21.

McLennan, S.M., Taylor, S.R., Kröner, A., 1983. Geochemical evolution of Archean shales from South Africa. I. The Swaziland and Pongola Supergroups. Precambrian Res. 22, 93–124.

Meckel, T., Brink, U., Williams, S., 2007. Sediment compaction rates and subsidence in deltaic plains: Numerical constraints and stratigraphic influences. Basin Res. 19, 19–31.

Middelburg, J.J., Nieuwenhuize, J., 1998. Carbon and nitrogen stable isotopes in

suspended matter and sediments from the Schelde Estuary. Marine Chemistry. 60(3-4), 217–225.

Middelburg, J.J., Nieuwenhuize, J., Slim, F.J., Ohowa, B., 1996. Sediment biogeochemistry in an east African mangrove forest (Gazi Bay, Kenya). Biogeochemistry. 34(3), 133–155.

Mil-Homens, M., Vale, C., Raimundo, J., Pereira, P., Brito, P., Caetano, M., 2014. Major factors influencing the elemental composition of surface estuarine sediments: The case of 15 estuaries in Portugal. Mar. Pollut. Bull. 84, 135–146.

Milliman, J., Farnsworth, K., 2013. River discharge to the coastal ocean: a global synthesis. Cambridge University Press, New York.

Milliman, J.D., Bonaldo, D., Carniel, S., 2016. Flux and fate of river-discharged sediments to the adriatic sea. Advances in Oceanography and Limnology. 7(2), 106–114.

Mimura, N., Horikawa, K., 2013. Review Sea level rise caused by climate change and its implications for society. Mimura, Nobuo. "Sea level rise caused by Clim. Chang. its Implic. Soc. Proc. Japan Acad. Ser. B. 89, 281–301.

Mishra, M., Sen, S., 2012. Provenance, tectonic setting and source-area weathering of Mesoproterozoic Kaimur Group, Vindhyan Supergroup, Central India. Geol. Acta. 10, 283–293.

Mungai, F., Kairo, J., Mironga, J., Kirui, B., Mangora, M., Koedam, N., 2019. Mangrove cover and cover change analysis in the transboundary area of Kenya and Tanzania during 1986–2016. J. Indian Ocean Reg. 15, 157–176.

Murphy, C.P., 1986. Thin section preparation of soils and sediments. United Kigdom:AB Academic Publishers.

Mutakyahwa, M.K.D., Ikingura, J.R., Mruma, A.H., 2003. Geology and geochemistry of bauxite deposits in Lushoto District, Usambara Mountains, Tanzania. J. African Earth Sci. 36, 357–369.

Nardin, W., Vona, I., Fagherazzi, S., 2021. Sediment deposition affects mangrove

forests in the Mekong delta, Vietnam. Cont. Shelf Res. 213, 104319.

Nasir, A., Lukman, M., Tuwo, A., Hatta, M., Tambaru, R., Nurfadilah, 2016. The use of C/N ratio in assessing the influence of land-based material in coastal water of South Sulawesi and Spermonde Archipelago, Indonesia. Frontiers in Marine Science. 3, 1–8.

Ndirangu, M.D., Chira, R.M., Wang'ondu, V., Kairo, J.G., 2017. Analysis of wave energy reduction and sediment stabilization by mangroves in Gazi Bay, Kenya. Bonorowo Wetl. 7, 83–94.

Nerem, R.S., Beckley, B.D., Fasullo, J.T., Hamlington, B.D., Masters, D., Mitchum, G.T., 2018. Climate-change–driven accelerated sea level rise detected in the altimeter era. Proc. Natl. Acad. Sci. U. S. A. 115, 2022–2025.

Nesbitt, H., Young, G., 1982. Early Proterozoic climates and plate motions inferred from major elements chemistry of lutites. Nature. 299, 715–717.

Nesbitt, H.W., Young, G.M., 1984. Prediction of some weathering trends of plutonic and volcanic rocks based on thermodynamic and kinetic considerations. Geochim. Cosmochim. Acta. 48, 1523–1534.

Nesbitt, H.W., Young, G.M., McLennan, S.M., Keays, R.R., 1996. Effects of chemical weathering and sorting on the petrogenesis of siliciclastic sediments, with implications for provenance studies. J. Geol. 104, 525–542.

Neubauer, S.C., 2008. Contributions of mineral and organic components to tidal freshwater marsh accretion. Estuar. Coast. Shelf Sci. 78, 78–88.

Neubauer, S.C., Anderson, I.C., Constantine, J.A., Kuehl, S.A., 2002. Sediment Deposition and Accretion in a Mid-Atlantic (U.S.A.) Tidal Freshwater Marsh. Estuar. Coast. Shelf Sci. 54, 713–727.

Nicholls, R.J., Adger, W.N., Hutton, C.W., Hanson, S.E., 2020. Delta Challenges and Trade-Offs from the Holocene to the Anthropocene. Deltas Anthr. 1–22.

Nicholls, R.J., Lincke, D., Hinkel, J., Brown, S., Vafeidis, A.T., Meyssignac, B., Hanson, S.E., Merkens, J.L., Fang, J., 2021. A global analysis of subsidence, relative sea

level change and coastal flood exposure. Nat. Clim. Chang. 11(4), 338–342.

Nicholson, S. E., 2018. The ITCZ and the seasonal cycle over equatorial Africa. Bulletin of the American Meteorological Society. 99(2), 337-348.

Nolte, S., Koppenaal, E.C., Esselink, P., Dijkema, K.S., Schuerch, M., De Groot, A. V., Bakker, J.P., Temmerman, S., 2013. Measuring sedimentation in tidal marshes: A review on methods and their applicability in biogeomorphological studies. J. Coast. Conserv. 17, 301–325.

Nyobe, J.M., Sababa, E., Bayiga, E.C., Ndjigui, P.D., 2018. Mineralogical and geochemical features of alluvial sediments from the Lobo watershed (Southern Cameroon): Implications for rutile exploration. Comptes Rendus Geosci. 350, 119–129.

Ochiewo, J., de la Torre-Castro, M., Muthama, C., Munyi, F., Nthuta, J.M., 2010. Socio-economic features of sea cucumber fisheries in southern coast of Kenya. Ocean Coast. Manag. 53, 192–202.

Okello, J.A., Kairo, J.G., Dahdouh-Guebas, F., Beeckman, H., Koedam, N., 2020. Mangrove trees survive partial sediment burial by developing new roots and adapting their root, branch and stem anatomy. Trees - Struct. Funct. 34, 37–49.

Okello, J.O., Schmitz, N., Kairo, J.G., Beeckman, H., Dahdouh-Guebas, F., Koedam, N., 2013. Self-sustenance potential of peri-urban mangroves: a case of Mtwapa Creek Kenya. J. Environ. Sci. Water Resour. 2, 277–289.

Okuku, E.O., Kiteresi, L.I., Owato, G., Mwalugha, C., Omire, J., Mbuche, M., Chepkemboi, P., Ndwiga, J., Nelson, A., Kenneth, O., Lilian, M., Brenda, G., 2020. Baseline meso-litter pollution in selected coastal beaches of Kenya: Where do we concentrate our intervention efforts? Mar. Pollut. Bull. 158, 111420.

Okuku, E.O., Tole, M., Bouillon, S., 2018. Role of a cascade of reservoirs in regulating downstream transport of sediment, carbon and nutrients: Case study of tropical arid climate Tana River Basin. Lakes Reserv. Res. Manag. 23, 43–55.

Ouyang, X., Lee, S.Y., Connolly, R.M., 2017. The role of root decomposition in global

mangrove and saltmarsh carbon budgets. Earth-Science Rev. 166, 53–63.

Paprotny, D., Vousdoukas, M.I., Morales-Nápoles, O., Jonkman, S.N., Feyen, L., 2020. Pan-European hydrodynamic models and their ability to identify compound floods. Nat. Hazards 101, 933–957.

Parnell, A.C., Phillips, D.L., Bearhop, S., Semmens, B.X., Ward, E.J., Moore, J.W., Jackson, A.L., Grey, J., Kelly, D.J., Inger, R., 2013. Bayesian stable isotope mixing models. Environmetrics. 24(6), 387–399.

Pastene, M., Quiroga, E., Hurtado, C.F., 2019. Stable isotopes and geochemical indicators in marine sediments as proxies for anthropogenic impact: A baseline for coastal environments of central Chile (33°S). Mar. Pollut. Bull. 142, 76–84.

Payo, A., Mukhopadhyay, A., Hazra, S., Ghosh, T., Ghosh, S., Brown, S., Nicholls, R.J., Bricheno, L., Wolf, J., Kay, S., Lázár, A.N., Haque, A., 2016. Projected changes in area of the Sundarban mangrove forest in Bangladesh due to SLR by 2100. Clim. Chang. 139(2), 279–291.

Perdue, E.M., Koprivnjak, J.F., 2007. Using the C/N ratio to estimate terrigenous inputs of organic matter to aquatic environments. Estuar. Coast. Shelf Sci. 73, 65–72.

Perri, F., Muto, F., Belviso, C., 2011. Links between composition and provenance of Mesozoic siliciclastic sediments from western Calabria (southern Italy). Ital. J. Geosci. 130, 318–329.

Petsch, S.T., 2013. Weathering of Organic Carbon, in: Treatise on Geochemistry: Second Edition. Elsevier Inc., 12, 217–238.

Phan, L.K., Van Thiel De Vries, J.S.M., Stive, M.J.F., 2015. Coastal mangrove squeeze in the Mekong Delta. J. Coast. Res. 31, 233–243.

Phillips, O.A., Falana, A.O., Adebayo, A.J., 2017. The geochemical composition of sediment as a proxy of provenance and weathering intensity: a case study of Southwest Nigeria's Coastal Creeks. Geol. Geophys. Environ. 43, 229.

Pietrafesa, L.J., Zhang, H., Bao, S., Gayes, P.T., Hallstrom, J.O., 2019. Coastal

Flooding and Inundation and Inland Flooding due to Downstream Blocking. J. Mar. Sci. Eng. 2019, Vol. 7, Page 336 7, 336.

Plaziat, J.-C., Cavagnetto, C., Koeniguer, J.-C., Baltzer, F., 2001. History and biogeography of the mangrove ecosystem, based on a critical reassessment of the paleontological record. Wetl. Ecol. Manag. 9(3), 161–180.

Polidoro, B.A., Carpenter, K.E., Collins, L., Duke, N.C., Ellison, A.M., Ellison, J.C., Farnsworth, E.J., Fernando, E.S., Kathiresan, K., Koedam, N.E., Livingstone, S.R., Miyagi, T., Moore, G.E., Ngoc Nam, V., Ong, J.E., Primavera, J.H., Salmo, S.G., Sanciangco, J.C., Sukardjo, S., Wang, Y., Yong, J.W.H., Nam, V.N., Ong, J.E., Primavera, J.H., Salmo, S.G., Sanciangco, J.C., Sukardjo, S., Wang, Y., Wan, J., Yong, H., 2010. The Loss of Species: Mangrove Extinction Risk and Geographic Areas of Global Concern. PLoS One. 5(4), e10095.

Power, P.E., 1969. Clay Mineralogy and Paleoclimatic Significance of Some Red Regoliths and Associated Rocks in Western Colorado. J. Sediment. Res. 39(3).

Prasad, M.B.K., Kumar, A., Ramanathan, A.L., Datta, D.K., 2017. Sources and dynamics of sedimentary organic matter in Sundarban mangrove estuary from Indo-Gangetic delta. Ecol. Process. 6, 1–15.

Prizomwala, S.P., Bhatt, N., Basavaiah, N., 2014. Provenance discrimination and Source-to-Sink studies from a dryland fluvial regime: An example from Kachchh, western India. Int. J. Sediment Res. 29, 99–109.

Pruseth, K.L., Yadav, S., Mehta, P., Pandey, D., Tripathi, J.K., 2005. No TitleProblems in microwave digestion of high-Si and high-Al rocks. Curr. Sci. 89, 1668–1671.

R Core Team, 2020. R: A language and environment for statistical computing. R Foundation for Statistical Computing, Vienna, Austria.

Rahayu, Y.P., Solihuddin, T., Kusumaningtyas, M.A., Afi Ati, R.N., Salim, H.L., Rixen, T., Hutahaean, A.A., 2019. The Sources of Organic Matter in Seagrass Sediments and Their Contribution to Carbon Stocks in the Spermonde Islands, Indonesia. Aquatic Geochemistry. 25(3), 161–178.

Rahman, A.F., Dragoni, D., El-Masri, B., 2011. Response of the Sundarbans coastline to sea level rise and decreased sediment flow: A remote sensing assessment. Remote Sens. Environ. 115, 3121–3128.

Rahman, M.M., Zimmer, M., Ahmed, I., Donato, D., Kanzaki, M. and Xu, M., 2021. Co-benefits of protecting mangroves for biodiversity conservation and carbon storage. Nature communications. 12(1), 1-9.

Raigemborn, M., Brea, M., Zucol, A., Matheos, S., 2009. Early Paleogene climate at mid latitude in South America: Mineralogical and paleobotanical proxies from continental sequences in Golfo San Jorge basin (Patagonia, Argentina). Geol. Acta. 7, 125–145.

Ray, R., Michaud, E., Aller, R.C., Vantrepotte, V., Gleixner, G., Walcker, R., Devesa, J., Le Goff, M., Morvan, S., Thouzeau, G., 2018. The sources and distribution of carbon (DOC, POC, DIC) in a mangrove dominated estuary (French Guiana, South America). Biogeochemistry. 138(3), 297–321.

Ricklefs, R.E., Schwarzbach, A.E., Renner, S.S., 2015. Rate of Lineage Origin Explains the Diversity Anomaly in the World's Mangrove Vegetation. 168, 805–810.

Rivera-Monroy, V.H., Kristensen, E., Lee, S.Y., Twilley, R.R., 2017. Mangrove ecosystems: A global biogeographic perspective: Structure, function, and services. Mangrove Ecosyst. A Glob. Biogeogr. Perspect. Structure, function, and services. Cham, Switzerland: Springer Interna-tional. pp. 1–399.

Rogers, K., 2021. Accommodation space as a framework for assessing the response of mangroves to relative sea level rise. Singap. J. Trop. Geogr. 42, 163–183.

Rogers, K., Saintilan, N., Woodroffe, C.D., 2014. Surface elevation change and vegetation distribution dynamics in a subtropical coastal wetland: Implications for coastal wetland response to climate change. Estuar. Coast. Shelf Sci. 149, 46–56.

Romañach, S.S., DeAngelis, D.L., Koh, H.L., Li, Y., Teh, S.Y., Raja Barizan, R.S., Zhai, L., 2018. Conservation and restoration of mangroves: Global status,

perspectives, and prognosis. Ocean Coast. Manag. 154, 72-82.

Rubel, F., Brugger, K., Haslinger, K., Auer, I., 2017. The climate of the European Alps: Shift of very high resolution Köppen-Geiger climate zones 1800-2100. Meteorologische Zeitschrift. 26(2), pp.115-125.

Rudnick, R.L., Gao, S., 2003. Composition of the continental crust. The crust. 3, 1–64.

Ruiz-Fernández, A.C., Agraz-Hernández, C.M., Sanchez-Cabeza, J.A., Díaz-Asencio, M., Pérez-Bernal, L.H., Chan Keb, C.A., López-Mendoza, P.G., Blanco y Correa, J.M., Ontiveros-Cuadras, J.F., Osti Saenz, J., Reyes Castellanos, J.E., 2018. Sediment Geochemistry, Accumulation Rates and Forest Structure in a Large Tropical Mangrove Ecosystem. Wetlands. 38, 307–325.

Rumolo, P., Barra, M., Gherardi, S., Marsella, E., Sprovieri, M., 2011. Stable isotopes and C/N ratios in marine sediments as a tool for discriminating anthropogenic impact. Journal of Environmental Monitoring. 13(12), 3399–3408.

Saintilan, N., Khan, N.S., Ashe, E., Kelleway, J.J., Rogers, K., Woodroffe, C.D., Horton, B.P., 2020. Thresholds of mangrove survival under rapid sea level rise. Science. 368(6495), 1118–1121.

Sajid, Z., Ismail, M.S., Hanif, T., 2020. Mineralogical and geochemical imprints to determine the provenance, depositional history and tectonic settings of Triassic turbidites in the Semanggol and Semantan Basins, Peninsular Malaysia. J. Asian Earth Sci. 203, 104539.

Saleh, M., Becker, M., 2018. New estimation of Nile Delta subsidence rates from InSAR and GPS analysis. Environ. Earth Sci. 2018 781 78, 1–11.

Sanders, C.J., Smoak, J.M., Naidu, A.S., Patchineelam, S.R., 2008. Recent Sediment Accumulation in a Mangrove Forest and Its Relevance to Local Sea level Rise (Ilha Grande, Brazil). J. Coast. Res. 242, 533–536.

Sarkar, S.K., Frančišković-Bilinski, S., Bhattacharya, A., Saha, M., Bilinski, H., 2004. Levels of elements in the surficial estuarine sediments of the Hugli River,

northeast India and their environmental implications. Environ. Int. 30, 1089–1098.

Sasmito, S.D., Kuzyakov, Y., Lubis, A.A., Murdiyarso, D., Hutley, L.B., Bachri, S., Friess, D.A., Martius, C., Borchard, N., 2020. Organic carbon burial and sources in soils of coastal mudflat and mangrove ecosystems. Catena. 187, 104414.

Sasmito, S.D., Murdiyarso, D., Friess, D.A., Kurnianto, S., 2016. Can mangroves keep pace with contemporary sea level rise? A global data review. Wetl. Ecol. Manag. 24, 263–278.

Schlünz B., S.R.R., 2000. Transport of terrestrial organic carbon to the oceans by rivers: re-estimating flux- and burial rates. Int. Earth Sci. 88(4), 599–606.

Schlüter, T., 1997. Geology of East Africa, XII. ed. Schweizerbart'sche Verlagsbuchhandlung.

Schuerch, M., Spencer, T., Temmerman, S., Kirwan, M.L., Wolff, C., Lincke, D., McOwen, C.J., Pickering, M.D., Reef, R., Vafeidis, A.T., Hinkel, J., Nicholls, R.J., Brown, S., 2018. Future response of global coastal wetlands to sea level rise. Nature. 561, 231–234.

Sensarma, S., Rajamani, V., Tripathi, J.K., 2008. Petrography and geochemical characteristics of the sediments of the small River Hemavati, Southern India: Implications for provenance and weathering processes. Sediment. Geol. 205, 111–125.

Shackleton, R., 1993. Tectonics of the lower crust: a view from the Usambara Mountains, NE Tanzania. J. Struct. Geol. 15, 663–671.

Shao, J., Yang, S., Li, C., 2012. Chemical indices (CIA and WIP) as proxies for integrated chemical weathering in China : Inferences from analysis of fl uvial sediments. Sediment. Geol. 265–266, 110–120.

Shao, J.Q., Yang, S.Y., 2012. Does chemical index of alteration (CIA) reflect silicate weathering and monsoonal climate in the Changjiang River basin? Chinese Sci. Bull. 57, 1178–1187.

Siddall, M., Rohling, E.J., Almogi-Labin, A., Hemleben, C., Meischner, D., Schmelzer, I., Smeed, D.A., 2003. Sea level fluctuations during the last glacial cycle. Nature. 423(6942), 853–858.

Silva, M.M.V.G., Cabral Pinto, M.M.S., Carvalho, P.C.S., 2016. Major, trace and REE geochemistry of recent sediments from lower Catumbela River (Angola). J. African Earth Sci. 115, 203–217.

Singh, M., Sharma, M., Jü Rgen Tobschall, H., 2005. Weathering of the Ganga alluvial plain, northern India: implications from fluvial geochemistry of the Gomati River. Appl. Geochemistry. 20, 1–21.

Singh, P., 2009. Geochemistry and provenance of stream sediments of the Ganga River and its major tributaries in the Himalayan region, India. Chem. Geol. 269, 220–236.

Sippo, J.Z., Lovelock, C.E., Santos, I.R., Sanders, C.J., Maher, D.T., 2018. Mangrove mortality in a changing climate: An overview. Estuar. Coast. Shelf Sci. 215, 241–249.

Smith, B.N., Epstein, S., 1971. Two Categories of 13C/12C Ratios for Higher Plants. Plant Physiol. 340–383.

Soares, M.L.G., 2009. A conceptual model for the responses of mangrove forests to sea level rise. J. Coast. Res. 267–271.

Spencer, C.J., Kirkland, C.L., Taylor, R.J.M., 2016. Strategies towards statistically robust interpretations of in situ U–Pb zircon geochronology. Geosci. Front. 7, 581–589.

Stringer, C.E., Trettin, C.C., Zarnoch, S.J., Tang, W., 2015. Carbon stocks of mangroves within the Zambezi River Delta, Mozambique. For. Ecol. Manage. 354, 139–148. https://doi.org/10.1016/j.foreco.2015.06.027

Sugden, A.M., 2020. Mangroves under sea level rise. Science. 368(6495), 1076-1078.

Sun, X., Li, C., Kuiper, K.F., Wang, J., Tian, Y., Vermeesch, P., Zhang, Z., Zhao, J., Wijbrans, J.R., 2018. Geochronology of detrital muscovite and zircon constrains

the sediment provenance changes in the Yangtze River during the late Cenozoic. Basin Res. 30, 636–649.

Swales, A., Bentley, S.J., Lovelock, C., Bell, R.G., 2007. Sediment processes and mangrove-habitat expansion on a rapidly-prograding Muddy Coast, New Zealand. Coast. Sediments '07 - Proc. 6th Int. Symp. Coast. Eng. Sci. Coast. Sediment Process. 40926.

Syvitski, J.P.M., 2008. Deltas at risk. Sustain. Science. 3, 23–32.

Syvitski, J.P.M., Kettner, A.J., Overeem, I., Hutton, E.W.J., Hannon, M.T., Brakenridge, G.R., Day, J., Vörösmarty, C., Saito, Y., Giosan, L., Nicholls, R.J., 2009. Sinking deltas due to human activities. Nat. Geosci. 2, 681–686.

Syvitski, J.P.M., Milliman, J.D., 2007. Geology, geography, and humans battle for dominance over the delivery of fluvial sediment to the coastal ocean. J. Geol. 115, 1–19.

Takagi, H., 2018. Long-Term Design of Mangrove Landfills as an Effective Tide Attenuator under Relative Sea level Rise. Sustainability. 10, 1045.

Tamooh, F., Meysman, F.J.R., Borges, A. V., Marwick, T.R., Van Den Meersche, K., Dehairs, F., Merckx, R., Bouillon, S., 2014. Sediment and carbon fluxes along a longitudinal gradient in the lower Tana River (Kenya). Journal of Geophysical Research: Biogeosciences. 119(7), 1340–1353.

Tamooh, F., Van Den Meersche, K., Meysman, F., Marwick, T.R., Borges, A. V., Merckx, R., Dehairs, F., Schmidt, S., Nyunja, J., Bouillon, S., 2012. Distribution and origin of suspended matter and organic carbon pools in the Tana River Basin, Kenya. Biogeosciences. 9(8), 2905–2920.

Taylor, S.R., McLennan, S.M., 1985. The continental crust: its composition and evolution. Blackwells. 301.

Temmerman, S., Kirwan, M.L., 2015. Building land with a rising sea. Science. 349(6248), 588–589.

Tesfamariam, E. G., Home, P. G., Gathenya, J. M., 2018. Statistical Analysis of

Relationships Between the Flow Regime and Riverine Ecosystems in The Umba River, Kenya. Journal of Environmnetal and Earth Sciences. 8(11), 13-24.

Tesfamariam, E., Home, P., Gathenya, J., 2021. Rainfall-runoff modelling to determine continuous time series of daily streamflow in the Umba River, Kenya. African J. Rural Dev. 5, 49–68.

Thornton, S.F., McManus, J., 1994. Application of Organic Carbon and Nitrogen Stable Isotope and C/N Ratios as source Indicators of Organic Matter Provenance in Estuarine Systems: Evidence From the Tay Estuary, Scotland. Estuarine, Coastal and Shelf Science. 38(3), 219–233.

Törnqvist, T.E., Wallace, D.J., Storms, J.E.A., Wallinga, J., van Dam, R.L., Blaauw, M., Derksen, M.S., Klerks, C.J.W., Meijneken, C., Snijders, E.M.A., 2008. Mississippi Delta subsidence primarily caused by compaction of Holocene strata. Nat. Geosci. 13(1), 173–176.

Tuda, A. O., Kark, S., Newton, A., 2019. Exploring the prospects for adaptive governance in marine transboundary conservation in East Africa. Marine Policy. 104, 75-84.

Turner, R.K., 2000. Integrating natural and socio-economic science in coastal management. J. Mar. Syst. 25, 447–460.

UNEP-Nairobi Convention and WIOMSA. 2021. Western Indian Ocean Marine Protected Areas Outlook: Towards achievement of the Global Biodiversity Framework Targets. UNEP and WIOMSA, Nairobi, Kenya, 298 pp.

Vermeesch, P., 2019. Exploratory Analysis of Provenance Data Using R and the Provenance Package. Minerals 9, 193.

Verschuren, D., Damsté, J. S. S., Moernaut, J., Kristen, I., Blaauw, M., Fagot, M., Haug, G. H., 2009. Half-precessional dynamics of monsoon rainfall near the East African Equator. Nature, 462(7273), 637-641.

von Fischer, J.C., Tieszen, L.L., 1995. Carbon Isotope Characterization of Vegetation and Soil Organic Matter in Subtropical Forests in Luquillo, Puerto Rico.

Biotropica. 27(2), 138-148.

Walling, D.E., 2013. The evolution of sediment source fingerprinting investigations in fluvial systems. J. Soils Sediments.13, 1658–1675.

Wang, A., Wang, Z., Liu, J., Xu, N., Li, H., 2021. The Sr/Ba ratio response to salinity in clastic sediments of the Yangtze River Delta. Chem. Geol. 559, 119923.

Wang, Z. L., Liu, C. Q., 2008. Geochemistry of rare earth elements in the dissolved, acid-soluble and residual phases in surface waters of the Changjiang Estuary. J. Oceanogr. 64, 407–416.

Wang'ondu, V., Kairo, J.G., Mwaura, F., Bosire, J., Dahdouh-Guebas, F., Koedam, N., 2009. Phenology of Avicennia marina (Forsk.) Vierh. in a Disjunctly-zoned Mangrove Stand in Kenya. West. Indian Ocean J. Mar. Sci. 9(2), 135-144.

Ward, R.D., Friess, D.A., Day, R.H., Mackenzie, R.A., 2016. Impacts of climate change on mangrove ecosystems: a region by region overview. Ecosyst. Heal. Sustain. 2(4), e01211.

Webb, E.L., Friess, D.A., Krauss, K.W., Cahoon, D.R., Guntenspergen, G.R., Phelps, J., 2013. A global standard for monitoring coastal wetland vulnerability to accelerated sea level rise. Nat. Clim. Chang. 3, 458–465.

Webb, J.R., Santos, I.R., Maher, D.T., Finlay, K., 2018. The Importance of Aquatic Carbon Fluxes in Net Ecosystem Carbon Budgets: A Catchment-Scale Review. Ecosyst. 22(3), 508–527.

White, W.M., Hofmann, A.W., 1982. Sr and Nd isotope geochemistry of oceanic basalts and mantle evolution. Nat. 296(5860), 821–825.

Woodroffe, C., 1981. Mangrove swamp stratigraphy and Holocene transgression, Grand Cayman Island, West Indies. Mar. Geol. 41, 271–294.

Woodroffe, C.D., 1985. Studies of a mangrove basin, Tuff Crater, New Zealand: III. The flux of organic and inorganic particulate matter. Estuar. Coast. Shelf Sci. 20, 447–461.

Woodroffe, C.D., 2018. Mangrove response to sea level rise: Palaeoecological

insights from macrotidal systems in northern Australia. Mar. Freshw. Res. 69, 917–932.

Woodroffe, C.D., Rogers, K., McKee, K.L., Lovelock, C.E., Mendelssohn, I.A., Saintilan, N., 2016. Mangrove Sedimentation and Response to Relative Sea level Rise. Annual Review of Marine Science. 8(1), 243–266.

Wooller, M.J., Morgan, R., Fowell, S., Behling, H., Fogel, M., 2016. A multiproxy peat record of Holocene mangrove palaeoecology from Twin Cays, Belize. The Holocene. 17(8), 1129–1139.

Wu, W., Xu, S., Lu, H., Yang, J., Yin, H., Liu, W., 2011. Mineralogy, major and trace element geochemistry of riverbed sediments in the headwaters of the Yangtze, Tongtian River and Jinsha River. J. Asian Earth Sci. 40, 611–621.

WWF Eastern Africa Marine Ecoregion (EAME). 2004. Towards the establishment of an ecologically representative network of Marine Protected Areas in Kenya, Tanzania and Mozambique. WWF: Dar es Salaam, Tanzania. 74 pp.

Wylie, L., Sutton-Grier, A.E., Moore, A., 2016. Keys to successful blue carbon projects: Lessons learned from global case studies. Mar. Policy 65, 76–84.

Xia, P., Meng, X., Zhang, Y., Zhang, J., Li, Z., Wang, W., Meng, X., Zhang, J., Li, Z., 2021. The Potential of Mangrove-Derived Organic Matter in Sediments for Tracing Mangrove Development During the Holocene Holocene Climatic and oceanographic changes in the west Pacific region View project Stand structure succession of typical mangrove assosiati. Estuaries and Coasts. 44, 1020–1035.

Xiao, H.Y., Liu, C.Q., 2010. Identifying organic matter provenance in sediments using isotopic ratios in an urban river. Geochemical Journal. 44(3), 181–187.

Xie, D., Schwarz, C., Brückner, M.Z.M., Kleinhans, M.G., Urrego, D.H., Zhou, Z., Maanen, B. van, 2020. Mangrove diversity loss under sea level rise triggered by bio-morphodynamic feedbacks and anthropogenic pressures. Environ. Res. Lett. 15, 114033.

Xing, L., Zhao, M., Gao, W., Wang, F., Zhang, H., Li, L., Liu, J., Liu, Y., 2014. Multiple

proxy estimates of source and spatial variation in organic matter in surface sediments from the southern Yellow Sea. Org. Geochem. 76, 72–81.

Xu, S., He, Z., Zhang, Z., Guo, Z., Guo, W., Lyu, H., Li, J., Yang, M., Du, Z., Huang, Y., Zhou, R., Zhong, C., Boufford, D.E., Lerdau, M., Wu, C.-I., Duke, N.C., Consortium, T.I.M., Shi, S., 2017. The origin, diversification and adaptation of a major mangrove clade (Rhizophoreae) revealed by whole-genome sequencing. Natl. Sci. Rev. 4, 721–734.

Yang, S.C., Riddin, T., Adams, J.B., Shih, S.S., 2014. Predicting the spatial distribution of mangroves in a South African estuary in response to sea level rise, substrate elevation change and a sea storm event. J. Coast. Conserv. 18, 459–469.

Yong, Y., Baipeng, P., Guangcheng, C., Yan, C., 2011. Processes of organic carbon in mangrove ecosystems. Acta Ecol. Sin. 31, 169–173.

Yu, F., Zong, Y., Lloyd, J.M., Huang, G., Leng, M.J., Kendrick, C., Lamb, A.L., W-S Yim, W., Yim, W.W.S., 2010. Bulk organic $\delta^{13}C$ and C/N as indicators for sediment sources in the Pearl River delta and estuary, southern China. Estuarine, Coastal and Shelf Science. 87(2010), 618–630.

Zanchettin, D., Bruni, S., Raicich, F., Lionello, P., Adloff, F., Androsov, A., Antonioli, F., Artale, V., Carminati, E., Ferrarin, C., Fofonova, V., Nicholls, R.J., Rubinetti, S., Rubino, A., Sannino, G., Spada, G., Thiéblemont, R., Tsimplis, M., Umgiesser, G., Vignudelli, S., Wöppelmann, G., Zerbini, S., 2021. Sea level rise in Venice: historic and future trends. Hazards Earth Syst. Sci 21, 2643–2678.

Zhang, J., 2017. Toward understanding the evolutionary histories and mechanisms of mangroves. Natl. Sci. Rev. 4, 737.

Zhang, K., He, D., Cui, X., Fan, D., Xiao, S., Sun, Y., 2019. Impact of Anthropogenic Organic Matter on the Distribution Patterns of Sediment Microbial Community from the Yangtze River, China. Geomicrobiology. 36(10), 881–893.

Zhuchenko, N.A., Chebykin, E.P., Stepanova, O.G., Chebykin, A.P., Gol'Dberg, E.L., 2008. Microwave digestion of bottom sediments from Lake Baikal for the

inductively coupled plasma mass-spectrometric determination of their elemental composition. J. Anal. Chem. 63, 943–949.

Zieliński, M., Dopieralska, J., Królikowska-Ciągło, S., Walczak, A., Belka, Z., 2021. Mapping of spatial variations in Sr isotope signatures (87Sr/86Sr) in Poland — Implications of anthropogenic Sr contamination for archaeological provenance and migration research. Sci. Total Environ. 775, 145792.

Zimmer, M. (2018). Ecosystem design: when mangrove ecology meets human needs. In Threats to Mangrove Forests. Springer, Cham. Berlin Germany. pp. 367-376.

Zindorf, M., März, C., Schnetger, B., 2020. Data report: wavelength-dispersive X-ray fluorescence–based geochemical data, Site U1418, IODP Expedition 341, Gulf of Alaska, in: In Jaeger, J.M., Gulick, S.P.S., LeVay, L.J., and the Expedition 341 Scientists, Proceedings of the Integrated Ocean Drilling Program, 341: College Station, TX (Integrated Ocean Drilling Pro-Gram).